Prepared for:

Rijkswaterstaat
Dienst Noord Holland

Effect of dredging on SPM concentrations in the North Sea

Set-up, validation and results of Delft3D model simulations

Report

4500150916

September 2010

Client **Rijkswaterstaat Dienst Noord-Holland**

Title **Effect of dredging on SPM concentrations in the North Sea**

Abstract

This report describes the set-up and the results from a 3D model to simulate the suspended sediment concentrations of a silt fraction and a sand fraction in part of the Wadden Sea and part of the North Sea and simulate the effects of overflow from dredging activities on these concentrations offshore Den Helder on three different days in 2007.

References RWS overeenkomst 4500150916

Rev.	Originator	Date	Remarks	Checked by	Approved by
0	B.T. Grasmeijer	24-dec-2009			
1	B.T. Grasmeijer	16-Feb-2010			
2	B.T. Grasmeijer	2-Sep-2010		J. Adema	B.T. Grasmeijer

Document Control	Contents	Status
Report number: 4500150916 Keywords: modelling, suspended sediment, silt, dreaging Project number: 4500150916 File location: Report_4500150916	text pages : 28 tables : 3 figures : 149 appendices : 1	☐ preliminary ☐ draft ☑ final

Alkyon
Hydraulic Consultancy & Research

postal address
PO Box 248
8300 AE, Emmeloord
The Netherlands

visiting address
Voorsterweg 28, Marknesse
tel : 0527 24 81 00
fax: 0527 24 81 11

e-mail
info@alkyon.nl
internet
http://www.alkyon.nl

Executive's summary

- A 3D model was set-up to simulate the suspended sediment concentrations of a silt fraction and a sand fraction in part of the Wadden Sea and part of the North Sea and simulate the effects of overflow from dredging activities on these concentrations offshore Den Helder.
- The model includes effects of a temporally and spatially varying wind field, waves and salinity.
- The model accurately represents observed water levels along the Dutch coast.
- The model represents natural background suspended sediment concentrations offshore Den Helder and the effects of a sediment plume from the Marsdiep tidal inlet reasonably well.
- The model results show encouraging agreement with observations of suspended sediment concentrations made on 17 September 2007.
- The model underestimates the observed suspended sediment concentrations on 1 and 2 October by about a factor 2. This means roughly that the model predicts 2 mg/l near the surface where 4 mg/l was observed.
- The model tends to underestimate the extent of the plume from the Marsdiep inlet into the North Sea.

- Sediment release rate due to overflow from a dredger have been schematized based on observed flow velocities and concentrations in the suction pipes on a dredger and the amount of sediment (dry weight) in the dredger. Data were made available by RWS Directie Noordzee.
- This resulted in a realistic dredging scenario 1 in which the release rate from the dynamic overflow plume was 130 kg/s and from the passive flume 20 kg/s. Simulation were made also for scenario 2 in which the release rates were a factor 2 higher, i.e. 260 kg/s from the dynamic plume and 40 kg/s from the passive plume.

- The added near-surface concentrations in the plume from overflow by dredging amount generally to 0.5-1 mg/l. The added concentrations may locally (up to 2 km from the dredging location) and temporally (1 or 2 hours) reach values of 2-4 mg/l.

- The added concentrations due to overflow from dredging are generally smaller than the natural background concentrations.

Recommendations

- Make synoptic and continuous measurements for a period of 1 month at 4 fixed locations (at 2 and 10 km in the ebb and flood direction of the dredging location), measuring 10 minute-averaged values of flow velocity magnitude and direction and suspended matter concentration (6 values per hour) at approx. 25 different heights above the bed. We suggest using a bottom mounted ADCP for this purpose.
- Take water samples at 12 different heights above the bed on 2 days to determine the suspended matter concentrations and grain size distributions of the sediment in suspension. These can be used to calibrate and validate the synoptic and continuous measurements.

Contents

1 Introduction

1.1 General

This report aims to provide information about the release of Suspended Particulate Matter (SPM) during sand mining. This knowledge is required for EIA of sand mining for beach nourishment.

1.2 Offshore sand extraction

Sand is commonly extracted from the sea bed by Trailing Suction Hopper Dredgers (TSHD) at locations seaward of the -20 m depth contour, but within the 12 miles zone (Van Duin et al., 2007; Van Prooijen et al., 2007), where the seabed contains 0.5 up to 4 % mud (silt, clay, particulate organic matter (POC), aggregates). During dredging a large part of the "fines" (mud and fine sands) flows into the overflow pipe of the ship and is released through the bottom of the ship at a depth of about 10 m below the water surface (Figure 1.1). It is assumed that it sinks quickly to the seabed where the larger part settles as a sand/mud mixture. The mud may erode sooner or later by tidal currents or by wave action. It is not clear what the critical shear stresses for erosion are. It is possible that a part of the mud forms temporarily a highly concentrated benthic suspension (HCBS) layer.

1.3 Background concentrations: T0

This report is targeted towards a particular sand extraction activity, i.e. offshore Huisduinen (Figure 1.2). A T0 measurement campaign was made in May 2007 to determine the natural background concentrations without sand extraction activities. However, observed concentrations were found to be relatively low. Values of up to 2.8 mg/l were found (Talmon, 2007). Grasmeijer et al (2009) report that the suspended matter concentrations measured during the T0 campaign are much smaller (factor 2 to 5) than MWTL mean and MWTL summer-mean concentrations and therefore not representative as a T0 condition.

1.4 Effect of sand extraction: T1

Direct effects of sand extraction on the suspended sediment concentrations were measured on board two ships that sampled the near-field, which is 300 – 1000 m up- or downstream of the TSHD during dredging cycles and mid-field in a 14.5 by 6 km region just to the North. Figure 1.2 shows the sand extraction areas and locations of the T1 observations.

Observations were made during three campaigns, namely

- 17 September 10:09 h -13:59 h
- 1 October 09:36 h – 15:53 h
- 2 October 05:57 h – 17:08 h

No significant differences between near-field and mid-field measurements were found (Talmon, 2008b). Note that tidal movements during flood phase are estimated 8 km to the north, and during ebb 4 km to the south. Wind speed > 3 Bft can change this. The September measurements near Huisduinen indicate that there are low concentrations

close to the TSHD (Fig. 3; cf Talmon, 2008a Bijlage B & Talmon, 2008b Bijlage B). Begin October higher concentrations were discerned near the Marsdiep Waddenzee outflow point at ebb. Overall concentrations are lowest in the west and highest in the east (Talmon 2008a).

2 Model set-up and validation

2.1 General

We followed a three-step approach to make 3D simulations of the flow, waves and sediment concentrations off the coast of Den Helder.

Firstly, we generated Kalman-filtered boundary conditions using the so-called SIMONA *kuststgrof* model that includes the entire Dutch coastal stretch along the North Sea (2D). Secondly, we adopted these boundary conditions to drive a DELFT3D version of the so-called *kuststrook* model (2D). Finally, we nested a detailed DELFT3D model into the *kuststrook* model (3D) to make detailed 3D simulations of flow, waves and sediment concentrations along the Dutch coastal stretch roughly from 100 km south to 80 km north of Texel and including part of the Wadden Sea between Texel, Vlieland, Terschelling and the Afsluitdijk.

2.2 Model versions

The SIMONA model applied here is version 0904 (April 2009). The DELFT3D model is version 3.28.04 with FLOW module version 3.60.01.9946 (17 December 2009) and SWAN version 4072abcd (24 August 2009).

2.3 Grid parameters

Kustgrof 2D

Figure 2.1 shows the grid of the 2D *kustgrof* model (SIMONA). The model grid consists of 487 x 128 cells. The cell size varies from about 5000m x 1250 m offshore to about 1400 m x 500 m nearshore. Figure 2.2 shows the grid cell area of the 2D *kustgrof* model and Figure 2.3 the bathymetry.

Kuststrook 2D

Figure 2.4 shows the grid of the 2D *kuststrook* model (DELFT3D). The model grid consists of 941x401 cells. The cell size varies from about 2500m x 625 m offshore to about 700 m x 250 m nearshore. This is a factor 2 finer than the *kustgrof* model. Figure 2.5 shows the grid cell area of the 2D *kuststrook* model and Figure 2.6 the bathymetry.

Detailed 3D

Figure 2.7 presents the grid of the detailed 3D model (DELFT3D). The model grid consists of 346x143 cells horizontally and 8 sigma layers vertically. The layer thickness from near-bed to the water surface is 2, 3, 5, 8, 13, 19, 25 and 25% of the water depth, which means that in 10 m water depth, the layer thickness of the lowest layer is 0.20 m, of the second lowest 0.30 m, etc. The horizontal resolution of the nested 3D model is the same as that of the *kuststrook* model. Figure 2.8 shows the grid cell area of the detailed 3D model and Figure 2.9 the bathymetry.

2.4 Time frame

Direct effects of sand extraction on the suspended sediment concentrations were measured on 17 September, and 1 and 2 October 2007. The purpose of this study is to simulate this period in particular.

With the SIMONA *kustgrof* and the DELFT3D *kuststrook* model we made simulation for the period from 1 June to 31 October 2007. This relatively long period facilitates flexibility in the selection of the final simulation period with the detailed 3D model. We applied a time step of 2 minutes for the SIMONA *kustgrof* model and 1 minute for the DELFT3D *kuststrook* model.

With the detailed 3D Delft3D model we made simulations covering 17 days from 16 September to 3 October 2007 comprising a complete spring-neap tidal cycle. The time step is 1 minute for all runs. We should note here that we restarted the detailed 3D model a number of times to push salinity and sediment fractions towards equilibrium.

2.5 Physical parameters

Table 2.1 presents the applied physical parameters in the DELFT3D FLOW module. Default values were applied in many cases. Important aspect in this study is the way in which the different fractions of sediment are schematized. The DELFT3D model facilitates two options, i.e. well-mixed or multiple layers. We applied 10 sediment layers each with thickness 0.01 m to schematize an inhomogeneous bed composition in the vertical direction.

We adopted the Van Rijn (2007) sediment transport module in DELFT3D. The module describes the sediment transport of fine silts to coarse sand in a unified framework.

Table 2.2 presents the applied parameters in the DELFT3D WAVE module. Also here default values were applied mostly. Hydrodynamics and grids from Delft3D Flow were used in DELFT3D WAVE. In order to make MPI parallel runs, we used a newer SWAN version (4072abcd) than was originally supplied with DELFT3D 3.28.04 (4051a).

For the silt fraction we adopted a median grain diameter of 30 μm. This is a compromise between the diameters observed during the T0 measurement campaign (20-60 μm) and the T1 campaign (10 μm); see Talmon (2007, 2008a, 2008b).

Table 2.1 Physical parameters as applied for the DELFT3D FLOW module

Parameter	Value
Roughness	
Roughness formula	Chezy
Roughness value	65
Stress formulation wave forces	Fredsoe
Wall roughness slip condition	Free
Viscosity	
Horizontal eddy viscosity (background)	1 m^2/s
Horizontal eddy diffusivity (background)	10 m^2/s
Vertical eddy viscosity (background)	0 m^2/s
Vertical eddy diffusivity (background)	0 m^2/s
Ozmidov length scale	0 m

Model for 3D turbulence	k-Epsilon
Sediment silt	
Reference density for hindered settling	1600 kg/m^3
Specific density	2650 kg/m^3
Dry bed density	1600 kg/m^3
Median sediment diameter	30 μm
Stratigraphy schematisation model	Multiple layers
Sediment sand	
Reference density for hindered settling	1600 kg/m^3
Specific density	2650 kg/m^3
Dry bed density	1600 kg/m^3
Median sediment diameter	200 μm
Stratigraphy schematisation model	Multiple layers
Morphology	
Update bathymetry during flow simulation	False
Include effect of sediment on fluid density	True
Equilibrium sand conc. profile at inflow boundaries	True
Spin-up interval before morphological changes	720 minutes
Minimum depth for sediment calculation	0.1 m
Van Rijn's reference height factor	1
Threshold sediment thickness	0.05 m
Estimated ripple height factor	2
Factor for erosion of adjacent cells	0
Current-related reference concentration factor	1
Current-related transport vector magnitude factor	1
Wave-related suspended transport vector	1
Wave-related bed-load transport vector	1
Wind	
Space and time varying wind and pressure on a separate curvilinear grid	True
Interpolation type	**Linear**

Table 2.2 Parameters as applied for the DELFT3D WAVE module

Parameter	**Value**
Hydrodynamics and grid	
Hydrodynamic results from DELFT3D FLOW	Bathymetry, water level, wind
Computational grid and bathymetry	Same as for DELFT3D FLOW
Spectral resolution	
Directional space	Circle
Number of directions	36
Boundaries	
Boundary 1	south: (345,2) to (345,20); EURPFM
Boundary 2	west: (345,1) to (0,0); K13APFM
Boundary 2	north: (0,2) to (0,35); SCHIERMNOND
Wave constants	
Minimum depth	0.05 m
Wave set-up	None
Forces	Wave energy dissipation rate

Wave processes	
Generation mode for physics	3rd generation
Depth-induced breaking	Alpha = 1, Gamma = 0.73
Non-linear triad interactions	Off
Bottom friction	Jonswap; Coefficient = 0.067
Diffraction	Off
Wind growth	Activated
White capping	Activated
Quadruplets	Activated
Wave propagation in spectral space	
Refraction	Activated
Frequency shift	Activated

2.6 Sediment transport module (Van Rijn, 2007)

We adopted the Van Rijn (2007) sediment transport module in DELFT3D. The module describes the sediment transport of fine silts to coarse sand in a unified framework. Van Rijn (2007) schematizes the grain size scale of the American Geophysical Union for sediments into five subclasses (Table 2.3).

Table 2.3 Sediment classes

Sediment class	**Sediment particle size range**
Coarse sand	0.5 – 2 mm
Fine sand	0.062 – 2 mm
Coarse silt	0.032 – 0.062 mm
Fine silt	0.008 – 0.032 mm
Clay + very fine silt	< 0.008 mm

The transport of bed material particles may be in the form of either bed-load or bed-load plus suspended load, depending on the size of the bed material particles and the flow conditions. The suspended load may also include some wash load (usually, clay dominated fraction smaller than 0.008 mm). In many rivers and coastal areas this clay-dominated fraction with particle sizes smaller than about 0.008 mm can hardly be observed in bed material samples, which indicates that there is not much exchange of this fraction with the bed.

Particle movement will occur when the instantaneous fluid force on a particle is just larger than the instantaneous resisting force related to the submerged particle weight and the friction coefficient. The degree of exposure of a grain with respect to the surrounding grains is an important parameter determining the forces at initiation of motion also. Cohesive forces are important when the bed consists of appreciable amounts of clay and silt particles.

Natural beds of fine sediments generally show cohesive effects due to the presence of cohesive, binding forces between the particles. For particle size smaller than 0.062 mm Van Rijn (2007) assumes that the critical bed-shear stress is affected by cohesive particle–particle interaction effects including clay coating ($\phi_{cohesive}$), by packing ($\phi_{packing}$) and by biological and organic material effects (ϕ_{bo}). Van Rijn (2007) represents the critical bed-shear stress as follows:

$$\begin{aligned} \tau_{cr} &= \phi_{bo}\phi_{packing}\phi_{cohesive}\tau_{cr,0} \quad \text{for particles } < 0.062 \text{ mm} \\ \tau_{cr} &= \phi_{bo}\phi_{cohesive}\tau_{cr,0} \quad \text{for particles } \geq 0.062 \text{ mm} \end{aligned} \tag{1}$$

The cohesive effect $\phi_{cohesive}$ is a function of the particle size for particles < 0.062 mm and is 1 for particles ≥ 0.062 mm. The packing effect $\phi_{packing}$ depends on the gelling volume concentration for particles < 0.062 mm and is 1 for particles ≥ 0.062 mm. Gelling refers to an immobile bed or viscoplastic bed. The biological and organic effects can be taken in to account by a user defined factor ϕ_{bo}.

The top panel in Figure 2.10 presents the critical bed shear stress for erosion based on the Van Rijn (2007) sediment transport model and for different values γ, which is a free model parameter affecting $\phi_{cohesive}$. Van Rijn (2007) found good agreement between observed values from Thorn (1981) and Dou (2000) and predictions for $\gamma = 1.5$. This results in a critical bed shear stress of about 0.1 N/m^2 for weakly consolidated fine sediments with sizes in the range 0.008-0.062 mm. Using 0.1 N/m^2 for field conditions results in a critical depth-averaged current velocity of about 0.32 m/ s. Using 0.2 N/m^2 results in a critical depth-averaged current velocity of about 0.42 m/s.

Important physical aspect included in the Van Rijn (2007) sediment transport module is that the suspended sediment diameter increases with concentration due to flocculation effects. Van Rijn (2007) presents a sediment fall velocity given by:

$$w_s = \phi_{floc}\phi_{hs}w_{s,0} \tag{2}$$

where ϕ_{floc} is the flocculation factor, ϕ_{hs} is the hindered settling factor, and $w_{s,0}$ is the sediment fall velocity of individual suspended particles in clear water (Van Rijn, 1993). The minimum fall velocity is set to 0.2 mm/s assuming a minimum floc size of about $16\,\mu$m.

The flocculation factor for particles finer than sand ($d < 62\ \mu$m) and salinities larger than a user defined salinity (herein 7.5 ppt) is represented by:

$$\phi_{floc} = \left[4 + \log\left(\frac{2c}{c_{gel}}\right)\right]^{\alpha} \tag{3}$$

with a minimum value of 1 and maximum of 10, and where $\alpha = d_{sand} / d_{50} - 1$ with $\alpha_{\min} = 0$ and $\alpha_{\max} = 3$, c is the mass concentration and c_{gel} is the gelling mass concentration (between 130 and 1722 kg/m^3). The α -factor caries linearly between 0 and 3 depending on the ratio of d_{sand} and d_{50}; $\alpha = 0$ for $d_{50} = 62\ \mu$m (sand, $\phi_{floc} = 1$) and $\alpha = 3$ for $d_{50} \leq 16\ \mu$m. The ϕ_{floc} factor gradually increases for particles decreasing from $62\ \mu$m to $16\ \mu$m. Flocculation is supposed to be fully active for a salinity value larger than about 5 ppt.

The transport module includes the commonly applied Richardson & Zaki (1954) expression for hindered settling, which is formulated in terms of the volume concentration as

$$\phi_{hs} = \left(1 - 0.65\frac{c_{vol}}{c_{vol,gel}}\right)^5 \quad (4)$$

where c_{vol} is the volume concentration and $c_{vol,gel}$ is the volume concentration for immobile sediment bed.

The effective sediment settling velocity including flocculation and hindered settling effects based on the above equations is shown in the lower panel of Figure 2.10 for three different particle sizes. The effective settling velocity of mud particles of 8 μm increases from 0.2 mm/s for c = 0.1 kg/m^3 to 2 mm/s for c = 2 kg/m^3. The flocculation process of mud particles of 16 μm proceeds somewhat slower. Hindered settling effects are dominant for c > 5 kg/m^3. The effective settling velocity of 32 μm particles increases from about 0.9 mm/s for c = 0.1 kg/m^3 to 2.2 mm/s for c = 30 kg/m^3.

Figure 2.11 shows examples of concentrations and settling velocities from test runs using a rectangular basin, illustrating the effect of a concentration dependent flocculation. The applied single suspended particle size is 26 μm , uniformly distributed over the entire bed (100%). The depth-averaged velocity is 1 m/s. Figure 2.11 shows that under these conditions the settling velocity increases from about 0.5 mm/s in the upper part of the water column where the concentration are about 0.25 kg/m^3 to more than 1 mm/s near the bed where the concentrations are more than 1.5 kg/m^3.

Figure 2.11 also illustrates that the effect of changing the number of vertical layers on the concentrations is almost negligible under the applied conditions with uni-directional constant flow. Results from test runs using a harmonic boundary condition consisting of sinusoidal time series with a 1 m/s amplitude showed similar behaviour under maximum flow. However, the effect of the number of layers is more distinct during slack tide (small flow velocities). Figure 2.12 shows examples of vertical distributions of concentration and velocity during slack tide. Although the near bed concentrations are similar for the different simulations, higher up in the water column the concentration and the settling velocity decreases more rapidly when using more layers. The concentrations at mid depth are about 20% smaller when applying 64 layers instead of 8. This occurs only around slack tide. The results for higher current velocities are similar to those shown in Figure 2.11. Because of computational efficiency and the limited effect of the number of layers under these conditions we adopted 8 layers in our schematization. Realistically simulating the temporal behaviour of the vertical distribution of high mud concentrations requires more layers but this is beyond the scope of the present study.

2.7 Boundary and initial conditions

Locations of the water level and wave stations

Figure 2.13 shows the locations of the water level stations from which the observations were used to generate Kalman-filtered boundary conditions with the 2D SIMONA *kustgrof* model. The blue triangles in Figure 2.13 denote the locations of the wave station from

which observations were used to generate wave boundary conditions for the nested Delft3D model.

Space and time varying wind and pressure data

Additional boundary conditions for both models involve space and time varying wind and pressure data provided by The Royal Netherlands Meteorological Institute (KNMI) in so-called GRIB (GRIdded Binary) format. GRIB is a mathematically concise data format commonly used in meteorology to store historical and forecast weather data. We converted the files to formats readable by the SIMONA and DELFT3D models. The model input consists of a pressure and a wind field every 6 hours between 1 September and 31 October 2007, which comes down to 240 pressure fields and 240 wind fields.

The spatially varying pressure will have an effect on the simulated water levels. The wind fields will not only affect the simulated water levels and flow pattern due to wind stress at the free surface but also the simulated waves due to wind growth.

Figure 2.14 shows an example of the adopted pressure field boundary condition on 10 September 2007 18:00 h. It can be seen from this figure that a low pressure area east of Denmark together with a high pressure area west of Ireland results in winds from a North-westerly direction along the Dutch coast. Figure 2.15 shows the adopted wind field boundary condition at the same moment. It can be seen that the wind speeds reach values of about 15 m/s on the North Sea, which is a near-gale force wind of 7 Beaufort.

Processes activated in DELFT3D WAVE included wind growth and white capping.

Offshore wind and wave conditions

Showing all of the pressure and wind fields would require a large number of figures in this report. Therefore, to be practical, Figure 2.16 gives an impression of the offshore wind and wave conditions at station K13APFM during the simulation period between 1 September and 31 October 2007. The following four events with near gale force winds (7 Beaufort) occurred:

- 10 September; wind direction NW
- 18 September; wind direction N
- 24-28 September (intermittent); wind direction SSW to NE
- 28 October: wind direction WSW

This results in significant wave heights of more than 3 m during these events. Maximum significant wave height during the simulation period is nearly 5 m and occurs on 10 September 2007, 22:20 h. The mean significant wave height during the simulation period is 1.5 m.

Wave mean periods T_{m02} of up to 7.6 s occur during the near-gale events. The mean T_{m02} value during the entire simulation period is 4.8 s. The wave direction more or less follows the wind direction.

Discharges

Figure 2.17 shows the locations of 8 river discharge points in the model. This concerns the Eems, Kornwerderzand, Den Oever, IJmuiden, Schelde Schelle, Lek (Hagestein), Waal

(Thiel) and Bergse Maas (Lith). Figure 2.18 presents the applied discharges as a function of time.

Initial bed composition

The initial sediment composition of the bed was obtained by running the model firstly with an overall 2.5% of silt and 97.5% of sand in 10 different sub layers of 1 cm each. We restarted the model runs a few times applying the bed composition resulting from the previous run. We modified the bed composition results from the first run setting the percentage of silt on the North Sea to 0.5% and sand on 99.5%. We did not make modifications to the simulated bed composition on the Wadden Sea. Figure 2.19 shows the initial fraction of silt in the bed material. Figure 2.20 shows the fraction of sand, which comes down to 1-silt fraction.

Boundary conditions for suspended sediment concentrations

Figure 2.21 presents the cross-shore transects from which the data were used to schematize boundary conditions of suspended sediment concentrations in the model. We adopted the Goeree (GO) transect as the southern boundary and the Terschelling (TS) transect for the northern boundary. As the period of interest falls in late summer, we adopted summer mean suspended sediment concentrations.

Figure 2.22 shows the cross-shore distribution of statistical parameters determined from total suspended matter concentrations in the Terschelling and Goeree transects. The Goeree summer-mean concentrations range from 4 mg/l at 2 km offshore to 9 mg/l at 70 km offshore. The Terschelling summer-mean concentrations range from 7mg/l at 4 km offshore to 2 mg/l at 70 km offshore. Noordwijk and Walcheren are shown as reference.

The above described boundary conditions have been prescribed at the open model boundaries. However, in a physical world, the inflowing water mass immediately after low water slack originates from the outflowing water mass a moment earlier. Consequently, the concentration of the in flowing water is not equal to the concentration that has been prescribed along this open boundary. It will take some time before the concentration reaches the prescribed value. In DELFT3D, this time lag (return time) is modelled by means of a Thatcher-Harleman boundary condition (Thatcher and Harleman, 1972). We adopted a Thatcher Harleman time lag of 180 minutes (3 hours).

Miscellaneous

Bed update was set to off, which means that the bed composition changes in the model without changing the bed level. The effect of sediment on the fluid density was set on. This means that the presence of sediment affects the flow and vice versa.

We applied a spin-up interval of 720 minutes before morphological changes (bed composition changes) take effect. This is done to eliminate effects of initialization of the flow on the bed composition.

2.8 Simulating overflow from dredger

Trailing suction hopper dredging

A trailing suction hopper dredger (THSD) is a ship that is equipped with one or two suction pipes that are lowered to the seabed during dredging. A sediment-water mixture is pumped up from the seabed into the hopper cargo space. Provided the sediment in the mixture is not too fine, a separation process takes place in the hopper under the action of gravity. The sediment settles in the hopper and the excess water is ultimately forced to flow overboard. The dredging process is continued until the ship is loaded to its capacity.

Basically, the loading process consists of three phases (Van Rijn 2005; Van Rhee, 2002):

- filling phase to overflow level; three layers are present in the hopper: a lower layer of settled sand, a sediment-water mixture and a top layer of clear water;
- overflow phase (5 to 15 min); the hopper is filled with sand and the excess water is forced out of the hopper by overflow through a pipe system; a high-concentration density current is present above the bed which effect gradually reduces in time; a low-concentration top layer is present near the water surface flowing in horizontal direction to the overflow system;
- final phase; high-concentration layer reaches the water surface and the overflow losses of sediment increases considerably; the maximum sediment concentrations in the overflow pipeline may be as large as 30% by volume when the hopper approaches its capacity .

After filling, the ship sails to the disposal location where the sediment load is disposed by opening doors in the bottom or by pumping the load ashore by use of the dredge pumps of the ship.

Depending on the sediment size distribution, the hopper geometry and other process parameters, the overflow can reach values up to 30% (in muddy environment) of the total volume of sediment pumped into the hopper and may cause significant environmental problems (Van Rijn, 2005).

In sandy conditions the total overflow generally amounts to about 5% to 10%. Van Rijn (2005) estimates the total overflow loss of a hopper with a volume of 5000 m^3 at about 350 m^3 (assuming loss of 7%) or about 500 tonnes of sediment (assuming a density of 1500 kg/m^3). This amount of sediment will be released (mixed) in the water column during sailing over a distance over the order of 1000 m, a width of about 30 m (about 3 times the width of the vessel) and a water depth of about 15 m. Assuming complete mixing, the sediment concentration due to overflow in this water volume of about $0.5x10^6$ m^3 will be about 1 kg/m^3 ($500x10^3$ kg of sediment in $0.5x10^6$ m^3 of water). Most of this sediment (coarser fractions) will rapidly sink to the bed; the fines (10% to 20%) will remain in suspension for some time (15 to 30 minutes). Van Rijn (2005) estimates the resulting increase in turbidity around the hopper at about 0.1 to 0.2 kg/m^3 (0.1 to 0.2 times 1 kg/m^3).

Sediment release mechanisms

Sediment can be released from dredgers by a wide range of mechanisms and at different levels in the water column (Van Maren et al., 2008). The mechanisms that give rise to the release are often complex. There are five main mechanisms by which sediment may be

released into the water column by a trailing suction hopper dredger: 1) Overflow from the hopper; 2) Use of Lean Mixture OverBoard (LMOB) systems; 3) Disturbance around the draghead; 4) Scour of the bed caused by the main propellers and bow thrusters. 5) Operation of de-gassing systems.

The LMOB system is used mainly when dredging in soft soils and is designed to prevent low density mixtures entering the hopper and occupying space, which could be used for the storage of higher density mixtures. The system operates by diverting the flow from the discharge side of the pump to a discharge point in the vessel's hull. LMOB is used intermittently, mainly at the commencement of a dredging run and when the ship is turning. The relative importance of these release mechanisms varies according to the nature of the soil being dredged and, in some cases, on operating restrictions imposed to minimise environmental effects. In addition, sediment may be put into suspension by the release of biogenic gas from disturbed, recently-dredged areas. In broad terms, there are two main operating modes that determine the general magnitude of sediment release: (1) non-cohesive, relatively coarse materials with overflow, or (2) cohesive or very fine materials without overflow.

Overflow is usually used when dredging sands, stiff clays and gravels. It is characterised by: 1) Major discharge of sediment from the overflow, when the hopper has been filled with mixture, including during turning between trailing runs; 2) Relatively minor re-suspension of sediment at the draghead; 3) Propeller scour (depending on water depth relative to the draft, and on the nature of the bed material); 4) No use of Light Mixture OverBoard (LMOB) systems. In this mode, the release of sediment through the overflow may be orders of magnitude larger than the other sediment release mechanisms.

Dredging without overflow usually occurs when dredging silts and soft clays. It is characterised 1) Use of the LMOB system; 2) Propeller scour (depending on water depth relative to the draft, and on the nature of the bed material); 3) Re-suspension of sediment by the draghead at or near the seabed.

We focus here on dredging of sand with overflow.

Dynamic and passive plume

When working with overflow, the sediment released by the overflow will be dominant and will probably completely obscure the sediment released by other mechanisms (Van Maren et al, 2008). If the density of the overflow is sufficiently high and the speed of the vessel through the water is sufficiently low, the plume will initially be very dynamic and will descend rapidly towards the bed as a density current, resulting in a very short space of time, in a well developed depth-related concentration gradient. The plume may be significantly wider near the bed than at the surface. After impinging on the bed, the plume spreads radially as a horizontal density current, where it gradually decelerates. Most of the sediment will be deposited on the seabed. As the dredger passes over the plume, some material may be entrained from the top of the plume by the propeller wake and redistributed back towards the surface (Van Maren et al, 2008), but the bulk of the released sediment will remain in the lower part of the water column.

If the overflow density is low and the vessel speed is high, the plume descent speed will be relatively slow. The plume will tend to mix rapidly with the surrounding water and will be diffused. A large proportion of the released sediment will be further disturbed by the propeller wake of the ship. The concentration gradient within the plume will initially

be weak. The shape of the plume (in cross-section) will be more columnar than that resulting from dynamic, high-density overflows.

The passive plume is defined as the sediment that is brought in suspension by dredging processes, slowly settles from suspension, and is advected by the ambient currents (Van Maren et al, 2008).

Sediment in the passive plume originates from:

1) Entrainment from the overflow plume and horizontal density current. To what extent the passive plume originates from a weakly dynamic or a dynamic overflow plume cannot be determined directly. However, the entrainment rate from a weakly dynamic overflow plume is higher than from a dynamic overflow plume. If the sediment flux in the passive plume is high compared to the total sediment release rate through the overflow, then the overflow plume was probably weakly dynamic. The more dynamic the overflow plume, the lower the relative fraction of overflow sediment in the passive plume.
2) Erosion of the horizontal density current or fresh deposit (both originating from the overflow), or the seabed, by propeller wash and the ship-induced return current. Erosion by ship-induced currents and propeller wash will increase with decreasing water depth.
3) Erosion of the seabed by the dragheads. The erosion rate by the dragheads is probably mainly dependent on the sailing speed of the vessel. The seabed erosion rate by the dragheads, the propeller wash, and ship-induced return currents has the same order of magnitude, but their contribution to the passive plume is substantially less then the contribution from the overflow discharge.

Schematizing the dynamic overflow plume

Rijkswaterstaat Directie Noordzee provided us with some representative numbers on concentrations and velocities in the two suction pipes of a trailing suction hopper dredger. The pipe diameter is 1 m.

The flow velocity magnitude in the two suction pipes ranges in this representative case between about 4.5 and 6 m/s (Figure 2.23 upper panel). The concentrations in the suction pipes range between 100 and 500 kg/m^3 (Figure 2.23 second panel). The resulting transport of sediment in the pipes ranges roughly between 500 and 2000 kg/s. The lower panel in Figure 2.23 presents the cumulative integral of the transports in the suction pipes (kg) and the dry mass in the hopper. The difference between the two is the overflow loss. The total amount of sediment in the overflow summed over entire suction period of 3720 seconds amounts to about 473.000 kg. Dividing this by the suction period gives a release rate by overflow of about 130 kg/s.

To get an indication of the variation of the overflow loss Figure 2.23a shows the same parameters as Figure 2.23 but for a different trip. The overflow loss for this second trip amounts to about 180 kg/s.

To account for the variation in overflow between different trips we made simulations for two scenarios, the first with an overflow loss of 130 kg/s and the second with twice this value. These values are of the same order as the mean of the time series presented by Van Maren et al. (2008) for the Den Helder TASS experiments (figure A.76-A.85 in their report).

To be conservative, we assume the above derived overflow losses to consist entirely of silt. In reality, part of the overflow loss will consist of sand that does not remain in suspension as easily as the silt fraction does.

In addition, to be conservative also we use the total overflow loss for the dynamic plume. In reality, large part of the overflow loss will descend rapidly to the bed and remain there (Van Maren et al, 2008).

This means that our approach will provide an upper limit for the increased turbidity from overflow loss by a dredger.

Schematizing the passive plume

Besides the above described dynamic overflow plume, sediment from the overflow loss may be present in a so-called passive plume. This sediment slowly settles from suspension and is advected by the ambient currents.

Van Maren et al. (2008) indicate a range for the sediment release from the passive plume of 1-20 kg/s. We will here adopt the maximum value of 20 kg/s.

To be conservative, we will add the passive plume sediment release to the total overflow loss we use for the dynamic plume. In reality both the passive and the dynamic plume are part of the total overflow loss.

As the sediment in the dynamic overflow plume is expected to settle relatively quickly to the bed we schematize this as being released in the lowest computational layer near the bed. The passive overflow plume settles relatively slowly to the bed and is therefore schematized as being released over the entire water column.

Discussion on the sediment release rates

Van Maren et al (2008) present an indicative range of sediment fluxes from a TSHD based on measurements in and offshore Hook of Holland in May 2007, and offshore Den Helder in September 2007. The overflow loss range is 250-2500 kg/s, which is in the same range as presented by Miedema & Van Rhee (2007). From the overflow loss, 1-20 kg/s is released in a dynamic plume and 1-20 kg/s in a passive plume. About 0.1-0.2 kg/s is resuspended by the drag heads. Van Maren et al. (2008) found that over 99% of the sediment from the overflow descends rapidly onto the bed.

Van Rijn (2005) estimates the amount of material brought into suspension from the overflow at about 1.3% of the dredged volume. In our case this would amount to 1.3% of about 7000 m^3 of sand and would result in 91 m^3 of overflow loss. Assuming a dry bed density of 1500 kg/m^3, this would amount to 136500 kg. With a dredging period of 1 hour (3600 seconds) the sediment release would amount to 38 kg/s.

We could also estimate the sediment release rate from the dredger by taking the transport rate through the suction pipes (about 1500 kg/s), assume a fraction of silt in the bed at 2% (which is realistic for the seabed concerned here) and assume that all of this silt is released by the dredger. This would result in a sediment release rate of 30 kg/s, which is of the same order as Van Rijn (2005).

We simulate the total overflow loss (and not a part) as being released in a dynamic plume and add the maximum value observed by Van Maren et al. (2008) for the passive plume. Consequently, the sediment release rates adopted in this study are more than a factor 6 larger than the range presented by Van Maren et al. (2008) and more than a factor 3 larger than those based on rules of thumb. In addition, we assume the sediment being released to consist entirely of silt. This approach will result in upper limit for the effect of dredging on the SPM concentrations.

2.9 Model validation

Water levels

Figure 2.24 compares observed and predicted water levels for the entire simulation period for stations Wierumergronden, Petten Zuid, IJmuiden Buitenhaven and Brouwershavense Gat 08 (WIERMGDN, PETTZD, IJMBTHVN and BROUWHVSGT08).

The simulated water levels show encouraging agreement with the observations. The goodness-of-fit R^2 is higher than 0.98 for all stations. Figure 2.25 zooms in on the period 10-20 October to illustrate the good agreement between simulations and observations in more detail.

Residual current pattern

The mean/residual circulation pattern of the North Sea is induced by the prevailing winds, the tide and by the density field (e.g. De Boer, 2009). The tidally induced residual flows are largest along the coastal regions where the Kelvin wave amplitudes are largest and are directed in the same direction as the propagation of the Kelvin wave (e.g. Tee, 1979, 1980; Ye & Garvine, 1998). A second source for residuals in the Southern Bight is the wind. The average WSW direction of the wind, the predominant cyclonic rotation of the wind fields in combination with the bottom slope of the North Sea are responsible for a cyclonic residual current (Otto et al., 1990). These tidal and wind driven residual currents are responsible for a net transport through the Channel northwards with an average velocity of a few cm/s (Figure 2.25a).

Figure 4.25b shows the depth-averaged residual current field based on our 3D model simulation for the period between 16 September and 2 October 2007. The pattern agrees qualitatively with that in Figure 2.25a. The residual flow pattern shows a northward net transport with flow velocity magnitudes increasing from south to north along the Noord-Holland coast. We should note that we adopted a temporally and spatially varying wind field where Figure 4.25a shows the residual pattern for a spatially and temporally constant SW wind so that only a qualitative comparison can be made.

Salinities

Figure 2.26 compares observed and predicted salinities in the upper part of the water column. Salinity observations are not as abundantly available as water level observations. We compare 11 observations from 4 different stations. Figure 2.26 shows that the difference between observed and predicted salinities is less than 10% for the stations Vliestroom and Noordwijk 10. Before the near-gale event of 24-28 September, accuracy is good also for the other two stations. However, predicted salinities are higher than

observed for the period between 28 September and 31 October for station Doove Balg West and Marsdiep Noord. Largest difference occurs on 9 September when the observed salinity at Doove Balg West is 19 psu whereas the predicted value is 27 psu.

Concentrations introduction

Figure 2.27 shows the locations and names of the T1 observations and the dredging area as schematized in DELFT3D. The maximum north-to-south distance between the different observation points is 6 km. The maximum east-to-west-distance is about 10 km. The dredging area schematized in DELFT3D is located at about 2 km south of the nearest observation. Figure 2.27a shows the date and time of the T1 observations using the water level at Den Helder as a reference.

Figures 2.28 to 2.31 show vertical distributions of simulated suspended solids concentrations for 6 locations offshore Den Helder, i.e. N1, N21, N2, N5, N24 and N7 (see Figure 2.27 for locations). The figures show results from 3 different simulations, i.e. without dredging, with dredging scenario 1 and with dredging scenario 2, and observed values at 3 heights above the bed.

The mean, minimum and maximum values shown in Figures 2.28 to 2.31 are based on a 13 hour time series on 17 September and 1 and 2 October.

Concentration profiles 17 September 2007

On 17 September 2007, the mean simulated distribution at location N1 (closest to Marsdiep inlet) ranges between about 20 mg/l near the bed to 3 mg/l near the water surface (Figure 2.28 upper left). The minimum values range from 1 mg/l near the bed to 0.4 mg/l near the surface. The maximum concentrations range from about 100 mg/l near the bed to about 10 mg/l near the water surface. The temporary effect of dredging amounts to 20-50% of the background concentration. The observed concentrations show encouraging agreement with the mean simulated distribution.

The upper right panel in Figure 2.28 shows that the mean simulated concentration at location N21 (west of N1 and 2 km north of the dredging location) on 17 September ranges from 6 mg/l near the bed to 2 mg/l near the water surface. The minimum ranges from 3 to 1 mg/l and the maximum from 25 to 5 mg/l. Dredging scenario 1 increases the mean concentrations by about 1 mg/l and scenario 2 by about 2 mg/l. Observations agree with the minimum simulated vertical distribution.

N2 is situated 5 km west of N21 and northwest from the dredging location. The mean simulated concentrations range from 5 mg/l near the bed to 2 mg/l near the surface, the minima from 2 to 1 mg/l and the maxima from 18 to 4 mg/l (Figure 2.28 middle left panel). The effect of dredging to 20-50% of the background concentration. The observed values are between the minimum and mean simulated distributions.

Location N5 is situated north of N1 and northwest of the dredging location and relatively close to the Marsdiep inlet. Mean simulated concentrations range from 9 mg/l near the bed to 3 mg/l near the water surface. The minimum values range between 2 and 1 mg/l, the maxima between 40 and 6 mg/l. It is interesting to see that the profiles for dredging scenario 1 show about 1 mg/l smaller concentrations than the profiles without dredging and the profiles for scenario 2 about 1 mg/l higher concentrations than without dredging. This may be due to the suspended sediment fall velocity being

dependent on the concentration in the Van Rijn (2007) sediment transport model (Figure 2.10 lower panel). This effect is represented by Equation (4) in Section 2.6. Increasing the concentrations e.g. by overflow increases the fall velocity in the model. This causes the sediments to settle to the bed more rapidly than without the extra concentration.

Location N24 is situated at about 5 km north of the dredging location. The mean simulated concentrations range from 6 mg/l near the bed to 2 mg/l near the surface (Figure 2.28 lower left panel). The minimum values range between 3 and 1 mg/l and the maxima between 24 and 5 mg/l. Dredging scenario 1 and 2 increase the concentrations by less than 0.5 mg/l. Observations agree with the minimum simulated vertical distribution.

Location N6 is situated west of N24 and northwest from the dredging location. Mean simulated concentrations range from 5 mg/l near the bed to 2 mg/l near the surface. Minimum values range between 2 and 1 mg/l and maxima between 15 and 4 mg/l. The effect of dredging to 20-50% of the background concentration. The observed values are between the minimum and mean simulated distributions.

Concentration profiles 1 October 2007

On 1 October 2007, the mean simulated distribution at location N1 (closest to Marsdiep inlet) ranges between about 31 mg/l near the bed to 5 mg/l near the water surface (Figure 2.29 upper left). The minimum values range from 2 mg/l near the bed to 1 mg/l near the surface. The maximum concentrations range from about 170 mg/l near the bed to about 13 mg/l near the water surface. The effect of dredging is small for both scenarios. The observed concentrations are of the same order as the maximum simulated values near the bed and at mid depth but are about 30 mg/l higher near the surface. This may be due to the outflow from Marsdiep with relatively high suspended sediment concentrations reaching farther offshore than the model predicts.

The mean simulated concentration without dredging at location N21 (west of N1 and 2 km north of the dredging location) on 1 October ranges from 2 mg/l near the bed to 1 mg/l near the water surface (Figure 2.29 upper right). The minimum ranges from 1 to 0.3 mg/l and the maximum from 3 to 2 mg/l. Dredging scenario 1 increases the mean concentrations by about 0.5 mg/l and scenario 2 by about 0.7 mg/l. Observations are about 2 mg/l higher than the maximum simulated vertical distribution.

At location N2 (west of N21 and northwest of the dredging location), the mean simulated concentrations range from 3 mg/l near the bed to 1 mg/l near the surface. The minima range from 2 to 0.3 mg/l and the maxima from 5 to 3 mg/l (Figure 2.29 middle left). It is interesting to see here that the profiles for dredging scenarios 1 and 2 show slightly smaller concentrations (< 0.5 mg/l smaller) than without dredging. The observed values are about 2 mg/l higher than simulated.

Mean simulated concentrations at N5 (north of N1 and northeast of the dredging location and relatively close to the Marsdiep inlet) range from 4 mg/l near the bed to 2 mg/l near the water surface. The minimum values range between 2 and 1 mg/l, the maxima between 24 and 3 mg/l. The profile for dredging scenario 1 shows about 0.5 mg/l higher concentrations than without dredging and that for scenario 2 about 1 mg/l higher. Observed values are about 5 mg/l higher than the simulated maxima.

Location N24 is situated at about 5 km north of the dredging location. The mean simulated concentrations range from 2 mg/l near the bed to 1 mg/l near the surface on 1 October 2007 (Figure 2.29 lower left). The minimum values range between 1 and 0.2 mg/l and the maxima between 3 and 1 mg/l. Dredging scenario 1 and 2 increase the concentrations by less than 0.5 mg/l. Observations are about 10 mg/l higher near the bed and 5 mg/l higher near the water surface than the maximum simulated vertical distribution.

Location N6 is situated west of N24 and northwest from the dredging location. Mean simulated concentrations range from 3 mg/l near the bed to 1 mg/l near the surface on 1 October 2007. Minimum values range between 2 and 0.5 mg/l and maxima between 8 and 2 mg/l. It is interesting to see that also here the profiles for dredging scenarios 1 and 2 show slightly smaller concentrations (< 0.5 mg/l smaller) than without dredging. The observed values are of the same order as the simulated maximum near the bed and about 2 mg/l higher than the simulated maximum near the surface.

Concentration profiles 2 October 2007

On 2 October 2007, the mean simulated distribution at location N1 (closest to Marsdiep inlet) ranges between about 12 mg/l near the bed to 3 mg/l near the water surface (Figure 2.30 upper left). The minimum values range from 2 mg/l near the bed to 1 mg/l near the surface. The maximum concentrations range from about 55 mg/l near the bed to about 5 mg/l near the water surface. The effect of dredging is small for both scenarios. The observed concentrations are about 10mg/l higher than the simulated maxima.

The mean simulated concentration without dredging at location N21 (west of N1 and 2 km north of the dredging location) on 1 October ranges from 2 mg/l near the bed to 1 mg/l near the water surface (Figure 2.30 upper right). The minimum ranges from 1 to 0.4 mg/l and the maximum from 3 to 1 mg/l. Dredging scenario 1 increases the mean concentrations by about 0.5 mg/l and scenario 2 by about 0.7 mg/l. Observations are about 5 mg/l higher than the maximum simulated vertical distribution.

At location N2 (west of N21 and northwest of the dredging location), the mean simulated concentrations range from 2 mg/l near the bed to 1 mg/l near the surface. The minima range from 1 to 0.6 mg/l and the maxima from 4 to 1 mg/l (Figure 2.30 middle left). The profiles for dredging scenarios 1 and 2 show slightly smaller concentrations (< 0.5 mg/l smaller) than without dredging. The observed values are about 2-4 mg/l higher than simulated.

Location N5 is situated north of N1 and northwest of the dredging location and relatively close to the Marsdiep inlet. On 2 October, the mean simulated concentrations range from 3 mg/l near the bed to 1 mg/l near the water surface (Figure 2.30 middle right). The minimum values range between 2 and 1 mg/l, the maxima between 11 and 2 mg/l. Dredging scenario 1 increases the mean concentrations by about 0.5 mg/l and scenario 2 by about 1.0 mg/l.

The mean simulated concentrations at N24 (about 5 km north of the dredging location) range from 2 mg/l near the bed to 0.5 mg/l near the surface on 1 October 2007 (Figure 2.30 lower left). The minimum values range between 0.8 and 0.3 mg/l and the maxima between 3 and 0.7 mg/l. Dredging scenario 1 and 2 increase the concentrations by less

than 0.5 mg/l. Observations are about 4-10 mg/l higher than the maximum simulated vertical distribution.

Location N6 is situated west of N24 and northwest from the dredging location. Mean simulated concentrations range from 2 mg/l near the bed to 1 mg/l near the surface. Minimum values range between 1 and 0.5 mg/l and maxima between 3 and 1 mg/l. The effect of dredging is small for scenario 1. Concentrations decrease slightly in scenario 2 as compared to the situation without dredging. The observed values are of the same order as simulated near the bed and about 1 mg/l higher near the surface.

It is interesting to see that the observed concentrations are generally higher on 1 and 2 October 2007 than on 17 September 2007. This is likely related to the preceding wave conditions. The observations on 17 September were preceded by a period of 5 days with calmer wave conditions (Hs < 2.5 m) than the 5 days period preceding 1 and 2 October with higher wave, particularly on 27 and 28 September with Hs > 4 m (see Figure 2.16). These higher wave brought much of the very fine silt in suspension and it takes some time for this very fine fraction to settle to the bed.

The underestimation of the suspended sediment concentrations by the model on 1 and 2 October may be related to the following:

1. The fraction of silt in the bed on the North Sea is higher than used in the model. Increasing the silt fraction would indeed increase the background concentrations and improve model performance for 1 and 2 October. However, this would also have the undesirable effect of increasing the concentrations on 17 September which would deteriorate model performance for these conditions.
2. The representative grain diameter for silt on the North Sea is smaller than that used in the model. However, like increasing the fraction of silt, decreasing the representative grain diameter for silt would improve model performance for 1 and 2 October but deteriorate that on 17 September.
3. The finest silt fractions in the bed on the North Sea have a longer history effect than can be represented with one single 30 μm fraction. The finest fractions in the bed have been released into suspension during the energetic conditions in the 5 days period preceding 1 and 2 October. In contrast, these fine particles have had the time to settle to the bed during the relatively calm period preceding 17 September 2007. This is consistent with the finding by Talmon (2008a, 2008b) that the median particle diameter of the material in suspension is generally smaller in 1 and 2 October than on 17 September 2007 (see their Figures C.4, C.5 and C.6).

Concentration maps 17 September 2007

Figures 2.31 to 2.42 show the horizontal spatial distribution of simulated suspended solids concentrations in the upper computational layer for 12 time steps during a tidal cycle on 17 September 2007. The observed values near the water surface are shown also. We should note here that the different observations have been made at different moments in time, which means that they cannot be compared one-on-one with the simulated maps. However, plotting them in the maps does facilitate comparing the orders of magnitude of the observations and the simulations and the horizontal spatial gradients.

Figure 2.31 to 2.42 show that the sediment plume from Marsdiep that has flowed out into the North Sea in southwest direction during the ebbing phase is advected

northward during the flooding phase (Figures 2.31-2.33). The plume centre point with concentrations of 5-10 mg/l reaches the measurement area around high tide (Figure 2.34). Concentrations in the measurement area decrease to 1-2 mg/l during the ebbing phase and a new plume is generated by the outflow from the Marsdiep (Figures 2.35-2.42). Concentrations in the Marsdiep inlet may reach values of 30-200 mg/l during the ebbing phase.

Concentration maps 1 October 2007

Figures 2.43 to 2.54 show the horizontal spatial distribution of simulated suspended solids concentrations in the upper computational layer for 12 time steps during a tidal cycle on 1 October 2007. The observed values near the water surface are shown as coloured symbols.

As on 17 September, also on 1 October the sediment plume from Marsdiep that has flowed out into the North Sea in southwest direction during the ebbing phase is advected northward during the flooding phase (Figures 2.43-2.44). The plume is not advected as far north as on 17 September, which might be due to the more northerly winds on 1 October (Figure 2.16). Concentrations in the measurement area decrease to 1-2 mg/l during the ebbing phase and a new plume is generated by the outflow from the Marsdiep (Figures 2.47-2.54). Concentrations in the Marsdiep inlet may reach values of 30-200 mg/l during the ebbing phase.

Concentration maps 2 October 2007

Figures 2.55 to 2.66 show the simulated suspended sediment concentrations in the upper part of the water column for the period 2 October 01:30 h to 2 October 12.30 h. Simulated concentrations are smaller than on 1 October. This is likely due to the wind direction that has changed from NNW to NE and wave heights that have decreased from 3 m on 30 September to less than 1 m on 2 October. Simulated concentrations are of the same order as measured for the measurement locations fartherst from Marsdiep but a factor 2-4 smaller than observed closer the Marsdiep tidal inlet.

3 Results

3.1 Flow velocities and wave conditions

17 September 2007

The measurement campaign on 17 September 2007 started in the morning at 10:09 h (high tide) and was finished in the afternoon at 13:59 h (ebbing phase before low tide).

The upper panels in Figures 3.1 to 3.12 present the flow pattern in the upper computational layer at different tidal stages during which the measurements were made. X-marks denote locations of the T1 observations. The lower panels show the spatial distribution of the significant wave height and the mean wave direction.

Northward directed flow velocities range between 0.6 to 0.8 m/s at the study area during the flooding phase (Figures 3.1-3.3). Waves come in from WSW directions and the significant height ranges between 0.8 and 1 m.

The current velocity decreases to 0.4-0.5 m/s just before high tide (Figure 3.4) and near-zero around high tide (Figures 3.5 and 3.6; start of the measurement campaign). The wave direction is west (W). The significant height remains between 0.8 and 1.0 m.

The southward directed flow velocities during the ebbing phase of the tide increase to values of about 0.5 m/s (Figures 3.7-3.10). The maximum ebb velocities are smaller than the maximum flood velocities. The last observation has been made during this maximum ebb flow. The wave direction has changed slightly to WNW and the significant height has increased to 1.0-1.2 m. Flow velocities drop to smaller values afterwards (Figures 3.11-3.12).

1 October 2007

The measurement campaign on 1 October 2007 started in the morning at 09:36 h (high tide) and was finished in the afternoon at 15:53 h (ebbing phase just before low tide).

Flow velocities amount to 0.6-0.7 m/s during the flooding phase 2.5 hours before the measurement campaign starts (Figure 3.13). This drops to 0.5-0.6 m/s after two hours (Figure 3.14 and 3.15) and about 0.4 m/s just before high tide at the start of the measurement campaign (Figure 3.16). Waves come in from NNW and the significant height ranges between 0.8 and 1 m.

Velocities are near zero at high tide (Figure 3.17) and increase in a southward direction towards 0.3-0.4 m/s on 11:30 h (Figures 3.18). The wave height is about 0.8 m. The velocity is southward directed and amounts to about 0.6 m/s during the ebbing phase of the tide (Figures 3.19-3.21). The wave direction has shifted to N direction and the significant height has decreased to 0.6-0.8 m. The flow velocity decreases to near-zero around low tide (Figures 3.22-3.24). The wave direction has changed to NNE and the significant wave height is about 0.6 m.

2 October 2007

The measurement campaign on 2 October 2007 started in the morning at 05:57 h (just after low tide) and was finished in the afternoon at 17:08 h (just before low tide).

Flow velocities are near-zero at the start of the campaign (Figure 3.25). Waves come in from NW and the significant height is about 0.6 m. Current velocities are northward directed during the flooding phase and increase to about 0.6 m/s (Figures 3.26-3.28). The wave direction remains NE and the significant height remains about 0.6 m.

The current velocities decrease to near-zero at high tide (Figures 3.29-3.31). The wave direction remains NE and significant height about 0.6 m. During the ebbing phase of the tide, current velocities are southward directed and increase to about 0.6 m/s near the end of the campaign (Figures 3.32-3.36). The significant wave height decreases to0.4-0.6 m and the mean wave direction remains NE.

3.2 Salinities

Salinities in the study area are to a small extent affected by fresh water outflow from Schelde Schelle, Bergse Maas, Waal, Lek and IJmuiden but to a larger extent by the fresh water outflow from Den Oever en Kornwerderzand (Figure 2.8). Variations in salinity affect the flow pattern and the flocculation of cohesive sediment.

The upper panel in Figure 3.36 presents the salinity distribution in the upper part of the water column during the first half of the 17 September measurement campaign (flooding phase) and the lower panel during the second half (ebbing phase). The salinities at the most eastward observation locations (closest to Marsdiep) are between 31 and 33 psu. At the most westward location the salinities are between 33 and 35 psu. The effect of the outflow of fresher water from the Marsdiep is relatively small.

The upper and lower panel in Figure 3.37 present the horizontal salinity distribution in the upper part of the water column during the 1 October measurement campaign for the flooding and ebbing phase of the tide, respectively. Salinities range between 29 and 31 psu for the measurement locations closest to the Marsdiep and between 33 and 35 psu for the locations further offshore. The difference between the flooding and ebbing phase of the tide is more pronounced than on 17 September with lower salinities at the measurement site during flood than during ebb. Salinities on 2 October show a similar behaviour (Figures 3.38).

3.3 Suspended sediment concentrations (effect of dredging)

Introduction

We schematized the sediment release rate from overflow by adopting two different scenarios. In scenario 1 we adopted a release rate from the dynamic overflow plume of 130 kg/s and from the passive flume of 20 kg/s (see Par. 2.8). In scenario 2 we adopted release rates that are a factor 2 higher, i.e. 260 kg/s from the dynamic plume and 40 kg/s from the passive plume.

The dynamic overflow plume settles relatively slowly to the bed and is therefore schematized as being released over the entire water column. We schematized the passive plume as being released in the lowest computational layer near the bed.

We used a dredging period of 1 hour with a return period of 3.4 hours. Dredging takes place during the entire simulation period.

We illustrate the effect of dredging on the suspended sediment concentrations by subtracting results from 2 simulations as follows:

$$C_{effect} = C_{with\ dredging} - C_{without\ dredging}$$

We will show the spatial variation of c_{effect} near the water surface.

17 September 2007 10:09 h -13:59 h

Figures 3.39 to 3.50 present the simulated effect of overflow from a dredger on the suspended sediment concentrations for 12 different time steps in a tidal cycle on 17 September 2007. The upper panels show the effect for dredging scenario 1, the lower panels for dredging scenario 2.

The dredging activities are shown in the same plot as the water level time series.

It can be seen from these figures that a relatively small sediment plume occurs near the dredging location (2 km south of the measurement area) during the flooding phase of the tide (Figure 3.39). Maximum added near-surface concentrations are 0.5-1.0 mg/l for scenario 1 and 1-2 mg/l for scenario 2.

The plume is advected northward during the flooding phase and maximum concentrations increase to 2-4 mg/l at high tide for scenario 1 and about 9 mg/l for scenario 2 (Figures 3.40-3.42). A second plume from a previous dredging activity shows up at about 10 km north of the measurement area in these plots. This is 20 km north of the dredging location. Maximum concentrations in this old plume amount to 0.5 mg/l both for scenario 1 and 2.

The second plume is likely caused by previous dredging activities and northward advection of the associated overflow plume during a tidal cycle on 16 September or earlier and resuspension of the overflow sediments during the flooding phase on 17 September. The second plume disappears from the plots just after high tide.

The original plume is advected back southward during the ebbing phase (Figures 3.43-3.50). Maximum near-surface concentrations amount to about 1-2 mg/l for the first scenario and 2-4 mg/l for the second. Concentrations decrease gradually to 0.5-1.0 mg/l at low tide for the first scenario and 1-2 mg/l for the second.

1 October 2007 09:36 h – 15:53 h

Figures 3.51 to 3.62 show the simulated effect of overflow on the suspended sediment concentrations for different time steps in a tidal cycle on 1 October 2007. On this day, the effect of dredging is more pronounced than on 17 September. The area affected is larger and the added concentrations are higher.

The dredging activities are shown in the same plot as the water level time series.

On 1 October 2007 during the flooding phase of the tide a small plume is visible at the most southward measurement location (Figure 3.51). Maximum near-surface concentrations amount to 0.5-1.0 mg/l for the first dredging scenario and 2-4 mg/l for the second but the area of influence is relatively small (about 1 km).

A larger area affected by overflow from dredging shows up in the plots just before high tide (Figures 3.52-3.53). This is likely due to previous dredging activities from which the plume has been advected north and south of the dredging location. The sediments from these plumes that have settled to the bed are resuspended by the flood velocities on 1 October 2007 around 07:30 h and 08:30 h (see Figure 3.14 and 3.15 for velocities and waves). Added near-surface concentrations generally amount to 0.5-1.0 mg/l for both dredging scenarios. Maxima of 1-2 mg/l occur locally.

It is interesting the see a difference between scenario 1 and 2. The added near-surface concentrations tend to show up more south of the measurement area for the first scenario and mainly north for the second scenario. This is likely related to the behaviour of the fall velocity formulations in the Van Rijn (2007) model. Increasing the concentrations e.g. by overflow increases the fall velocity in the model. This causes the sediments to settle to the bed more rapidly than without the extra concentration.

Added near-surface concentrations decrease during the ebbing phase of the tide (Figure 3.54-3.62).

The affected area stretches from about 20 km south of the dredging area to 40 km north on 1 October 2007. This is much larger than on 17 September.

2 October 2007 05:57 h – 17:08 h

Figures 3.63 to 3.74 show the simulated effect of overflow on the suspended sediment concentrations on 2 October 2007. The dredging activities are shown in the same plot as the water level time series.

Maximum added near-surface concentrations due to overflow amount to about 0.5-1 mg/l during the flooding phase for the first scenario and 1-2 mg/l for the second scenario (Figures 3.63-3.68). It is interesting to see that the effect on 2 October is smaller than that on 1 October, which is likely due to the smaller wave heights in the area (e.g. compare Figure 3.14 with Figure 3.27).

Added near-surface concentrations decrease just after high tide (Figures 3.69-3.71) and increase slightly during the ebbing phase to maximum values of 1-2 mg/l just before low tide for both scenarios. The affected area stretches from about 10 km south of the dredging location to about 40 km north.

3.4 Sediment deposition

We investigated the observed (in simulations and measurements) relatively small effect of sediment release from the overflow on the suspended sediment concentrations by checking the simulated amount of sediment deposited on/in the bed and the amount in suspension for 4 different areas around the dredging location.

Figure 3.77 shows the selected areas and accompanying percentages of silt from the overflow deposited in the seabed on 2 October 2007 23:30 (end of simulation). We selected rectangular areas of 2x4 km, 4x8 km, 8x16 km and 16x32 km with the dredging location in the centre.

The percentages of overflow sediment deposited in the seabed are 12, 24, 43 and 49% in these areas, respectively. The percentages in suspension are 0, 1, 4 and 6%. This means that 46% of the total amount of sediment released by the overflow during the simulation is present outside the largest area selected here. This is not surprising considering the residual current pattern with a northward average velocity of a few cm/s. For example, assuming a small residual current velocity of 2 cm/s, the silt particles have travelled 24 km north over a period of two weeks. This is about 4 km north of the largest area selected here.

More interesting is however that largest part of the sediment released from overflow has settled to the bed in the areas selected and only a small percentage is stirred up in suspension. This is consistent with the relatively small increase of the suspended sediment concentrations observed in the simulations and consistent with findings by Van Maren et al. (2008) for the dredging activities concerned here.

4 Summarizing conclusions and recommendations

Conclusions

- A 3D model was set-up to simulate the suspended sediment concentrations of a silt fraction and a sand fraction in part of the Wadden Sea and part of the North Sea and simulate the effects of overflow from dredging activities on these concentrations offshore Den Helder.
- The model includes effects of a temporally and spatially varying wind field, waves and salinity.
- The model accurately represents observed water levels along the Dutch coast.
- The model realistically represents natural background suspended sediment concentrations offshore Den Helder and the effects of a sediment plume from the Marsdiep tidal inlet
- The model results show encouraging agreement with observations of suspended sediment concentrations made on 17 September 2007.
- The model underestimates the observed suspended sediment concentrations on 1 and 2 October by about a factor 2. This means roughly that the model predicts 2 mg/l near the surface where 4 mg/l was observed.
- The model tends to underestimate the extent of the plume from the Marsdiep inlet into the North Sea.

- Sediment release rate due to overflow from a dredger have been schematized based on observed flow velocities and concentrations in the suction pipes on a dredger and the amount of sediment (dry weight) in the dredger. Data were made available by RWS Directie Noordzee.
- This resulted in a realistic dredging scenario 1 in which the release rate from the dynamic overflow plume was 130 kg/s and from the passive flume 20 kg/s. Simulation were made also for scenario 2 in which the release rates were a factor 2 higher, i.e. 260 kg/s from the dynamic plume and 40 kg/s from the passive plume.

- The added near-surface concentrations in the plume from overflow by dredging amount generally to 0.5-1 mg/l. The added concentrations may locally (up to 2 km from the dredging location) and temporally (1 or 2 hours) reach values of 2-4 mg/l.

- The added concentrations due to overflow from dredging are generally smaller than the natural background concentrations.

Recommendations

- Make synoptic and continuous measurements for a period of 1 month at 4 fixed locations (at 2 and 10 km in the ebb and flood direction of the dredging location), measuring 10 minute-averaged values of flow velocity magnitude and direction and suspended matter concentration (6 values per hour) at approx. 25 different heights above the bed. We suggest using a bottom mounted ADCP for this purpose.
- Take water samples at 12 different heights above the bed on 2 days to determine the suspended matter concentrations and grain size distributions of the sediment in suspension. These can be used to calibrate and validate the synoptic and continuous measurements.

References

De Boer, G.J., 2009. On the interaction between tides and stratification in the Rhine Region of Freshwater Influence. Ph.D. thesis. Technische Universiteit Delft, Delft.

De Kok, J.M. 2004. Slibtransport langs de Nederlandse kust: bronnen, fluxen en concentraties. Report RIKZ/OS/2004.148w

Deltares, 2009. DELFT3D FLOW. Simulation of multi-dimensional hydrodynamic flows and transport phenomena, including sediments. User manual. Version 3.14. Revision 7864. 16 July 2009.

Gordon, H.R., W. R. McCluney (1975) Estimation of the depth of sunlight penetration in the sea for remote sensing. Applied Optics, 14, 413-416.

Grasmeijer, B.T., Eleveld, M.A., Van Banning, G., 2009. Evaluation of SPM measurements in the North Sea. Research in the framework of the EIA sand extraction North Sea 2008-2012. Alyon, Emmeloord (Oct. 2009).

Hitchcock, D.H., Bell, S., 2004. Physical impacts of marine aggregate dredging on seabed resources in coastal deposits. Journal of Coastal Research 20(1): 101-114.

Kraaijeveld, M., Fioole, A., 2005. Vertroebeling tijdens en na baggeren met sleephopperzuiger in het Noordzeekanaal. RIZA rapport 2005.006 (jan. 2005).

Laane, R.W.P.M., Sonneveldt, H.L.A., Van der Weyden, H.J., Loch, J.P.G. and Groeneveld, G. 1999. Trends in the spatial and temporal distribution of metals (Cd, Cu, Zn and Pb) and organic compounds (PCBs and PAHs) in Dutch coastal zone sediments from 1981 to 1996: a model case study for Cd and

Otto, L., Zimmerman, J.T.F., Furnes, G.K., Mork, M., Saetre, R., and Becker, G., 1990. Review of the physical oceanography of the North Sea. Netherlands Journal of Sea Research, 26(2-4): 161-238.

Peters, SW.M.., van der Woerd, H.J., Eleveld, M.A., in prep. Ovatie-2 Final report. IVM report.

Rast, M.,. Bezy, J.L., S. Bruzzi S., 1999. The ESA Medium Resolution Imaging Spectrometer MERIS – a review of the instrument and its mission. Int. j. remote sensing 20 (9), 1681-1702.

Talmon, A.M., 2007. Meetrapport SiltProfilermetingen 22 – 24 mei 2007 voor de Noord-Hollandse kust. Deltares rapport Z4426 (dec. 2007).

Talmon, A.M., 2008a. Meetrapport SiltProfilermetingen 17 september, 1 en 2 oktober 2007 voor de Noord-Hollandse kust. Deltares rapport Z4481 (juni 2008).

Talmon, A.M., 2008b. Meetrapport suspensiemetingen Ms. Zirfea bij zandwinning 17, 18 en 19 september voor de Noord-Hollandse kust. Deltares rapport Z4521 (sept.008)

Thatcher, M. L. and R. F. Harleman, 1972. A mathematical model for the prediction of unsteady salinity intrusion in estuaries. Tech. Rep. 144. 64, 225, 226

Tee, K.T., 1979. The Structure of Three-Dimensional Tide-Induced Current. Part I: Oscillating Currents. Journal of Physical Oceanography, 9(5): 930-944.

Tee, K.T., 1980. The Structure of Three-Dimensional Tide-Induced Current. Part II: Residual Currents. Journal of Physical Oceanography, 10(12): 2035-2057.

Van Duin, C.F., Gotjé, W, Jaspers, C.J., Kreft, M., 2007. MER winning ophoogzand Noordzee 2008 t/m 2017. Rapport Grondmij, Stichting La Mer (nov. 2007).

Van Maren, B., Rodger, J., Koomans, R. 2008. Measurements of sediment release from Trailing SuctionHopper Dredgers, May and September 2007. Deltares, SSB, HR Wallingford, Medusa.

Van Prooijen, B., Bliek, B., Los, H., Desmit, X., 2007. Winning ophoogzand Noordzee 2008-2017. Slibtransport, nutriëntentransport en primaire productie. Rapport Svasek voor Stichting La Mer (nov 2007)

Van Rijn, L.C., Grasmeijer, B.T. Ruessink, B.G., 2000. Measurement errors of instruments for velocity, wave height, sand concentration and bed levels in field conditions. Department of Physical Geography, University of Utrecht. November 2000. Coast3D.

Ye, J. and Garvine, R.W., 1998. A model study of estuary and shelf tidally driven circulation. Continental Shelf Research, 18(10): 1125-1155.

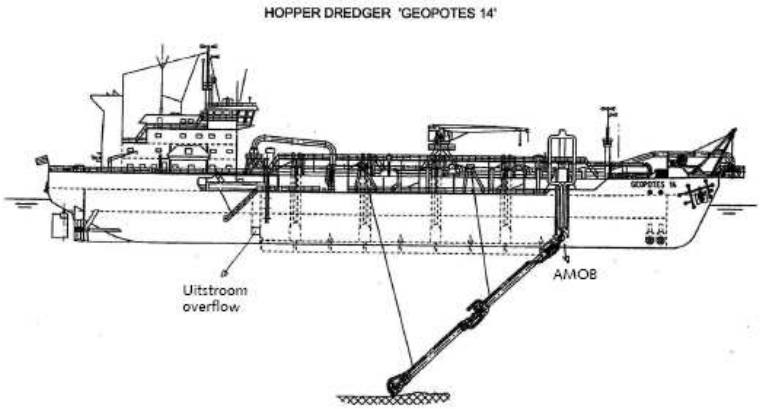

A Trailing Suction Hopper Dredger with two suction pipes, spill gaps at the bottom for overflow and AMOB (top). In−situ view into the container (middle) and vertical mixing by the propeller (lower)

Alkyon Hydraulic Consultancy & Research	A2273	Fig. 1.1

plotzandwin_v03

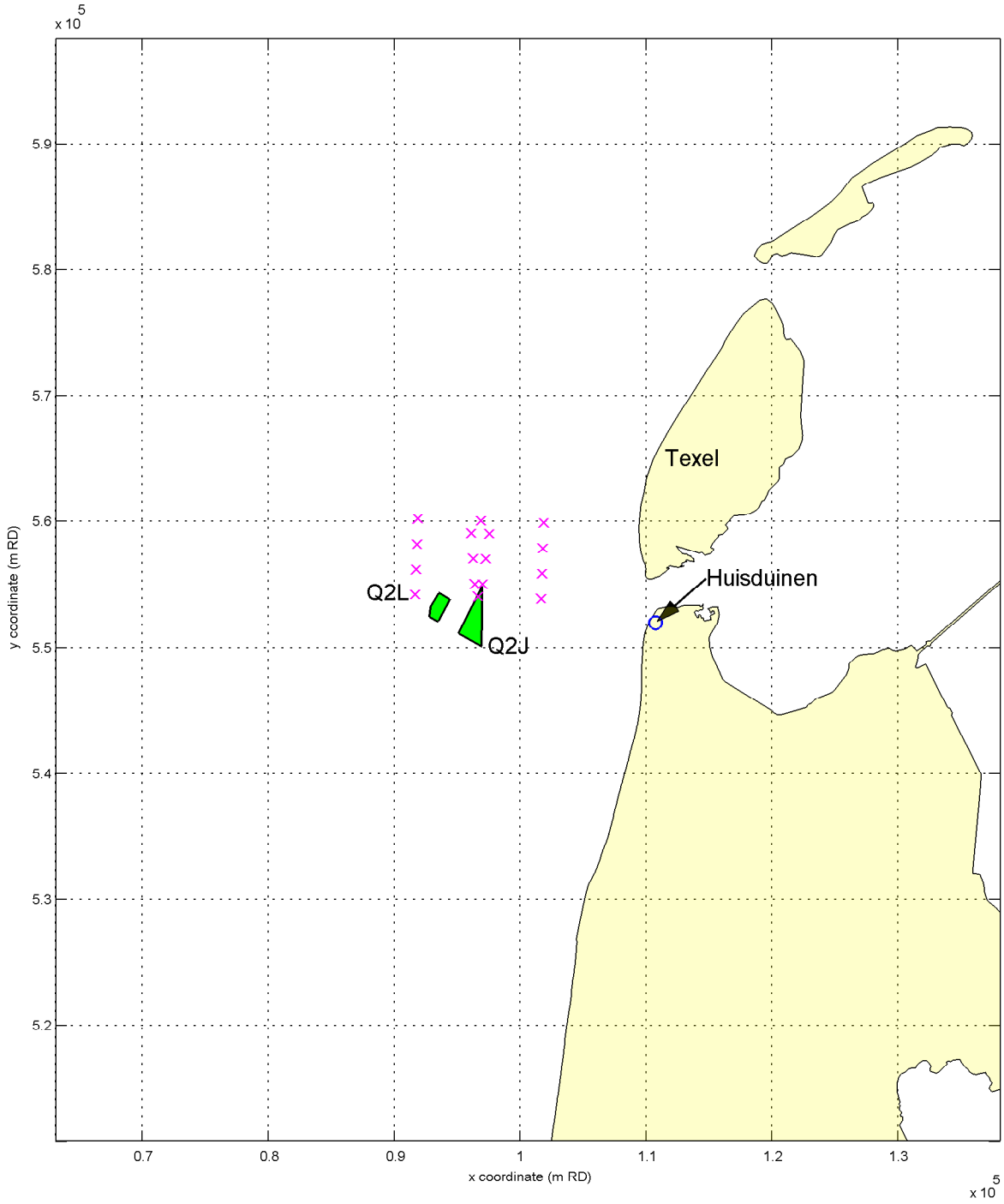

Sand extraction locations offshore Huisduinen (Q2L and Q2J) x-marks denote locations of T1 observations		
	Noordzee	
Alkyon Hydraulic Consultancy & Research	A2273	Fig. 1.2

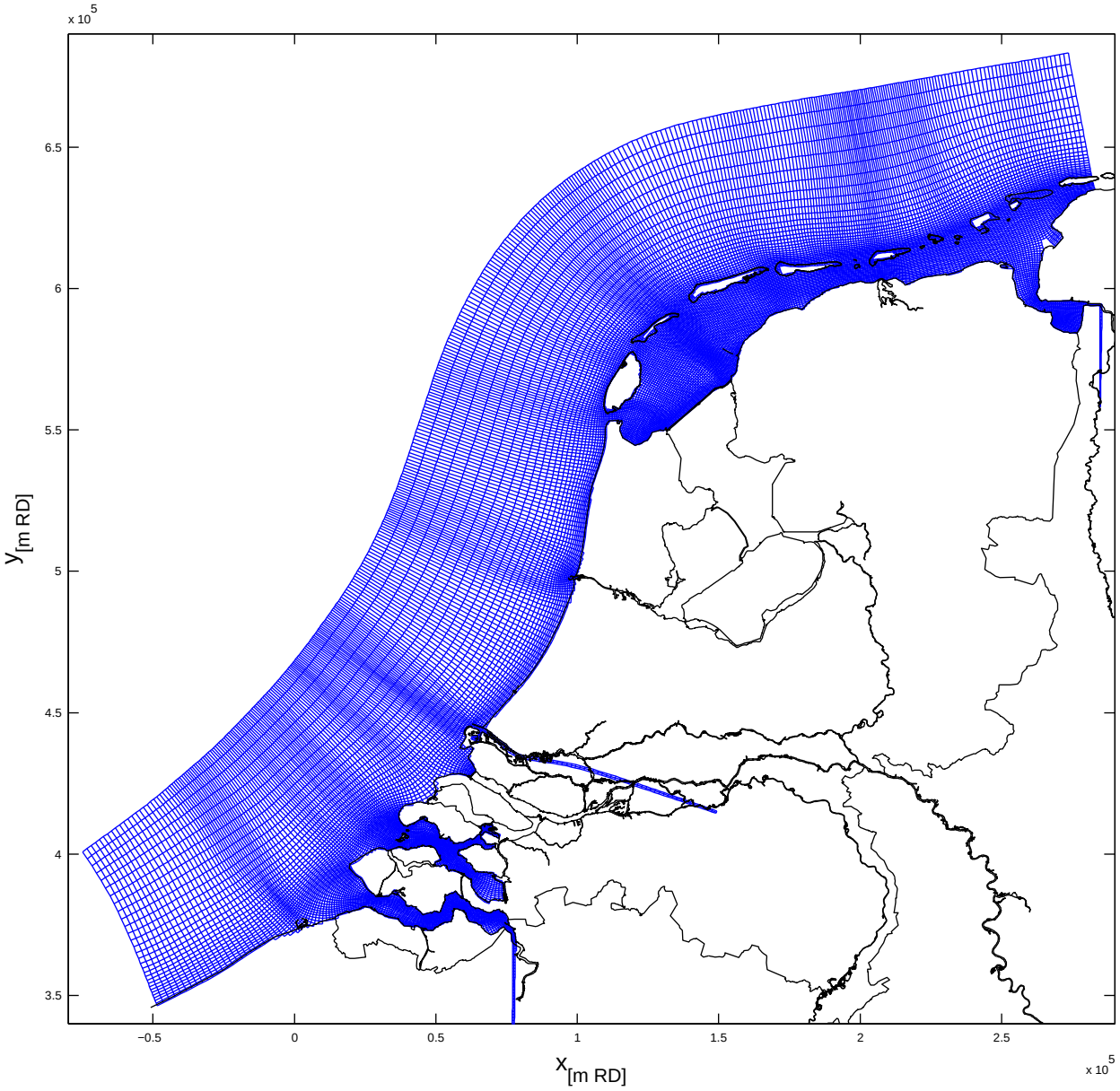

The grid adopted in the Simona *kustgrof* model		
	Simona	
Alkyon Hydraulic Consultancy & Research	A2273	Fig. 2.1

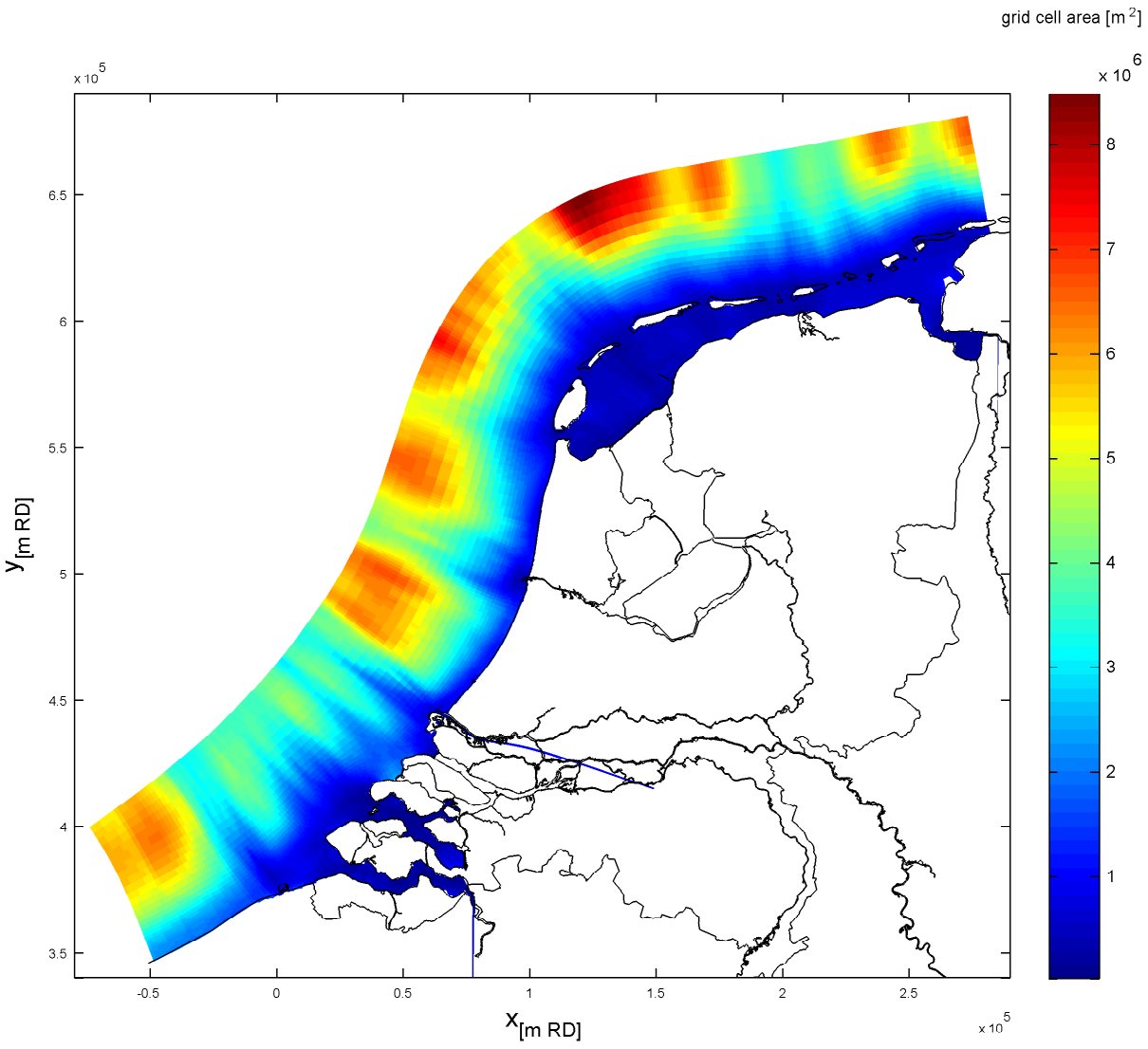

The grid cell area in the Simona *kustgrot* model		
	Simona	
Alkyon Hydraulic Consultancy & Research	A2273	Fig. 2.2

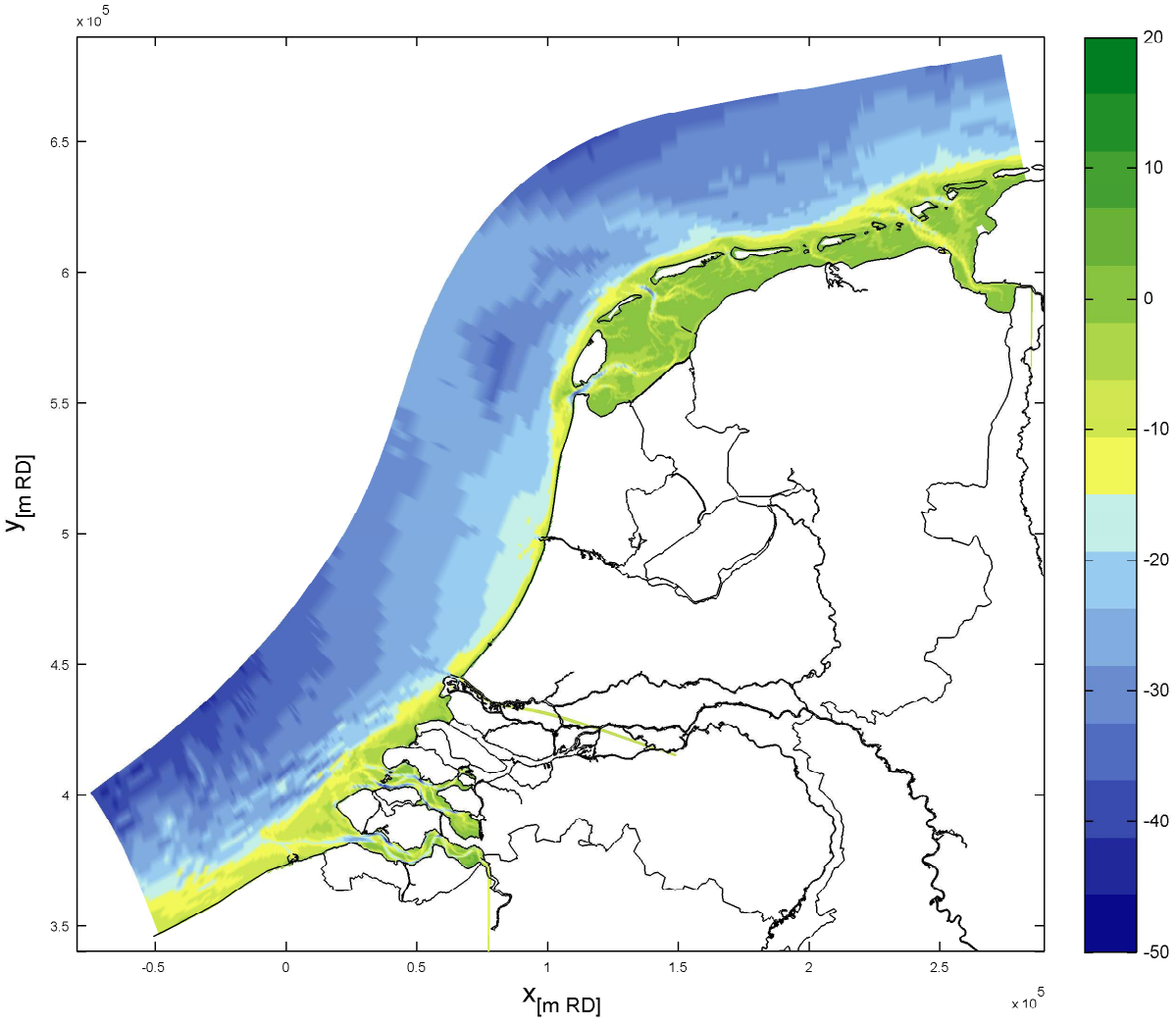

The bathymetry in the Simona *kustgrof* model		
	Simona	
Alkyon Hydraulic Consultancy & Research	A2273	Fig. 2.3

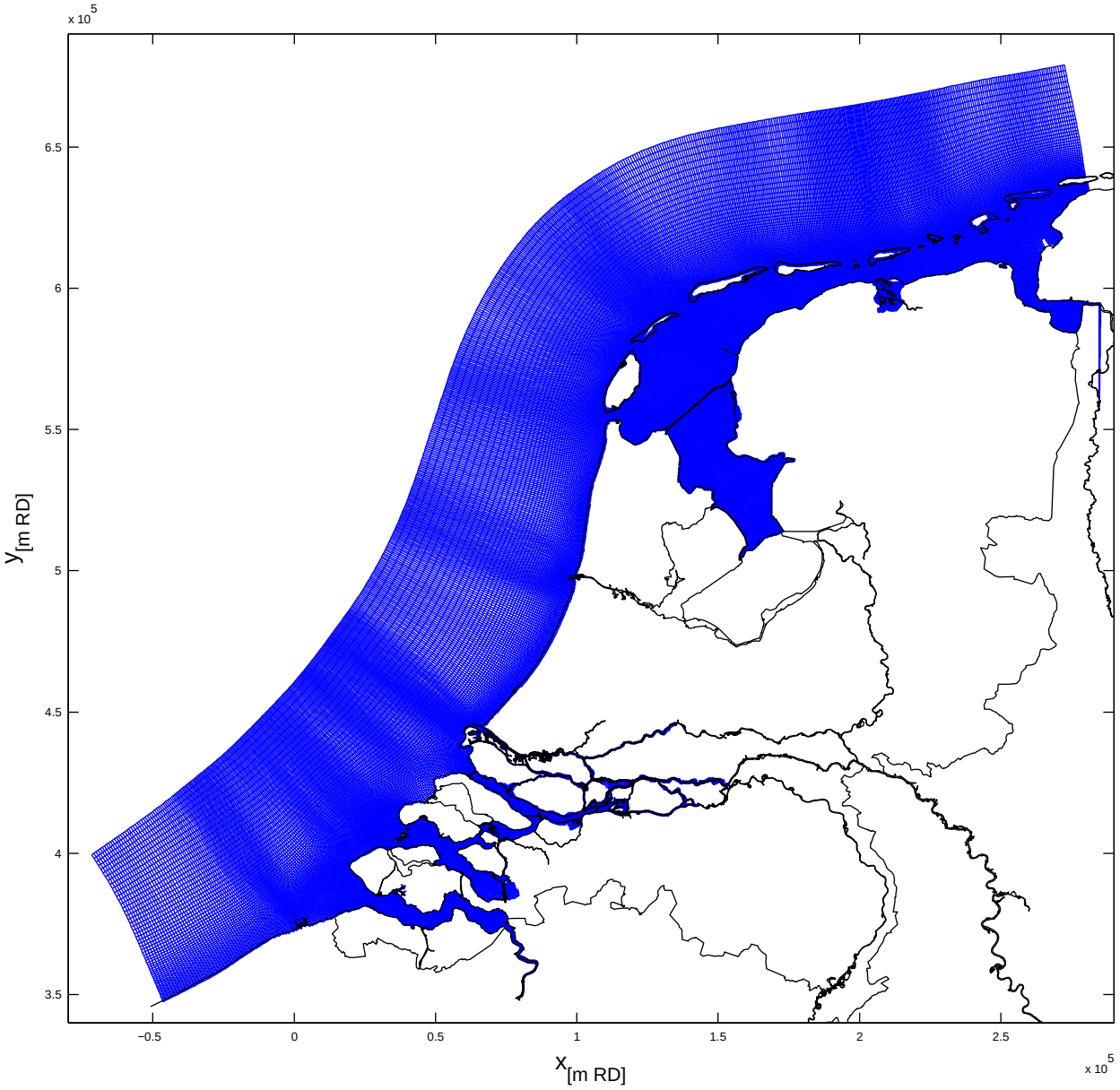

The grid adopted in the Delft3D *kuststrook* model		
	Delft3D	
Alkyon Hydraulic Consultancy & Research	A2273	Fig. 2.4

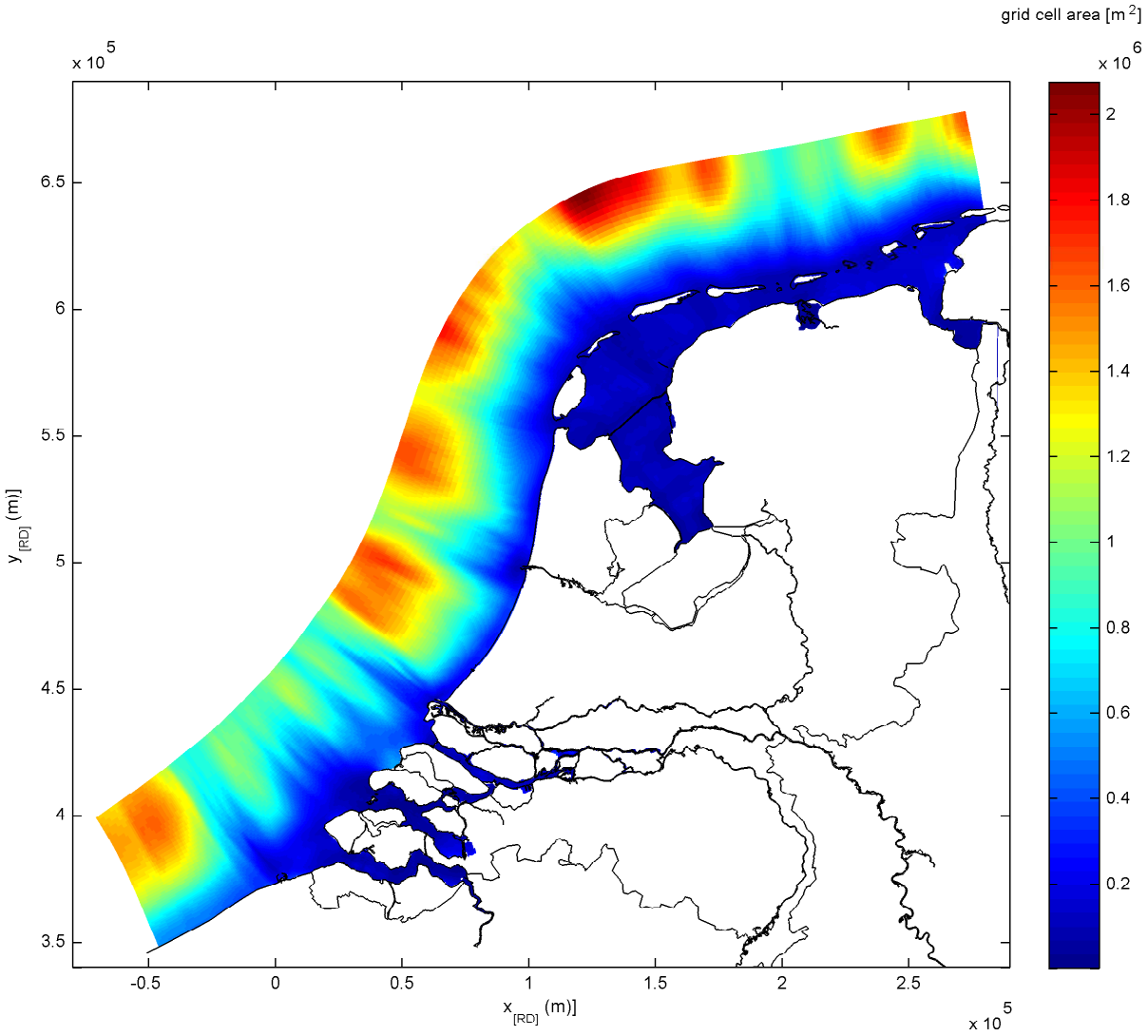

The grid cell area in the Delft3D *kuststrook* model		
	Delft3D	
Alkyon Hydraulic Consultancy & Research	A2273	Fig. 2.5

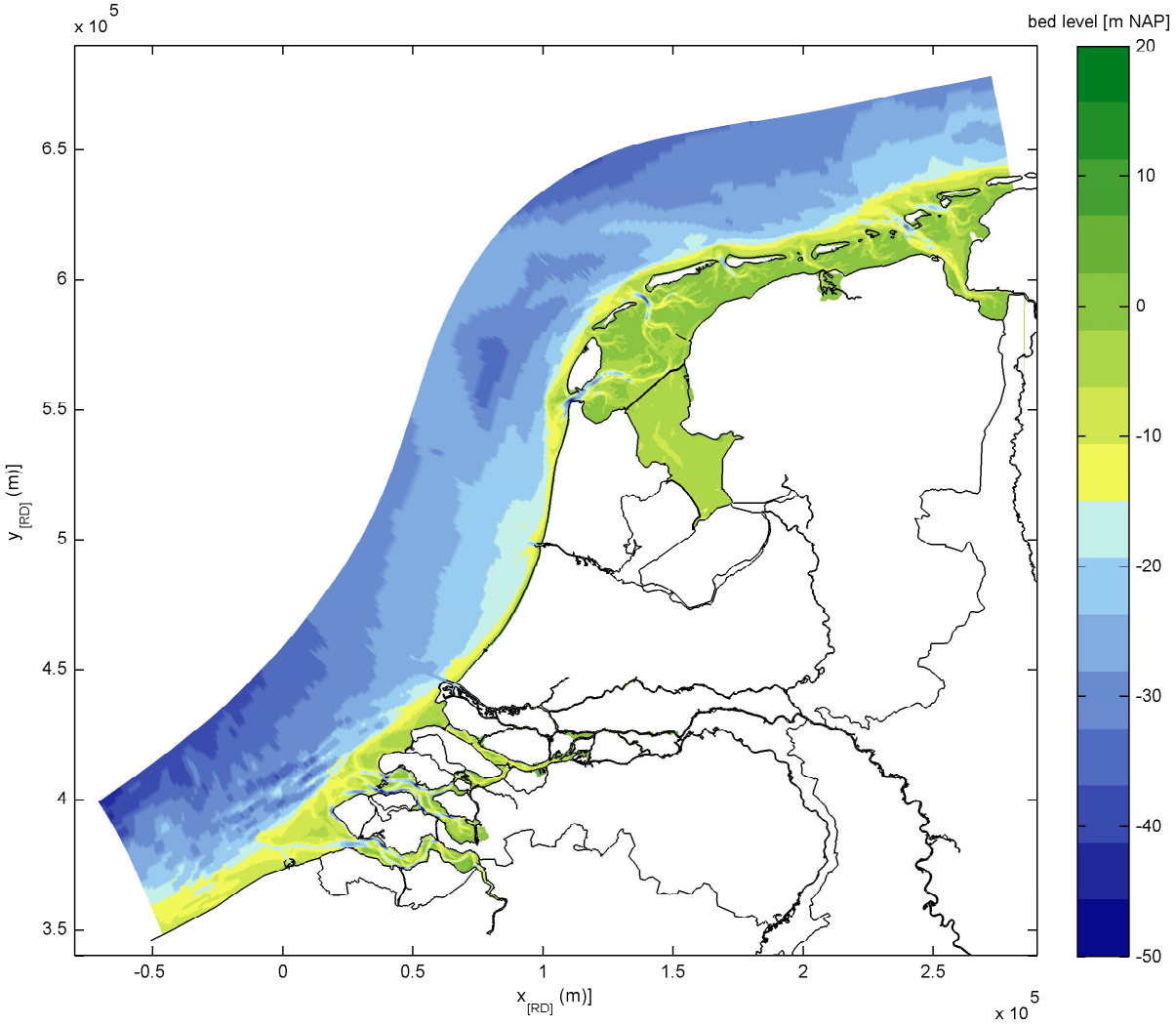

The bathymetry in the Delft3D *kuststrook* model		
	Delft3D	
Alkyon Hydraulic Consultancy & Research	A2273	Fig. 2.6

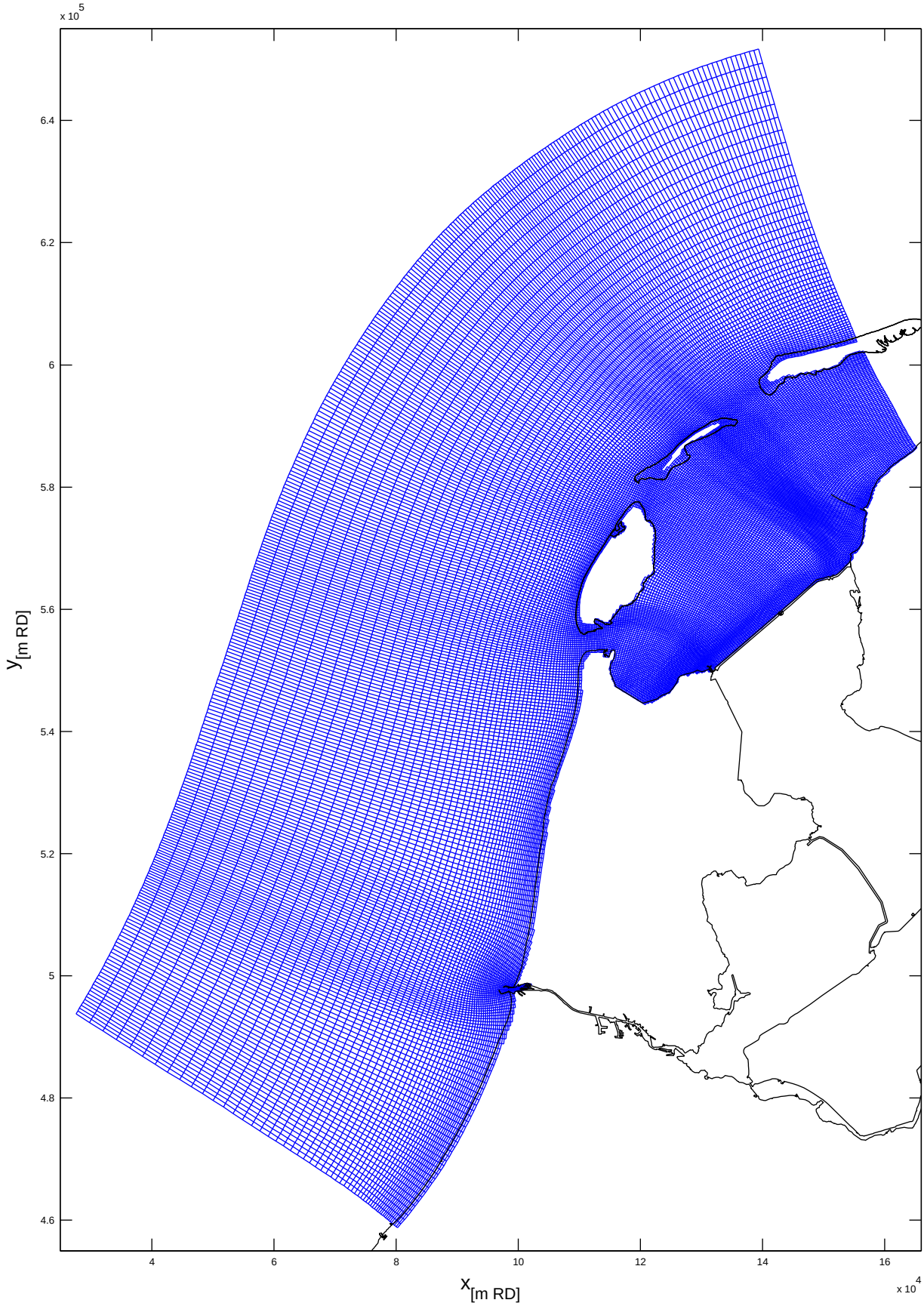

The grid adopted in the detailed 3D Delft3D model that was nested in the 2D Delft3D *kuststrook* model

Delft3D

Alkyon Hydraulic Consultancy & Research

A2273

Fig. 2.7

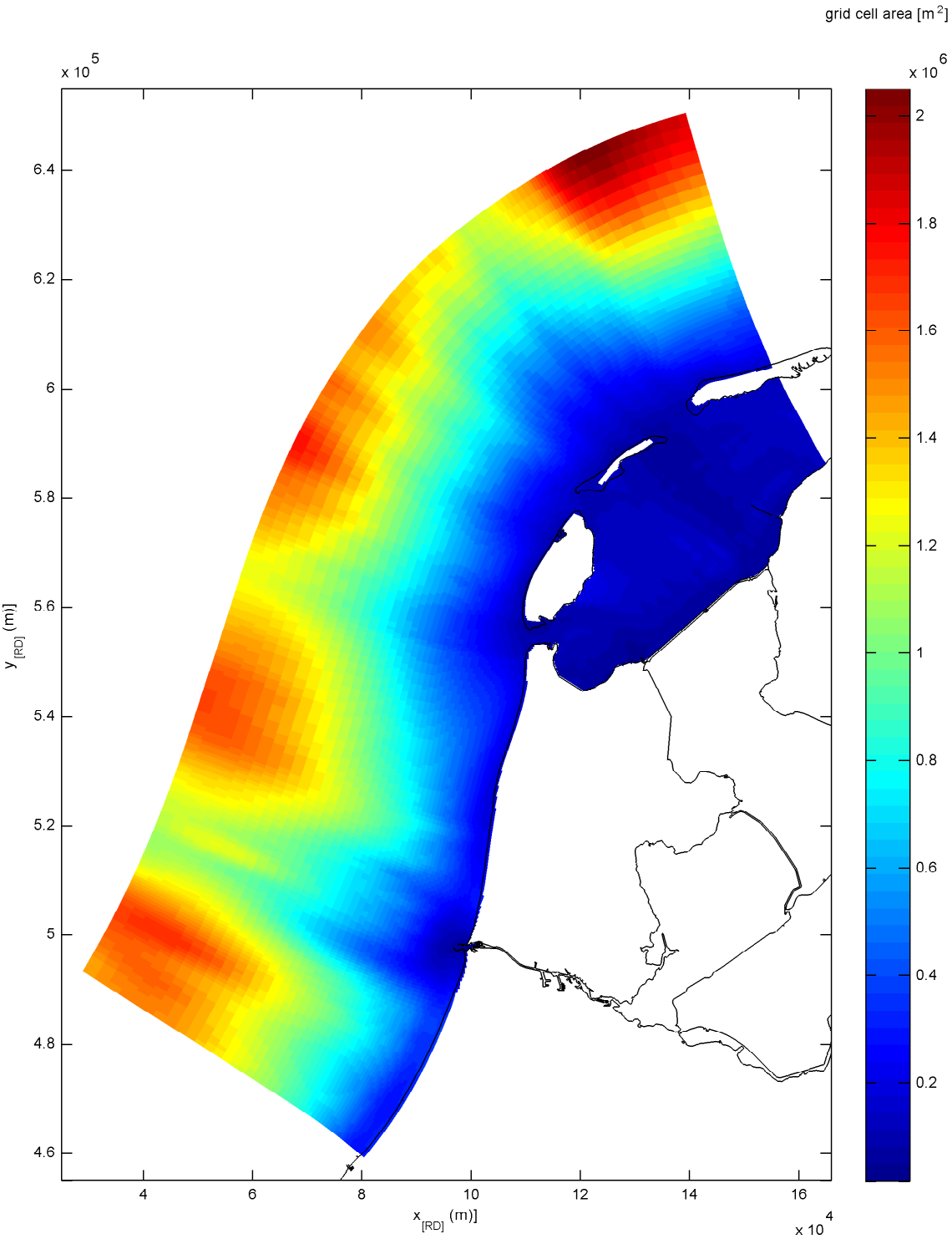

The grid cell area in the detailed 3D Delft3D model that was nested in the 2D Delft3D *kuststrook* model

Delft3D

Alkyon Hydraulic Consultancy & Research

A2273

Fig. 2.8

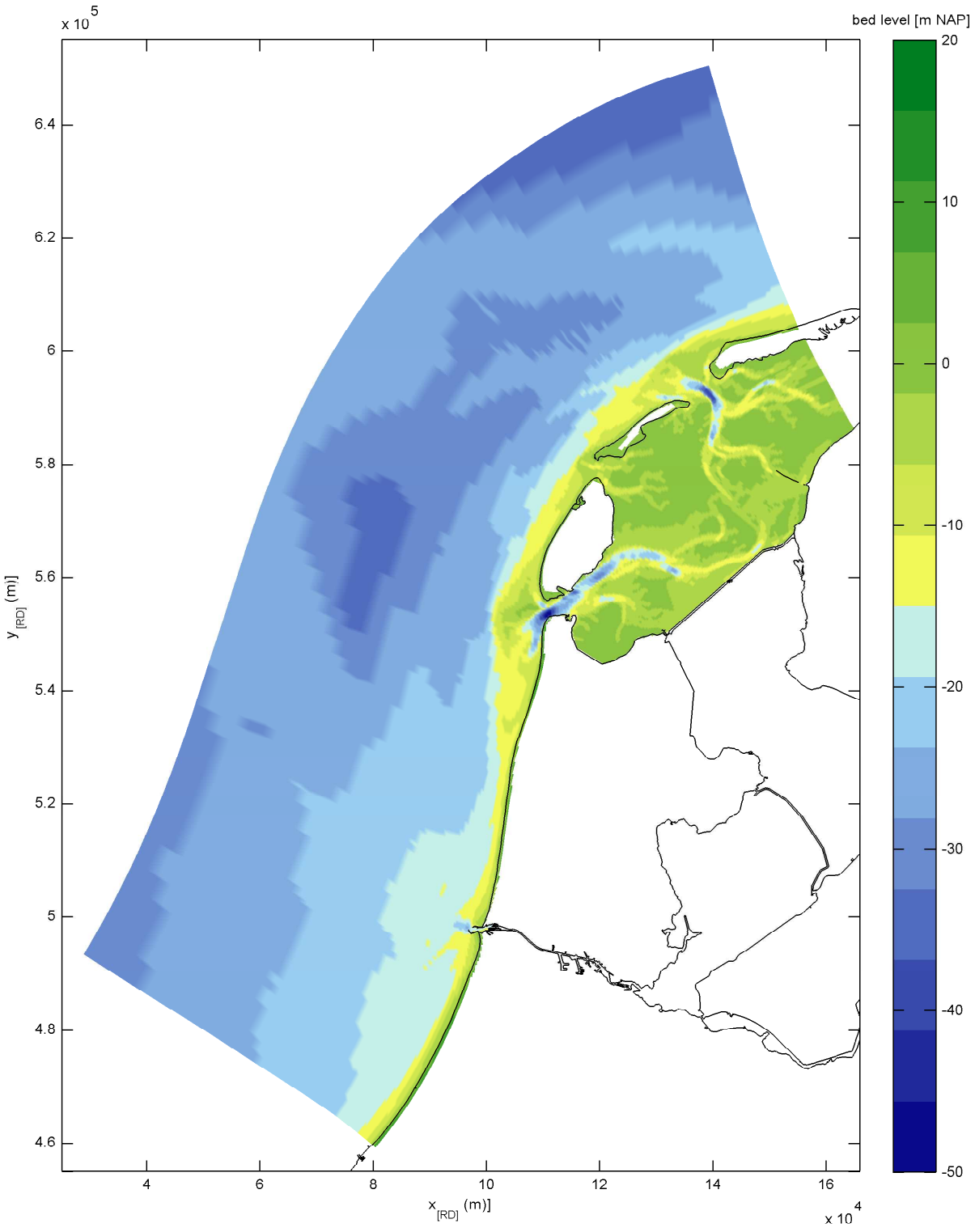

The bathymetry in the detailed 3D Delft3D model that was nested in the 2D Delft3D *kuststrook* model

Delft3D

Alkyon Hydraulic Consultancy & Research | A2273 | Fig. 2.9

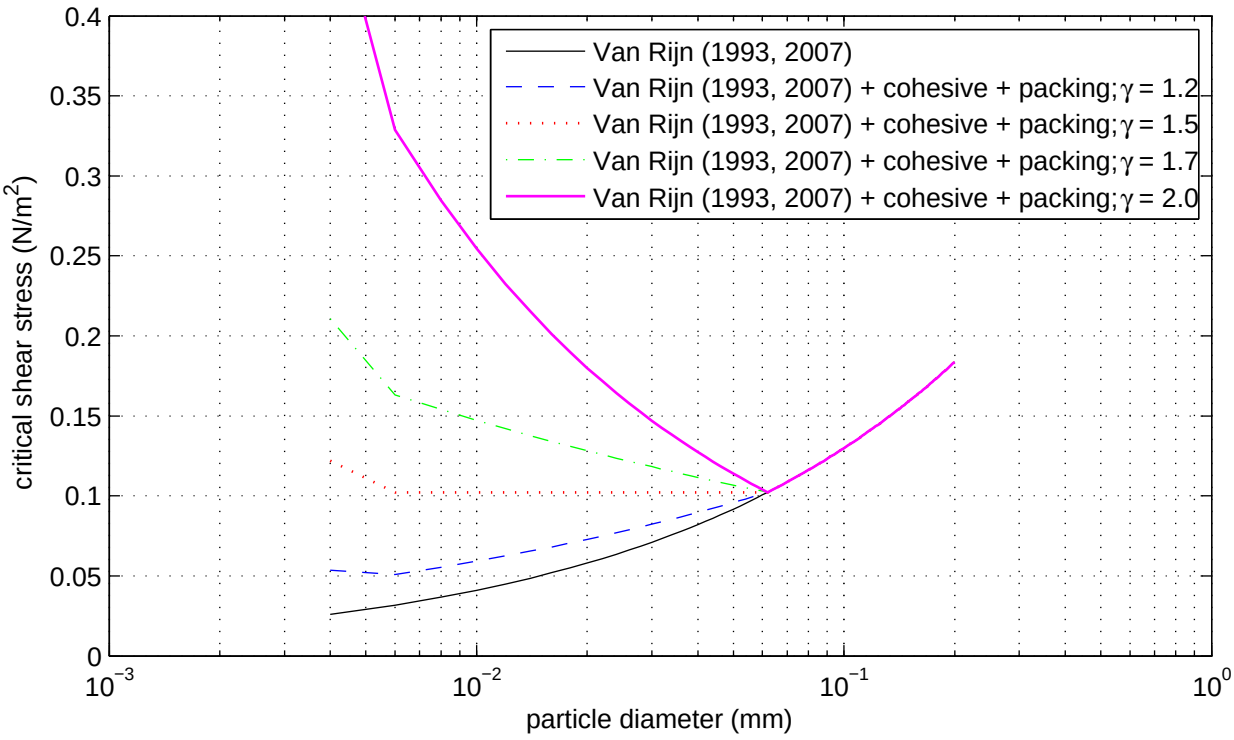

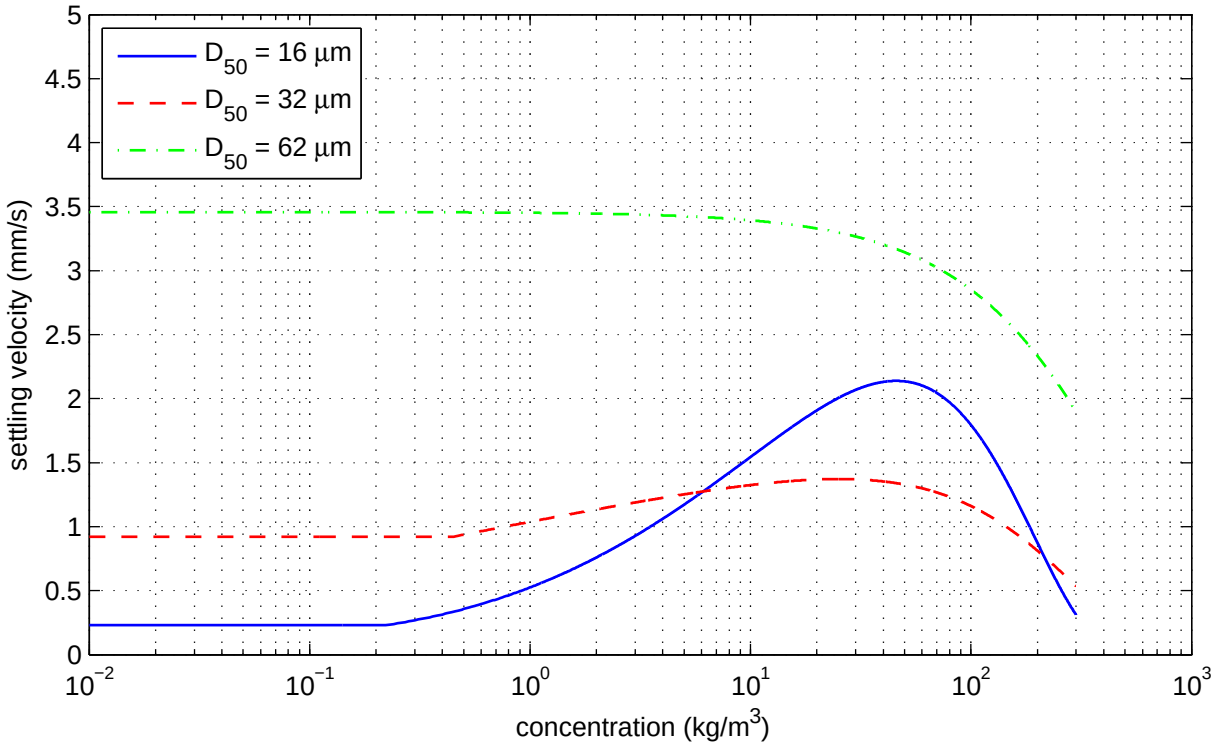

Critical shear stress for erosion and flocculation and hindered settling effect on the settling velocity in the the Van Rijn (2007) sediment transport model		
	Van Rijn (2007)	
Alkyon Hydraulic Consultancy & Research	A2229	Fig. 2.10

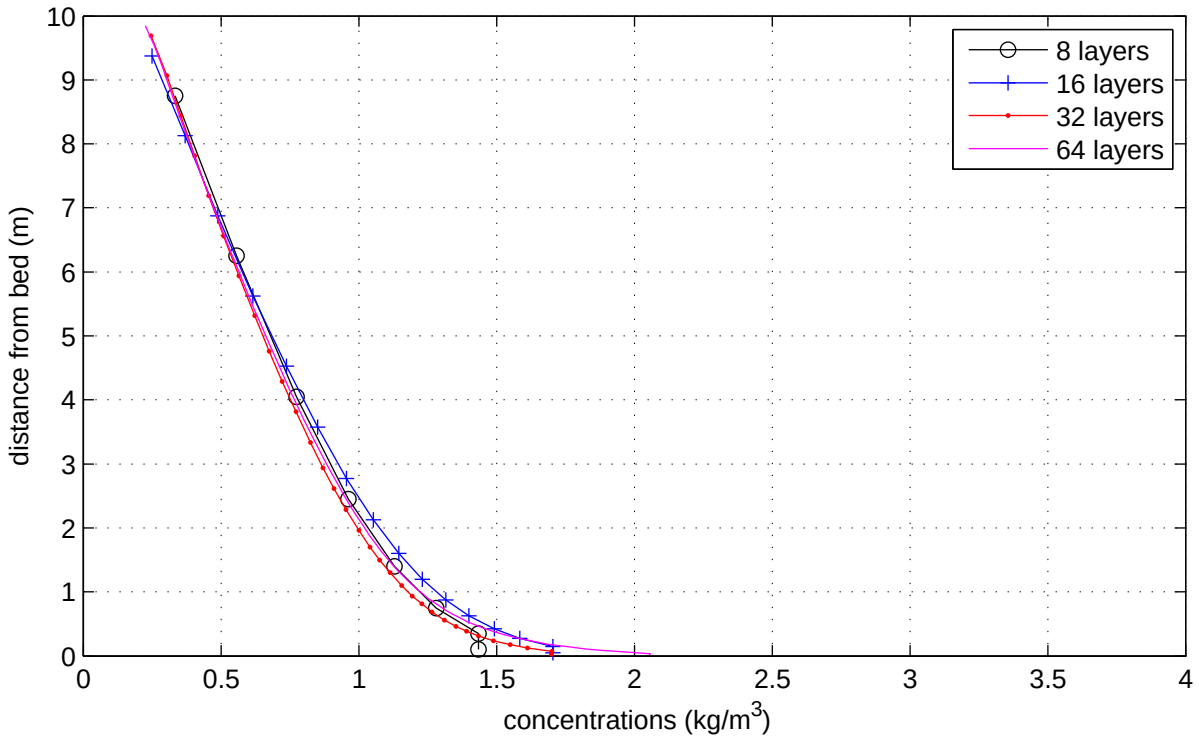

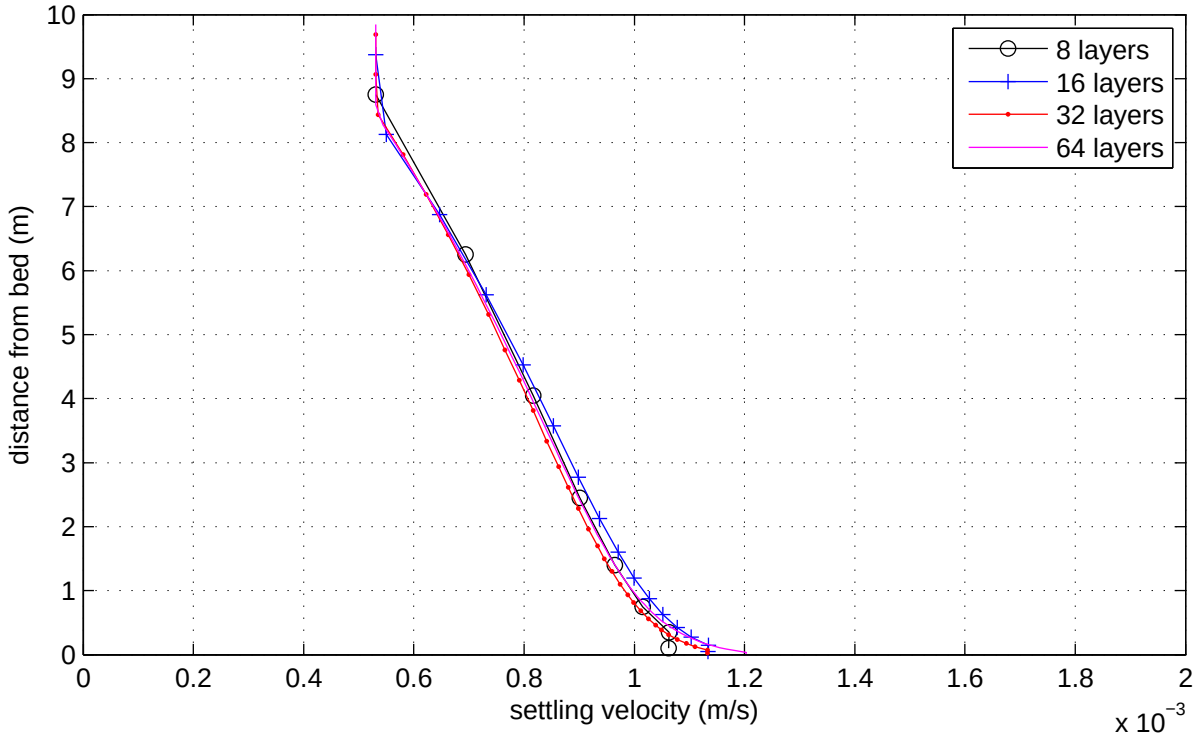

Examples of concentrations (upper) and settling velocities (lower) from Delft3D test runs using different numbers of layers, in a rectangular basin with h = 10 m, Um = 1 m/s and D = 26 µm		
	Van Rijn (2007)	
Alkyon Hydraulic Consultancy & Research	A2273	Fig. 2.11

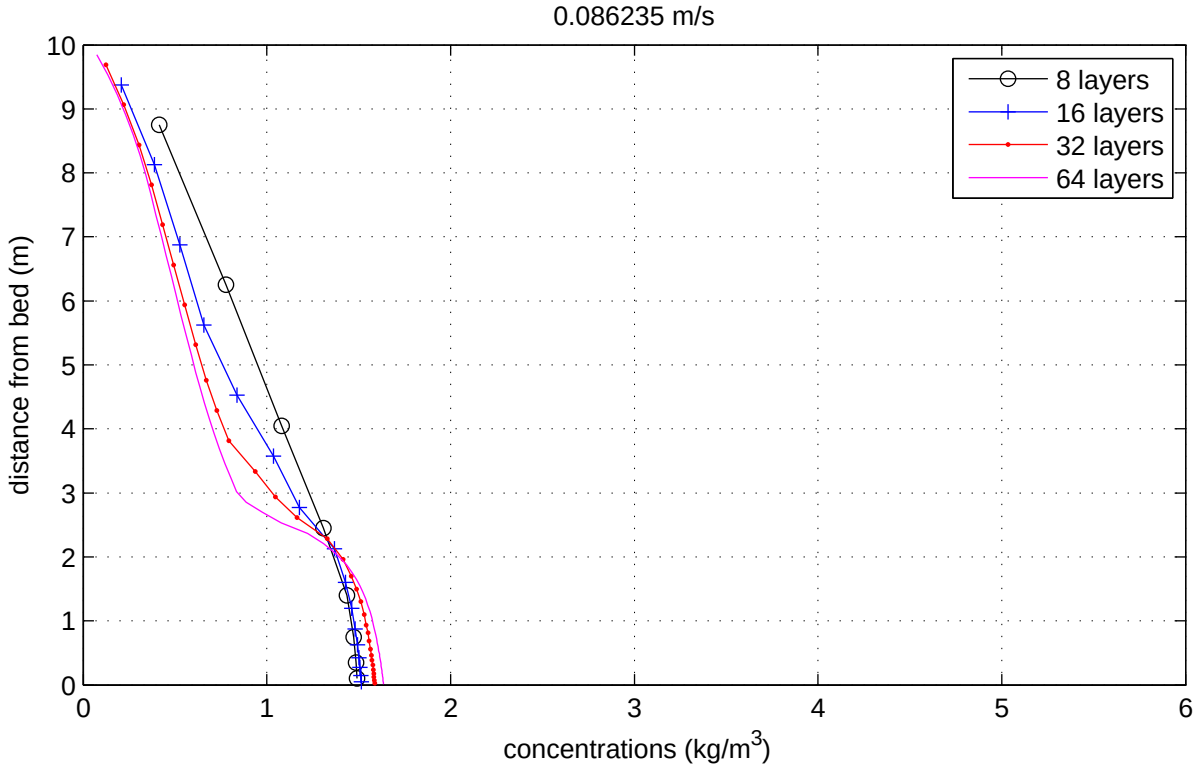

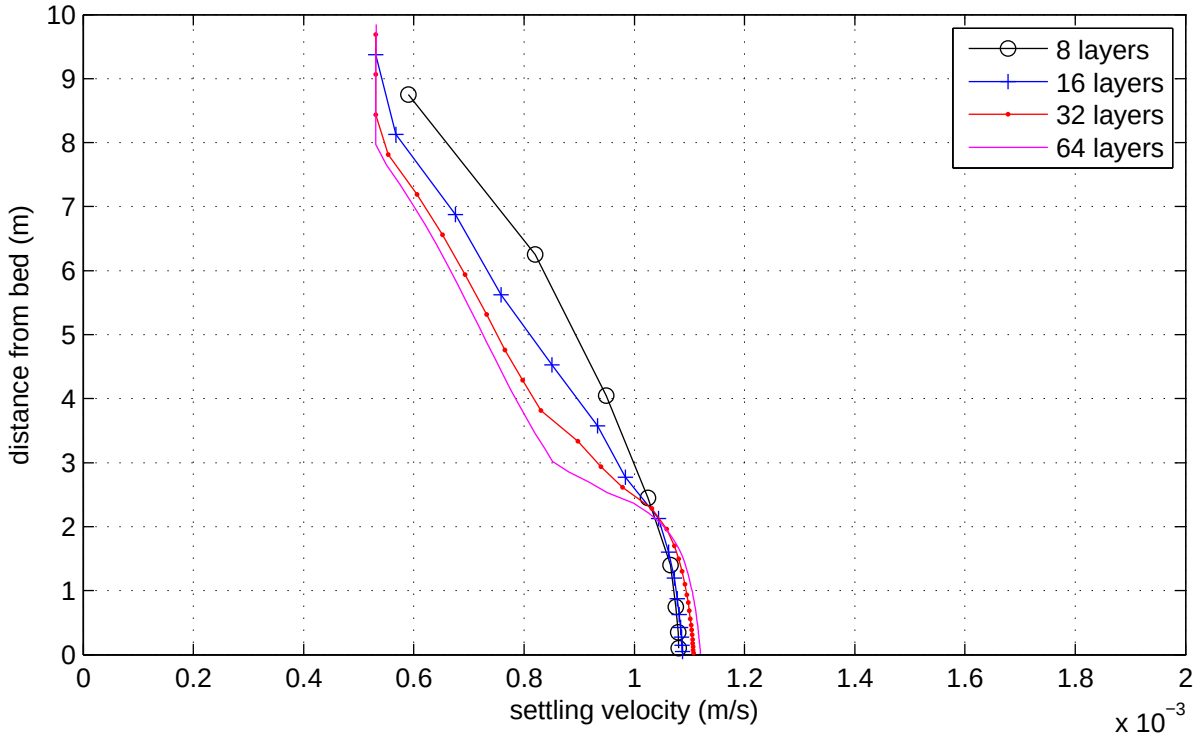

Examples of concentrations (upper) and settling velocities (lower) from Delft3D test runs using different numbers of layers, in rectangular basin with h = 10 m, sinusoidal velocity signal around slack and D = 26 μm

Van Rijn (2007)

Alkyon Hydraulic Consultancy & Research | A2273 | Fig. 2.12

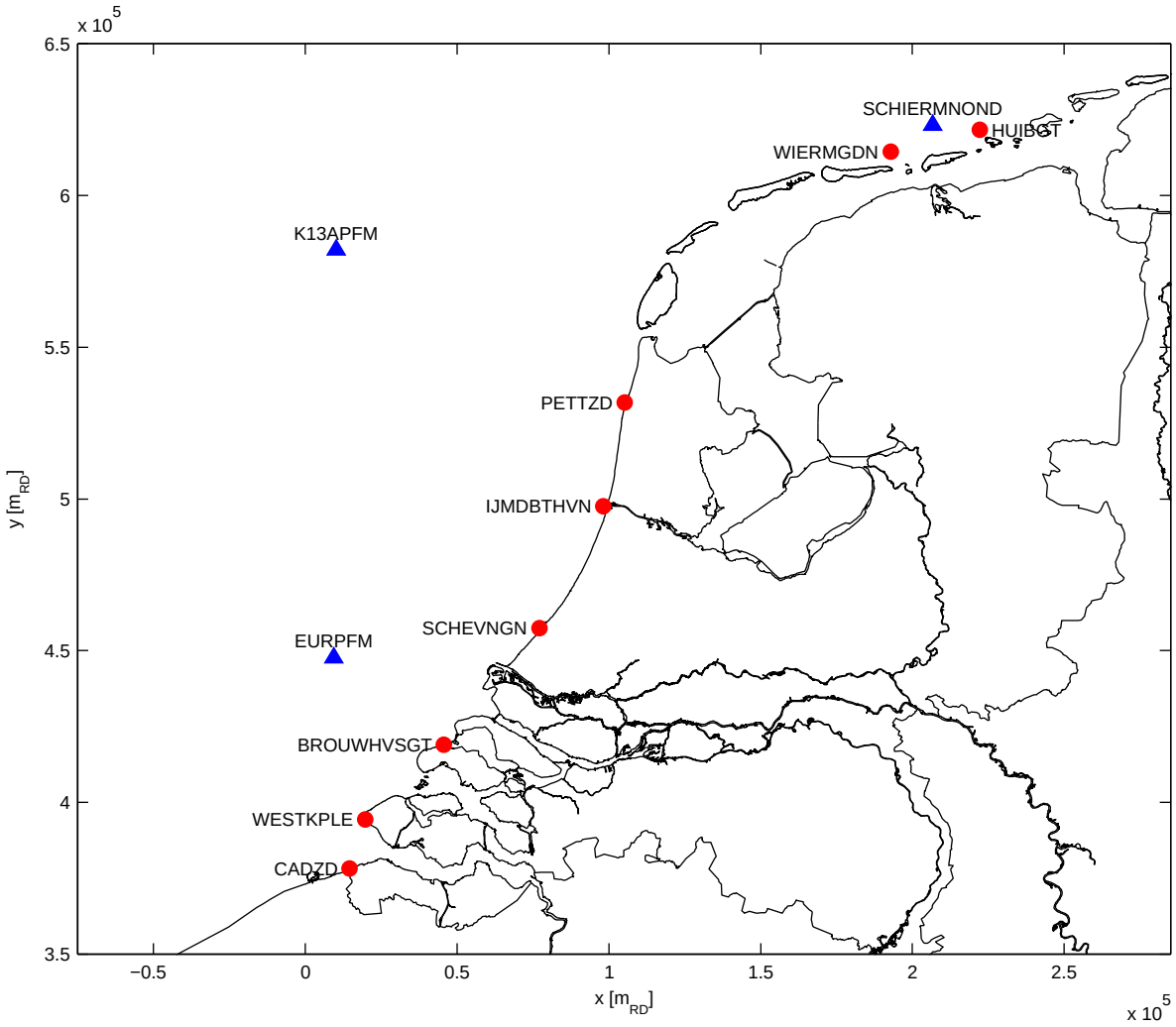

Locations and names of the 8 water level stations (red circles) used to generate Kalman−filtered boundary conditions and wave stations (blue triangles) for wave boundary conditions

Alkyon Hydraulic Consultancy & Research	A2273	Fig. 2.13

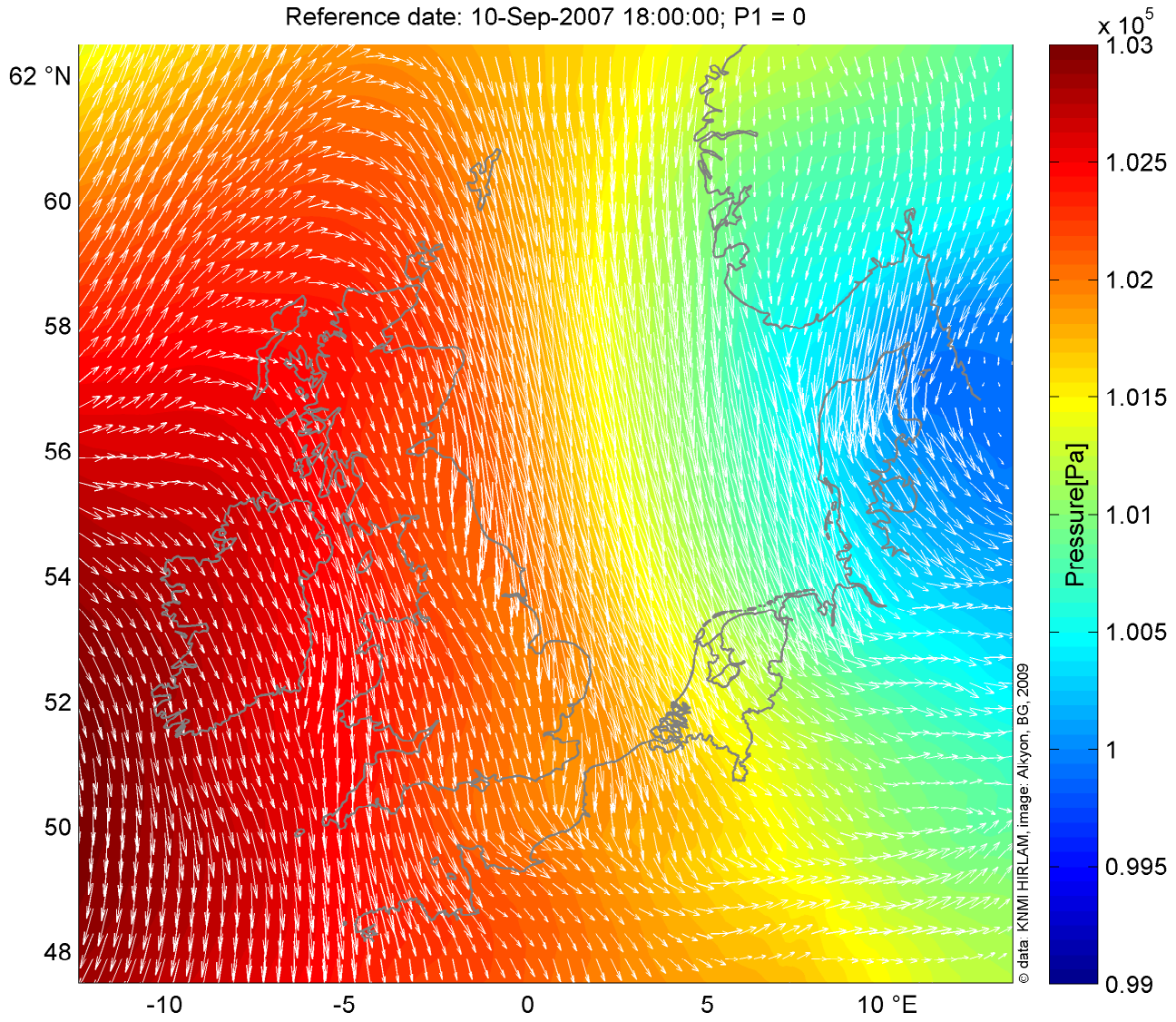

Example of spatially varying pressure field Reference date: 10-Sep-2007 18:00:00; P1 = 0 Arrows denote wind speed and wind direction		
	KNMI HIRLAM	
Alkyon Hydraulic Consultancy & Research	A2273	Fig. 2.14

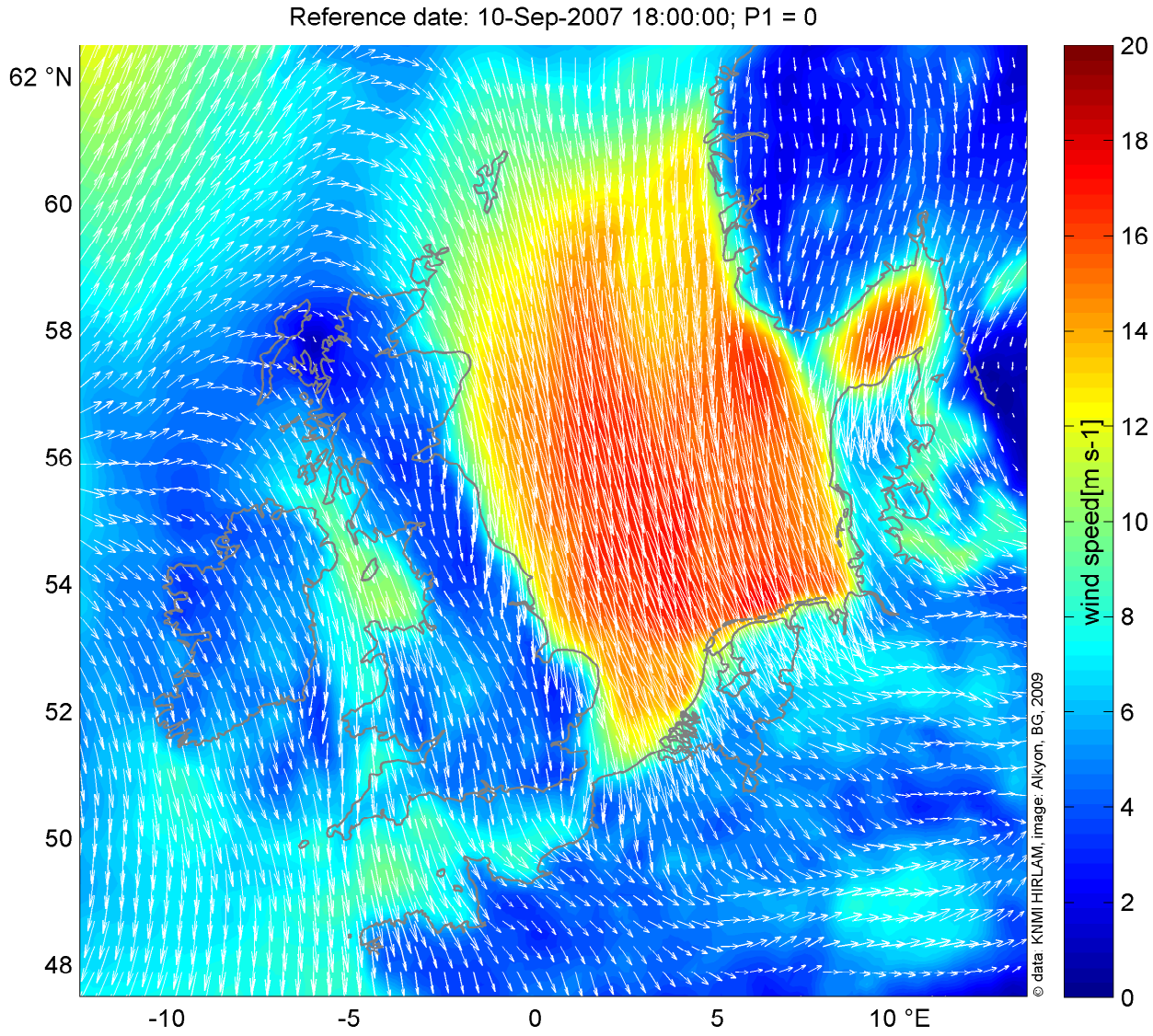

Example of spatially varying wind speed field Reference date: 10-Sep-2007 18:00:00; P1 = 0 Arrows denote wind speed and wind direction		
	KNMI HIRLAM	
Alkyon Hydraulic Consultancy & Research	A2273	Fig. 2.15

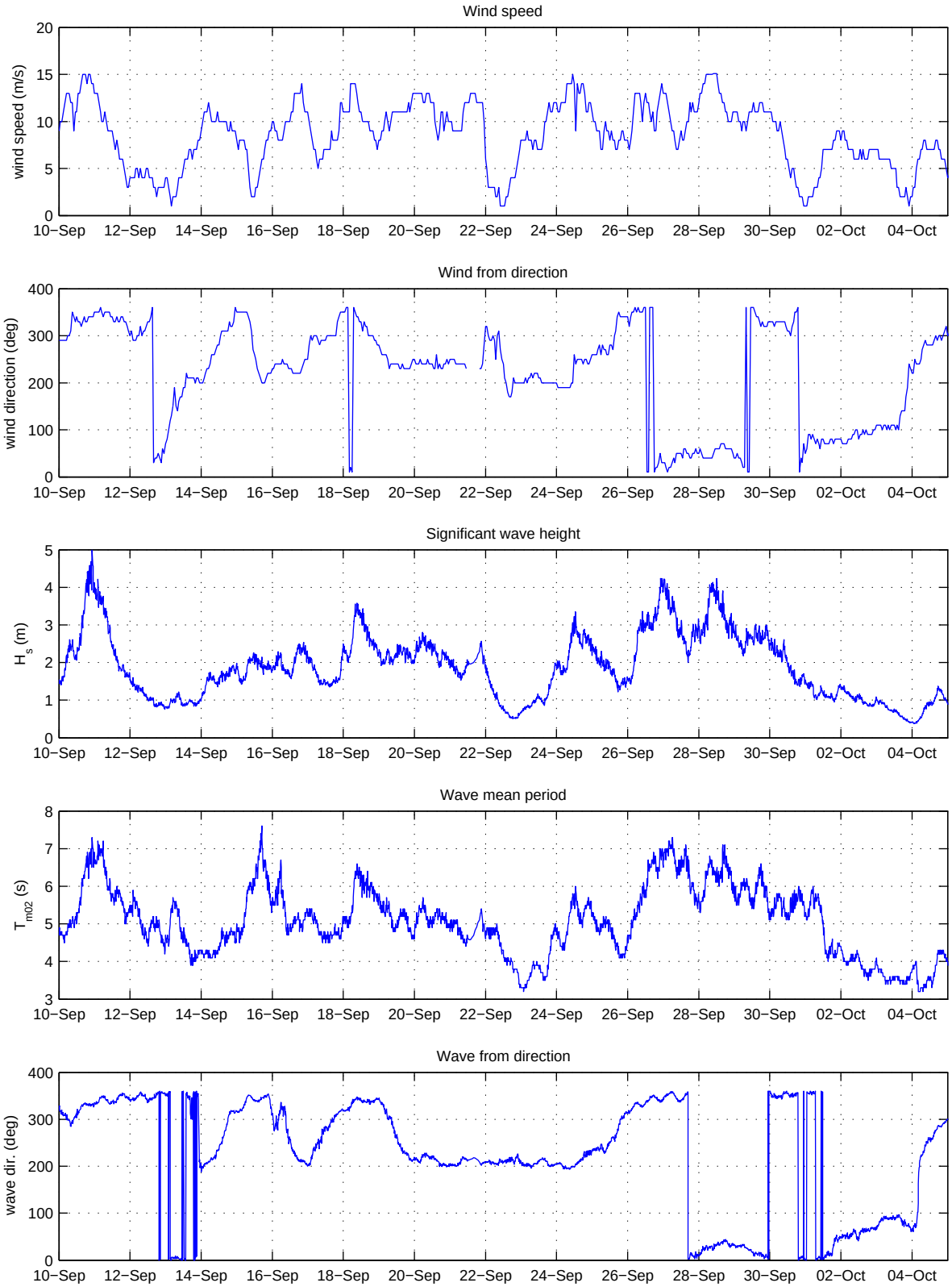

Observed wind and wave conditions from station K13a platform (K13APFM)		
	KNMI; OET Data	
Alkyon Hydraulic Consultancy & Research	A2273	Fig. 2.16

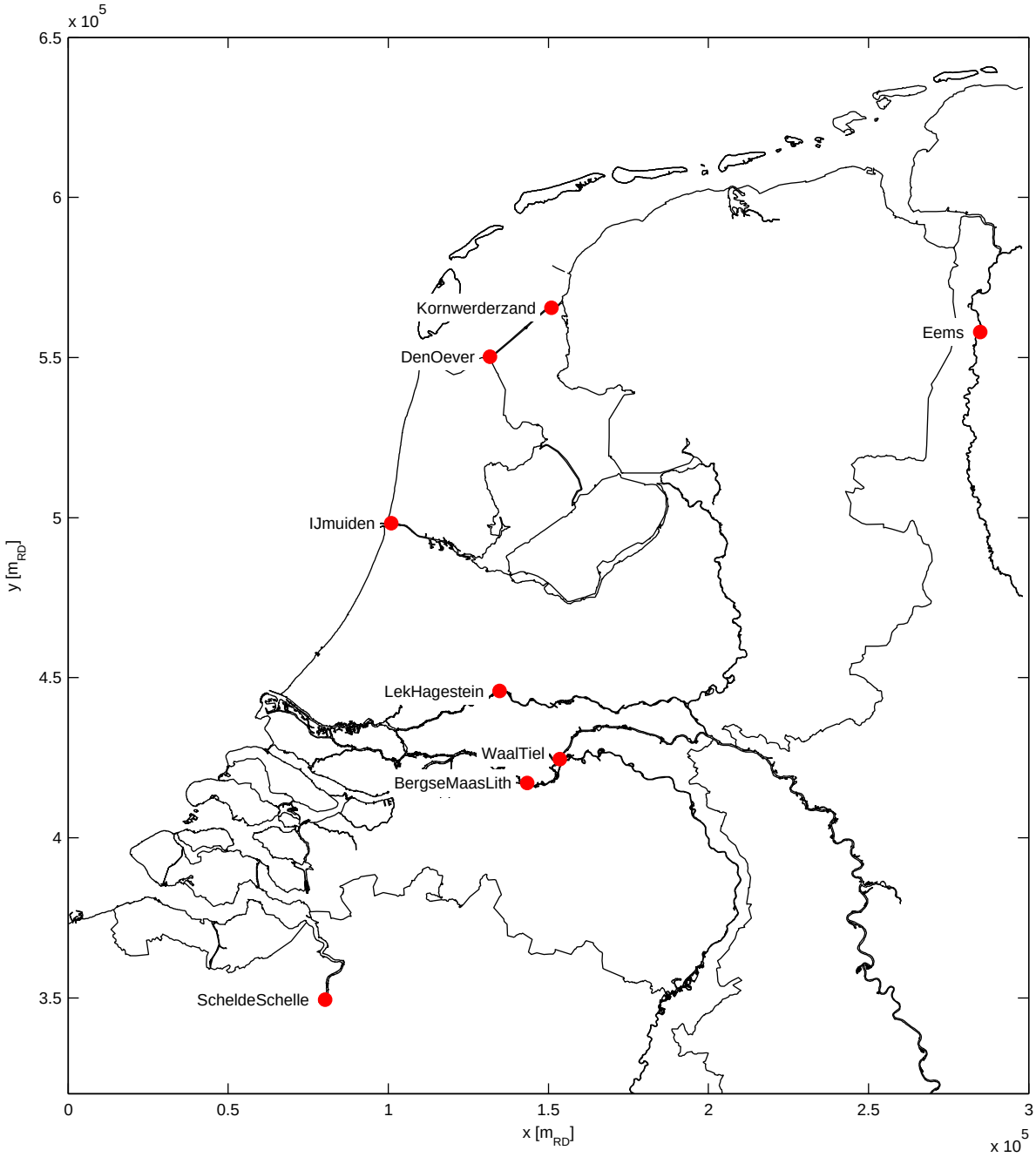

Locations and names of the 8 discharge points (red circles) as adopted in Simona and Delft3D models

Alkyon Hydraulic Consultancy & Research	A2273	Fig. 2.17

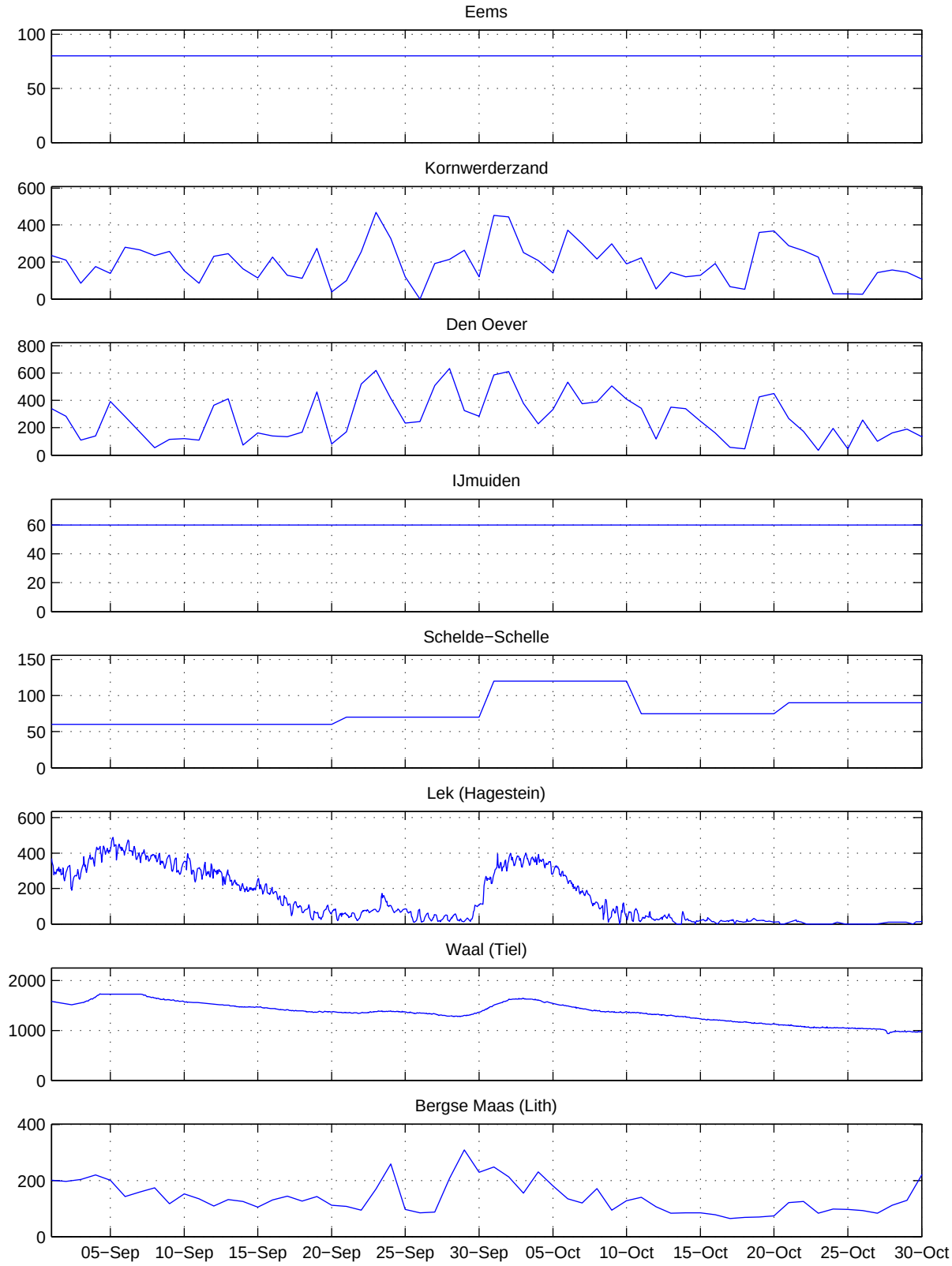

Discharges at the 8 discharge points
as adopted in Simona and Delft3D models

Alkyon Hydraulic Consultancy & Research | A2273 | Fig. 2.18

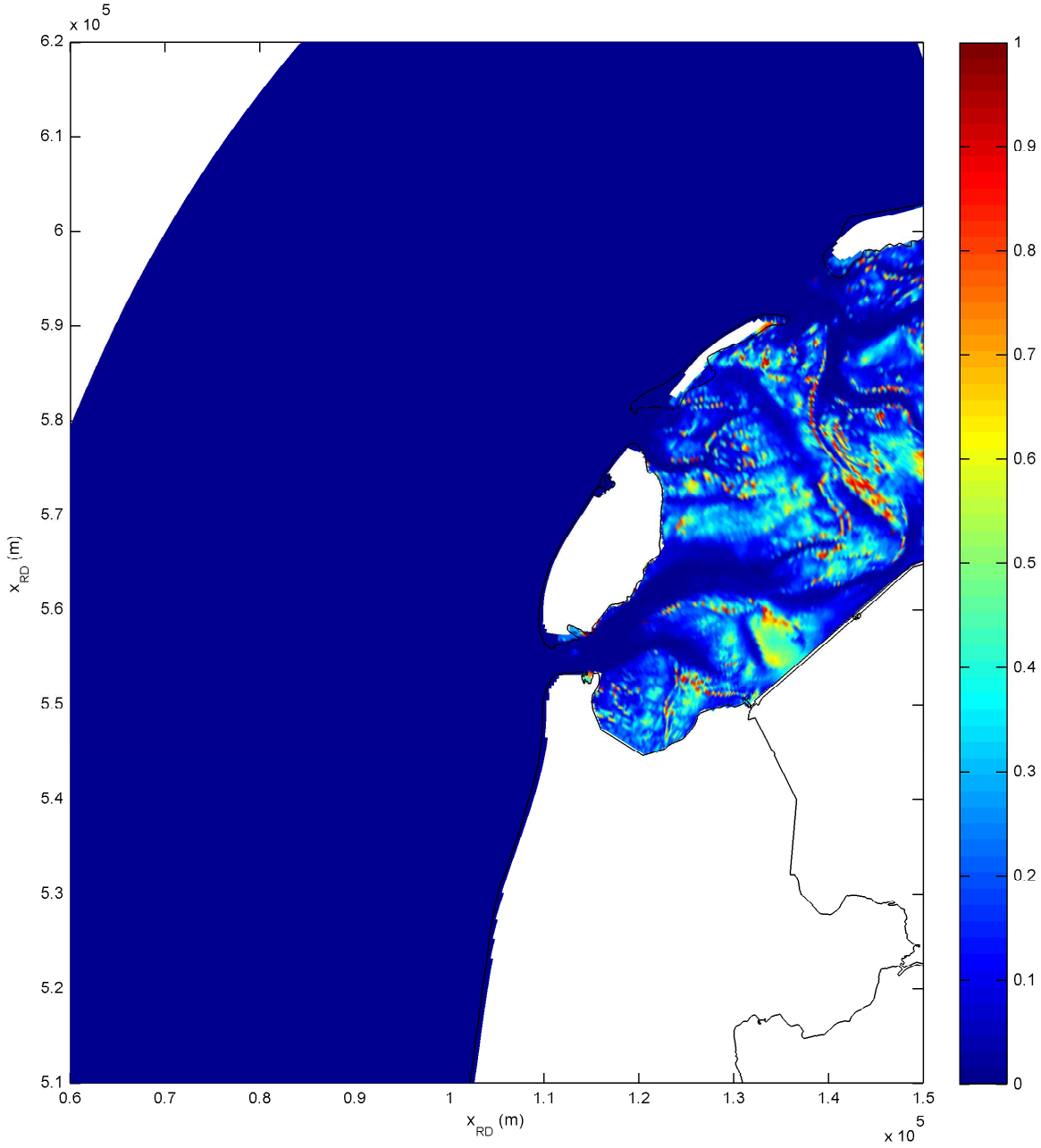

Initial mass fraction of silt in the upper 0.01 m in the bed North Sea modified after first runs		
	Delft3D	
Alkyon Hydraulic Consultancy & Research	A2229	Fig. 2.19

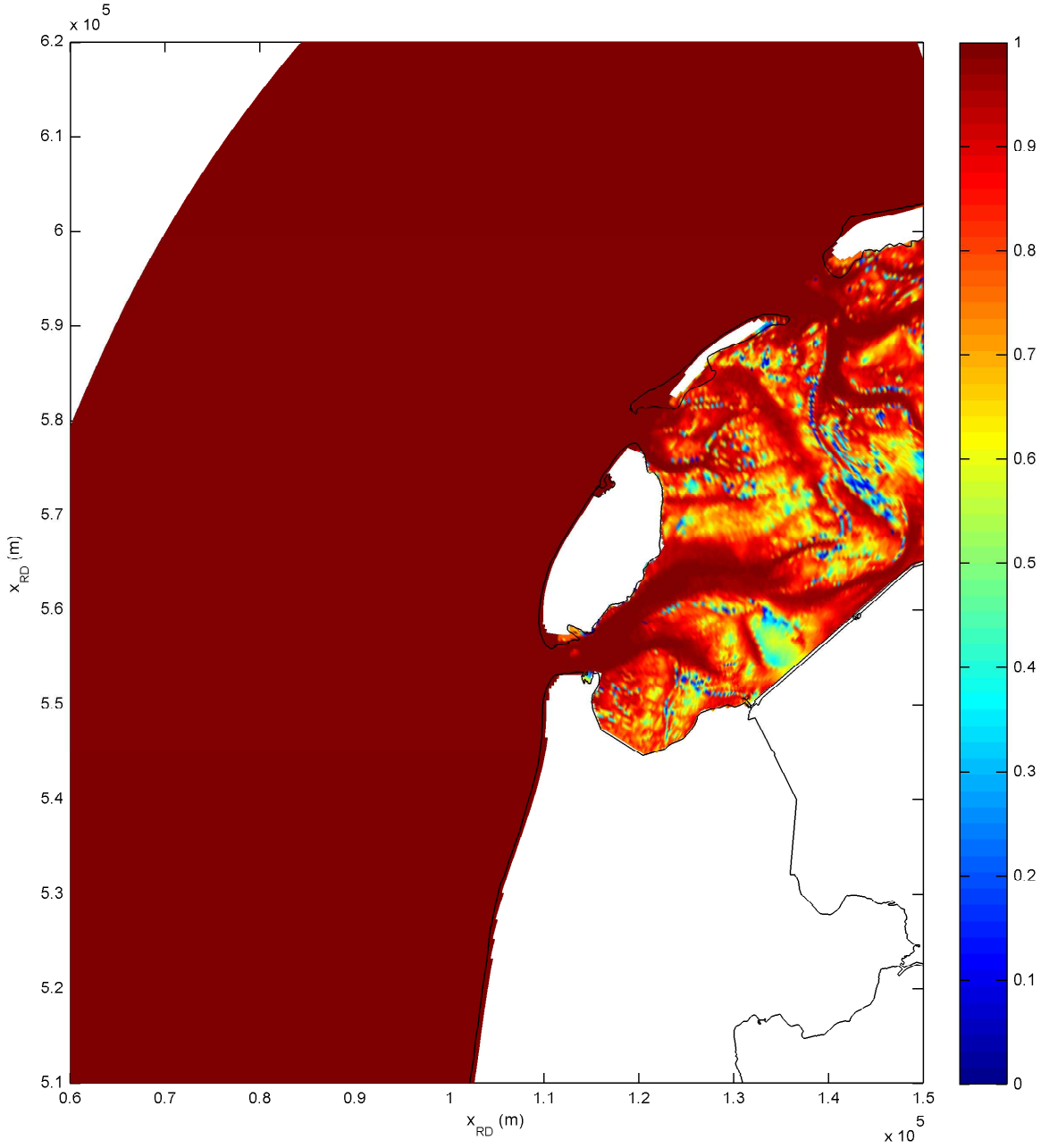

Initial mass fraction of sand in the upper 0.01 m in the bed North Sea modified after first runs		
	Delft3D	
Alkyon Hydraulic Consultancy & Research	A2229	Fig. 2.20

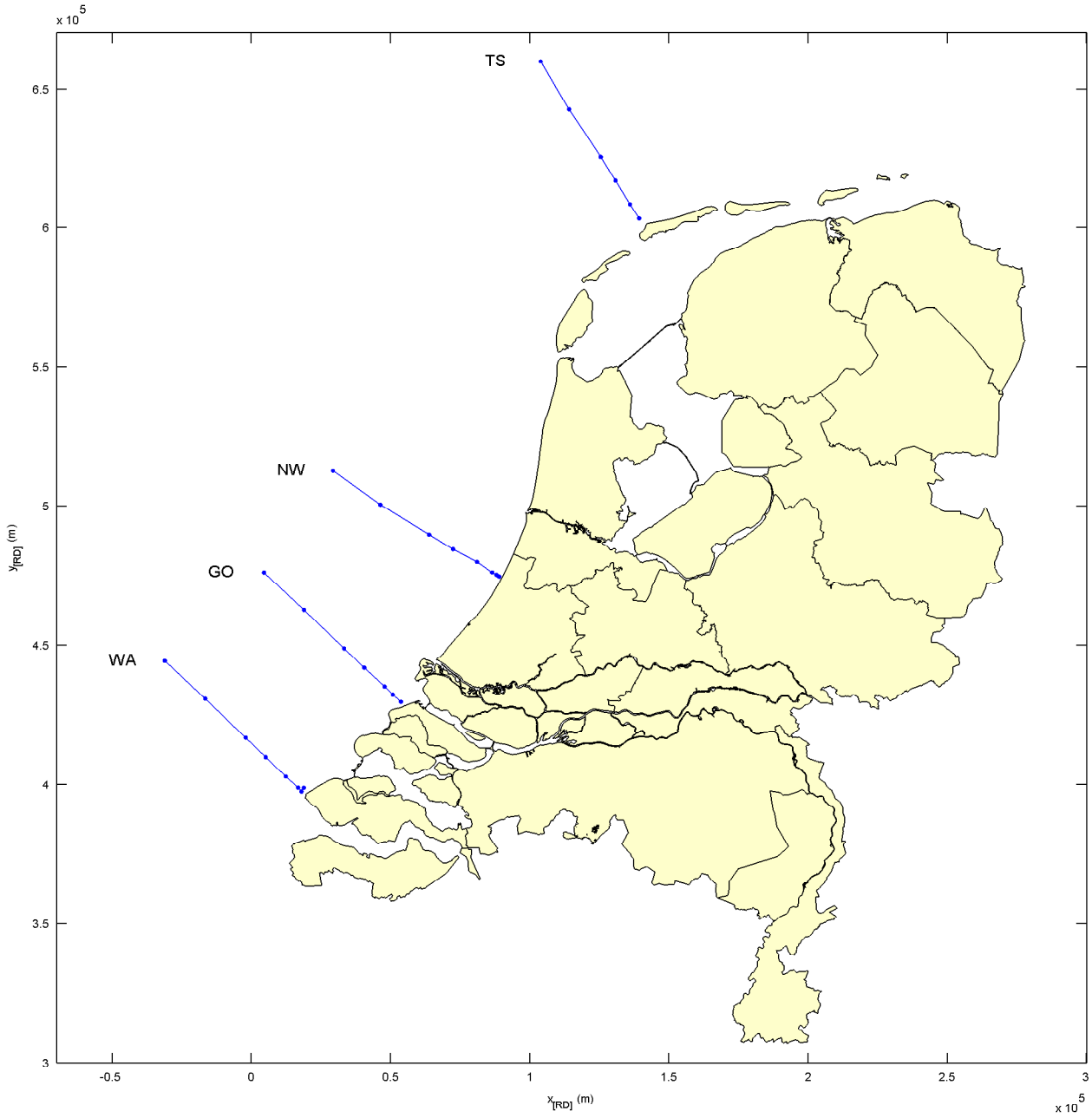

Suspended sediment concentration boundaries from Waterbase for the period 1975-2008 GO and TS have been applied in the Delft3D model		
	Waterbase 1975-2008	
Alkyon Hydraulic Consultancy & Research	A2273	Fig. 2.21

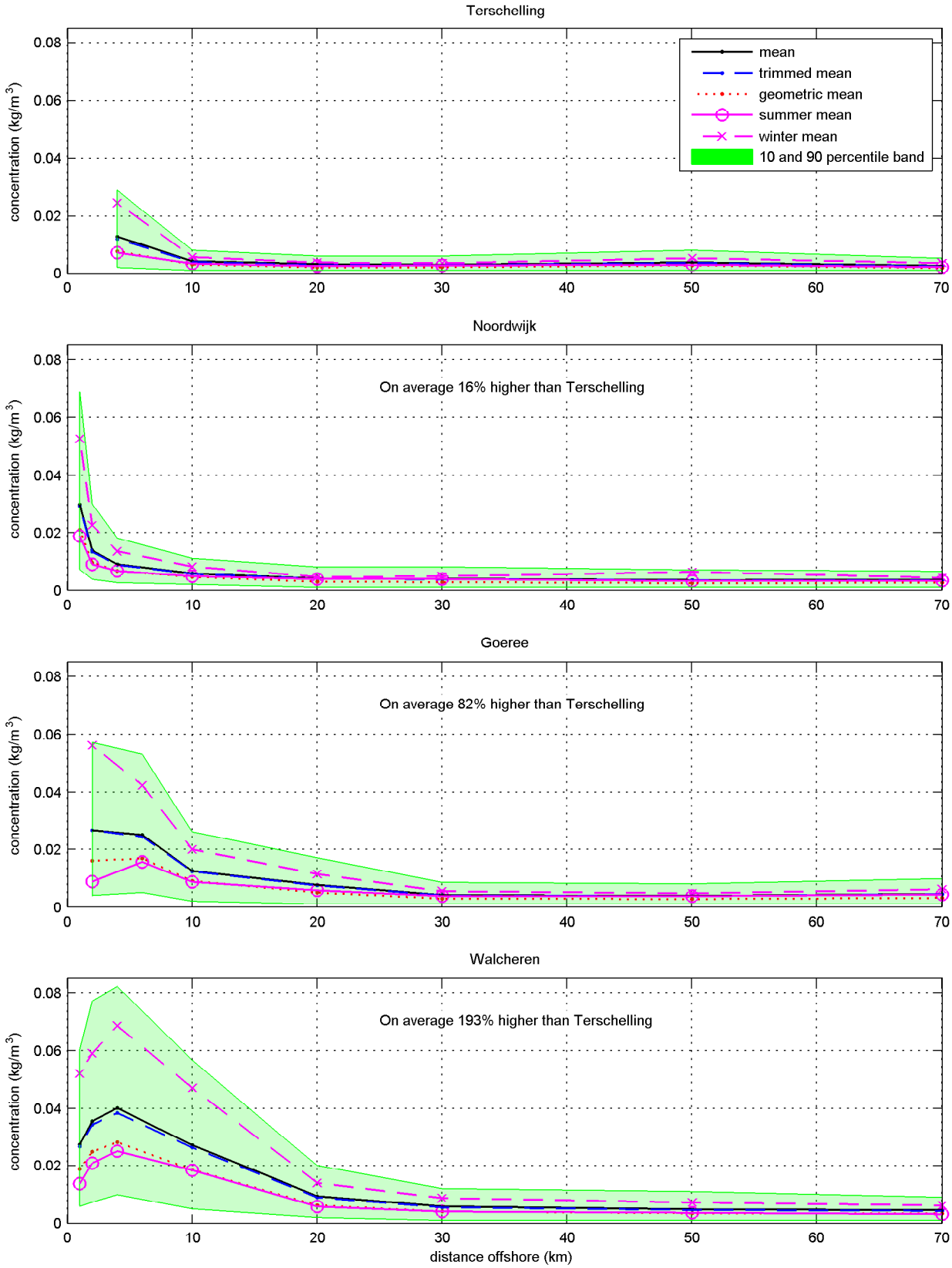

Cross-shore distribution of total suspended matter concentration (kg/m^3)
Statistical parameters based on 1975-2008 Waterbase data
Terschelling and Goeree were adopted for the model boundaries

Waterbase 1975-2008

Alkyon Hydraulic Consultancy & Research

A2273

Fig. 2.22

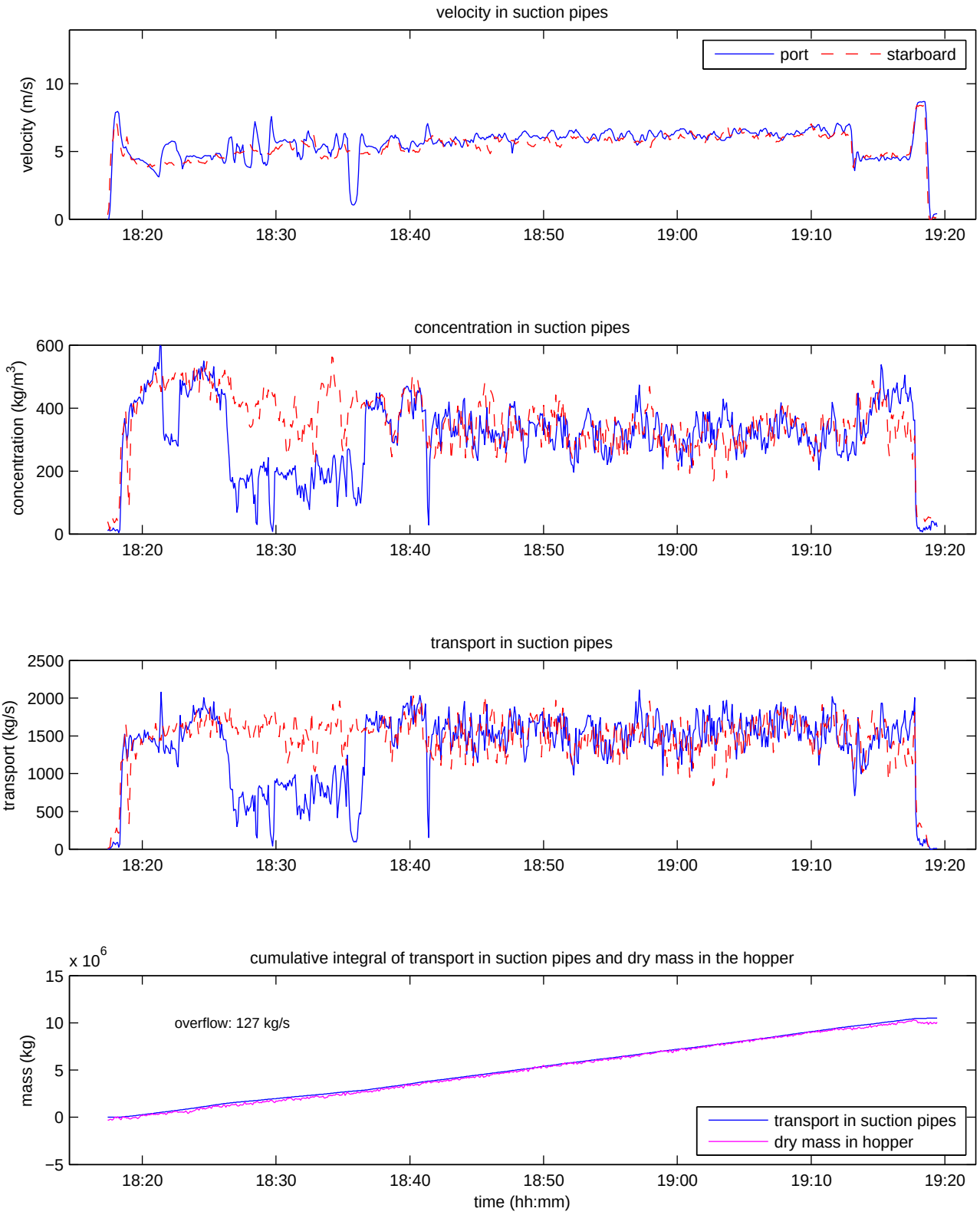

Velocity, concentration, transport and cumulative transport in suction pipes of the dredger, and dry mass in the hopper date: 26−Aug−2007, trip−id: 1188145865		
	source: RWS DNZ	
Alkyon Hydraulic Consultancy & Research	A2273	Fig. 2.23

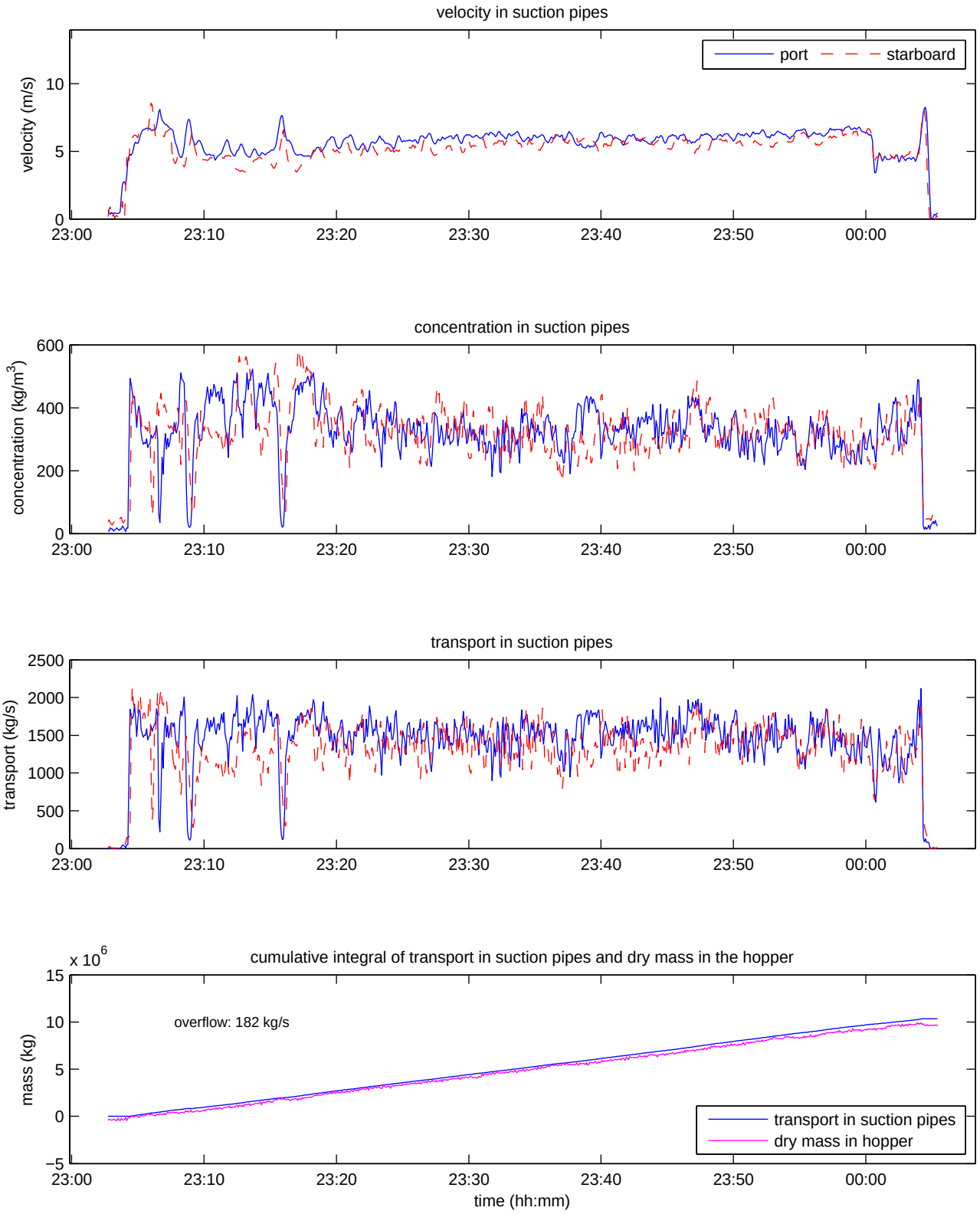

Velocity, concentration, transport and cumulative transport in suction pipes of the dredger, and dry mass in the hopper date: 26−Aug−2007, trip−id: 1188162060		
	source: RWS DNZ	
Alkyon Hydraulic Consultancy & Research	A2273	Fig. 2.23a

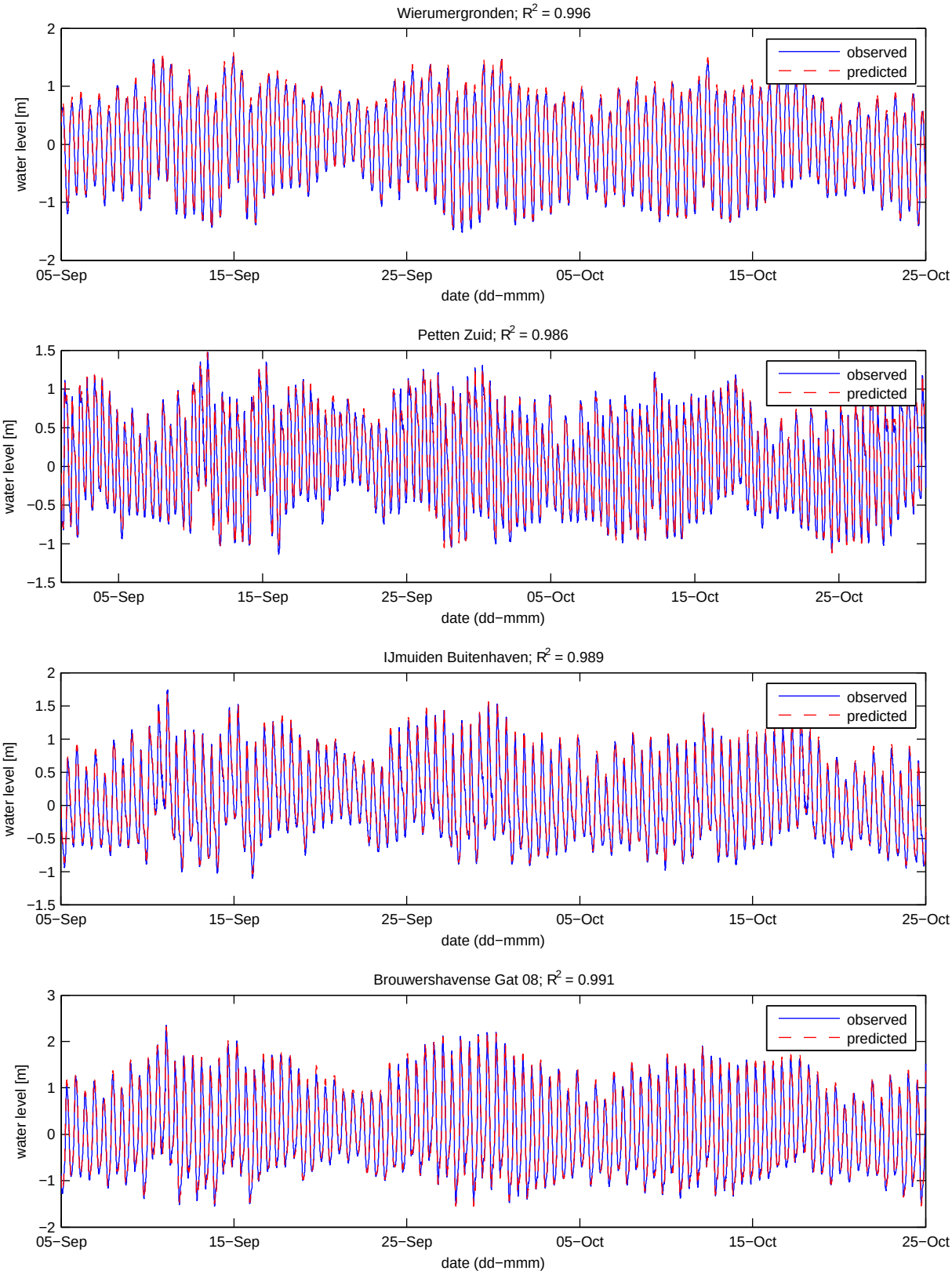

Observed and predicted water levels
for stations Wierumergronden, Petten Zuid,
IJmuiden Buitenhaven and Brouwershavense Gat 08

Alkyon Hydraulic Consultancy & Research | A2273 | Fig. 2.24

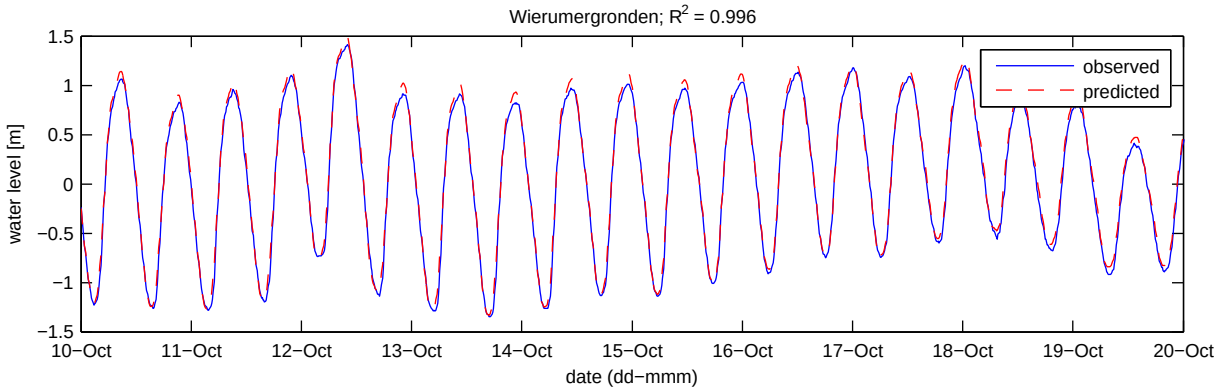

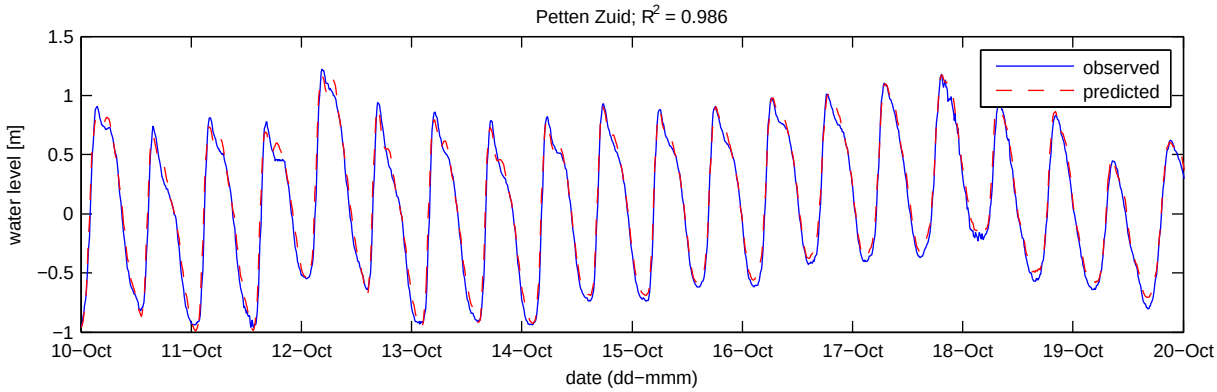

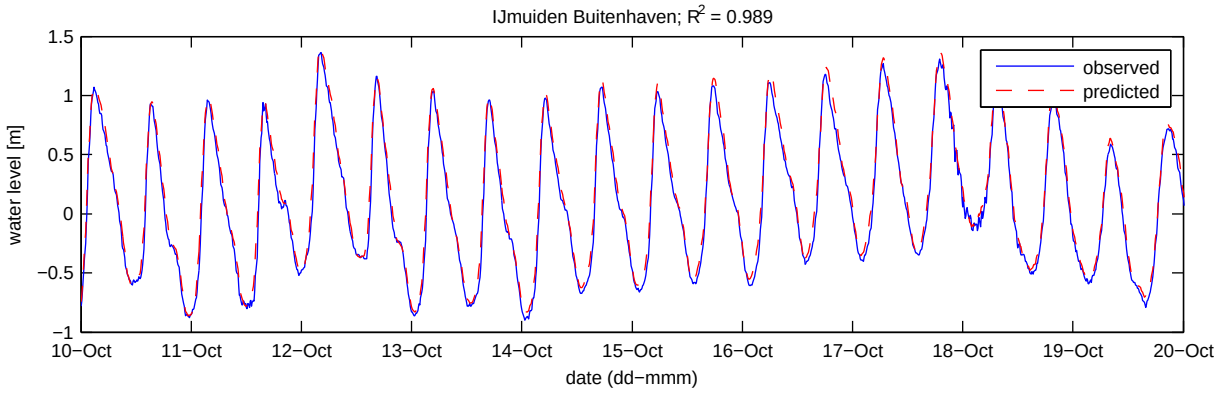

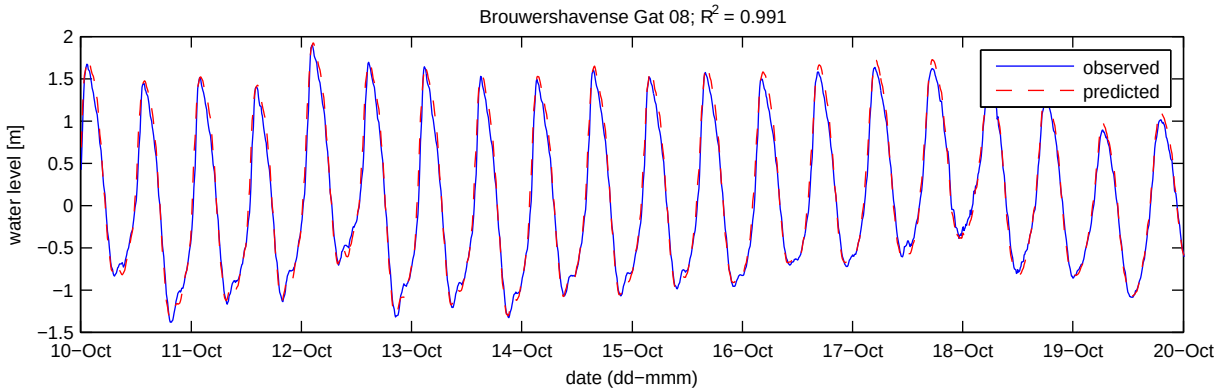

Observed and predicted water levels (zoom in on Fig 2.24)
for stations Wierumergronden, Petten Zuid,
IJmuiden Buitenhaven and Brouwershavense Gat 08

Alkyon Hydraulic Consultancy & Research | A2273 | Fig. 2.25

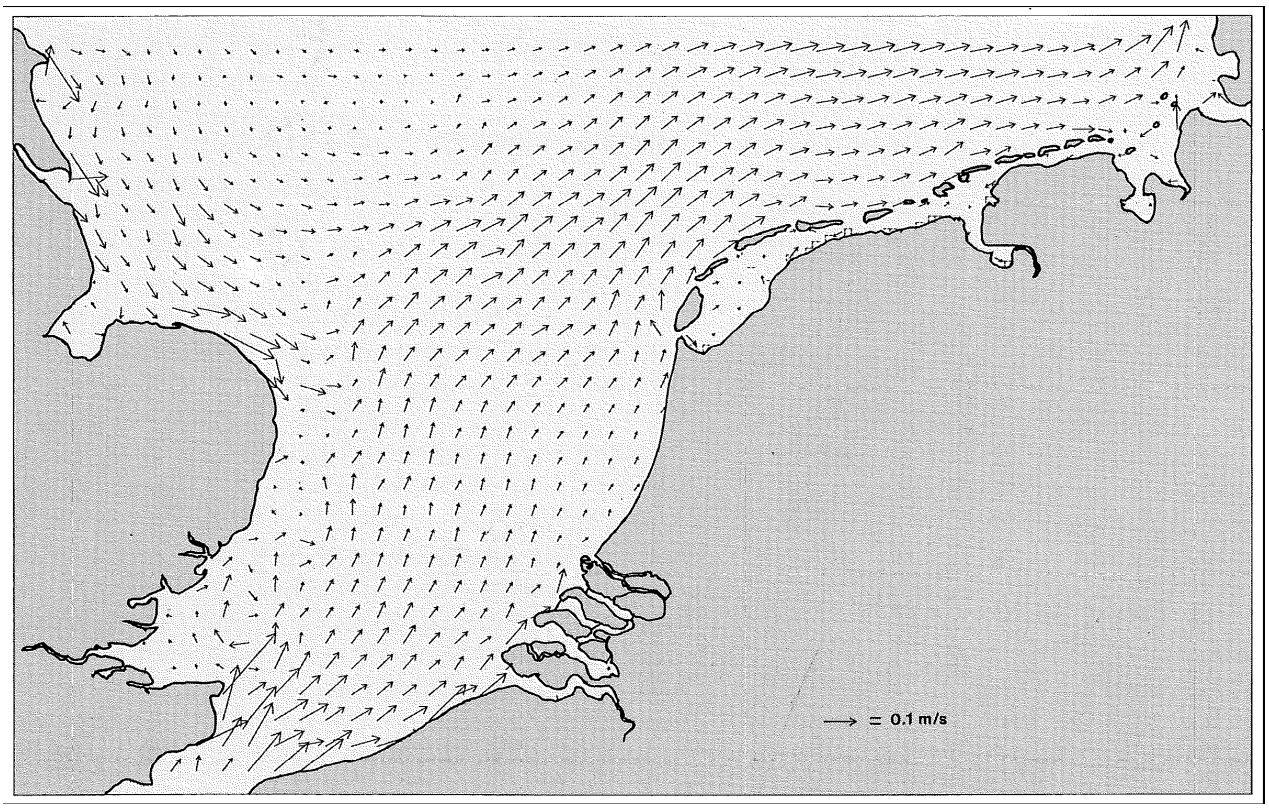

Deph−averaged residual current field for 4.5 m/s SW wind field from De Ruijter et al. (1987) Fig. 7		
	De Ruijter et al (1987)	
Alkyon Hydraulic Consultancy & Research	A2273	Fig. 2.25a

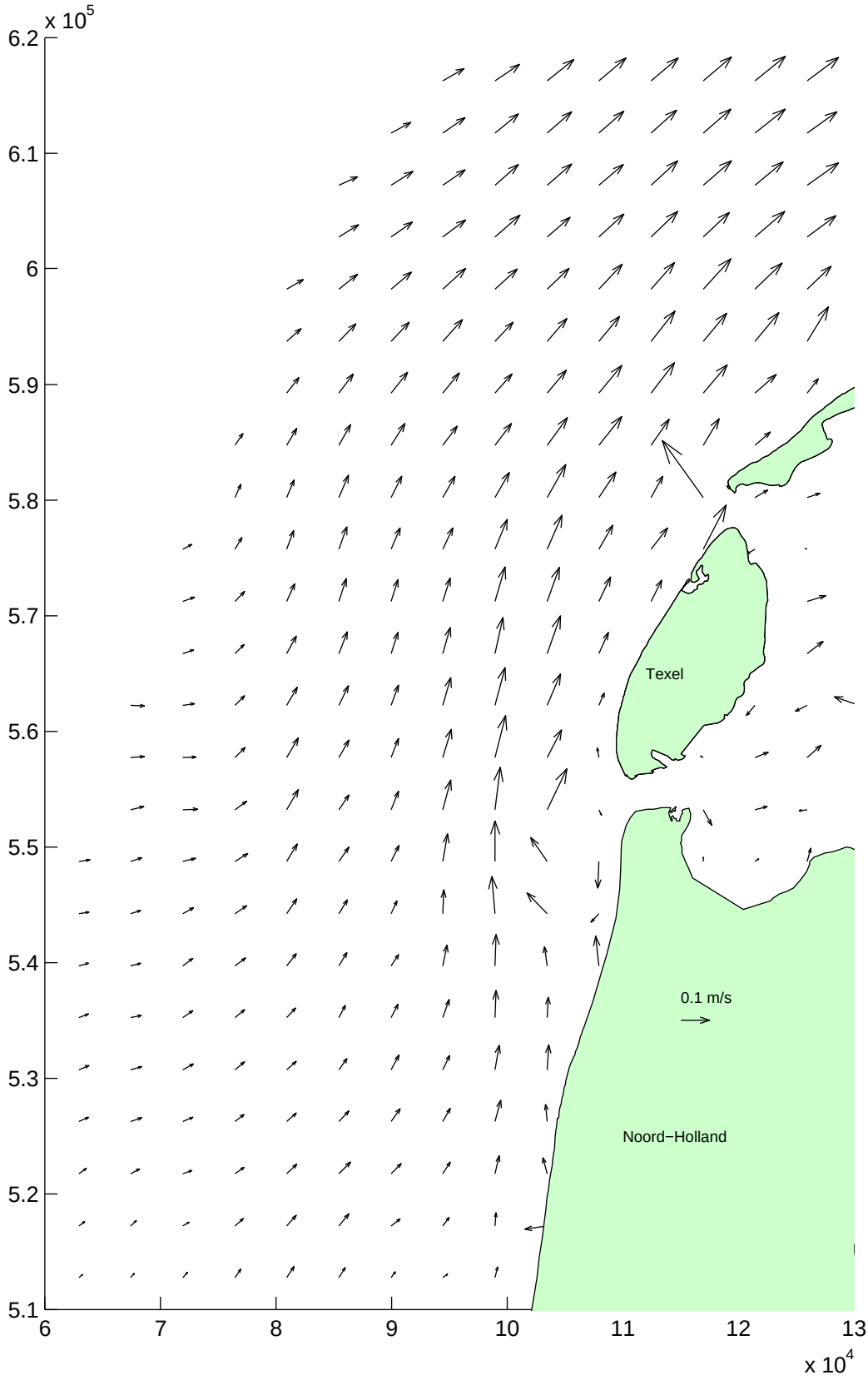

Depth−averaged residual current field based on 3D simulations incl. effects of wind, waves, sediment and salinity for the period 16−Sep−2007 10:30:00 − 02−Oct−2007 23:30:00	Delft3D	
Alkyon Hydraulic Consultancy & Research	A2273	Fig. 2.25b

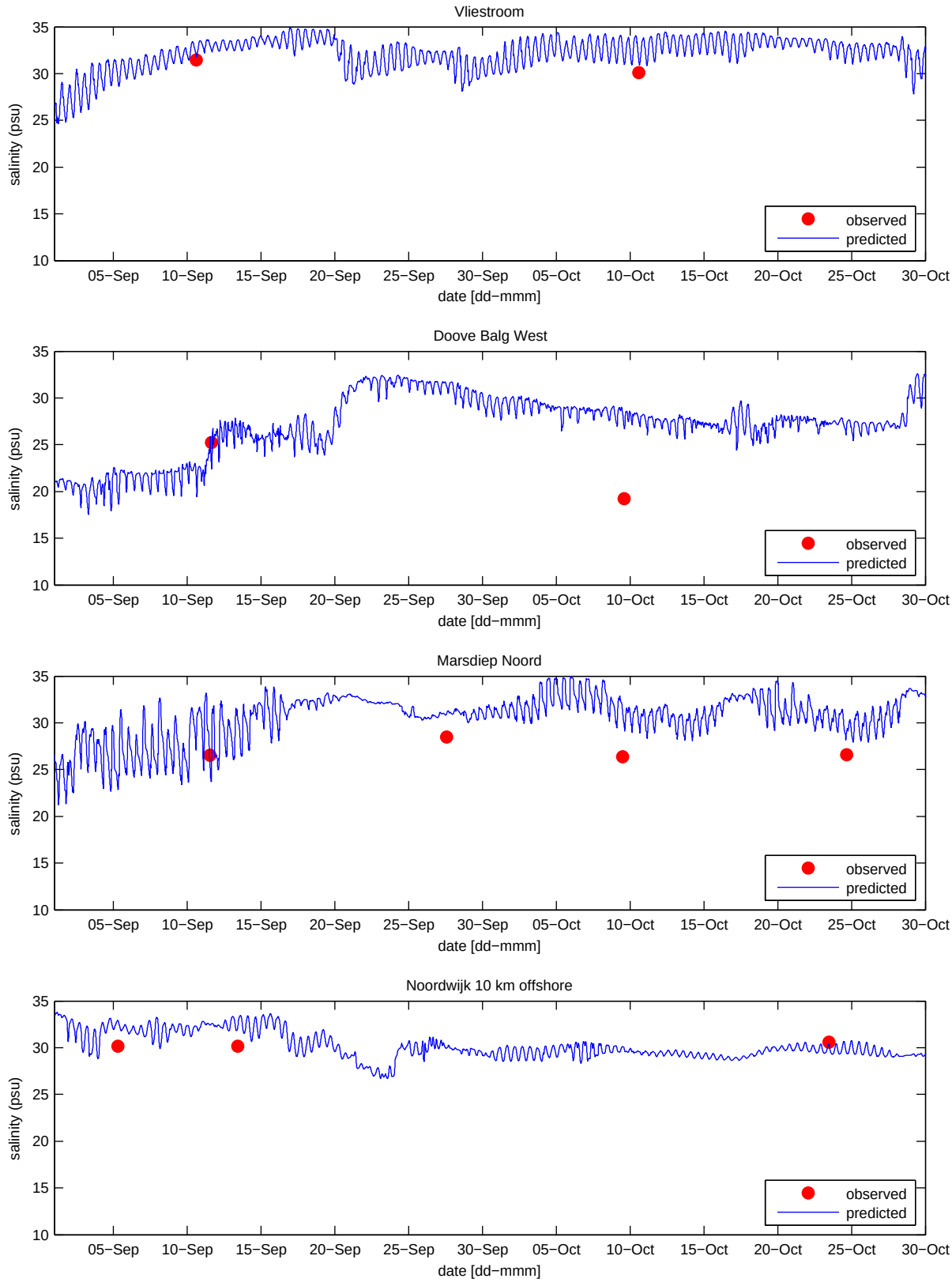

Observed and predicted salinities
for stations Vliestroom, Doove Balg West, Marsdiep Noord
and Noordwijk 10 km offshore

Alkyon Hydraulic Consultancy & Research | A2273 | Fig. 2.26

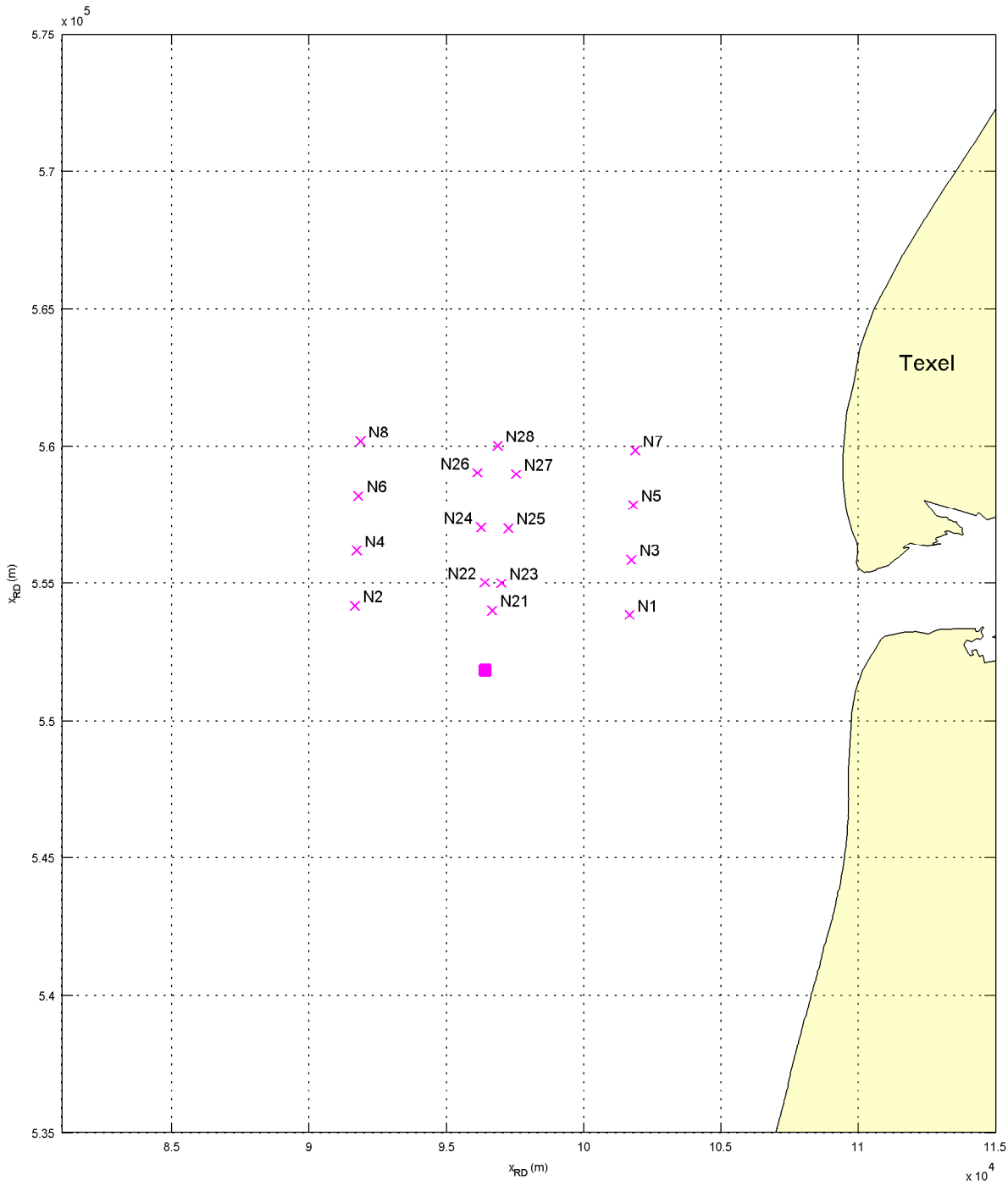

Locations and names of the T1 observations and the dredging location as schematized in Delft3D (square-mark)		
Alkyon Hydraulic Consultancy & Research	A2273	Fig. 2.27

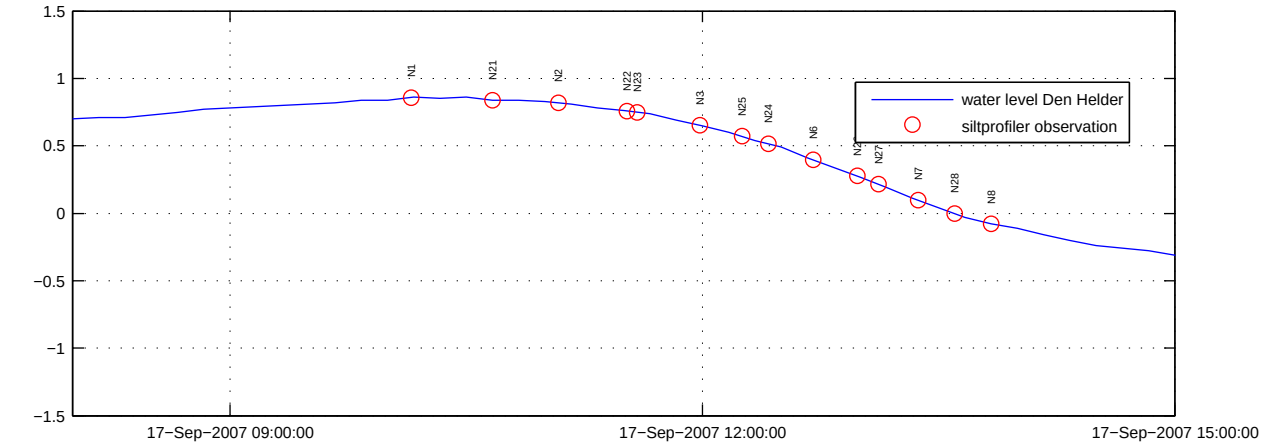

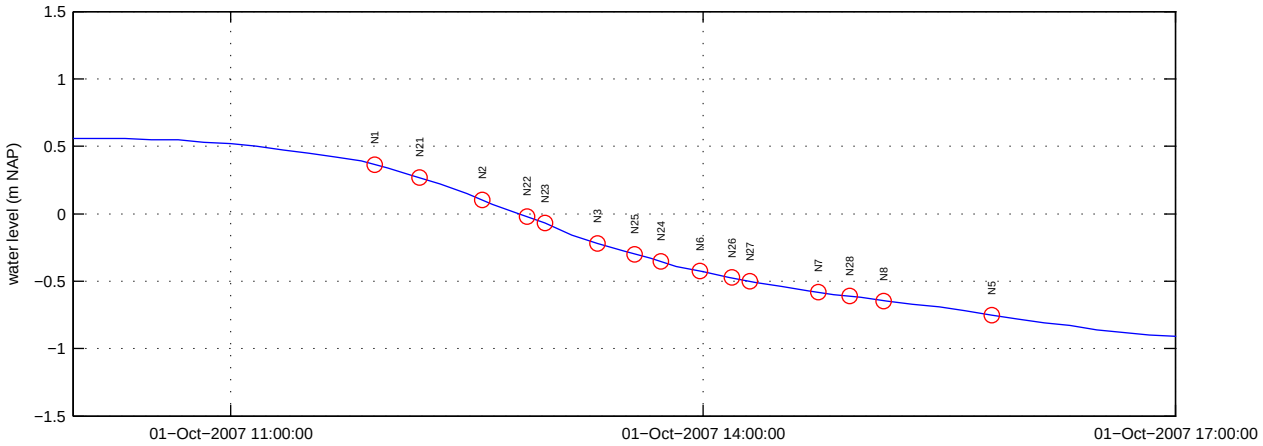

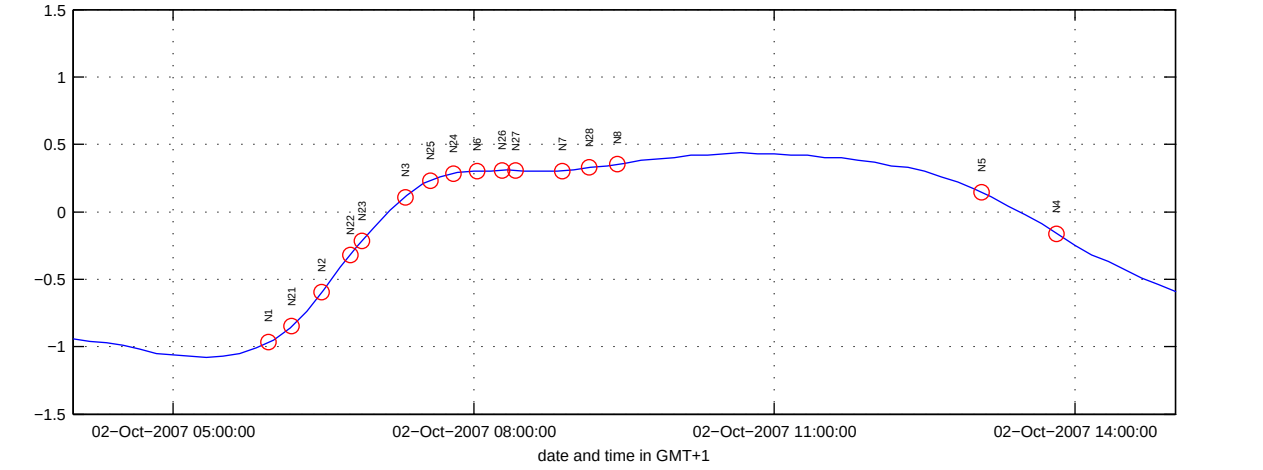

Date and time of T1 silt profiler measurements using water level at Den Helder as reference 17 September and 1 and 2 October 2007		
	Silt Profiler	
Alkyon Hydraulic Consultancy & Research	A2273	Fig. 2.27a

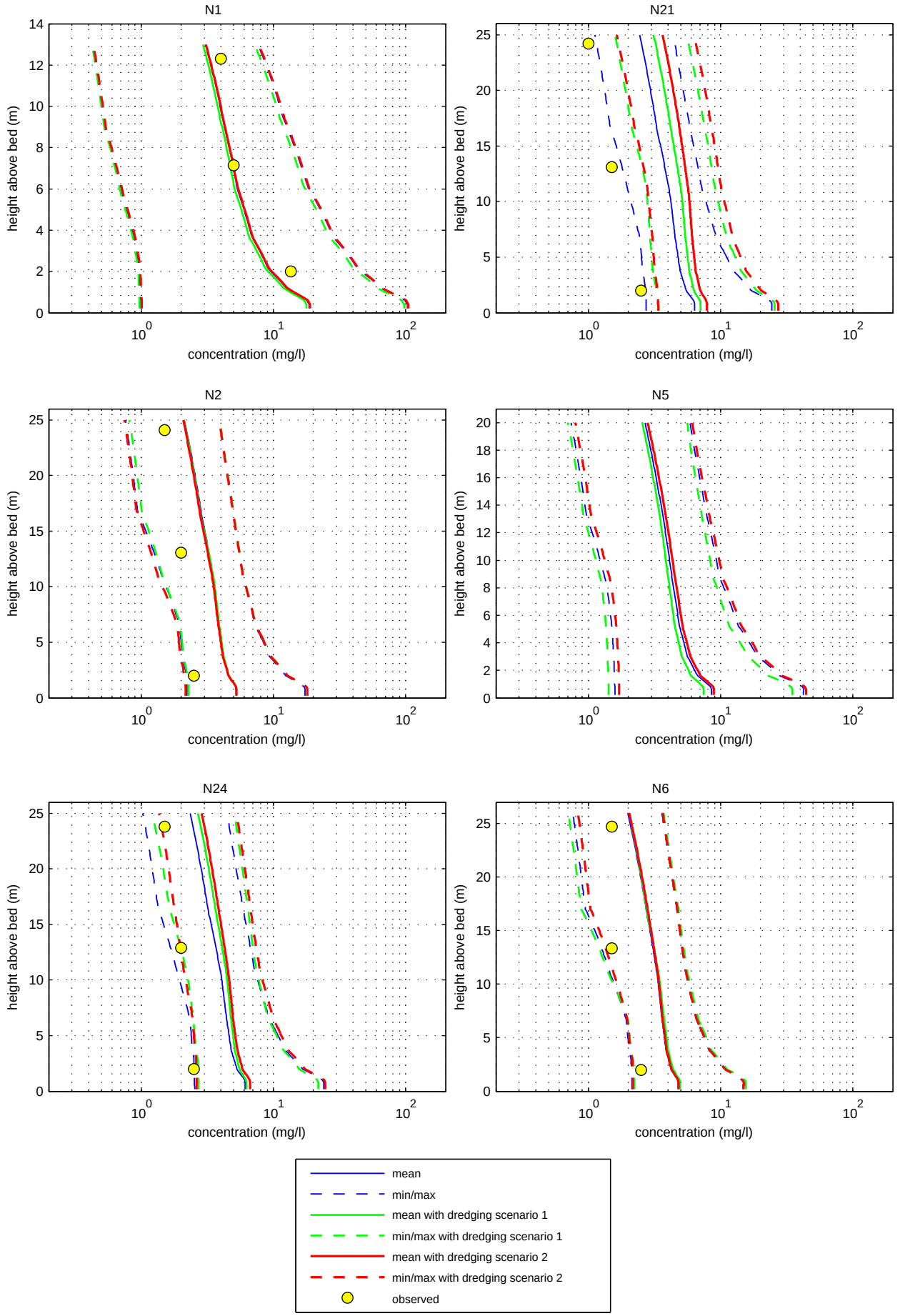

Vertical distribution of simulated suspended solids concentrations (mg/l) (mean, min. and max.), and observed values at N1, N21, N2, N5, N24 and N6 on 17 September 2007

Alkyon Hydraulic Consultancy & Research | A2273 | Fig. 2.28

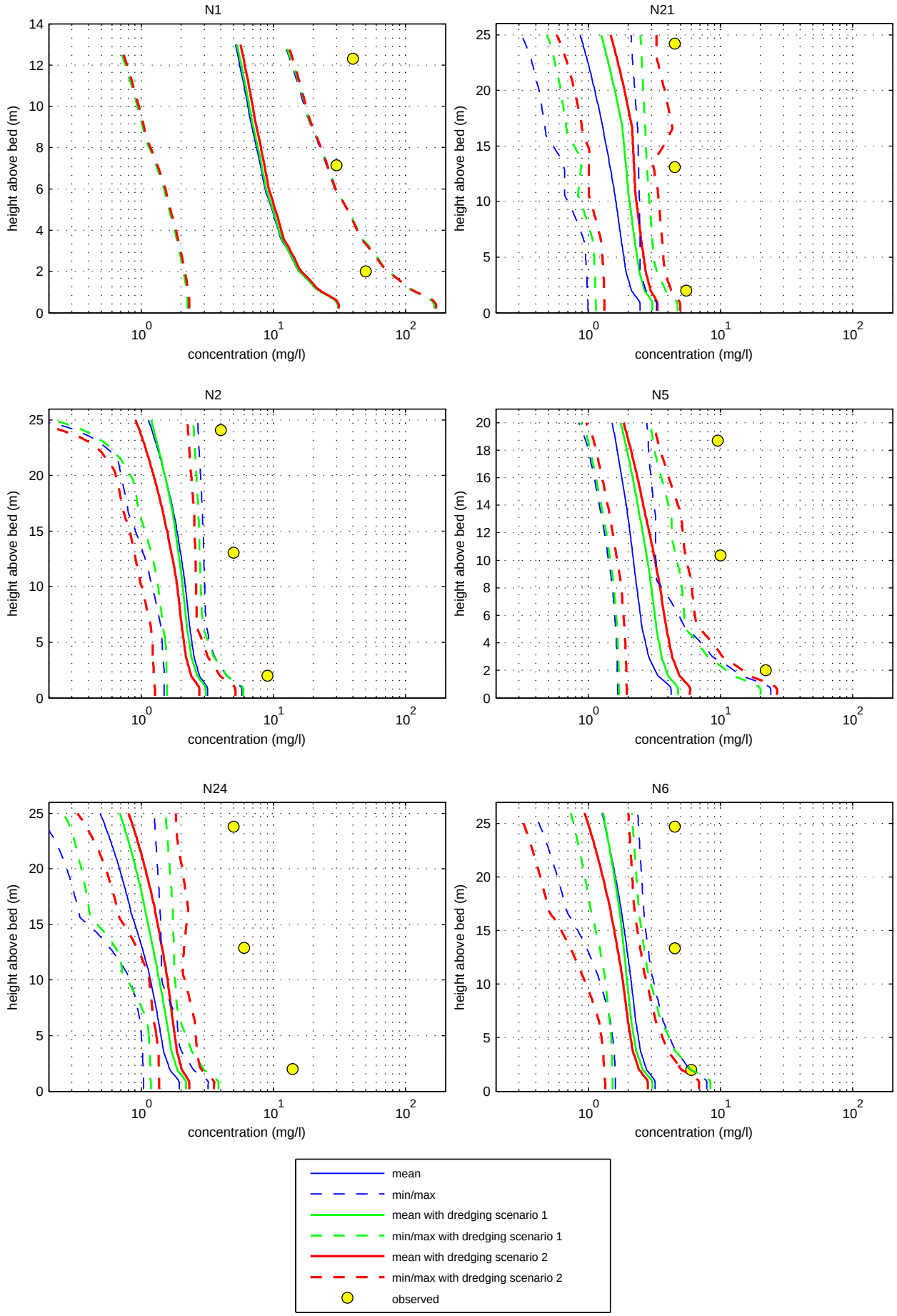

Vertical distribution of simulated suspended solids concentrations (mg/l) (mean, min. and max.), and observed values at N1, N21, N2, N5, N24 and N6 on 1 October 2007

Alkyon Hydraulic Consultancy & Research | A2273 | Fig. 2.29

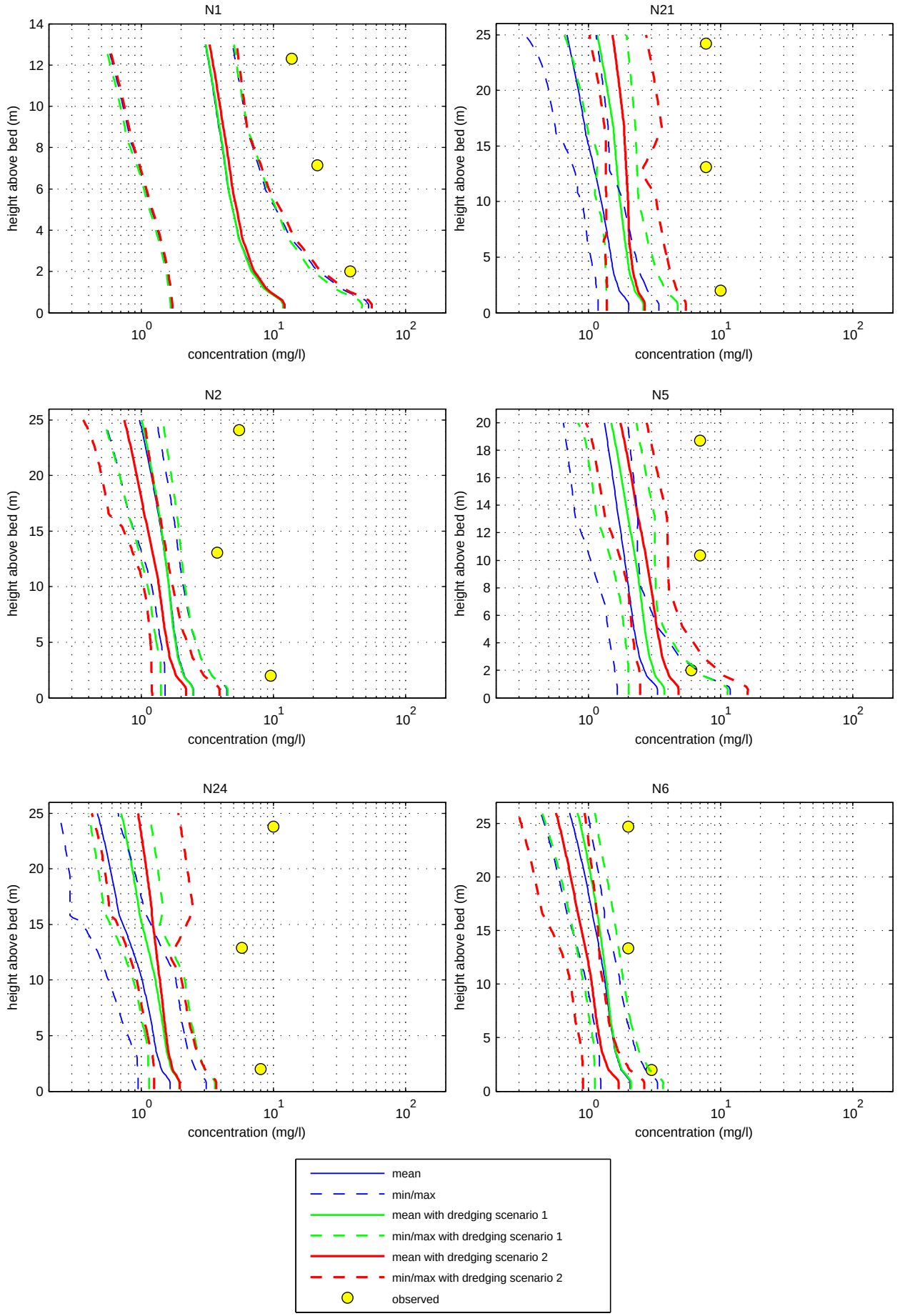

Vertical distribution of simulated suspended solids concentrations (mg/l) (mean, min. and max.), and observed values at N1, N21, N2, N5, N24 and N6 on 2 October 2007

Alkyon Hydraulic Consultancy & Research | A2273 | Fig. 2.30

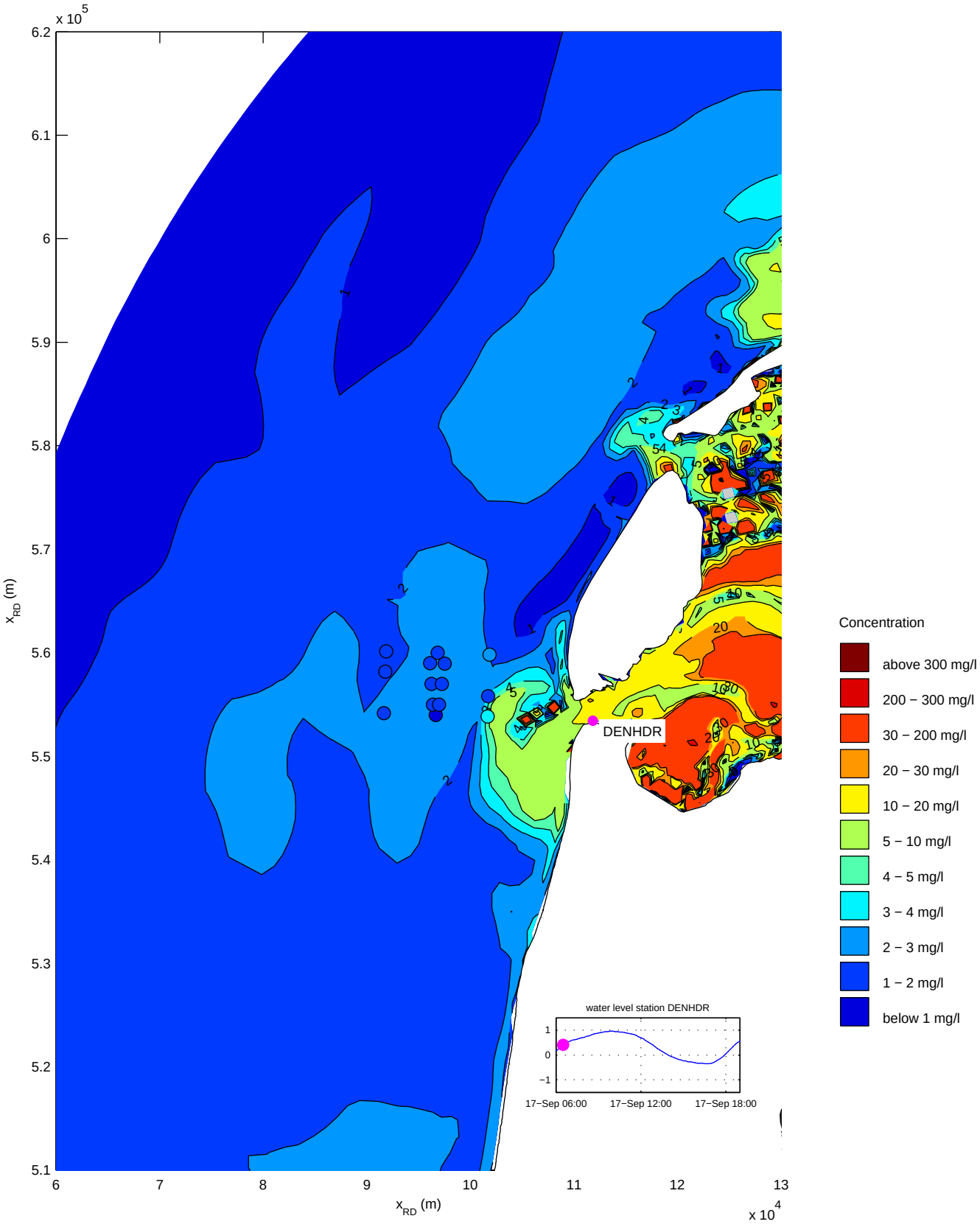

Simulated silt concentrations (mg/l) date and time: 17−Sep−2007 06:30:00 coloured symbols denote the T1 observations		
	trim−kh07intgraded36	
Alkyon Hydraulic Consultancy & Research	A2273	Fig. 2.31

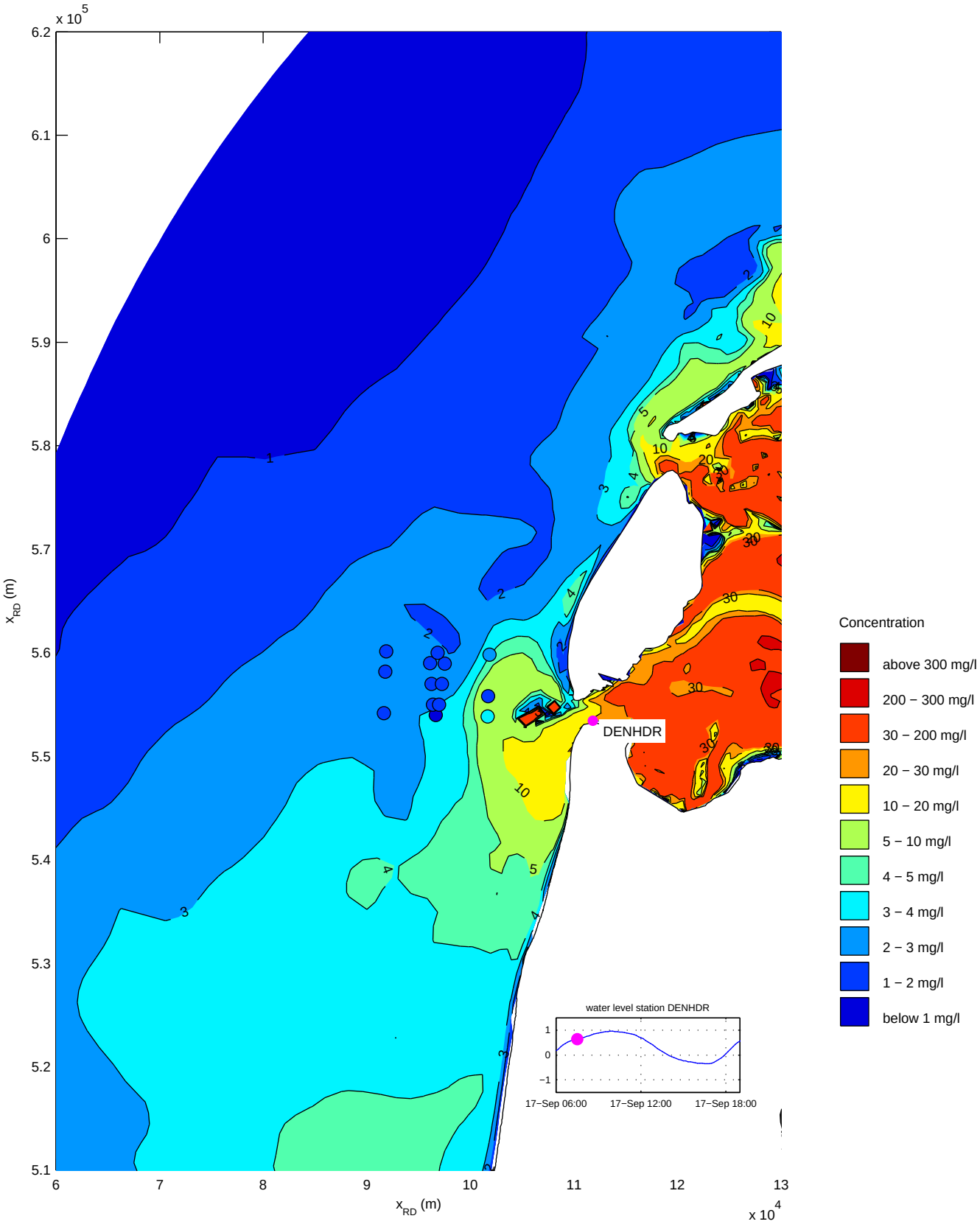

Simulated silt concentrations (mg/l) date and time: 17−Sep−2007 07:30:00 coloured symbols denote the T1 observations		
	trim−kh07intgraded36	
Alkyon Hydraulic Consultancy & Research	A2273	Fig. 2.32

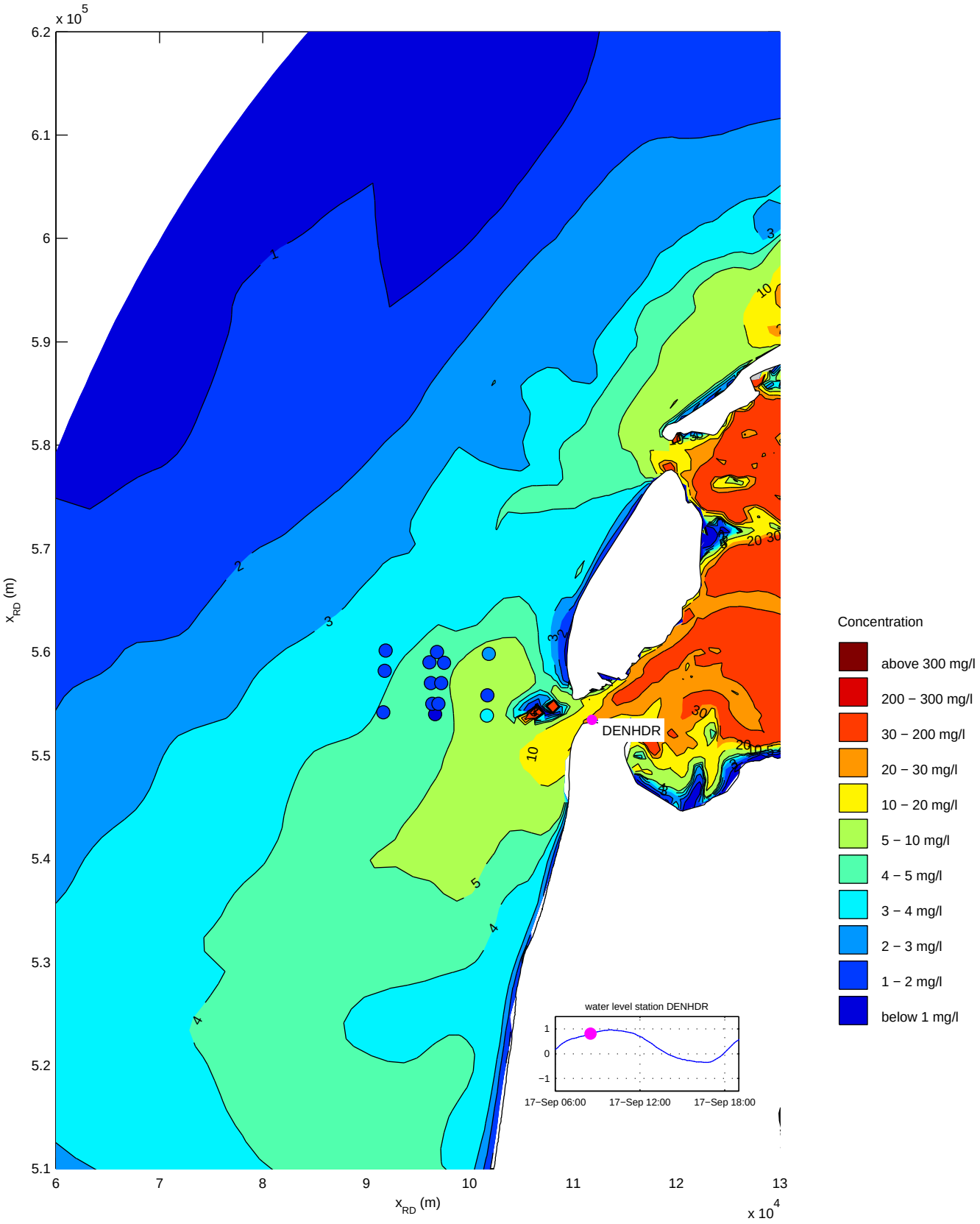

Simulated silt concentrations (mg/l) date and time: 17−Sep−2007 08:30:00 coloured symbols denote the T1 observations		
	trim−kh07intgraded36	
Alkyon Hydraulic Consultancy & Research	A2273	Fig. 2.33

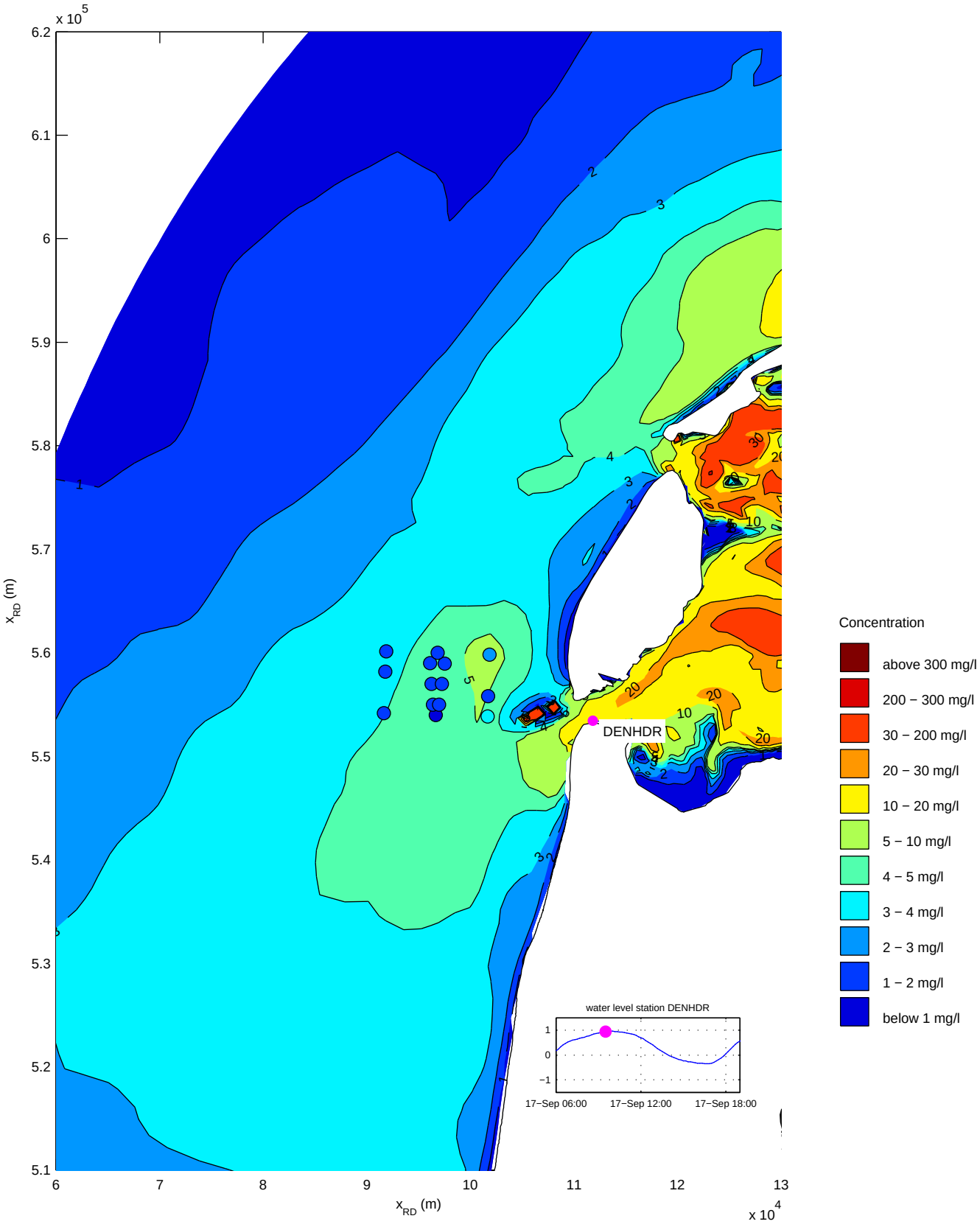

Simulated silt concentrations (mg/l) date and time: 17−Sep−2007 09:30:00 coloured symbols denote the T1 observations		
	trim−kh07intgraded36	
Alkyon Hydraulic Consultancy & Research	A2273	Fig. 2.34

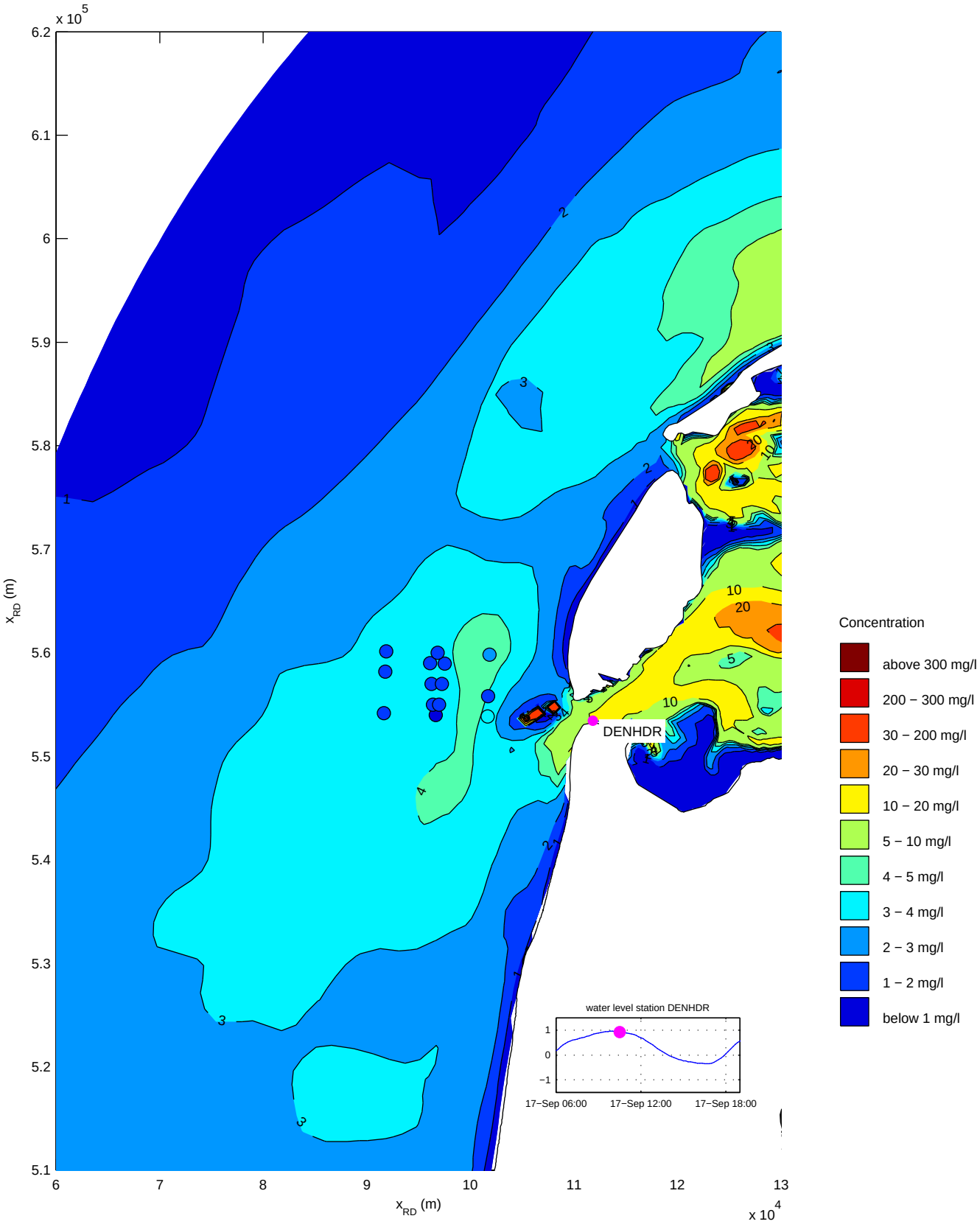

Simulated silt concentrations (mg/l) date and time: 17−Sep−2007 10:30:00 coloured symbols denote the T1 observations		
	trim−kh07intgraded36	
Alkyon Hydraulic Consultancy & Research	A2273	Fig. 2.35

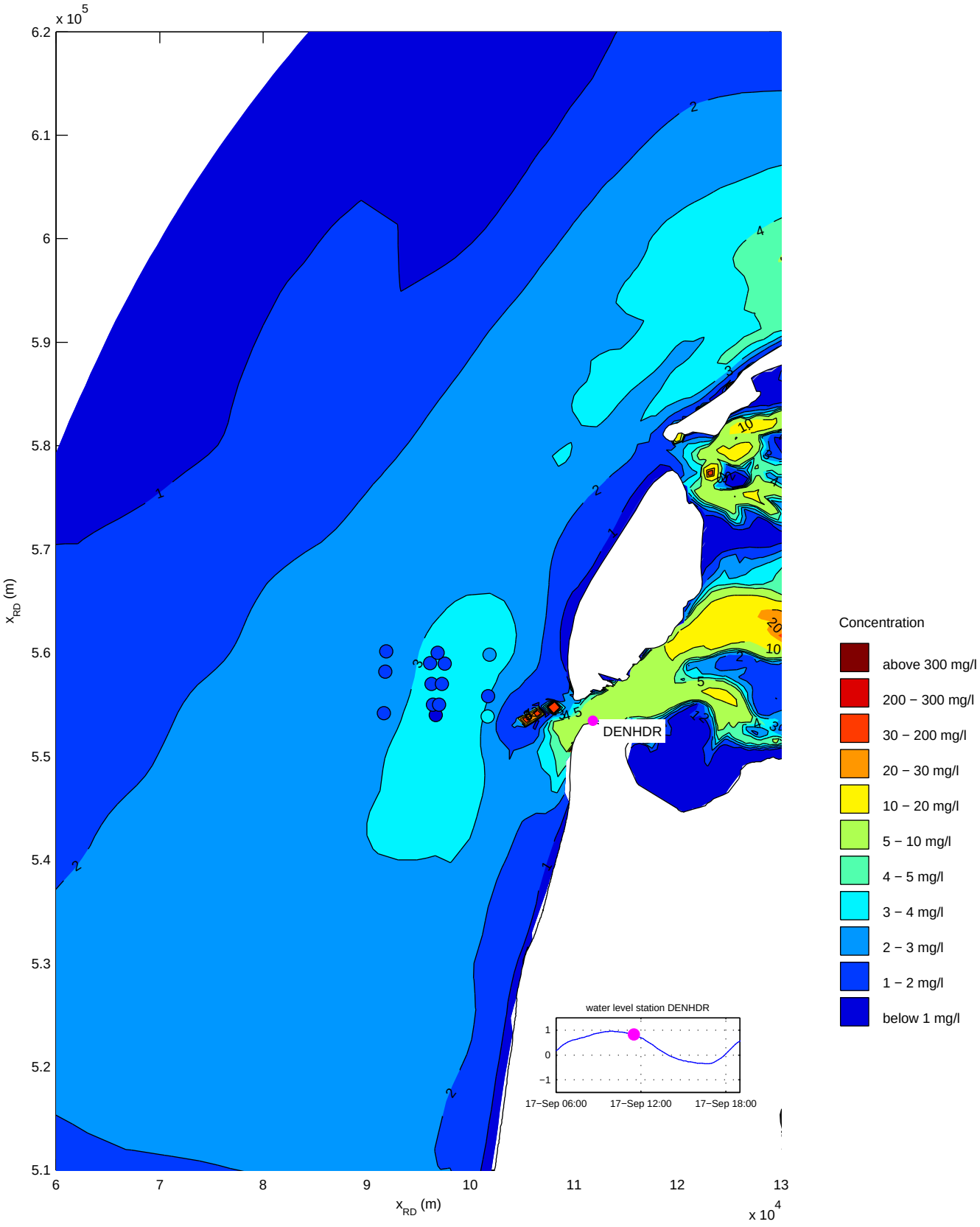

Simulated silt concentrations (mg/l) date and time: 17−Sep−2007 11:30:00 coloured symbols denote the T1 observations		
	trim−kh07intgraded36	
Alkyon Hydraulic Consultancy & Research	A2273	Fig. 2.36

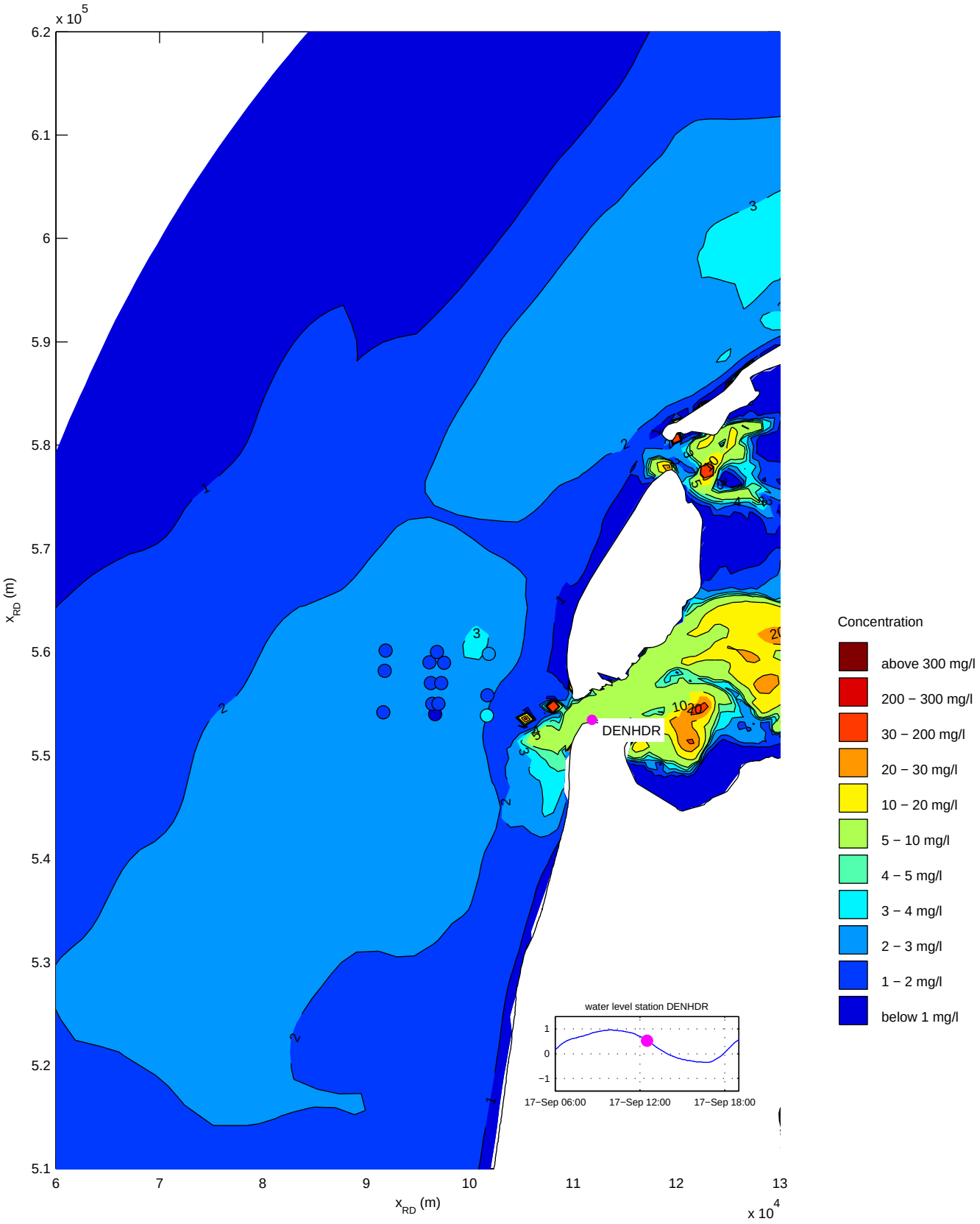

Simulated silt concentrations (mg/l) date and time: 17−Sep−2007 12:30:00 coloured symbols denote the T1 observations		
	trim−kh07intgraded36	
Alkyon Hydraulic Consultancy & Research	A2273	Fig. 2.37

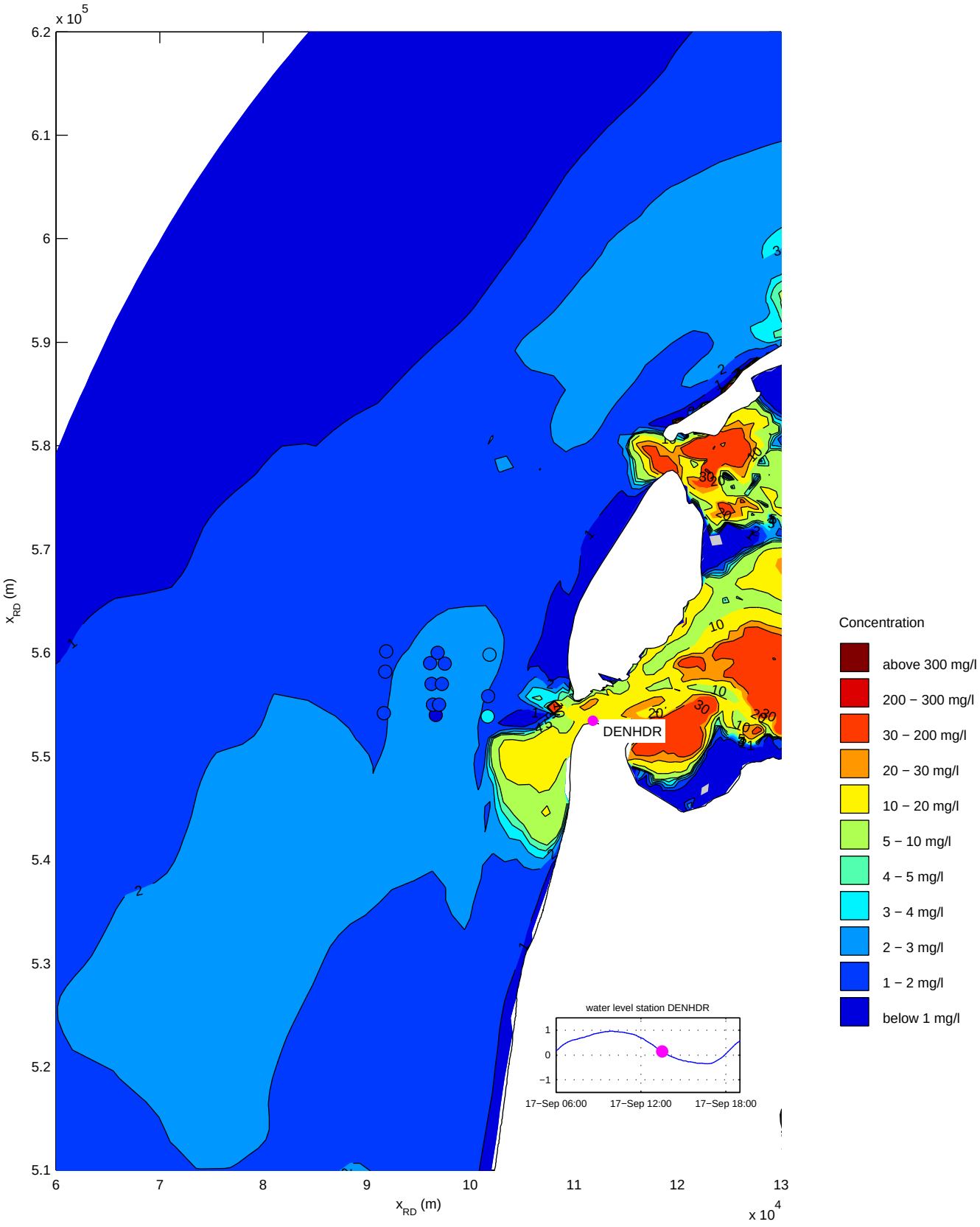

Simulated silt concentrations (mg/l) date and time: 17−Sep−2007 13:30:00 coloured symbols denote the T1 observations		
	trim−kh07intgraded36	
Alkyon Hydraulic Consultancy & Research	A2273	Fig. 2.38

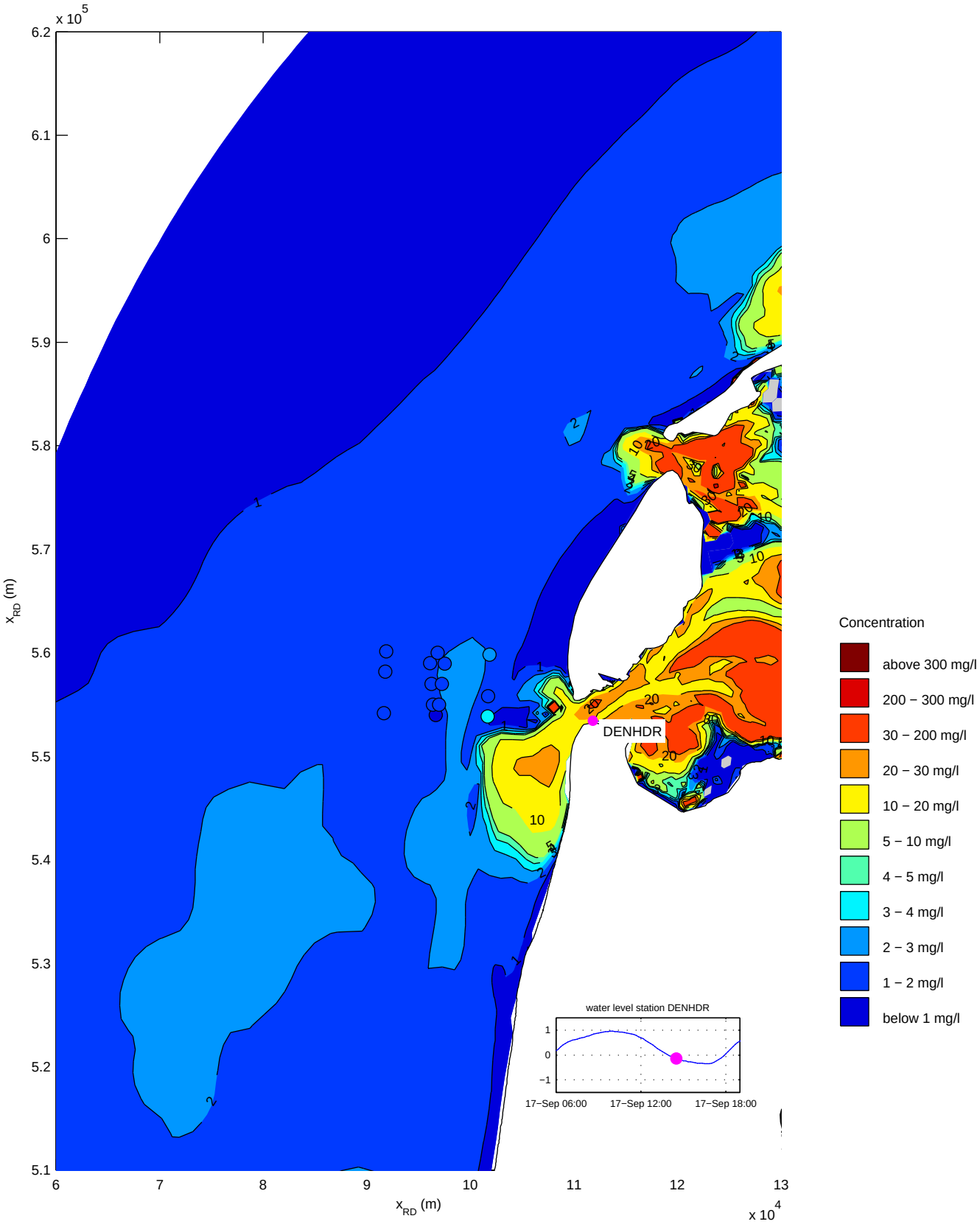

Simulated silt concentrations (mg/l) date and time: 17−Sep−2007 14:30:00 coloured symbols denote the T1 observations		
	trim−kh07intgraded36	
Alkyon Hydraulic Consultancy & Research	A2273	Fig. 2.39

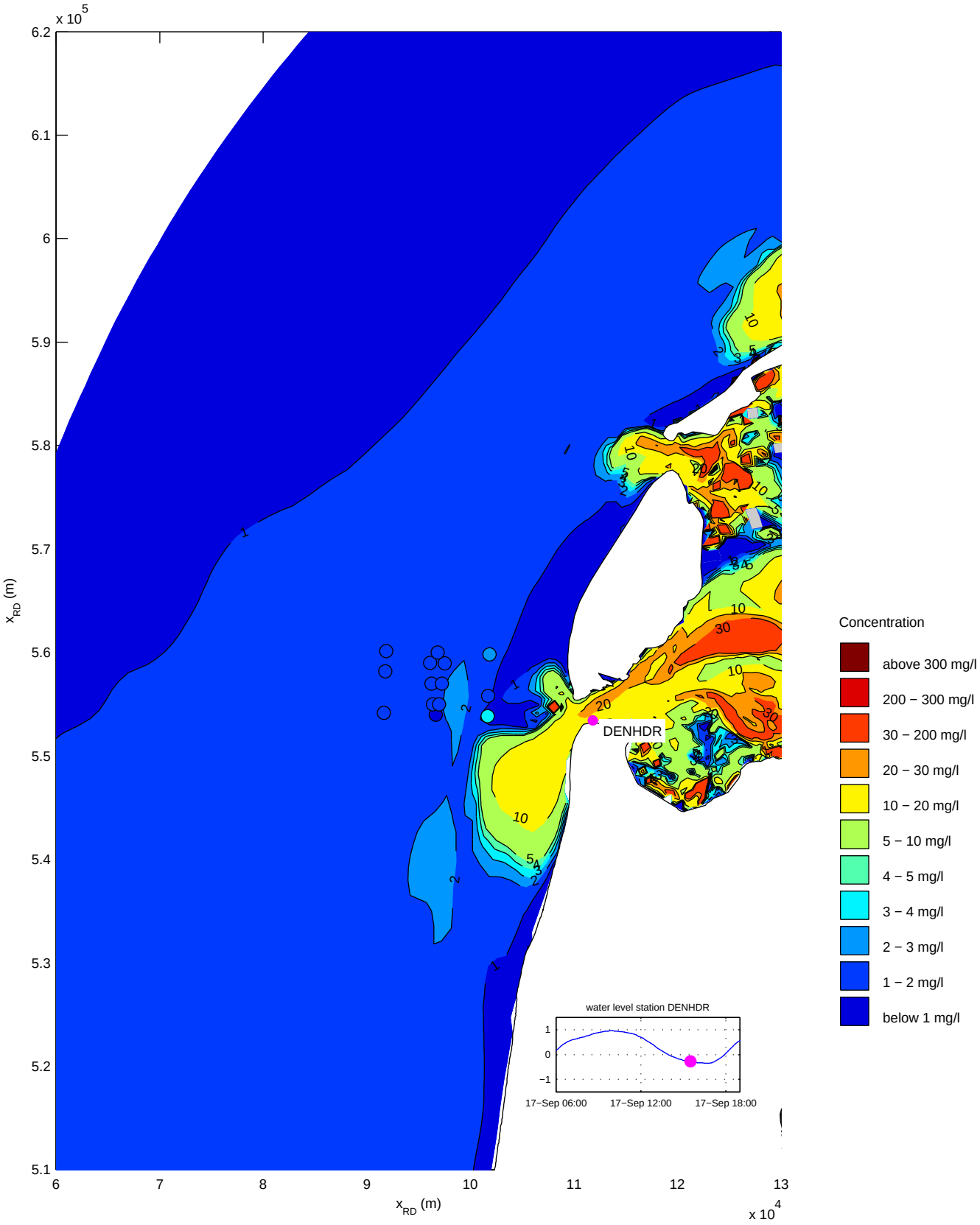

Simulated silt concentrations (mg/l) date and time: 17−Sep−2007 15:30:00 coloured symbols denote the T1 observations		
	trim−kh07intgraded36	
Alkyon Hydraulic Consultancy & Research	A2273	Fig. 2.40

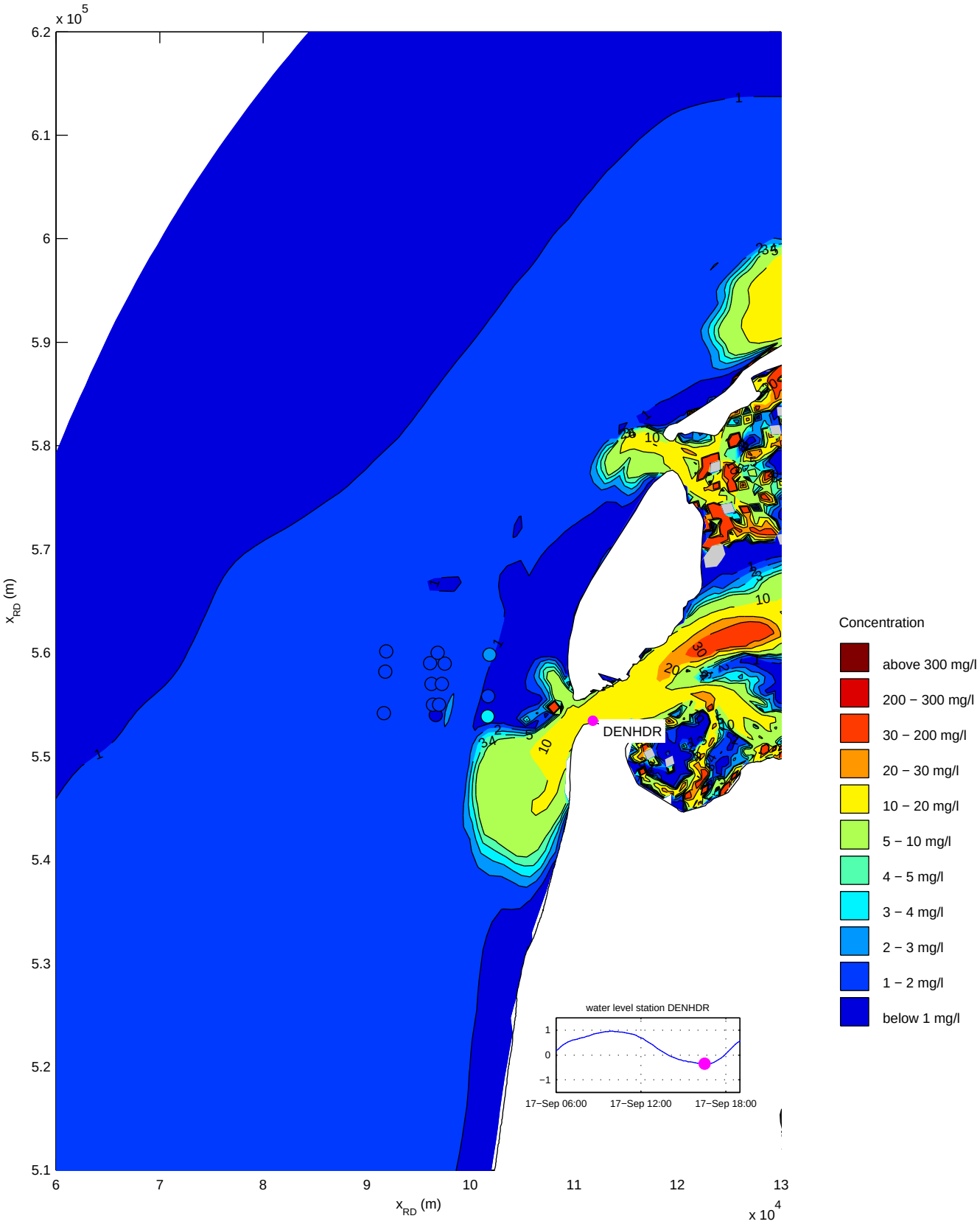

Simulated silt concentrations (mg/l) date and time: 17−Sep−2007 16:30:00 coloured symbols denote the T1 observations		
	trim−kh07intgraded36	
Alkyon Hydraulic Consultancy & Research	A2273	Fig. 2.41

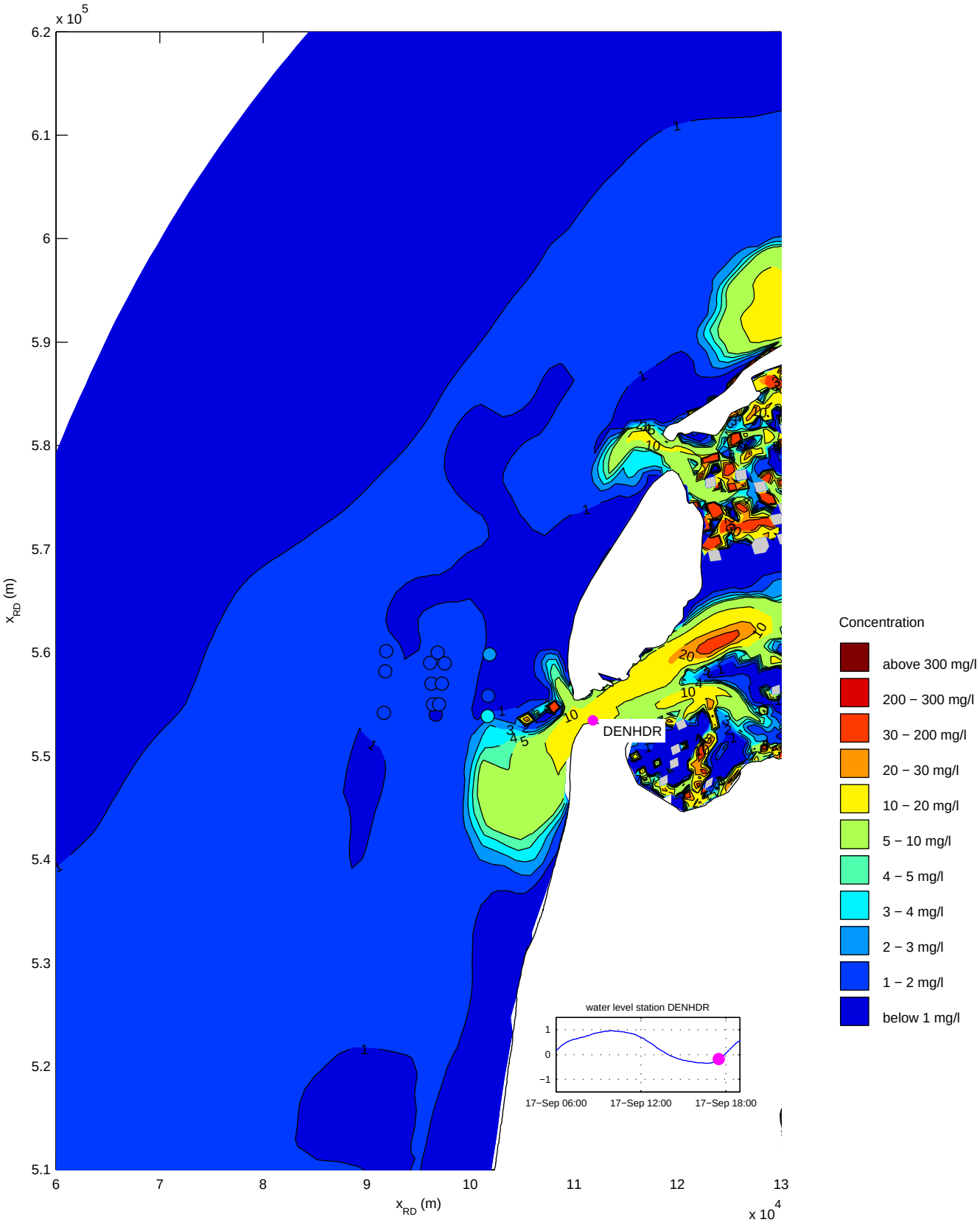

Simulated silt concentrations (mg/l) date and time: 17−Sep−2007 17:30:00 coloured symbols denote the T1 observations		
	trim−kh07intgraded36	
Alkyon Hydraulic Consultancy & Research	A2273	Fig. 2.42

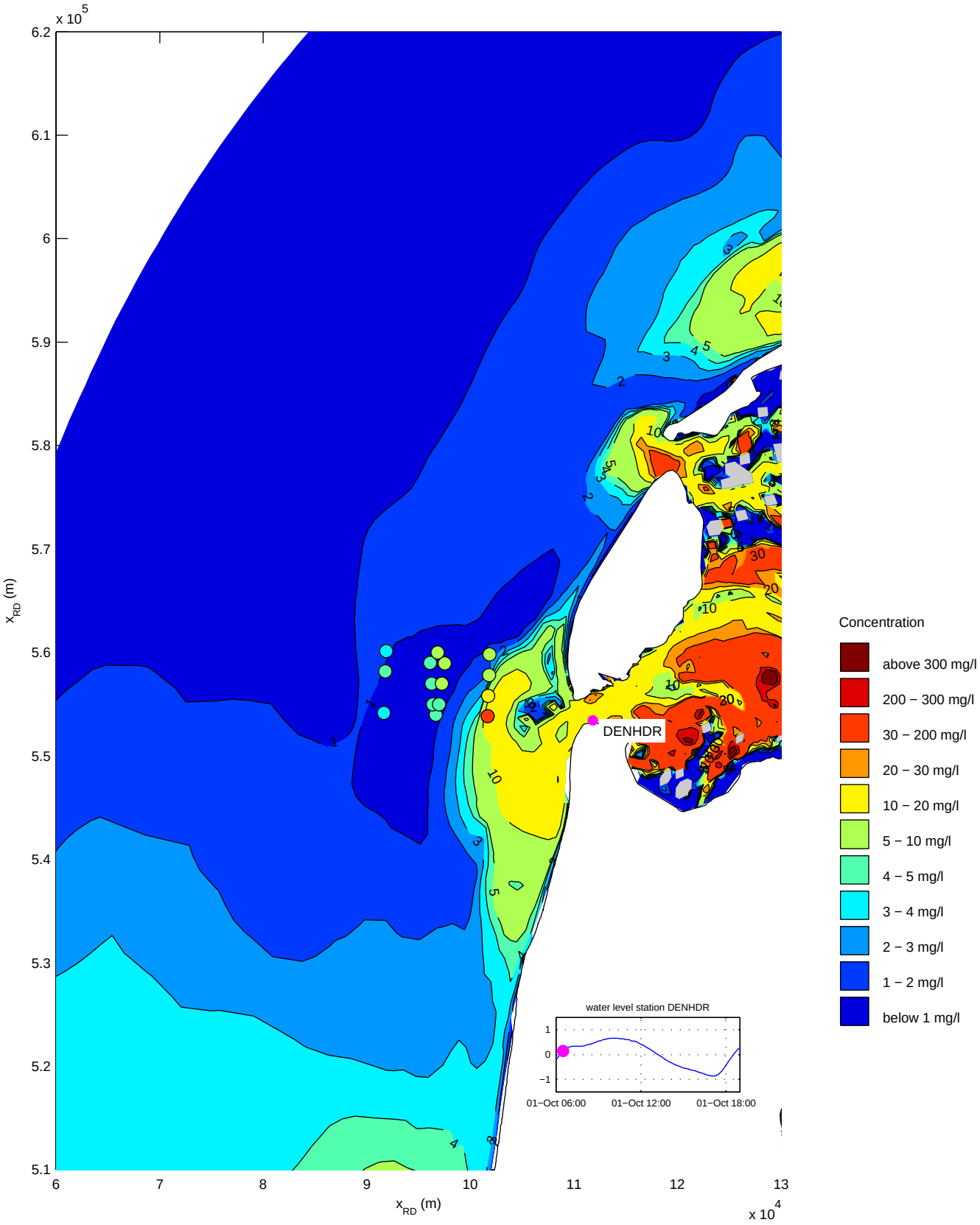

Simulated silt concentrations (mg/l) date and time: 01−Oct−2007 06:30:00 coloured symbols denote the T1 observations		
	trim−kh07intgraded36	
Alkyon Hydraulic Consultancy & Research	A2273	Fig. 2.43

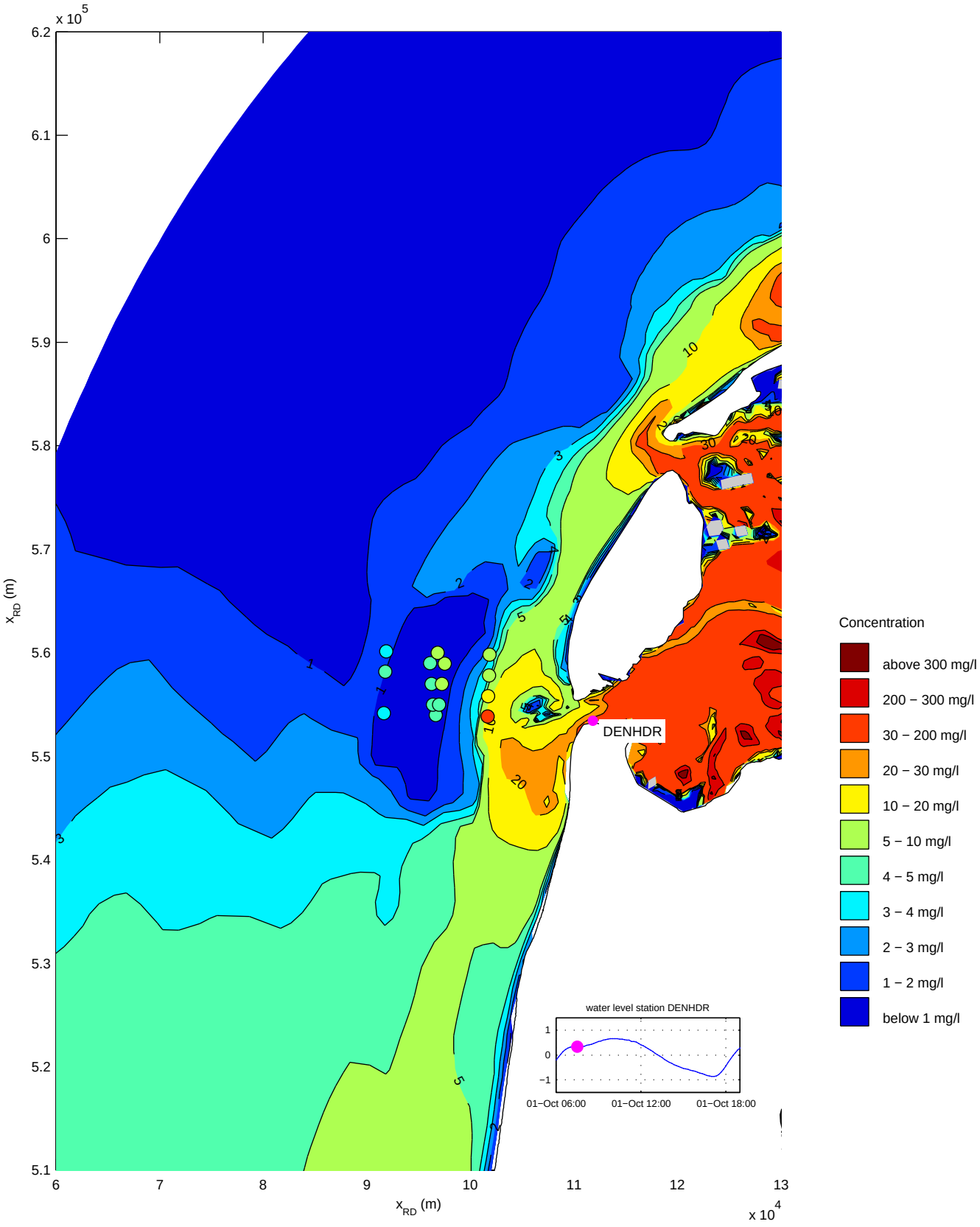

Simulated silt concentrations (mg/l) date and time: 01−Oct−2007 07:30:00 coloured symbols denote the T1 observations		
	trim−kh07intgraded36	
Alkyon Hydraulic Consultancy & Research	A2273	Fig. 2.44

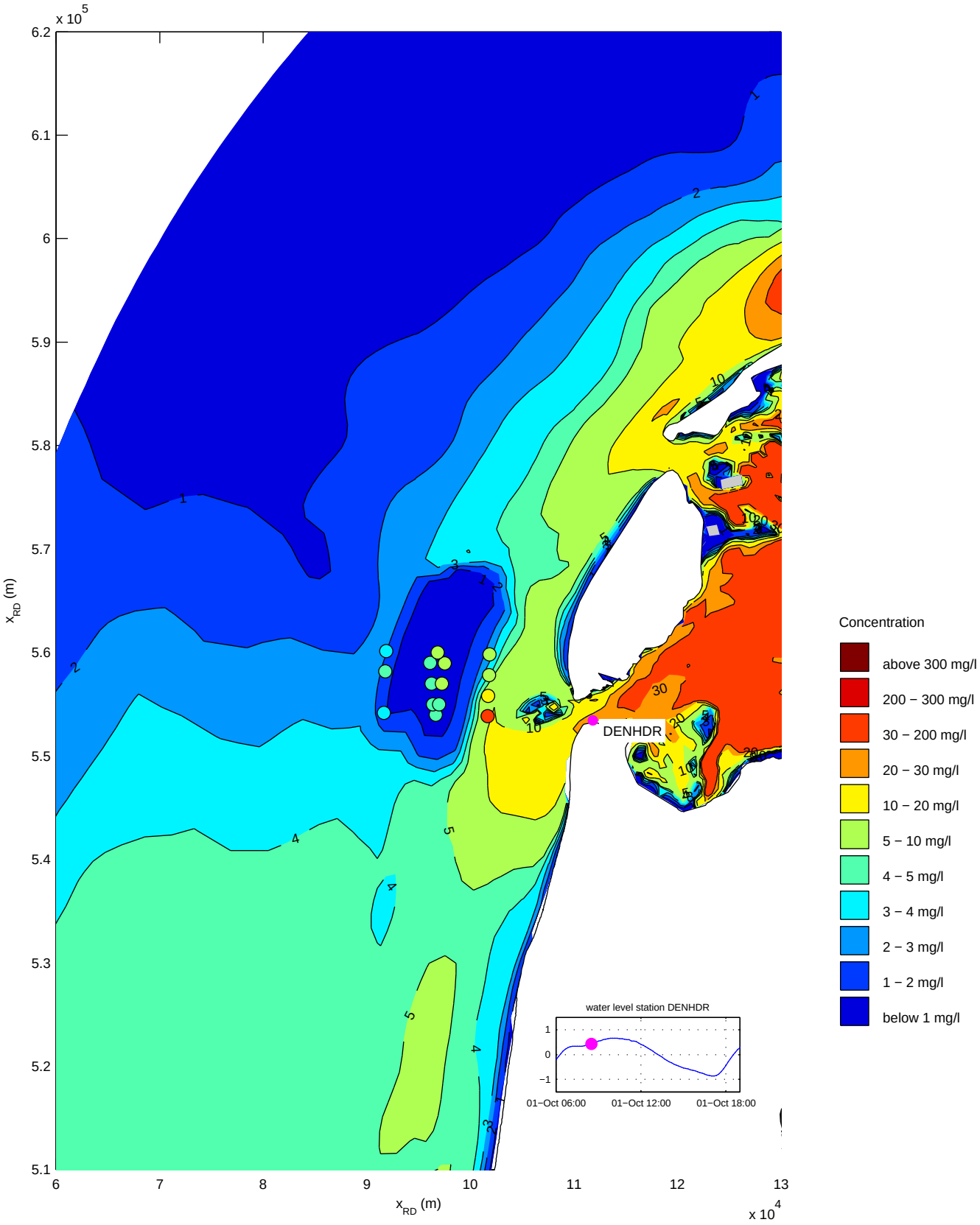

Simulated silt concentrations (mg/l) date and time: 01−Oct−2007 08:30:00 coloured symbols denote the T1 observations		
	trim−kh07intgraded36	
Alkyon Hydraulic Consultancy & Research	A2273	Fig. 2.45

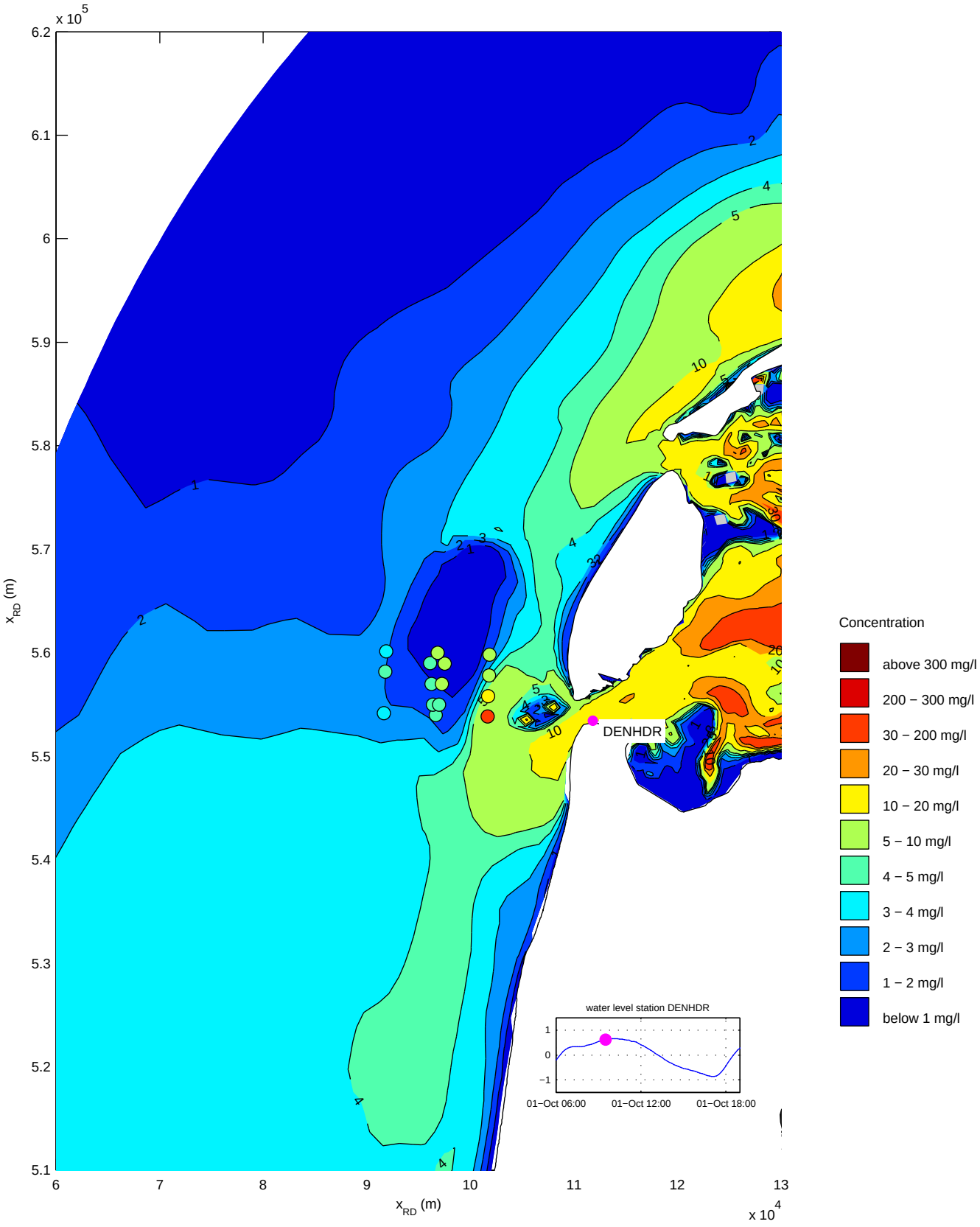

Simulated silt concentrations (mg/l) date and time: 01−Oct−2007 09:30:00 coloured symbols denote the T1 observations		
	trim−kh07intgraded36	
Alkyon Hydraulic Consultancy & Research	A2273	Fig. 2.46

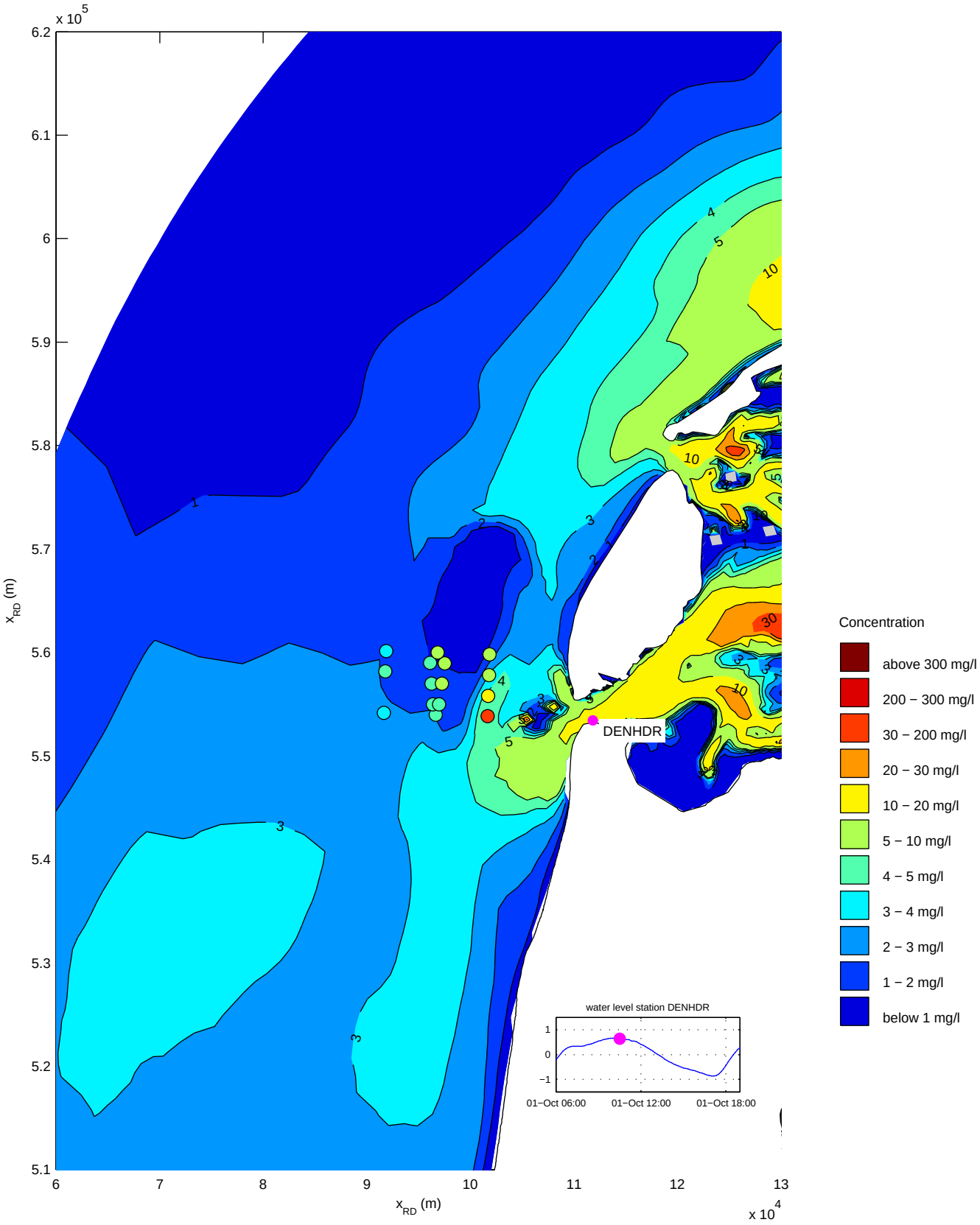

Simulated silt concentrations (mg/l) date and time: 01−Oct−2007 10:30:00 coloured symbols denote the T1 observations		
	trim−kh07intgraded36	
Alkyon Hydraulic Consultancy & Research	A2273	Fig. 2.47

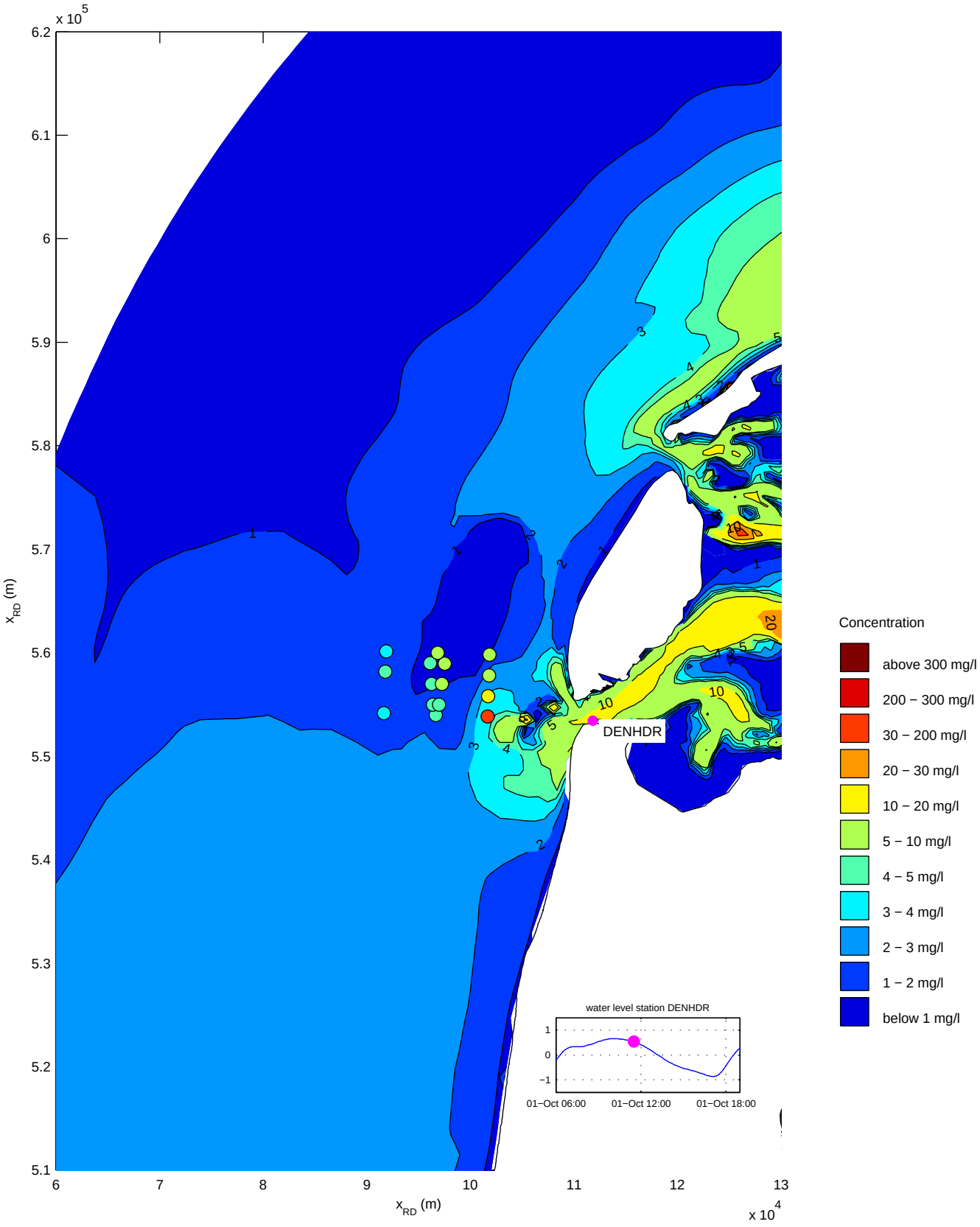

Simulated silt concentrations (mg/l) date and time: 01−Oct−2007 11:30:00 coloured symbols denote the T1 observations		
	trim−kh07intgraded36	
Alkyon Hydraulic Consultancy & Research	A2273	Fig. 2.48

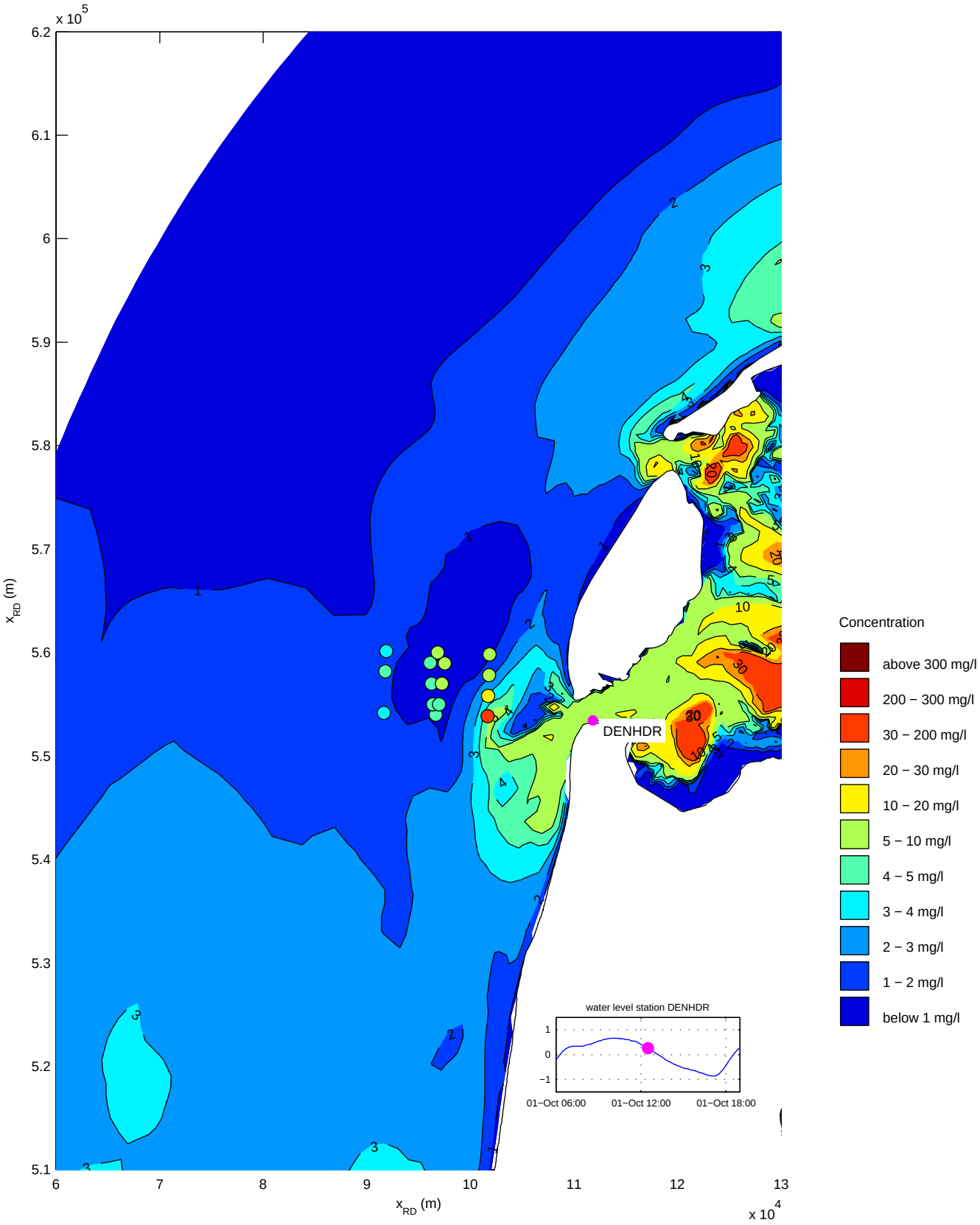

Simulated silt concentrations (mg/l) date and time: 01−Oct−2007 12:30:00 coloured symbols denote the T1 observations		
	trim−kh07intgraded36	
Alkyon Hydraulic Consultancy & Research	A2273	Fig. 2.49

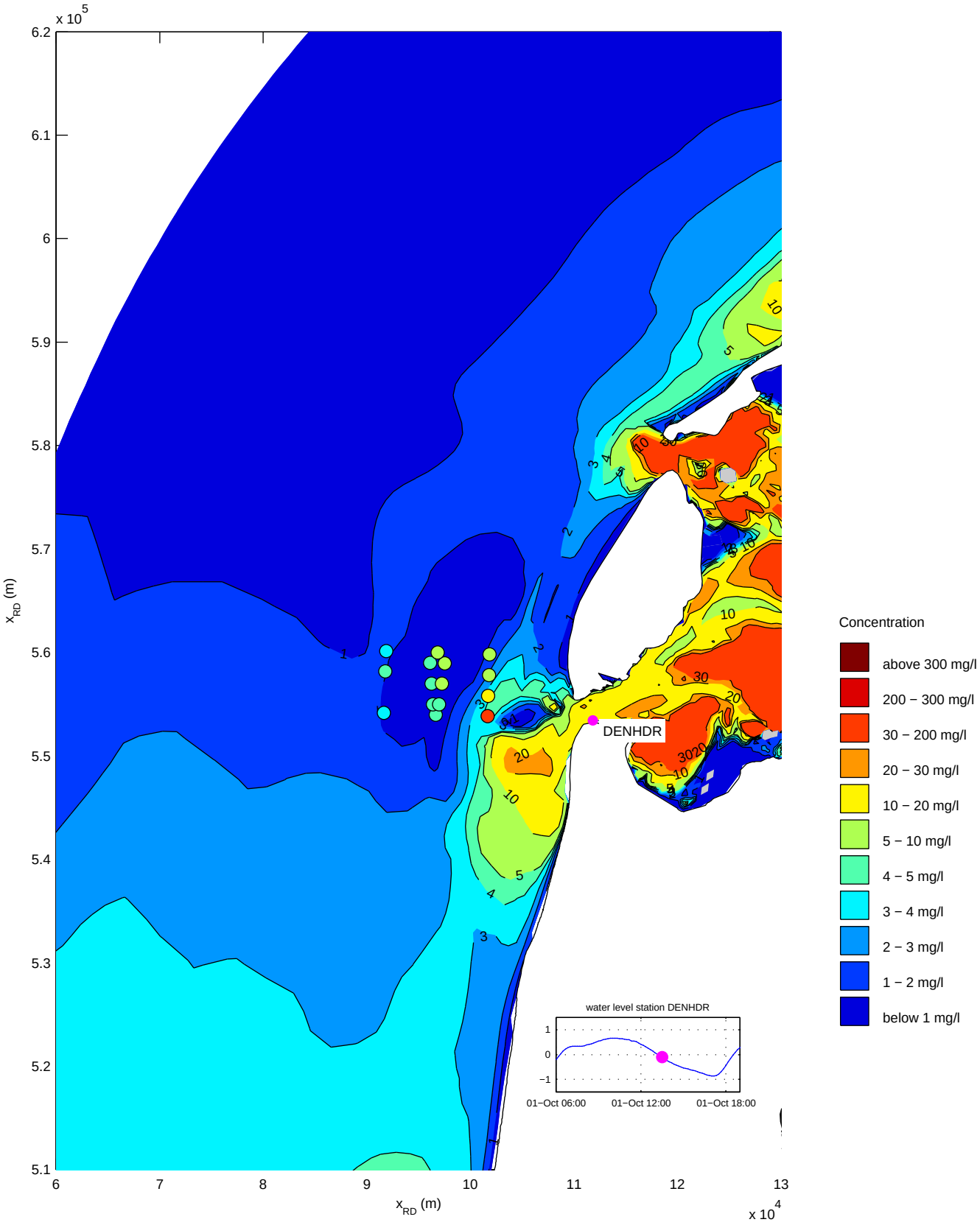

Simulated silt concentrations (mg/l) date and time: 01−Oct−2007 13:30:00 coloured symbols denote the T1 observations		
	trim−kh07intgraded36	
Alkyon Hydraulic Consultancy & Research	A2273	Fig. 2.50

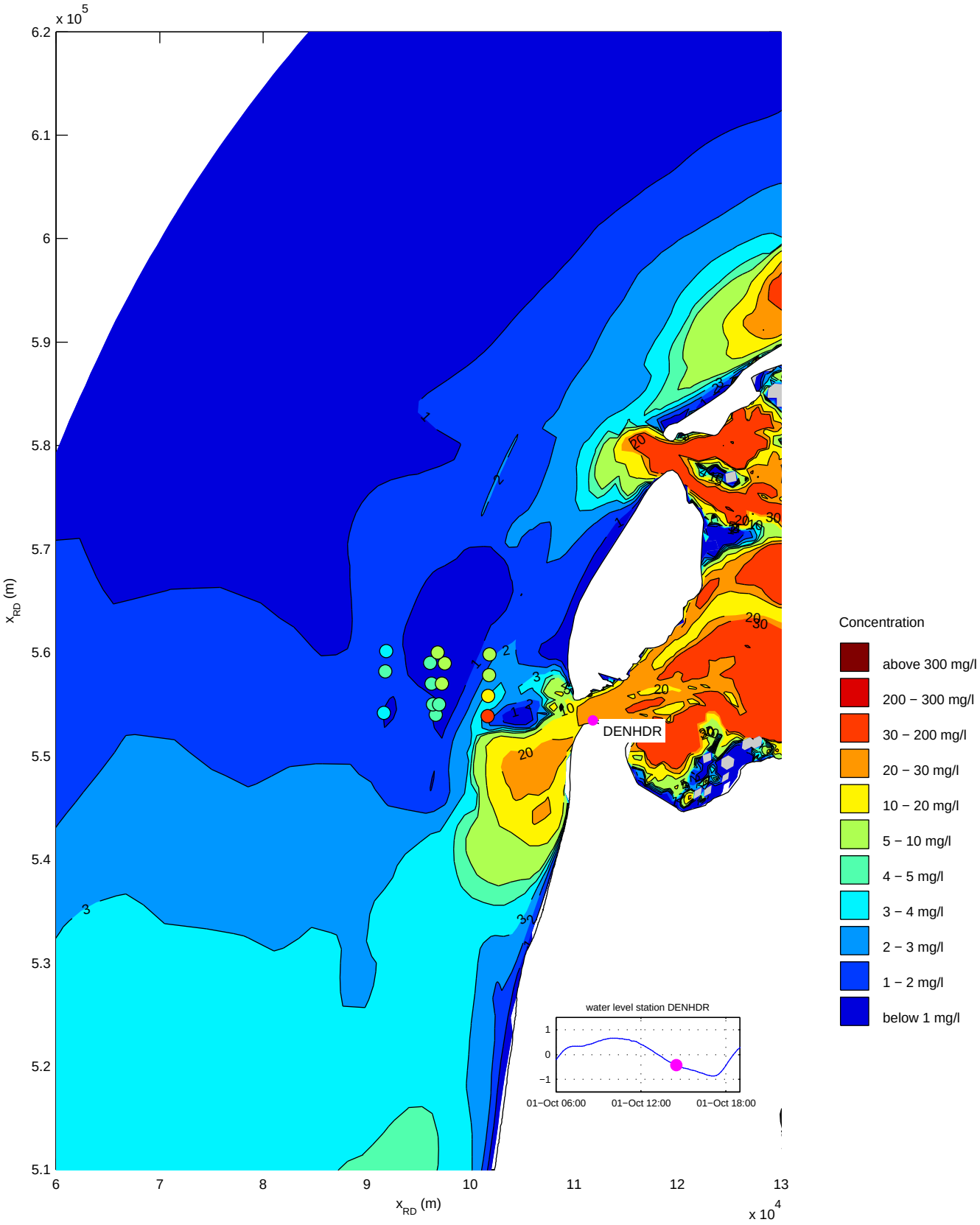

Simulated silt concentrations (mg/l) date and time: 01−Oct−2007 14:30:00 coloured symbols denote the T1 observations		
	trim−kh07intgraded36	
Alkyon Hydraulic Consultancy & Research	A2273	Fig. 2.51

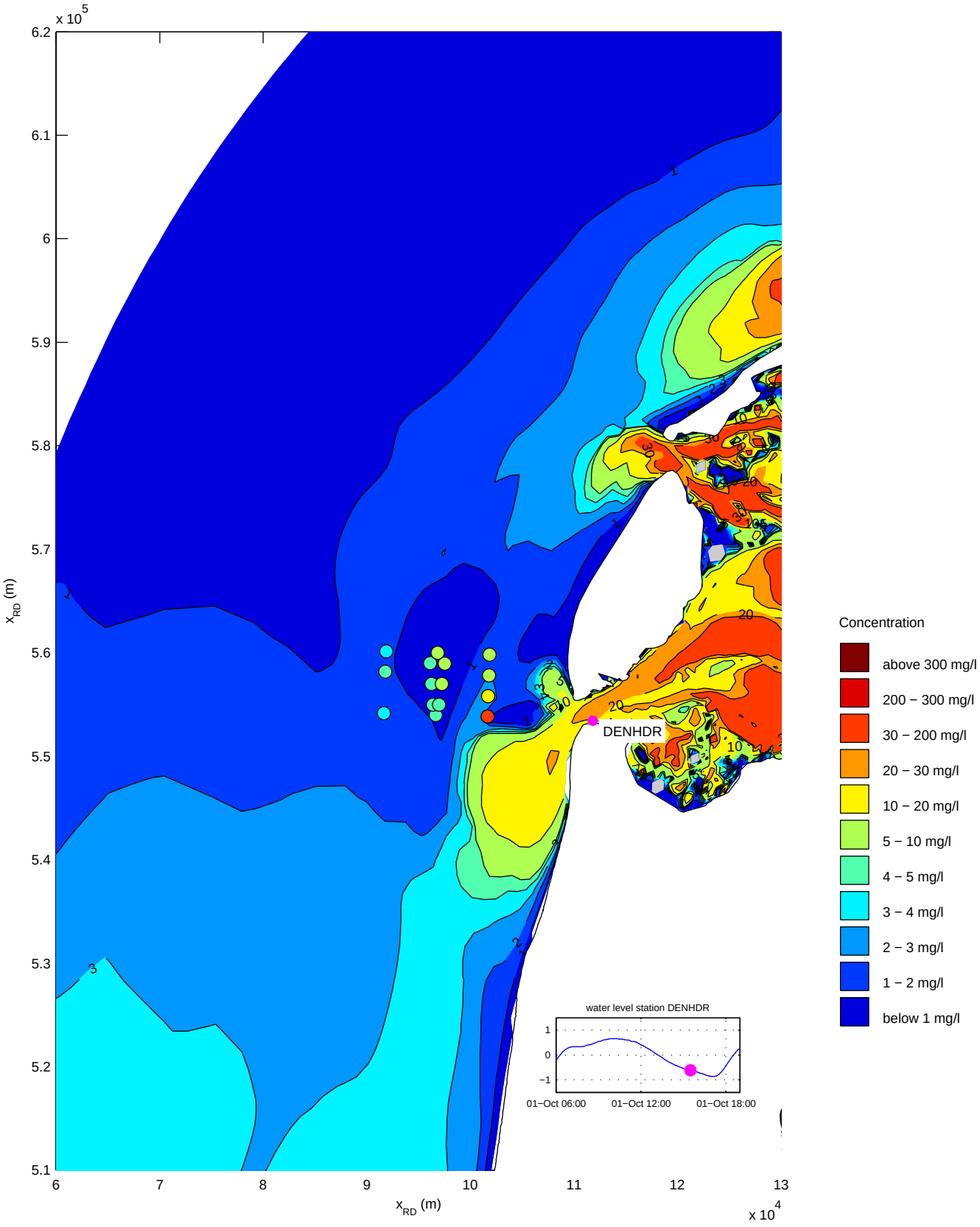

Simulated silt concentrations (mg/l) date and time: 01−Oct−2007 15:30:00 coloured symbols denote the T1 observations		
	trim−kh07intgraded36	
Alkyon Hydraulic Consultancy & Research	A2273	Fig. 2.52

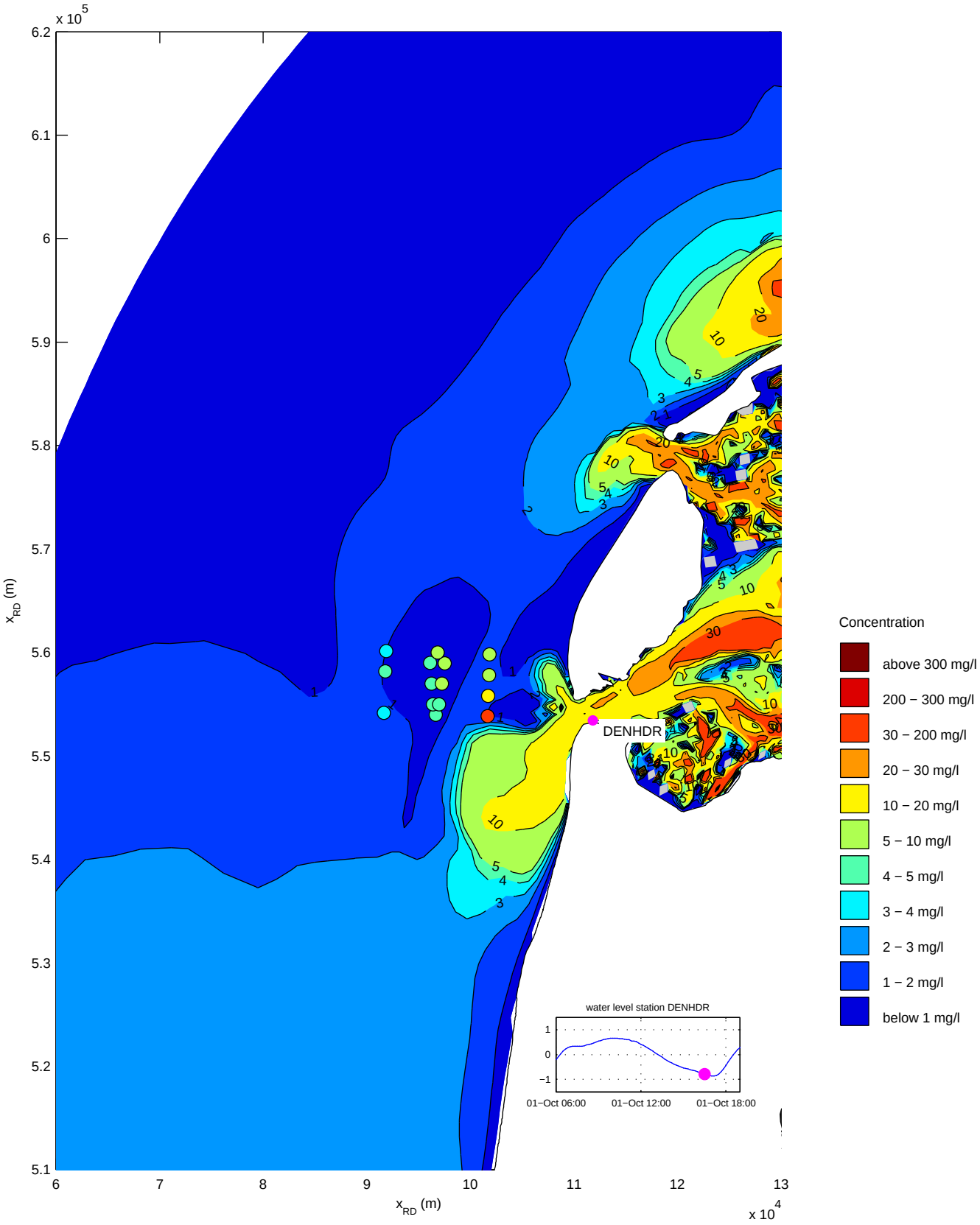

Simulated silt concentrations (mg/l) date and time: 01−Oct−2007 16:30:00 coloured symbols denote the T1 observations		
	trim−kh07intgraded36	
Alkyon Hydraulic Consultancy & Research	A2273	Fig. 2.53

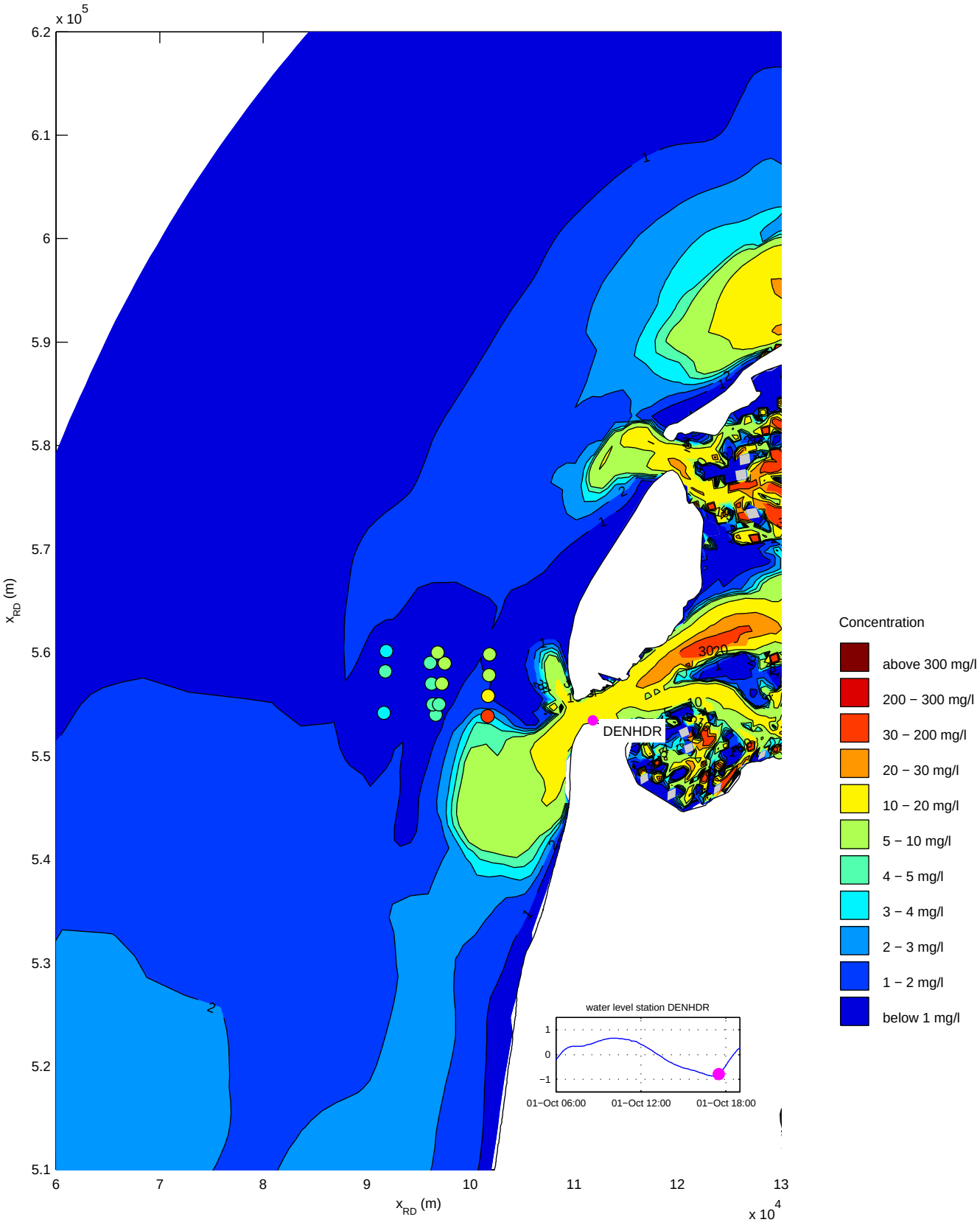

Simulated silt concentrations (mg/l) date and time: 01−Oct−2007 17:30:00 coloured symbols denote the T1 observations		
	trim−kh07intgraded36	
Alkyon Hydraulic Consultancy & Research	A2273	Fig. 2.54

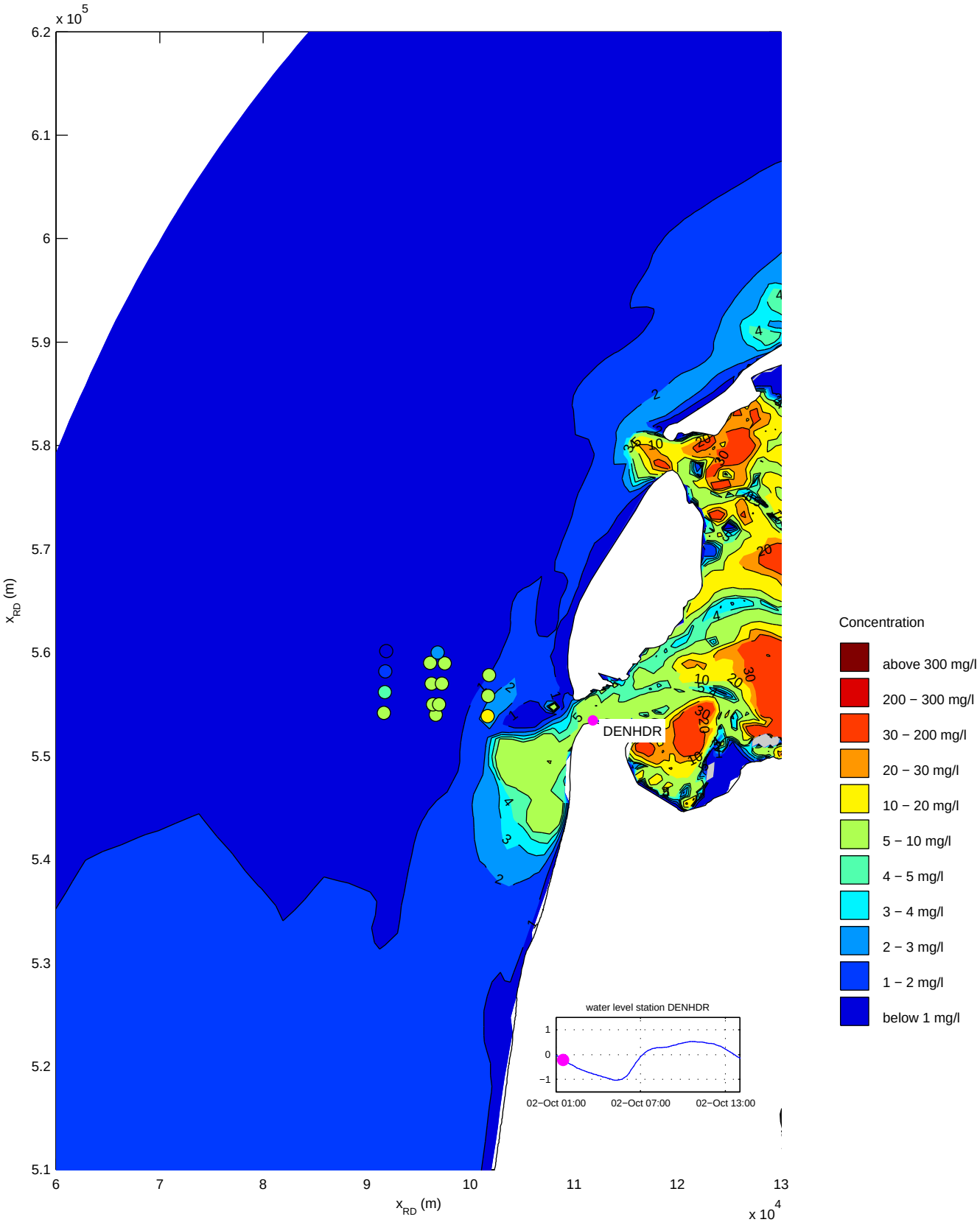

Simulated silt concentrations (mg/l) date and time: 02−Oct−2007 01:30:00 coloured symbols denote the T1 observations		
	trim−kh07intgraded36	
Alkyon Hydraulic Consultancy & Research	A2273	Fig. 2.55

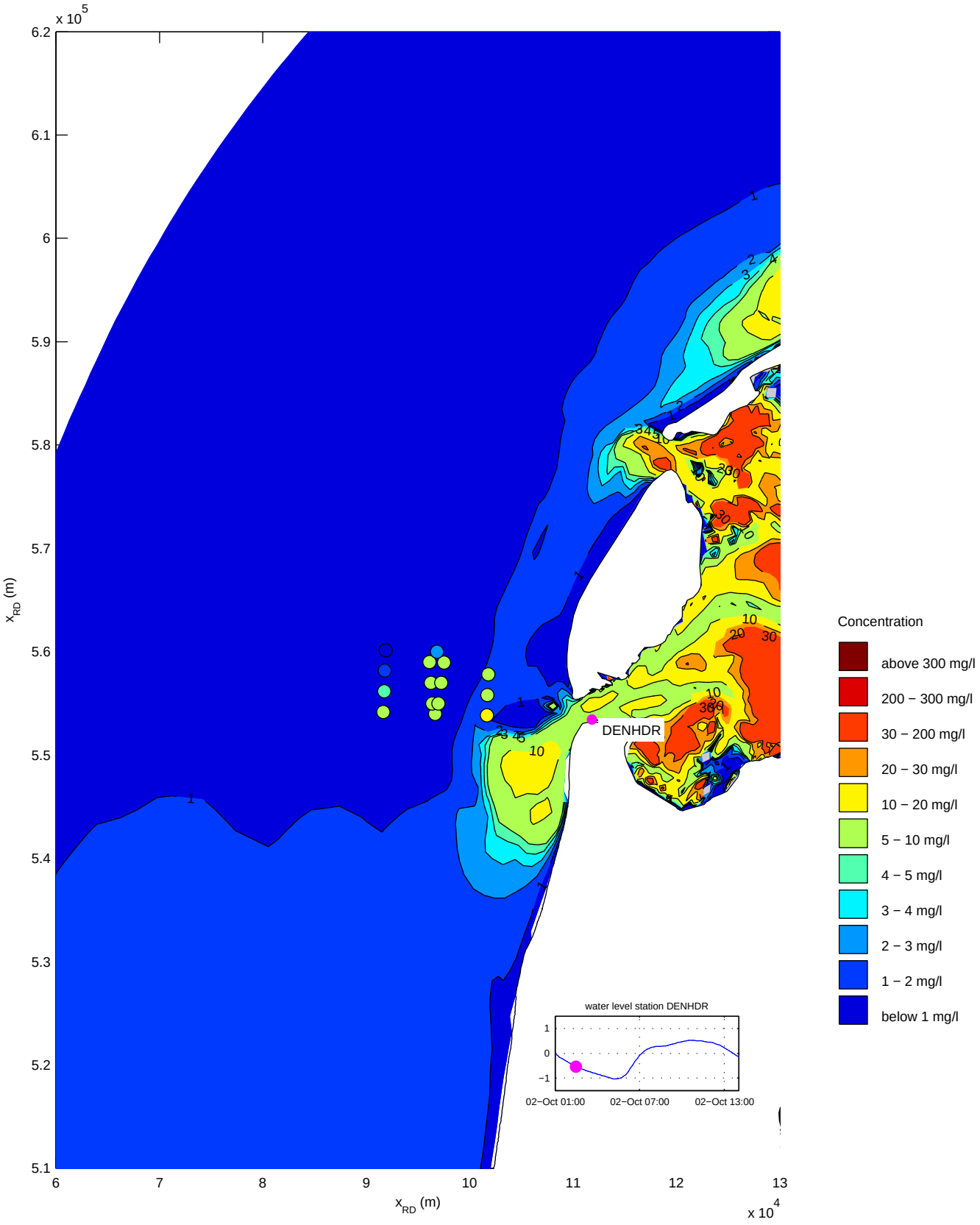

Simulated silt concentrations (mg/l) date and time: 02−Oct−2007 02:30:00 coloured symbols denote the T1 observations		
	trim−kh07intgraded36	
Alkyon Hydraulic Consultancy & Research	A2273	Fig. 2.56

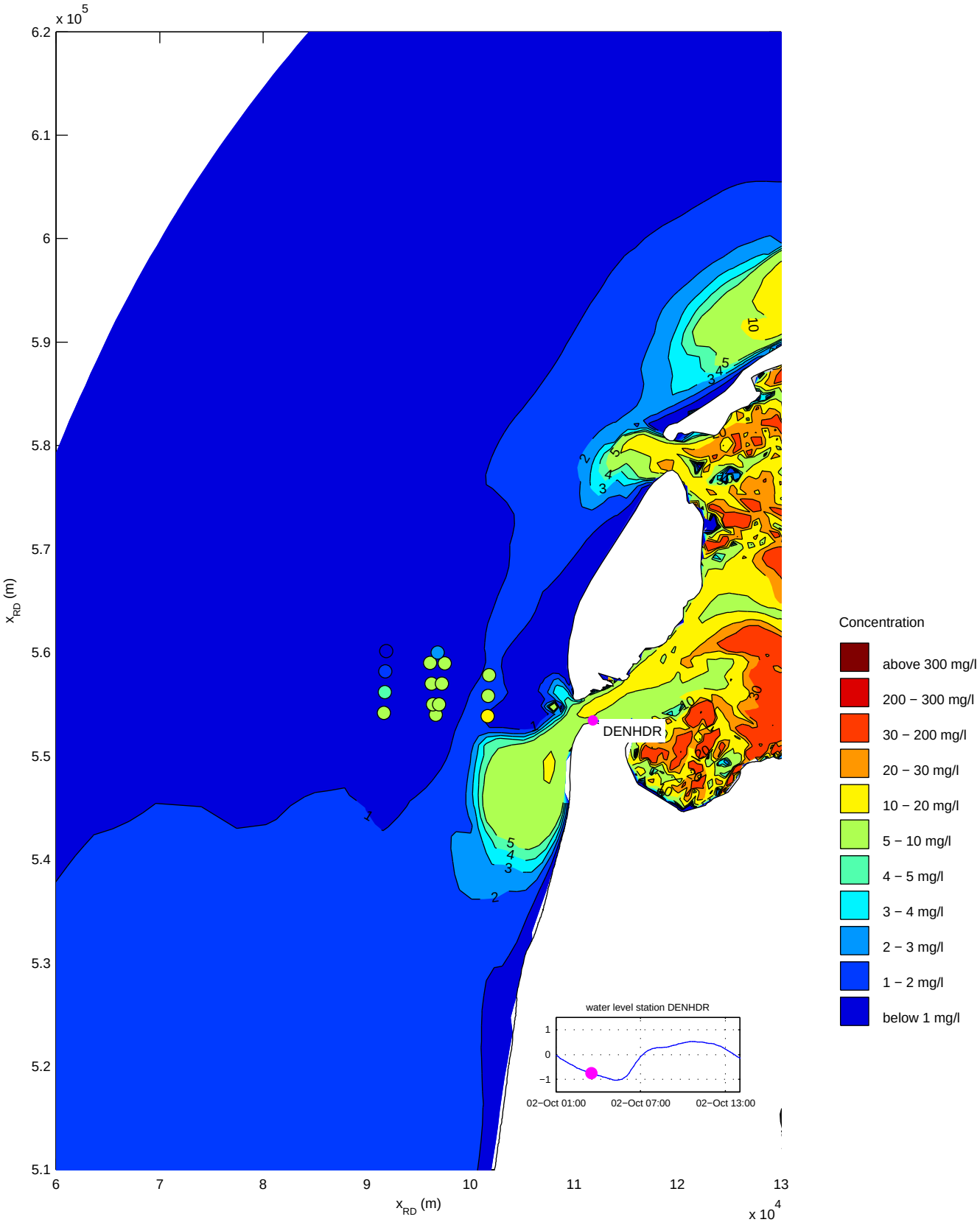

Simulated silt concentrations (mg/l) date and time: 02−Oct−2007 03:30:00 coloured symbols denote the T1 observations		
	trim−kh07intgraded36	
Alkyon Hydraulic Consultancy & Research	A2273	Fig. 2.57

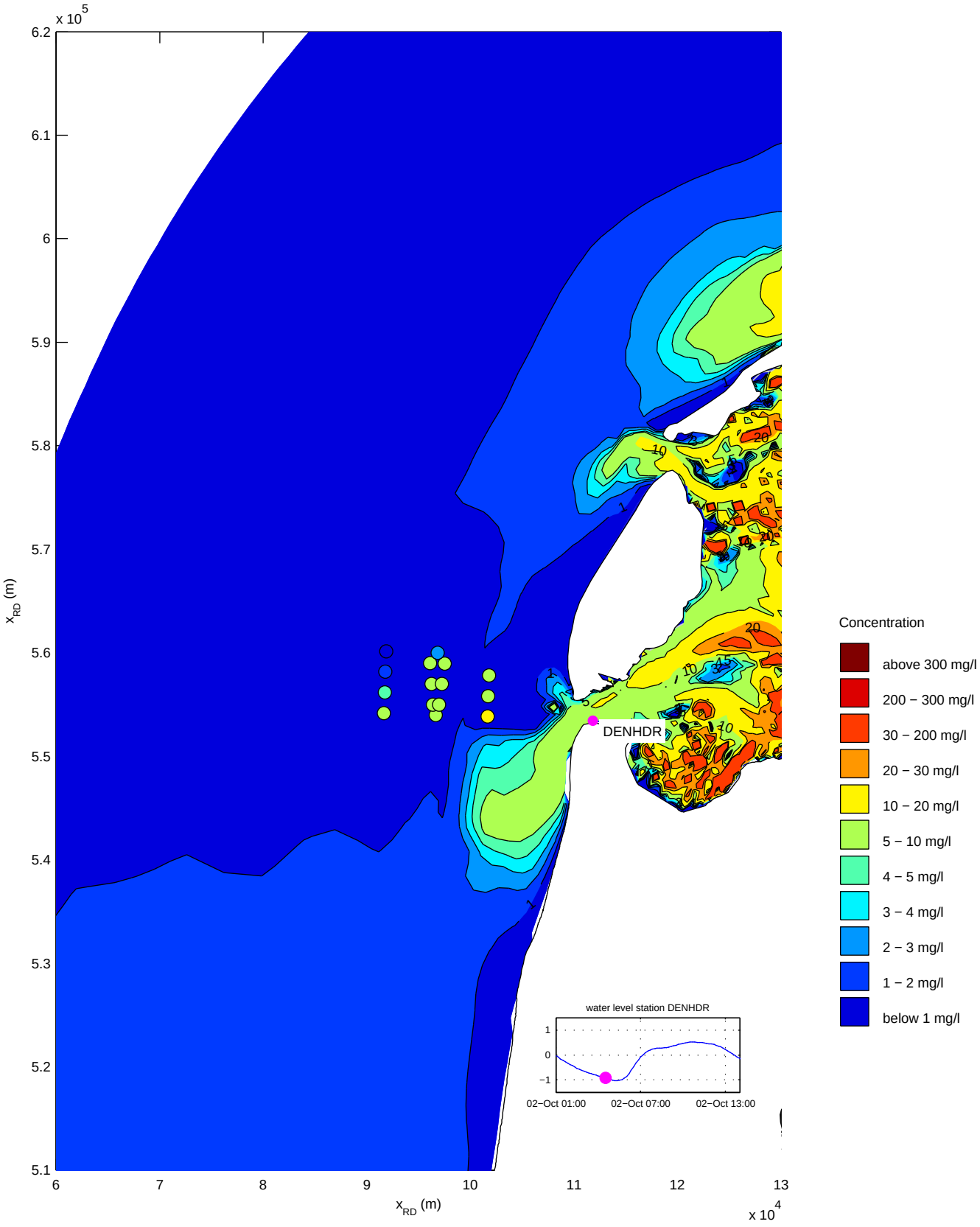

Simulated silt concentrations (mg/l) date and time: 02−Oct−2007 04:30:00 coloured symbols denote the T1 observations		
	trim−kh07intgraded36	
Alkyon Hydraulic Consultancy & Research	A2273	Fig. 2.58

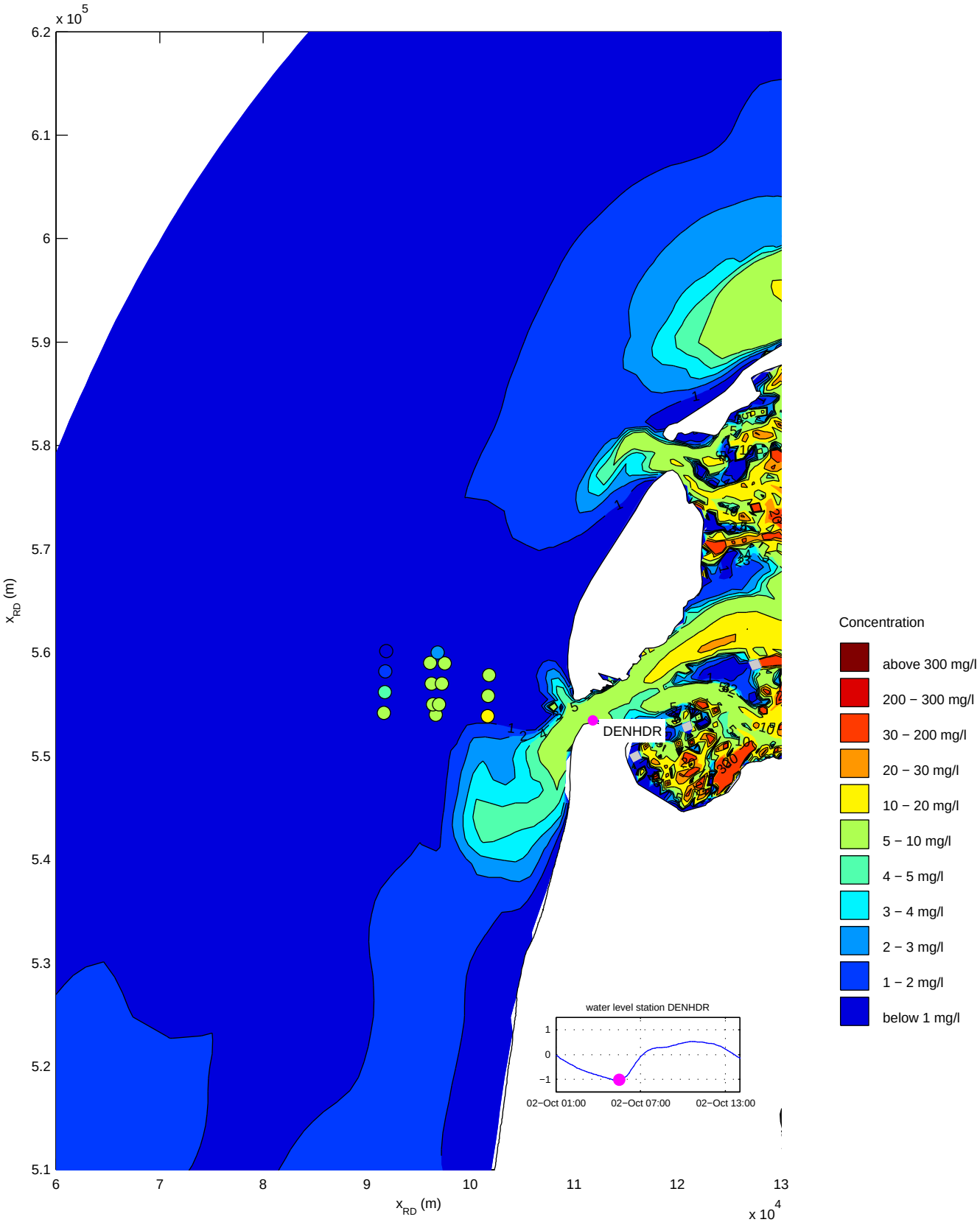

Simulated silt concentrations (mg/l) date and time: 02−Oct−2007 05:30:00 coloured symbols denote the T1 observations		
	trim−kh07intgraded36	
Alkyon Hydraulic Consultancy & Research	A2273	Fig. 2.59

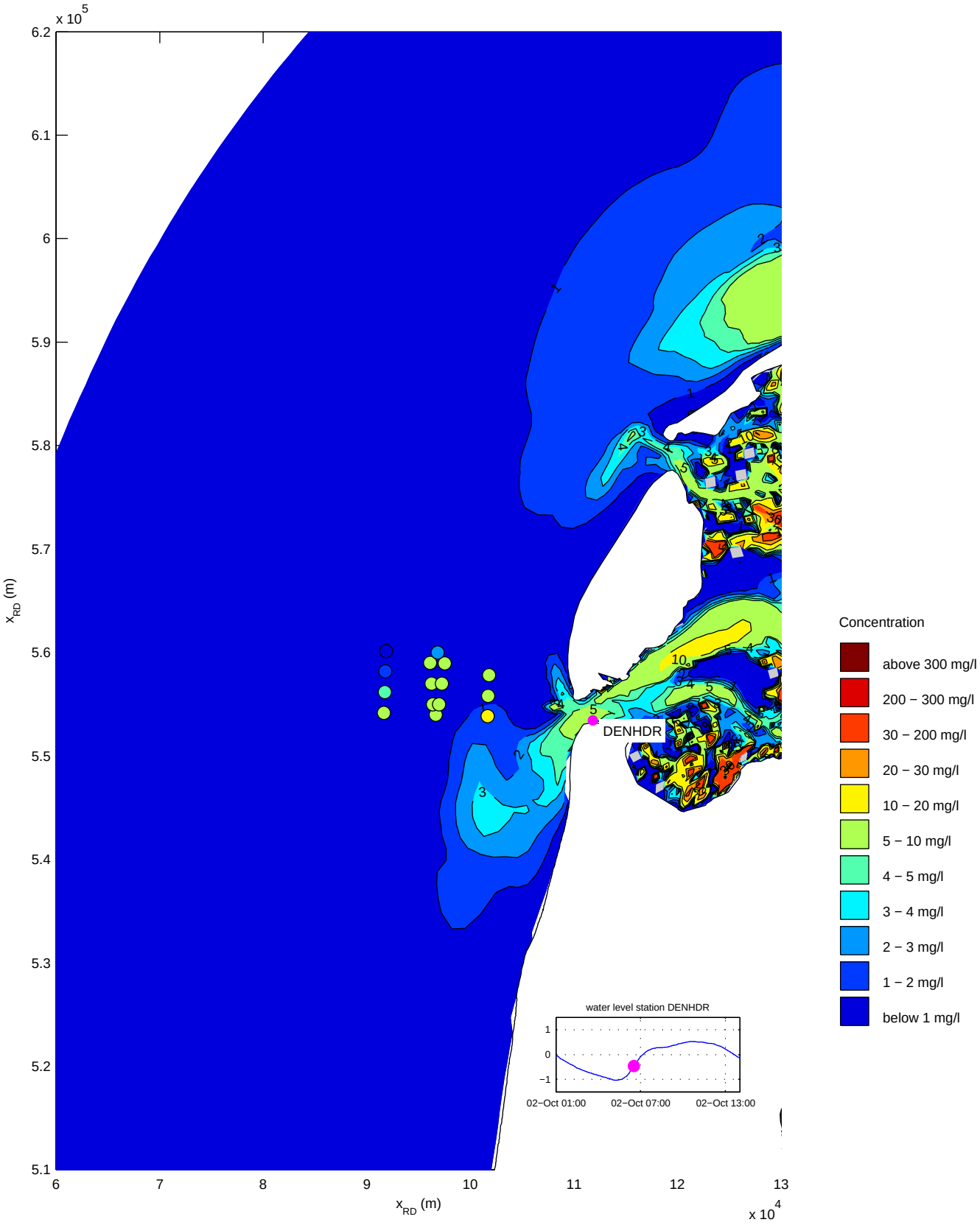

Simulated silt concentrations (mg/l) date and time: 02−Oct−2007 06:30:00 coloured symbols denote the T1 observations		
	trim−kh07intgraded36	
Alkyon Hydraulic Consultancy & Research	A2273	Fig. 2.60

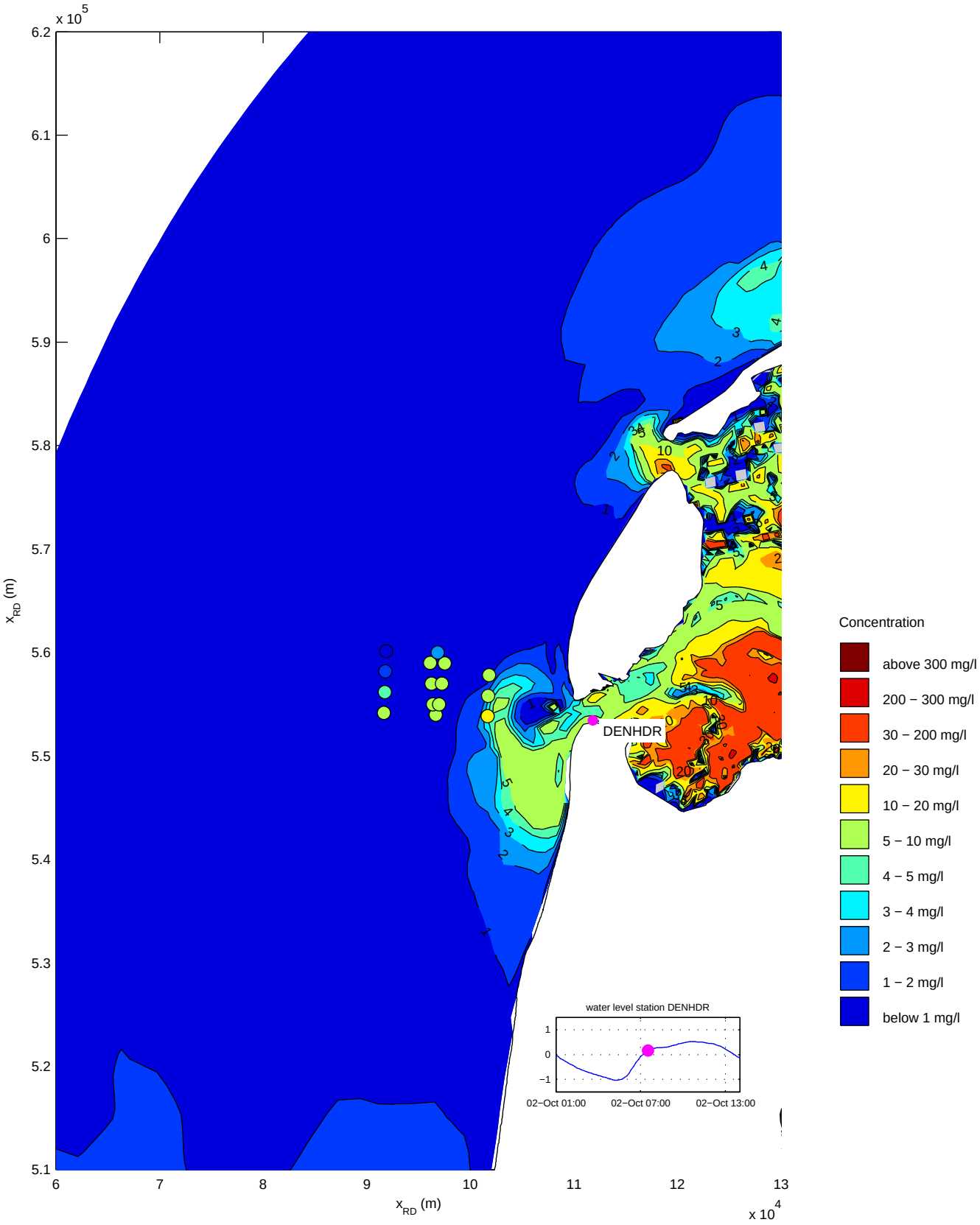

Simulated silt concentrations (mg/l) date and time: 02−Oct−2007 07:30:00 coloured symbols denote the T1 observations		
	trim−kh07intgraded36	
Alkyon Hydraulic Consultancy & Research	A2273	Fig. 2.61

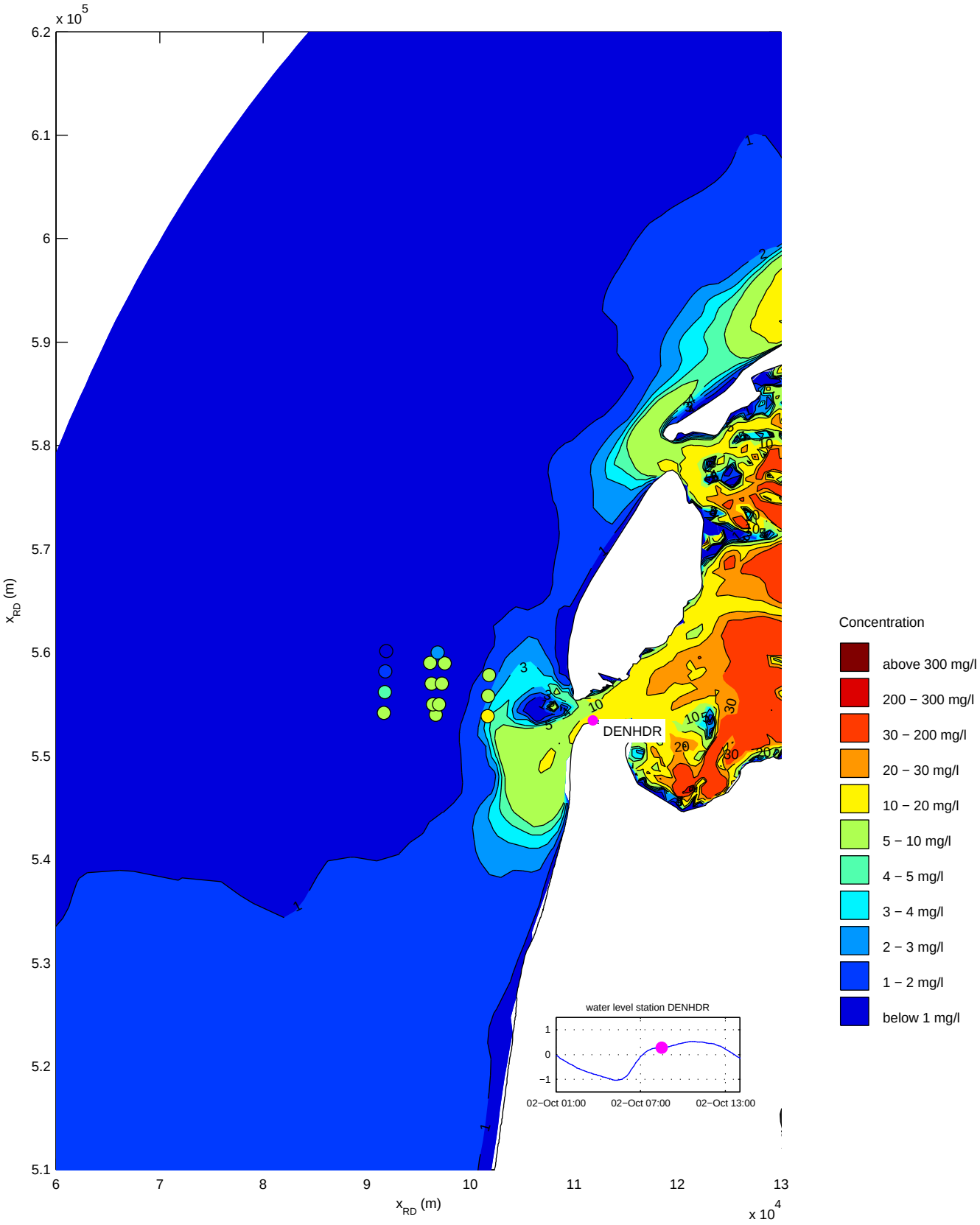

Simulated silt concentrations (mg/l) date and time: 02−Oct−2007 08:30:00 coloured symbols denote the T1 observations		
	trim−kh07intgraded36	
Alkyon Hydraulic Consultancy & Research	A2273	Fig. 2.62

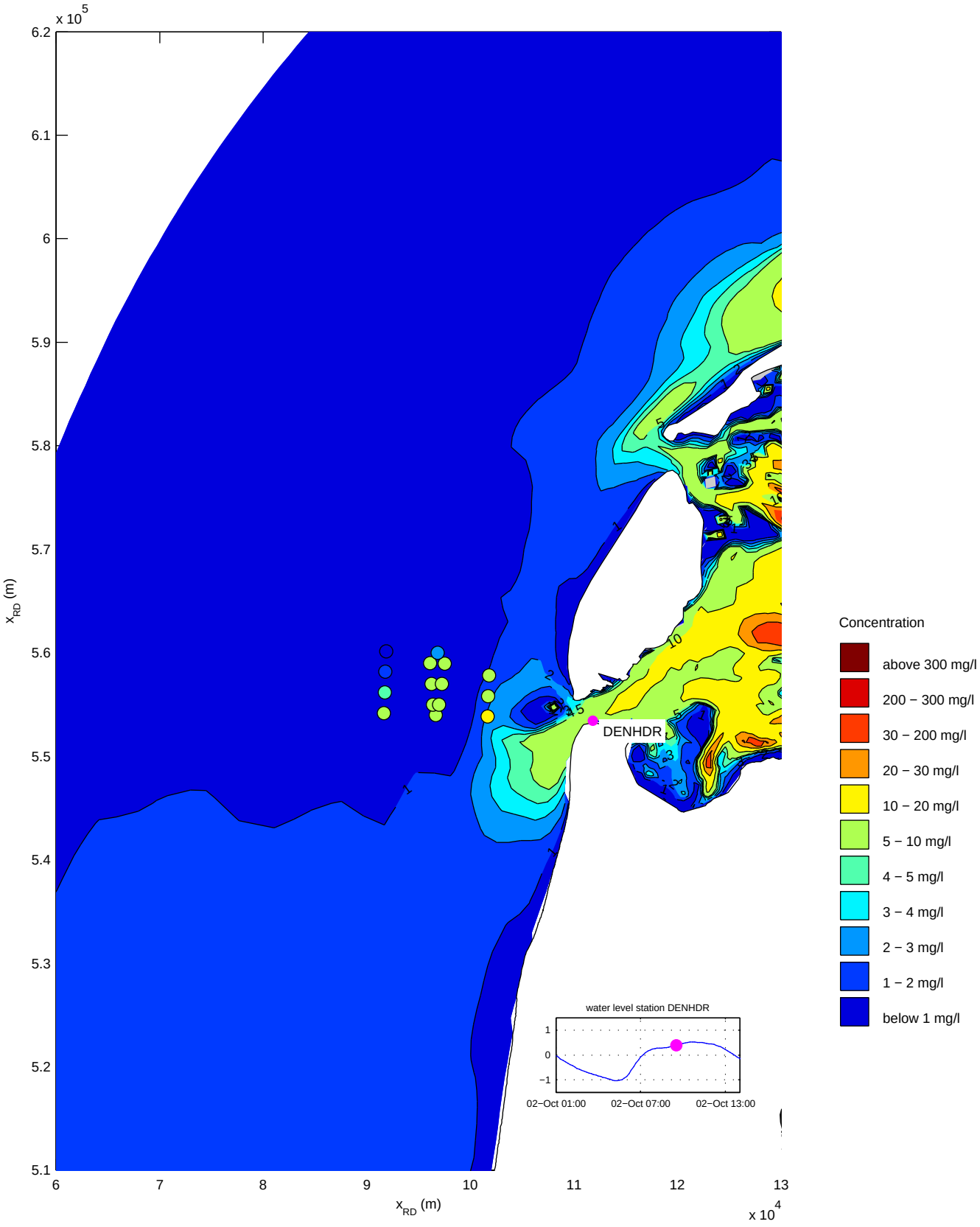

Simulated silt concentrations (mg/l) date and time: 02−Oct−2007 09:30:00 coloured symbols denote the T1 observations		
	trim−kh07intgraded36	
Alkyon Hydraulic Consultancy & Research	A2273	Fig. 2.63

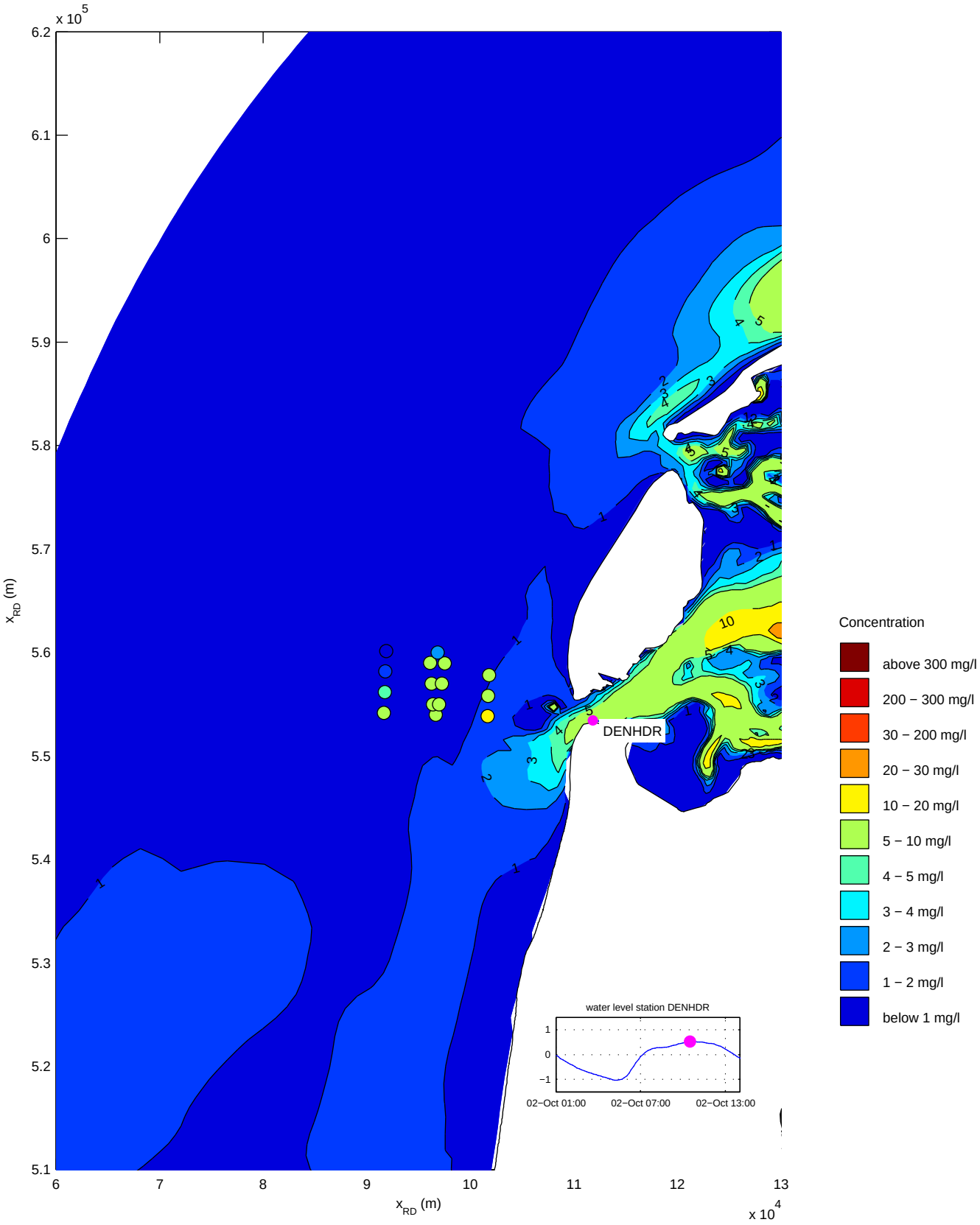

Simulated silt concentrations (mg/l) date and time: 02−Oct−2007 10:30:00 coloured symbols denote the T1 observations		
	trim−kh07intgraded36	
Alkyon Hydraulic Consultancy & Research	A2273	Fig. 2.64

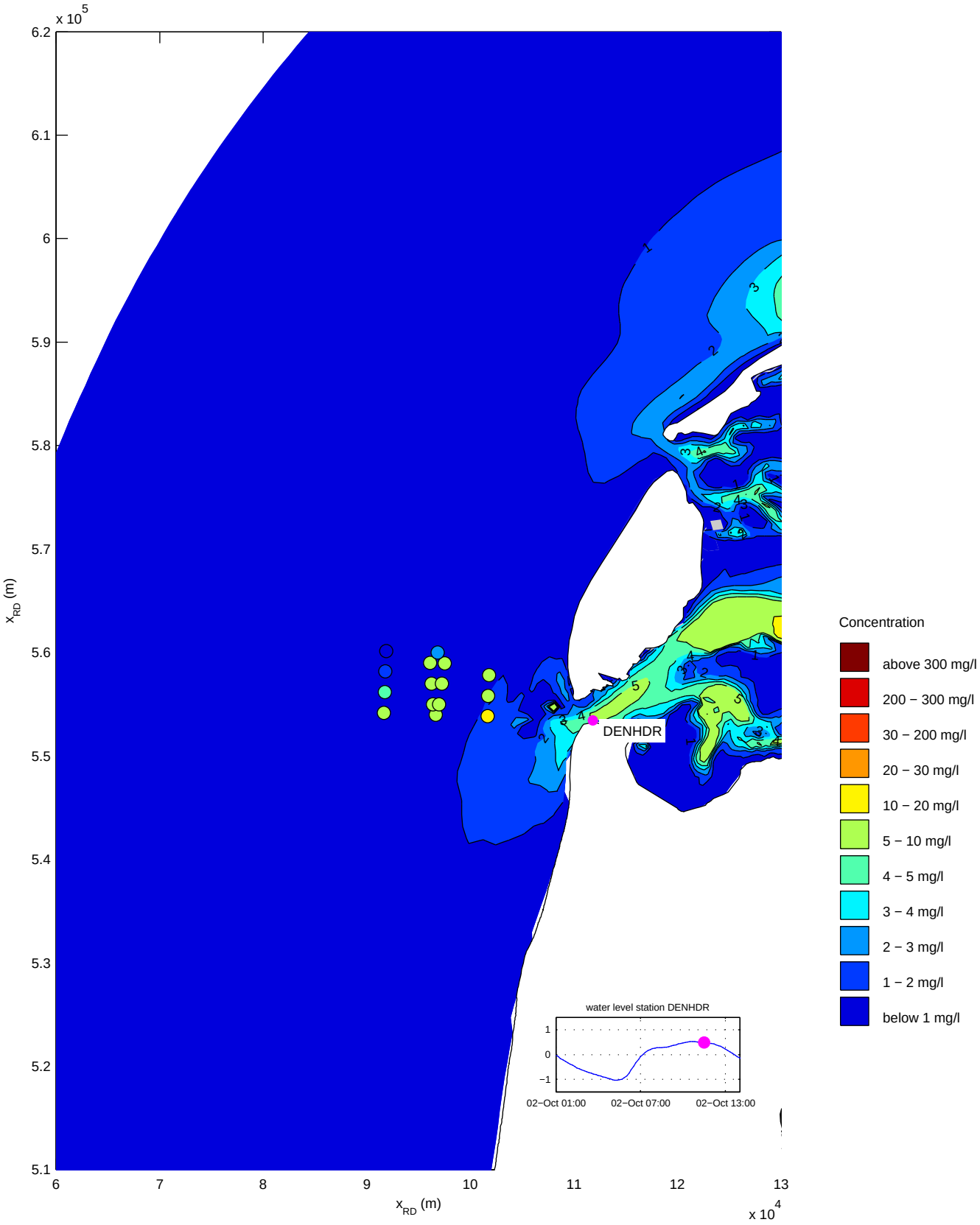

Simulated silt concentrations (mg/l) date and time: 02−Oct−2007 11:30:00 coloured symbols denote the T1 observations		
	trim−kh07intgraded36	
Alkyon Hydraulic Consultancy & Research	A2273	Fig. 2.65

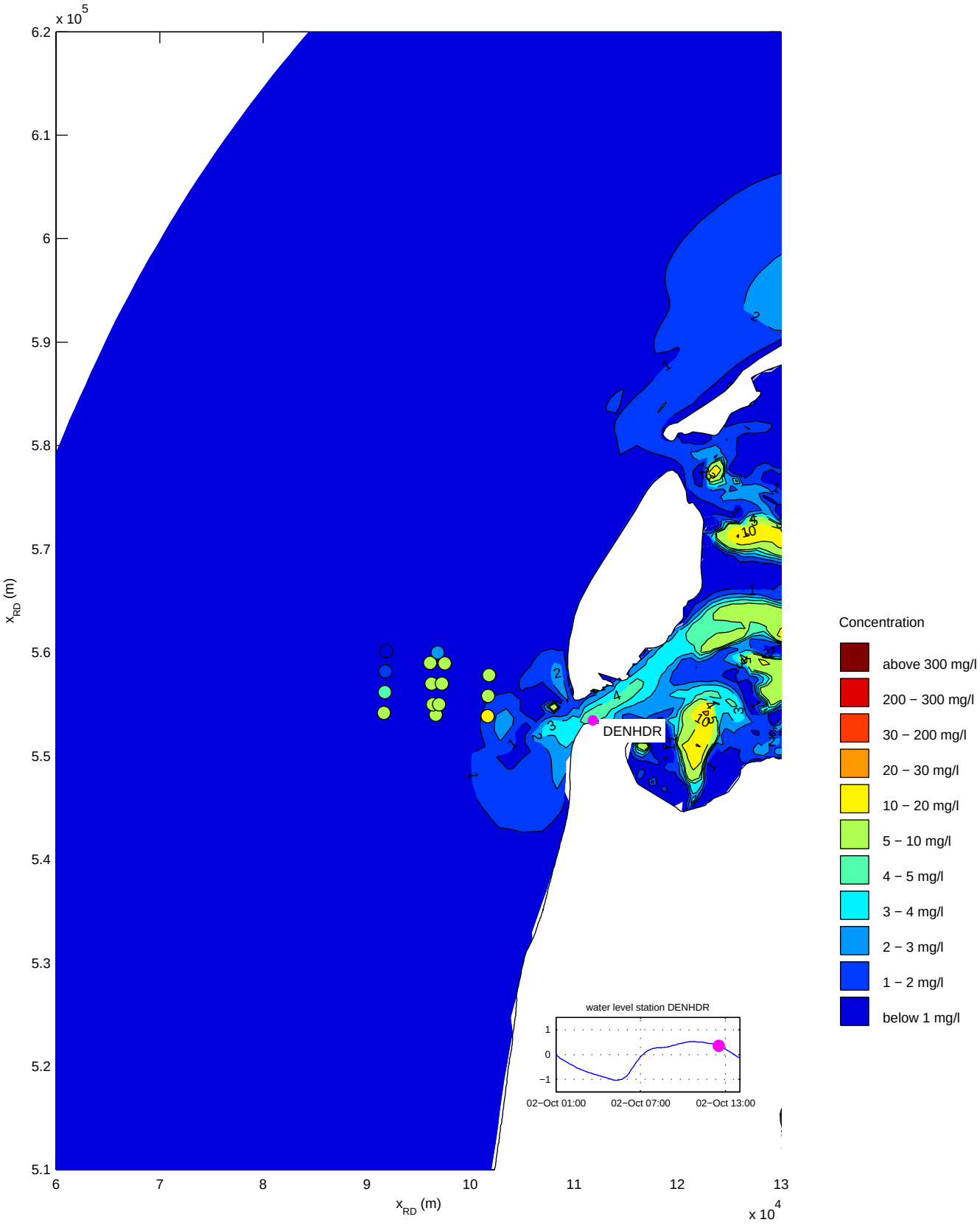

Simulated silt concentrations (mg/l) date and time: 02−Oct−2007 12:30:00 coloured symbols denote the T1 observations		
	trim−kh07intgraded36	
Alkyon Hydraulic Consultancy & Research	A2273	Fig. 2.66

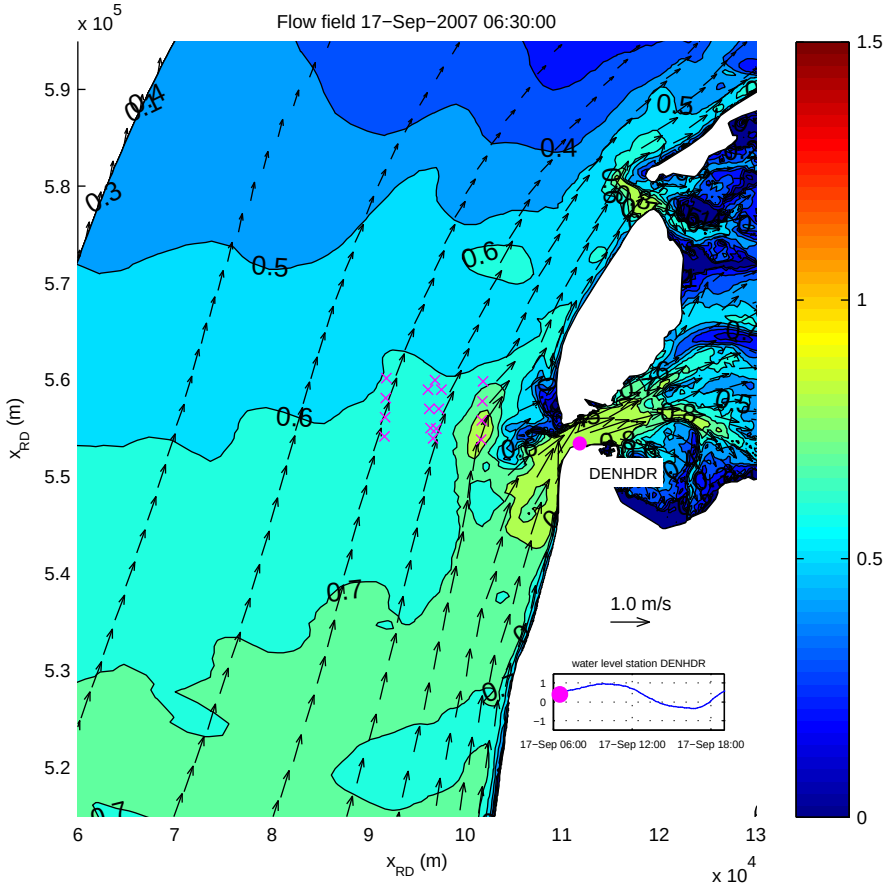

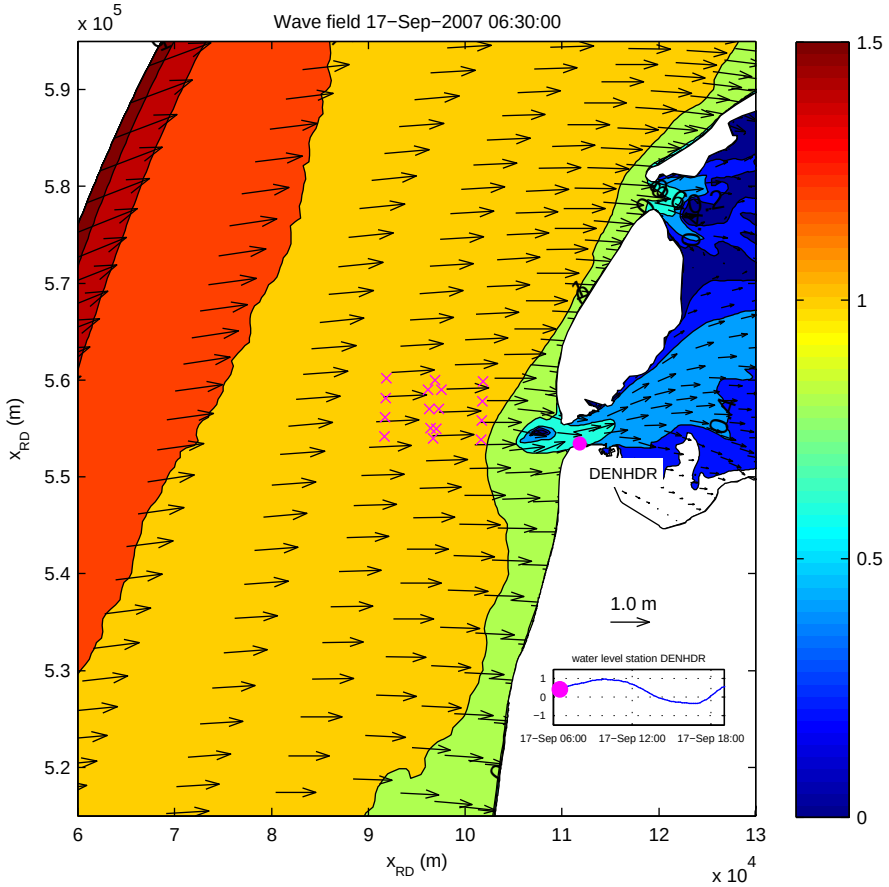

Simulated flow velocities in upper layer (m/s) and sigificant wave heights (m)
date and time: 17−Sep−2007 06:30:00
x−marks denote locations of T1 observations

Alkyon Hydraulic Consultancy & Research	A2273	Fig. 3.1

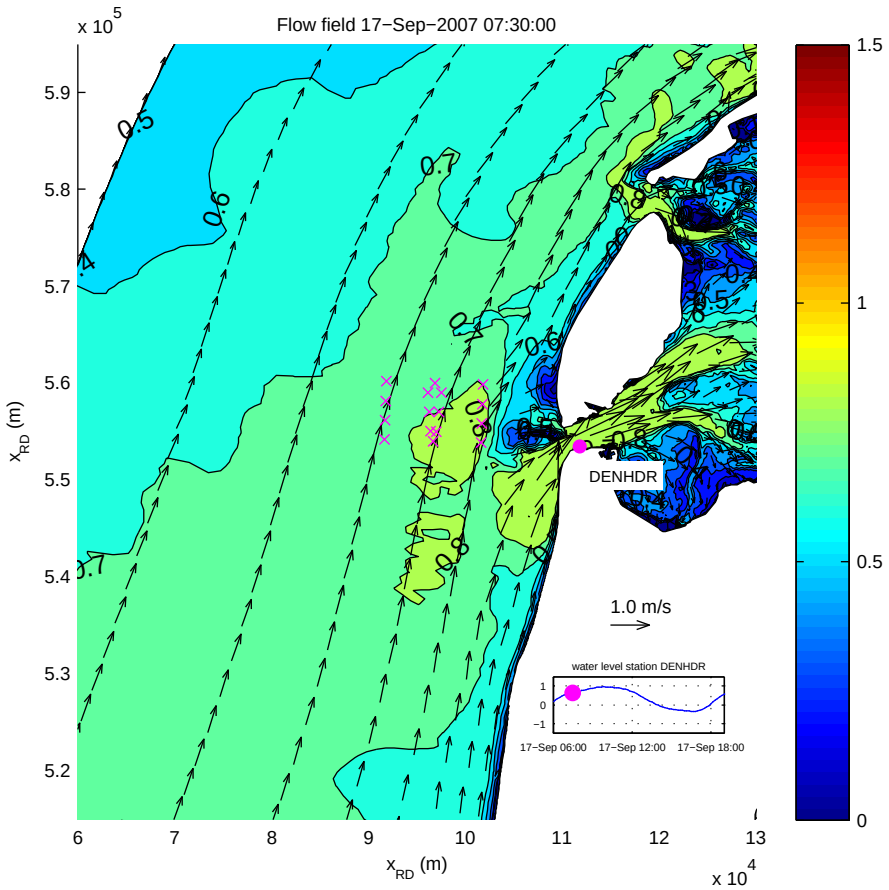

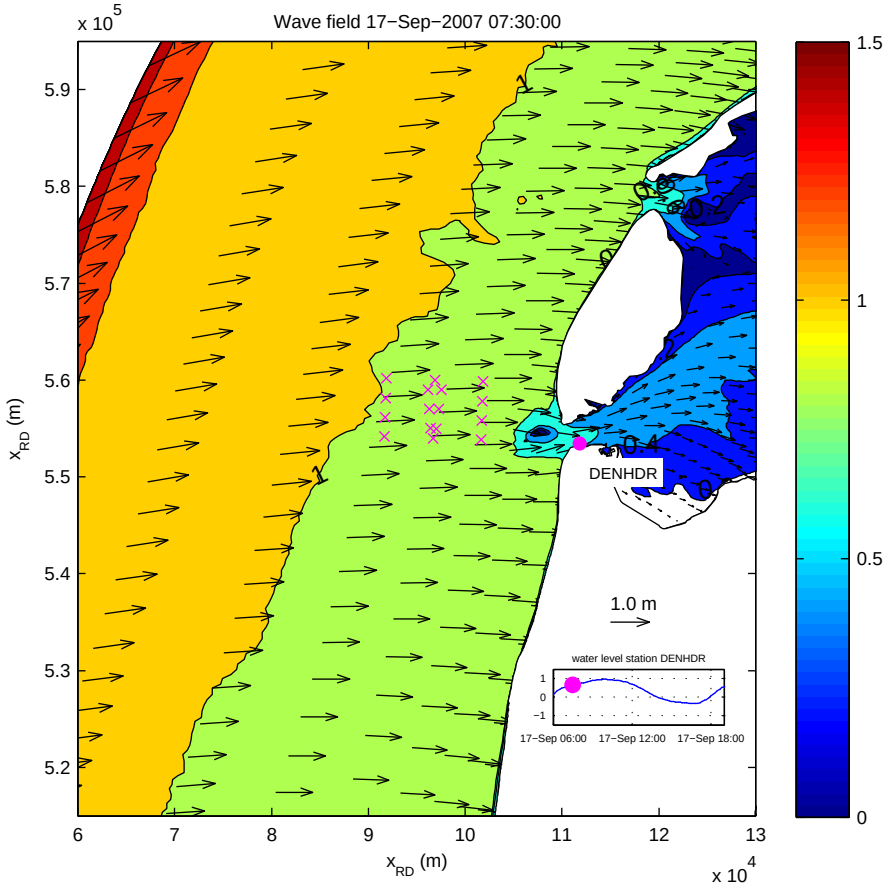

Simulated flow velocities in upper layer (m/s) and sigificant wave heights (m)
date and time: 17−Sep−2007 07:30:00
x−marks denote locations of T1 observations

Alkyon Hydraulic Consultancy & Research | A2273 | Fig. 3.2

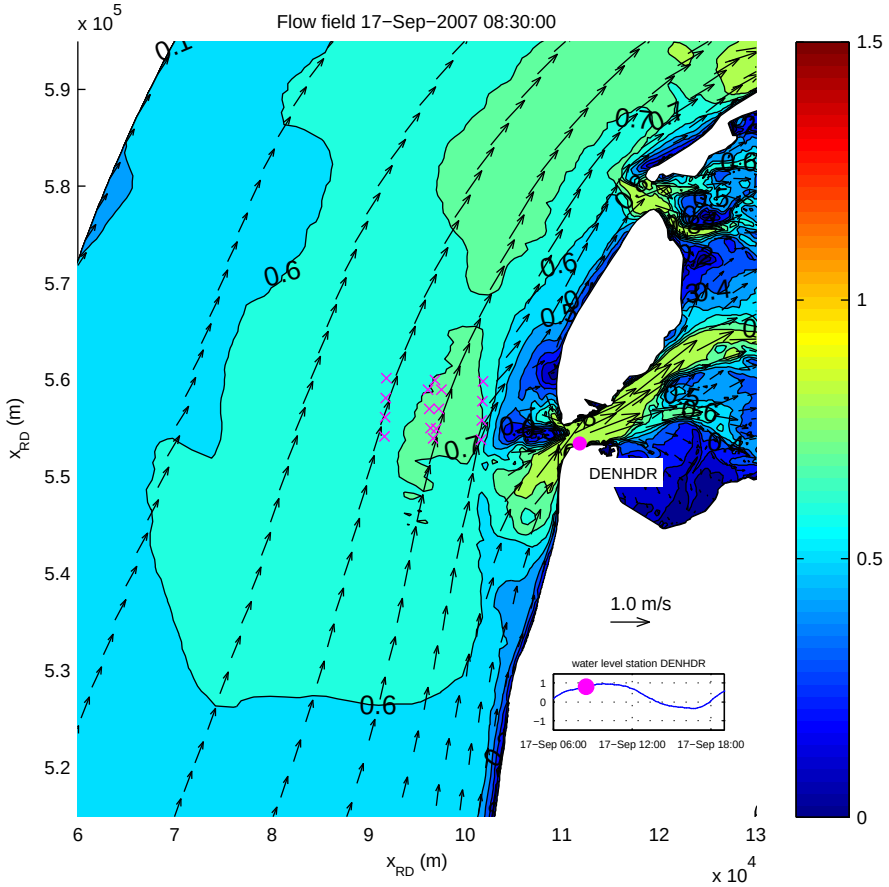

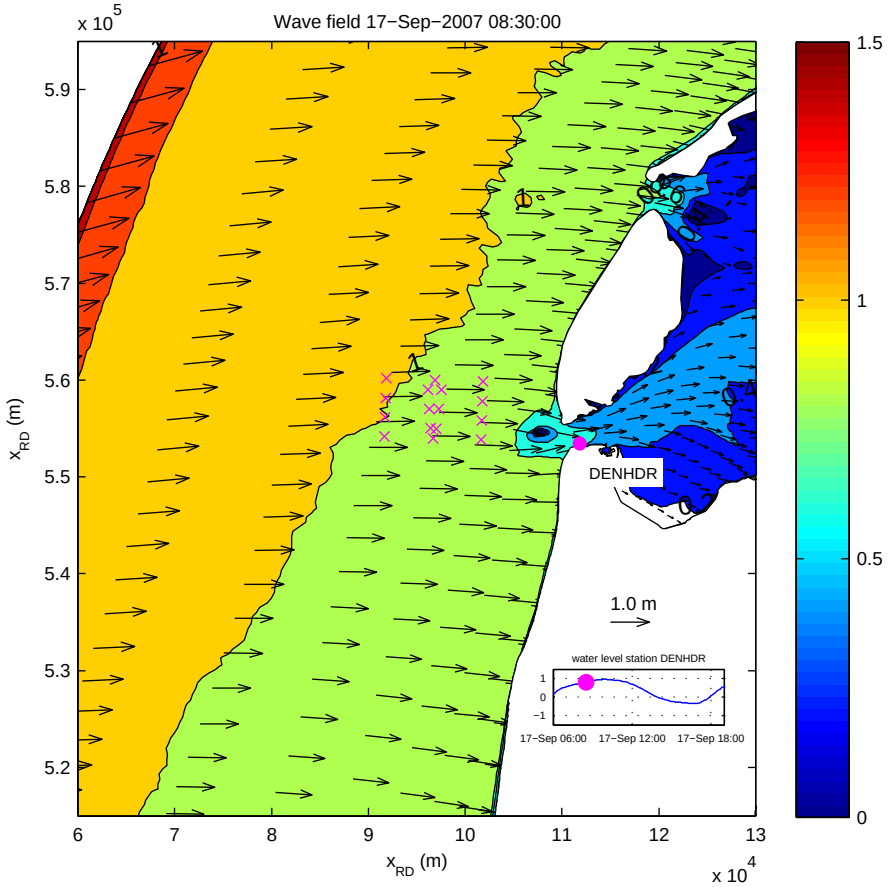

Simulated flow velocities in upper layer (m/s) and sigificant wave heights (m)
date and time: 17−Sep−2007 08:30:00
x−marks denote locations of T1 observations

Alkyon Hydraulic Consultancy & Research	A2273	Fig. 3.3

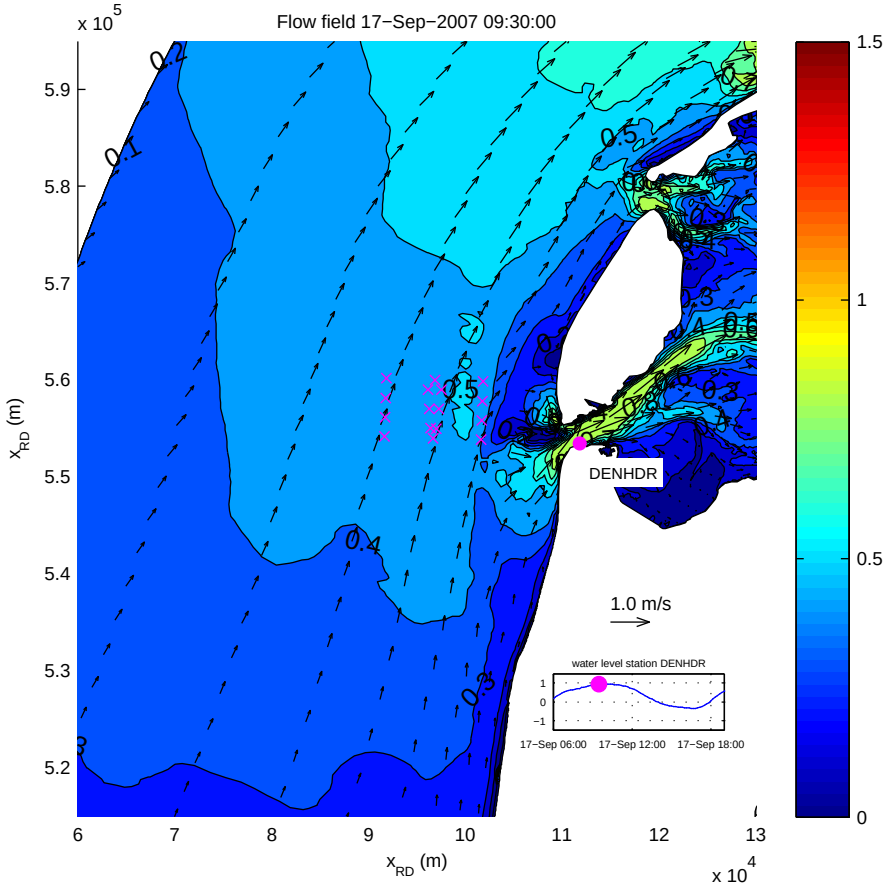

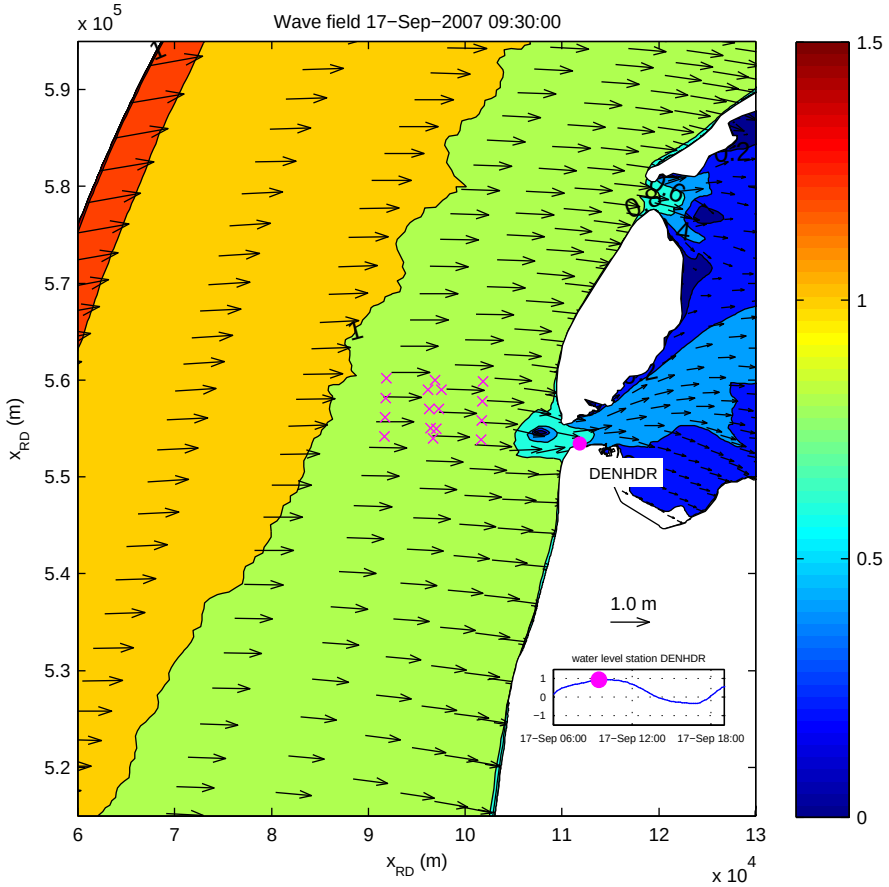

Simulated flow velocities in upper layer (m/s) and sigificant wave heights (m)
date and time: 17−Sep−2007 09:30:00
x−marks denote locations of T1 observations

Alkyon Hydraulic Consultancy & Research	A2273	Fig. 3.4

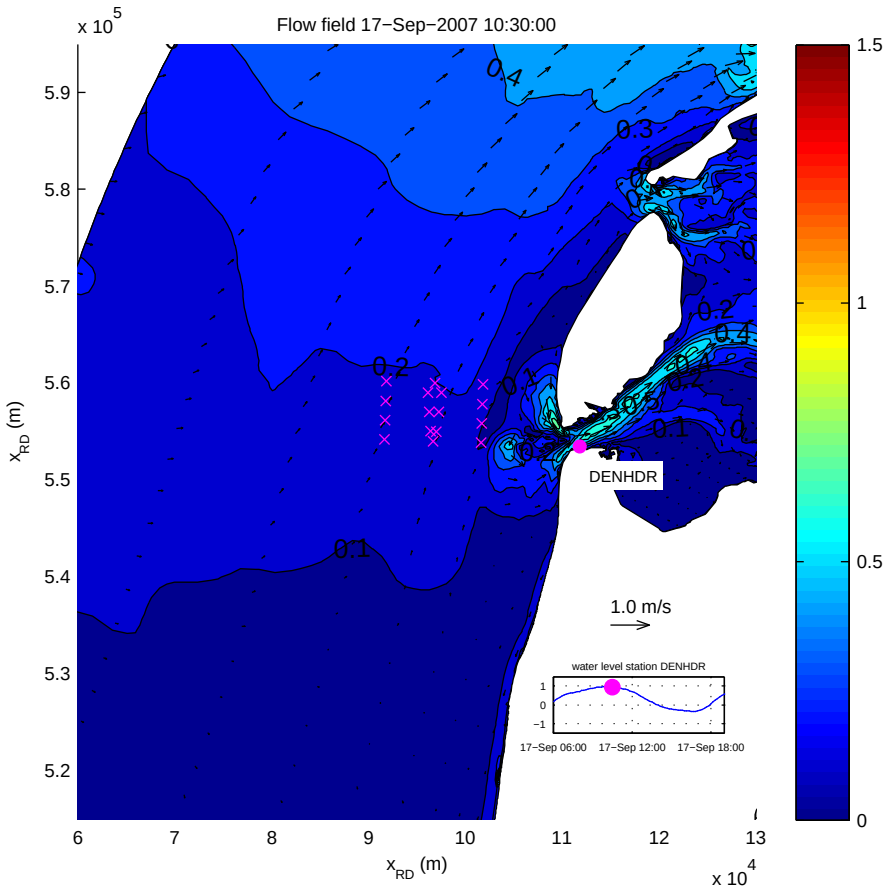

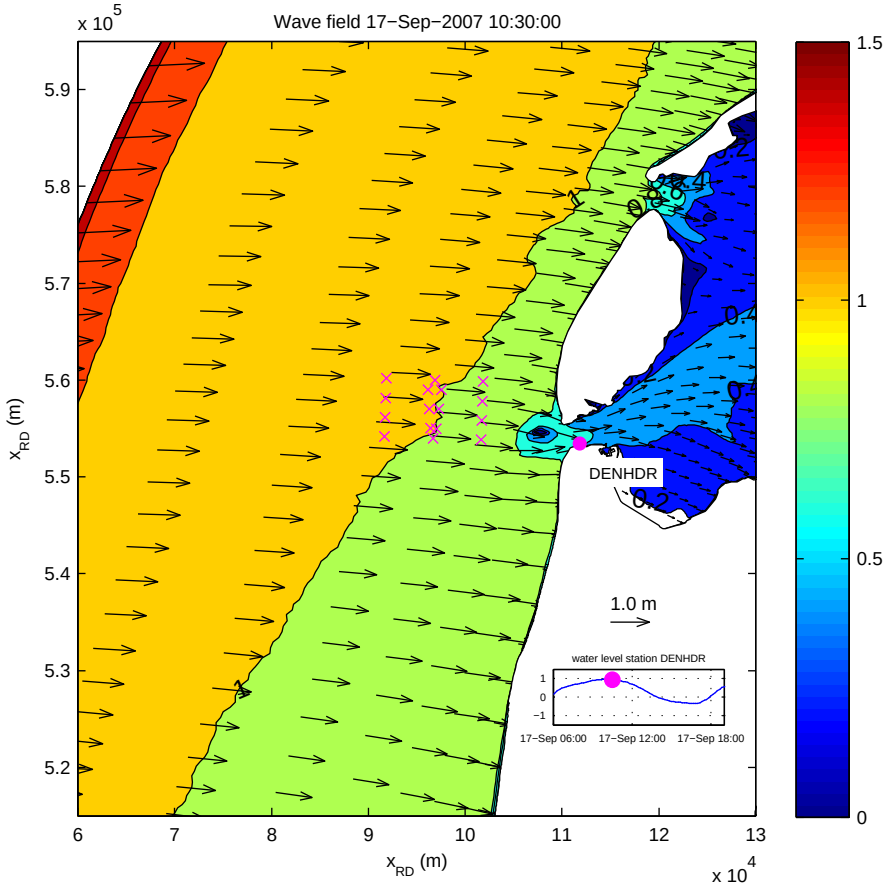

Simulated flow velocities in upper layer (m/s) and sigificant wave heights (m)
date and time: 17−Sep−2007 10:30:00
x−marks denote locations of T1 observations

Alkyon Hydraulic Consultancy & Research	A2273	Fig. 3.5

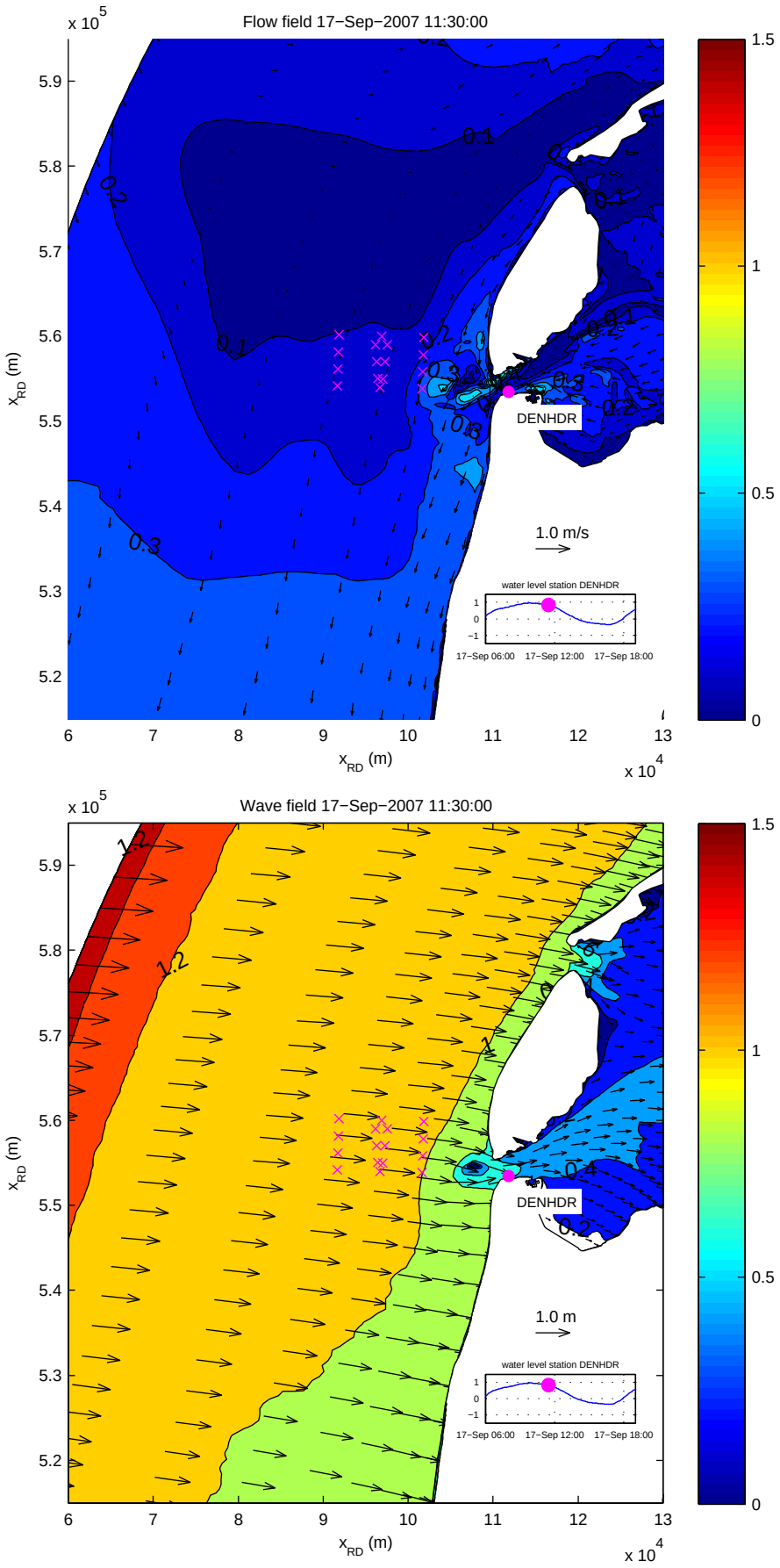

Simulated flow velocities in upper layer (m/s) and sigificant wave heights (m)
date and time: 17−Sep−2007 11:30:00
x−marks denote locations of T1 observations

Alkyon Hydraulic Consultancy & Research	A2273	Fig. 3.6

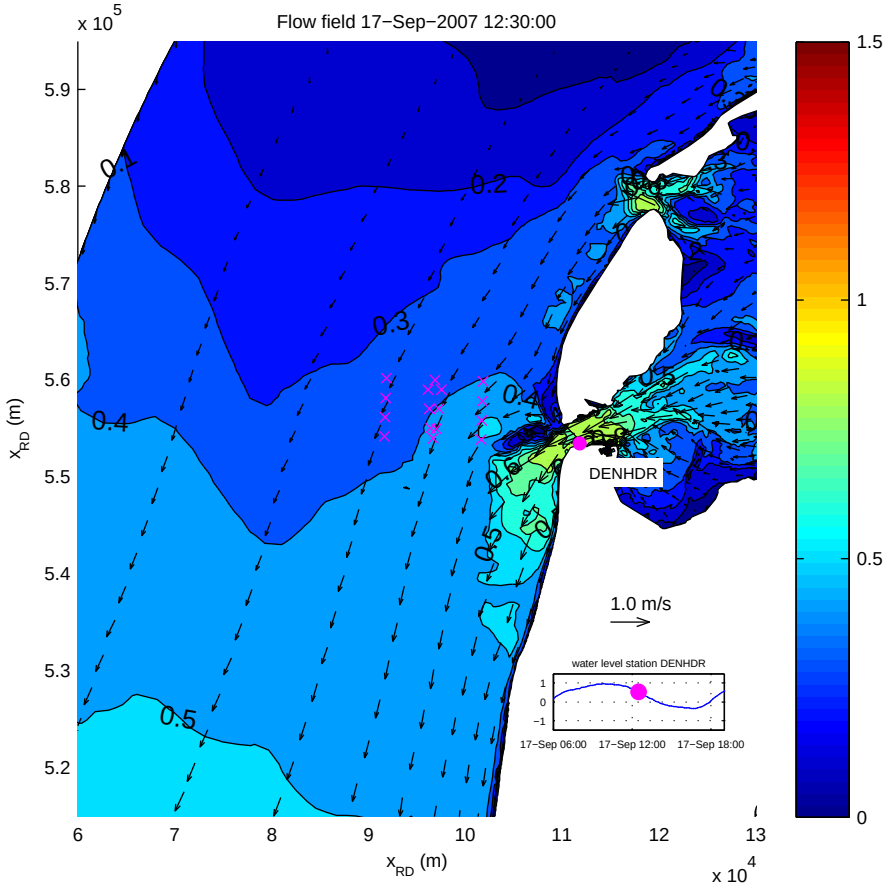

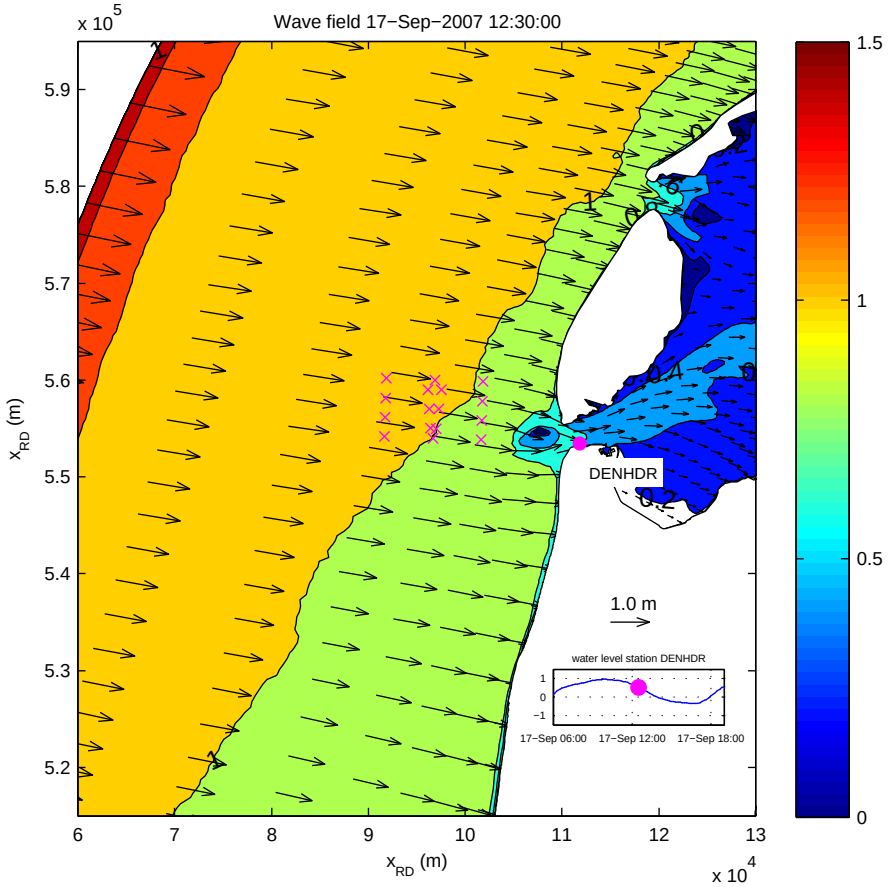

Simulated flow velocities in upper layer (m/s) and sigificant wave heights (m)
date and time: 17−Sep−2007 12:30:00
x−marks denote locations of T1 observations

Alkyon Hydraulic Consultancy & Research	A2273	Fig. 3.7

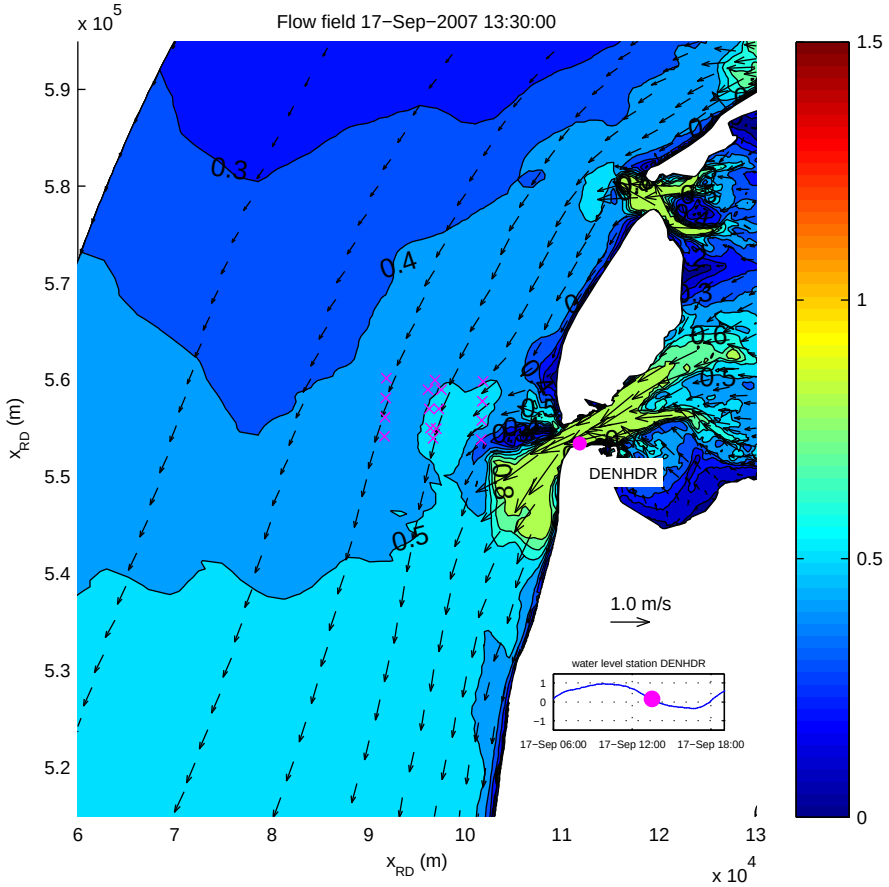

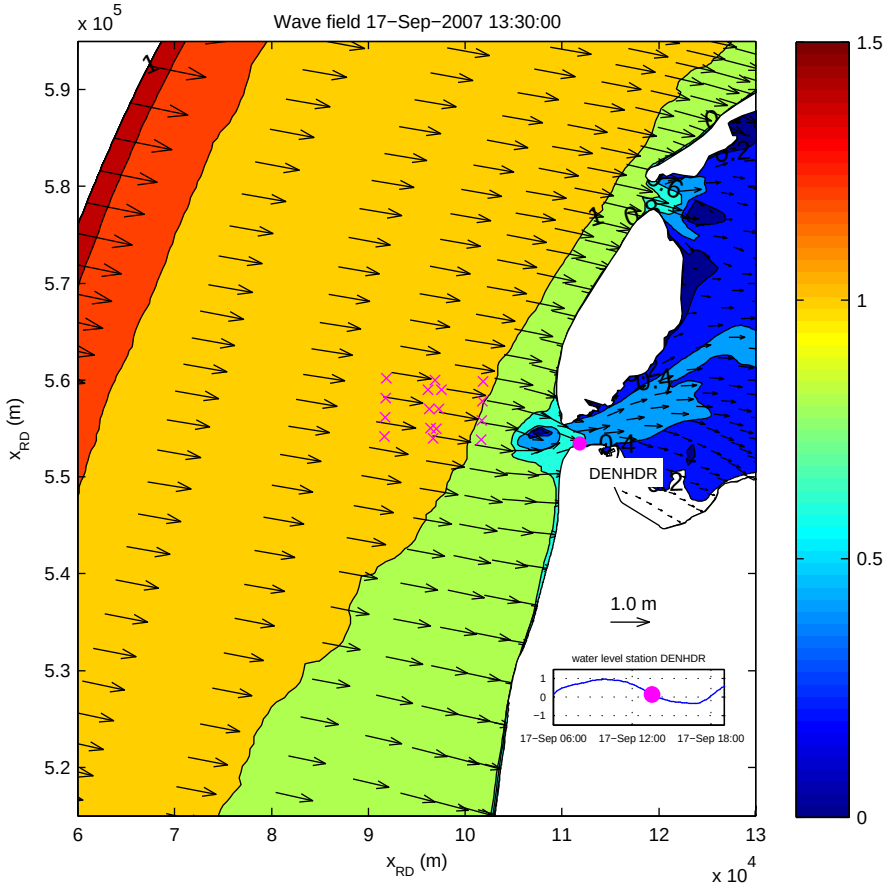

Simulated flow velocities in upper layer (m/s) and sigificant wave heights (m)
date and time: 17−Sep−2007 13:30:00
x−marks denote locations of T1 observations

Alkyon Hydraulic Consultancy & Research	A2273	Fig. 3.8

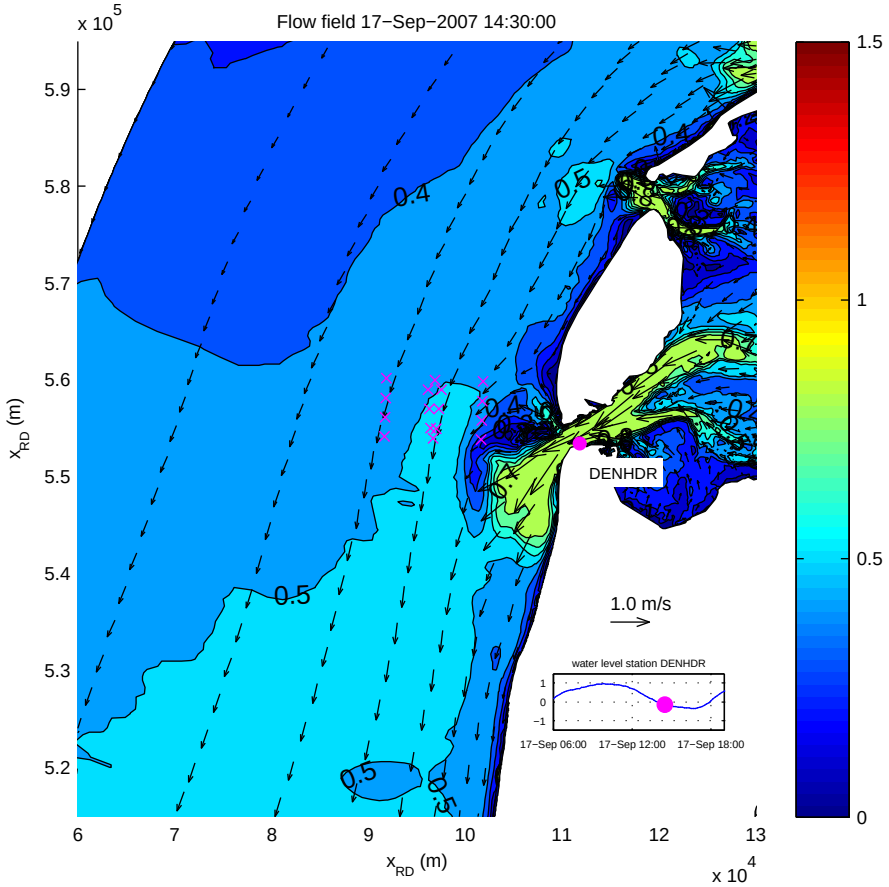

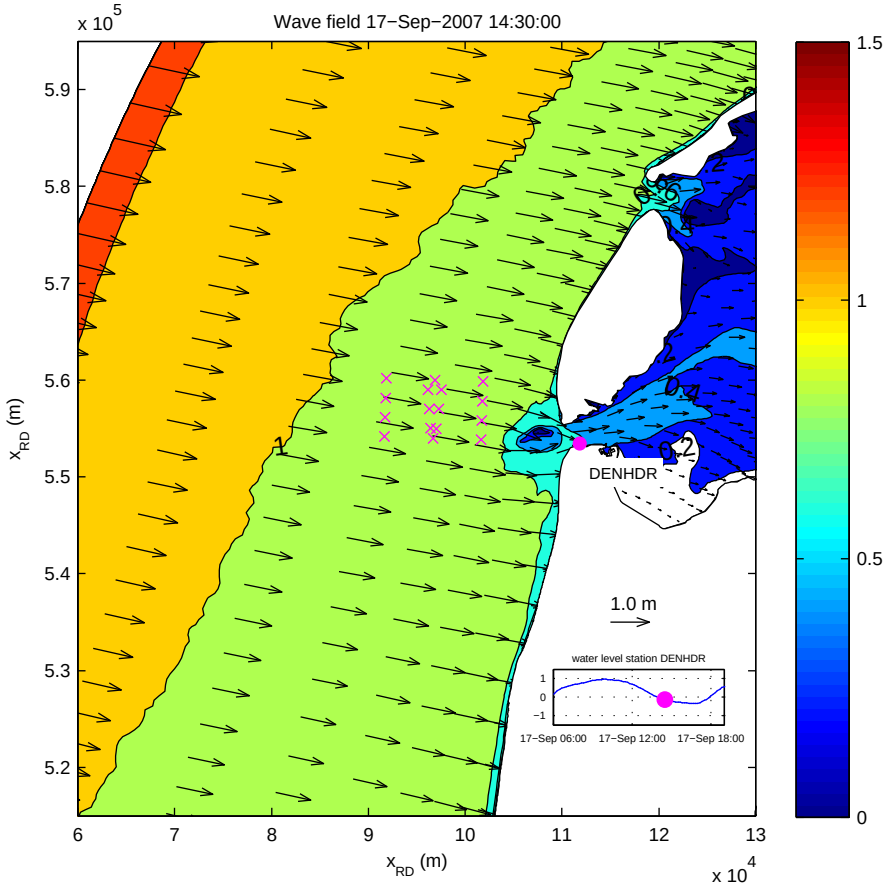

Simulated flow velocities in upper layer (m/s) and sigificant wave heights (m)
date and time: 17−Sep−2007 14:30:00
x−marks denote locations of T1 observations

Alkyon Hydraulic Consultancy & Research	A2273 Fig. 3.9

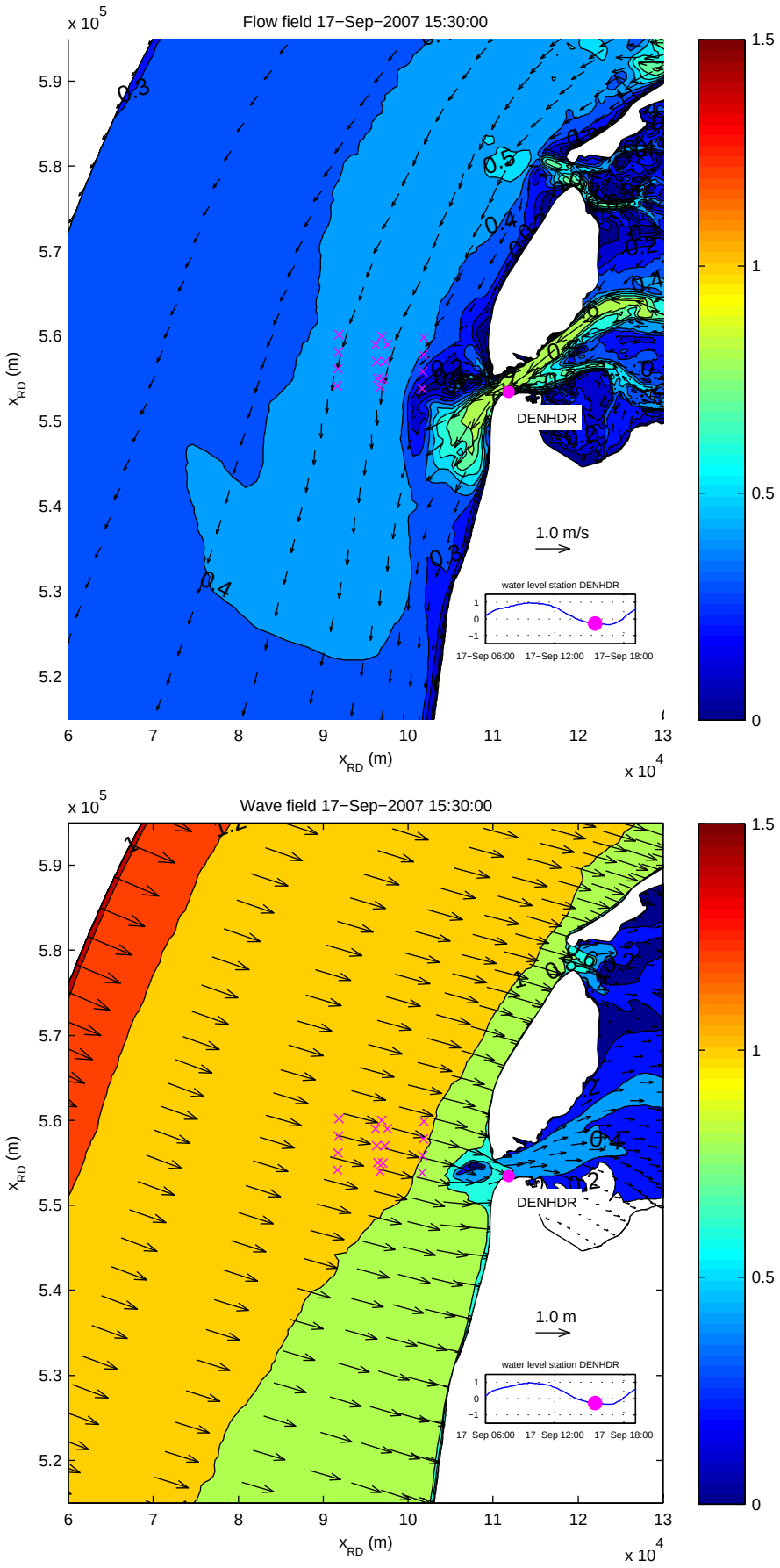

Simulated flow velocities in upper layer (m/s) and sigificant wave heights (m)
date and time: 17−Sep−2007 15:30:00
x−marks denote locations of T1 observations

Alkyon Hydraulic Consultancy & Research	A2273	Fig. 3.10

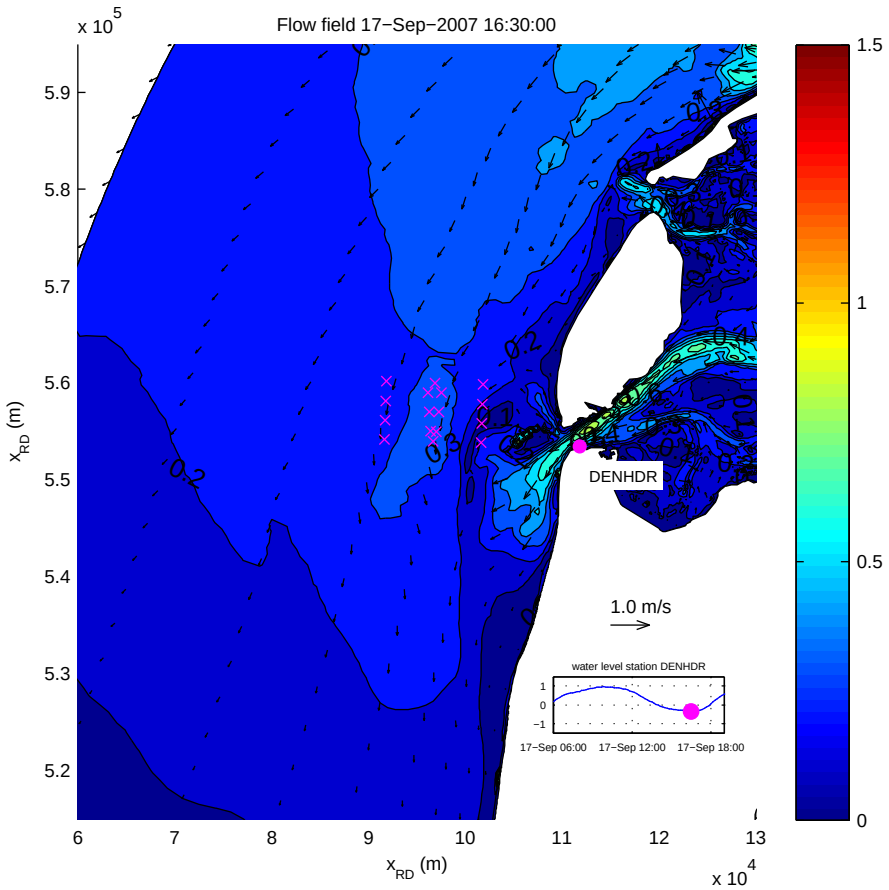

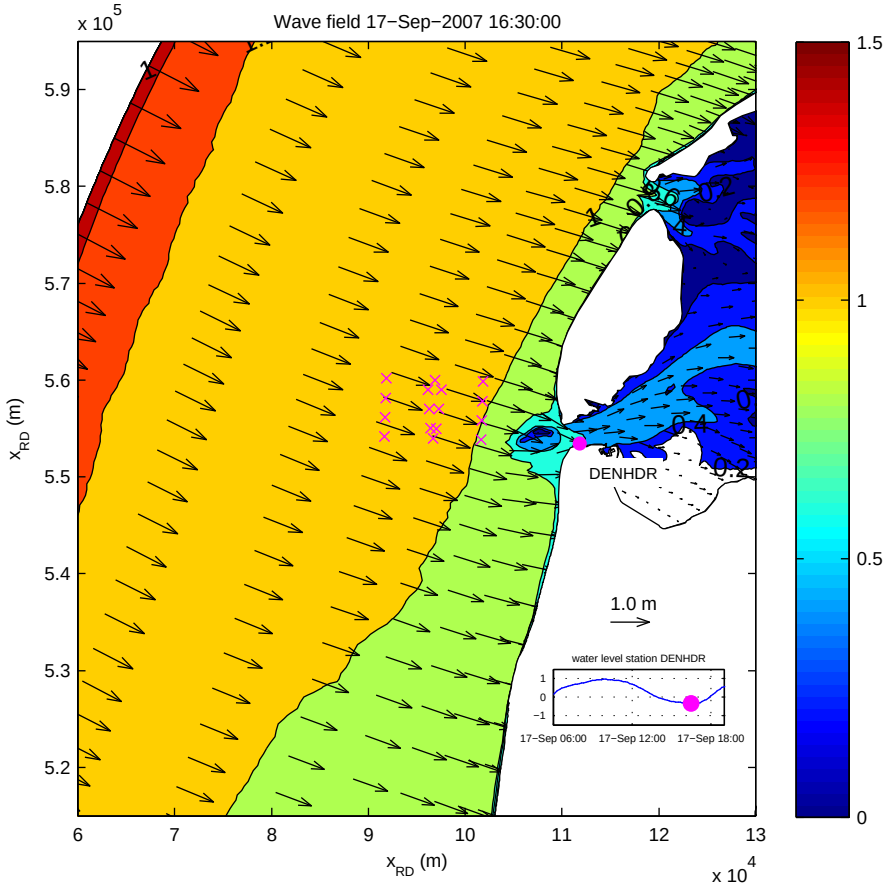

Simulated flow velocities in upper layer (m/s) and sigificant wave heights (m)
date and time: 17−Sep−2007 16:30:00
x−marks denote locations of T1 observations

Alkyon Hydraulic Consultancy & Research	A2273	Fig. 3.11

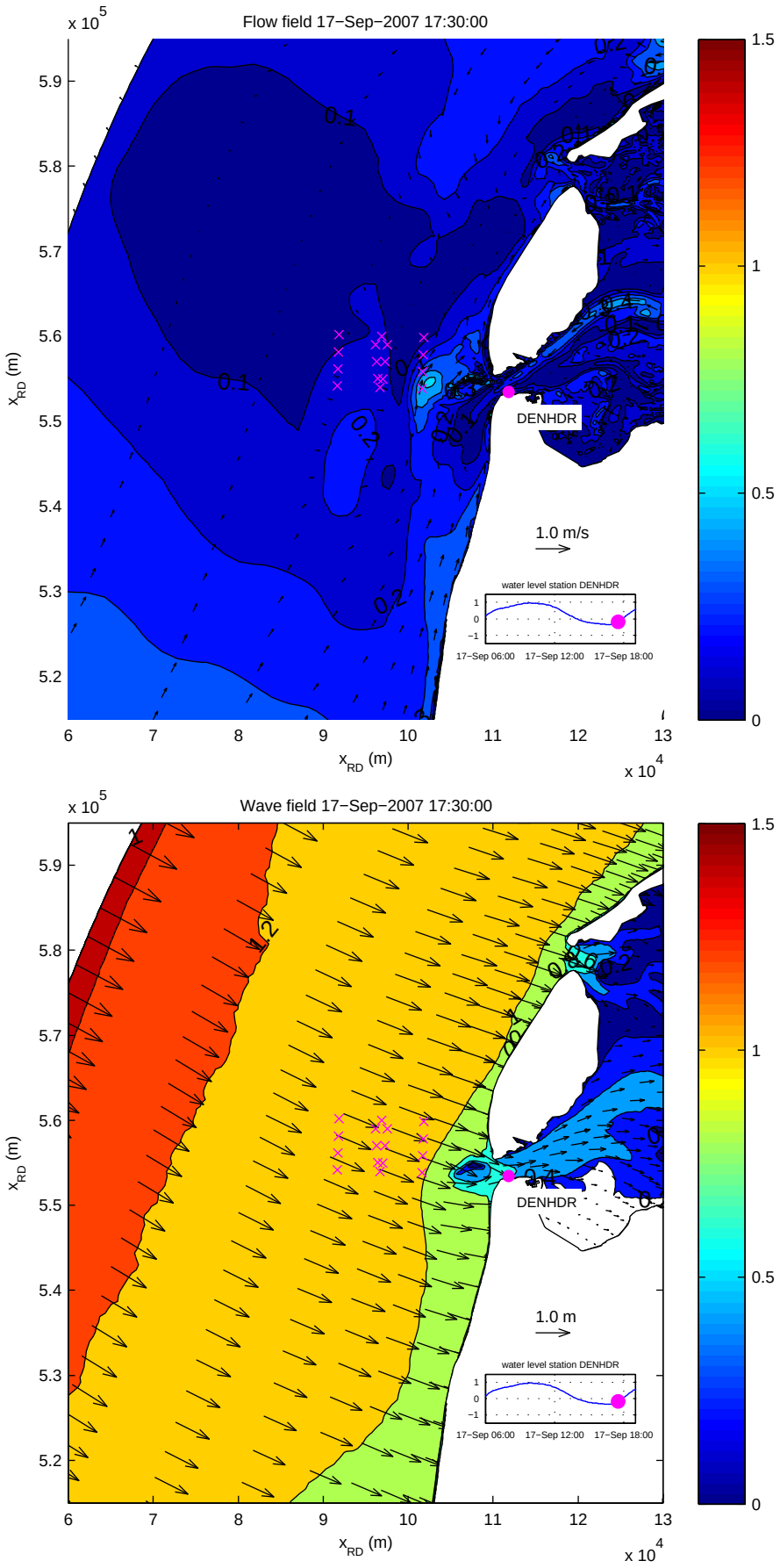

Simulated flow velocities in upper layer (m/s) and sigificant wave heights (m)
date and time: 17−Sep−2007 17:30:00
x−marks denote locations of T1 observations

Alkyon Hydraulic Consultancy & Research	A2273	Fig. 3.12

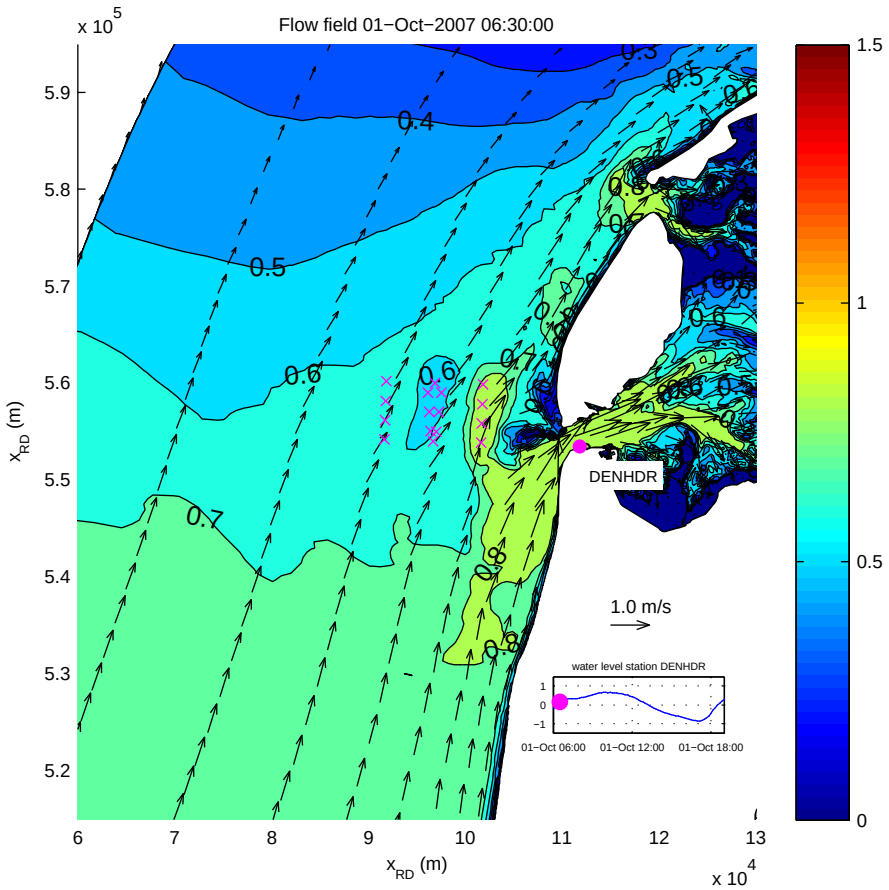

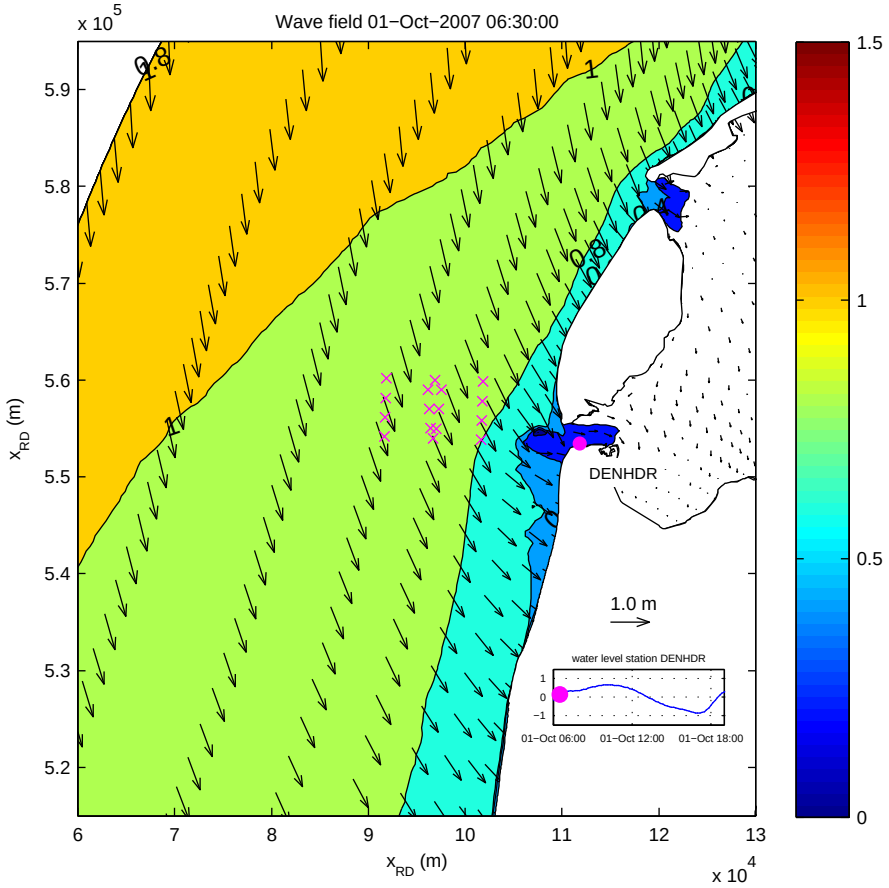

Simulated flow velocities in upper layer (m/s) and sigificant wave heights (m)
date and time: 01−Oct−2007 06:30:00
x−marks denote locations of T1 observations

Alkyon Hydraulic Consultancy & Research	A2273	Fig. 3.13

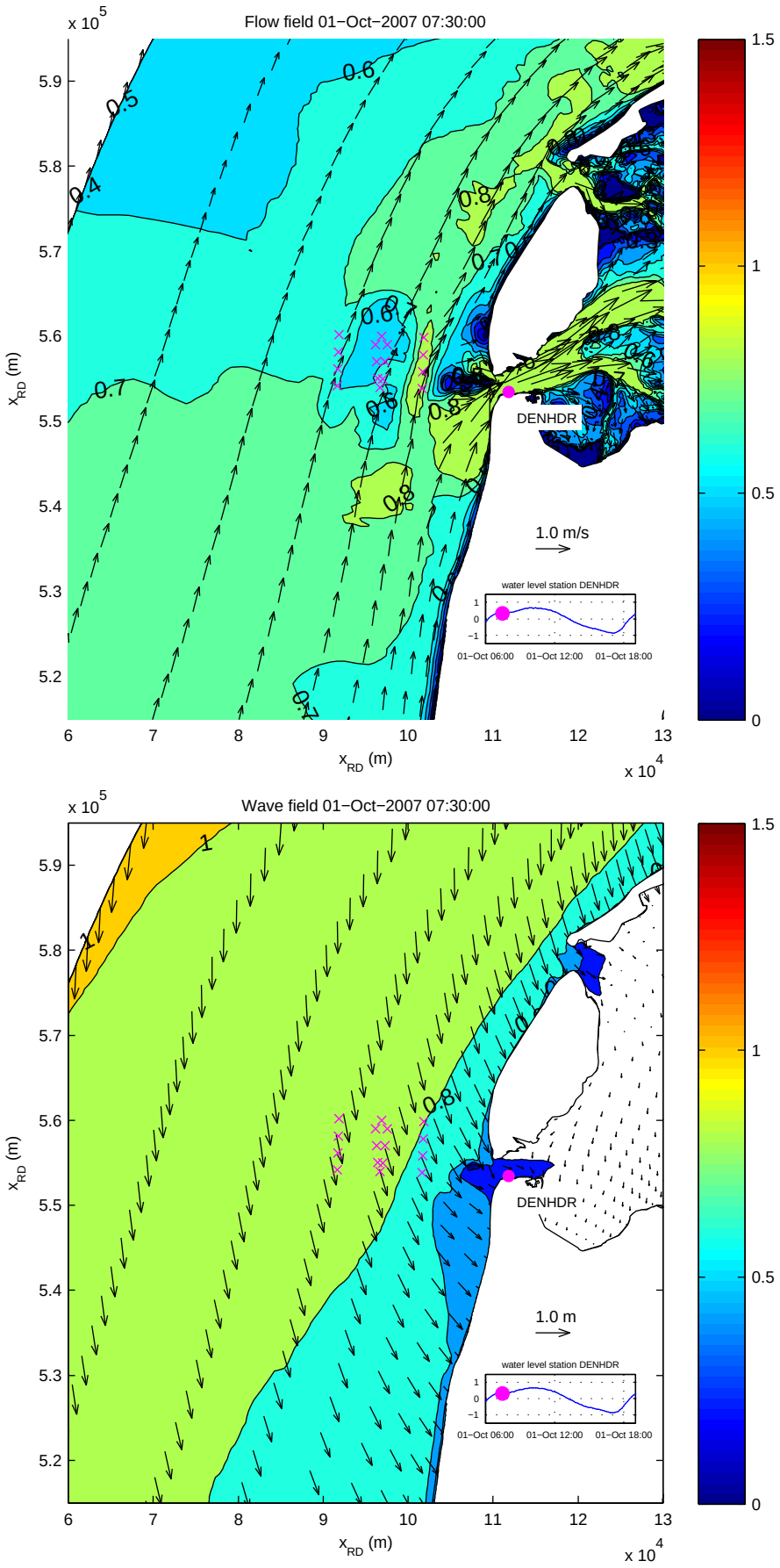

Simulated flow velocities in upper layer (m/s) and sigificant wave heights (m)
date and time: 01−Oct−2007 07:30:00
x−marks denote locations of T1 observations

Alkyon Hydraulic Consultancy & Research	A2273	Fig. 3.14

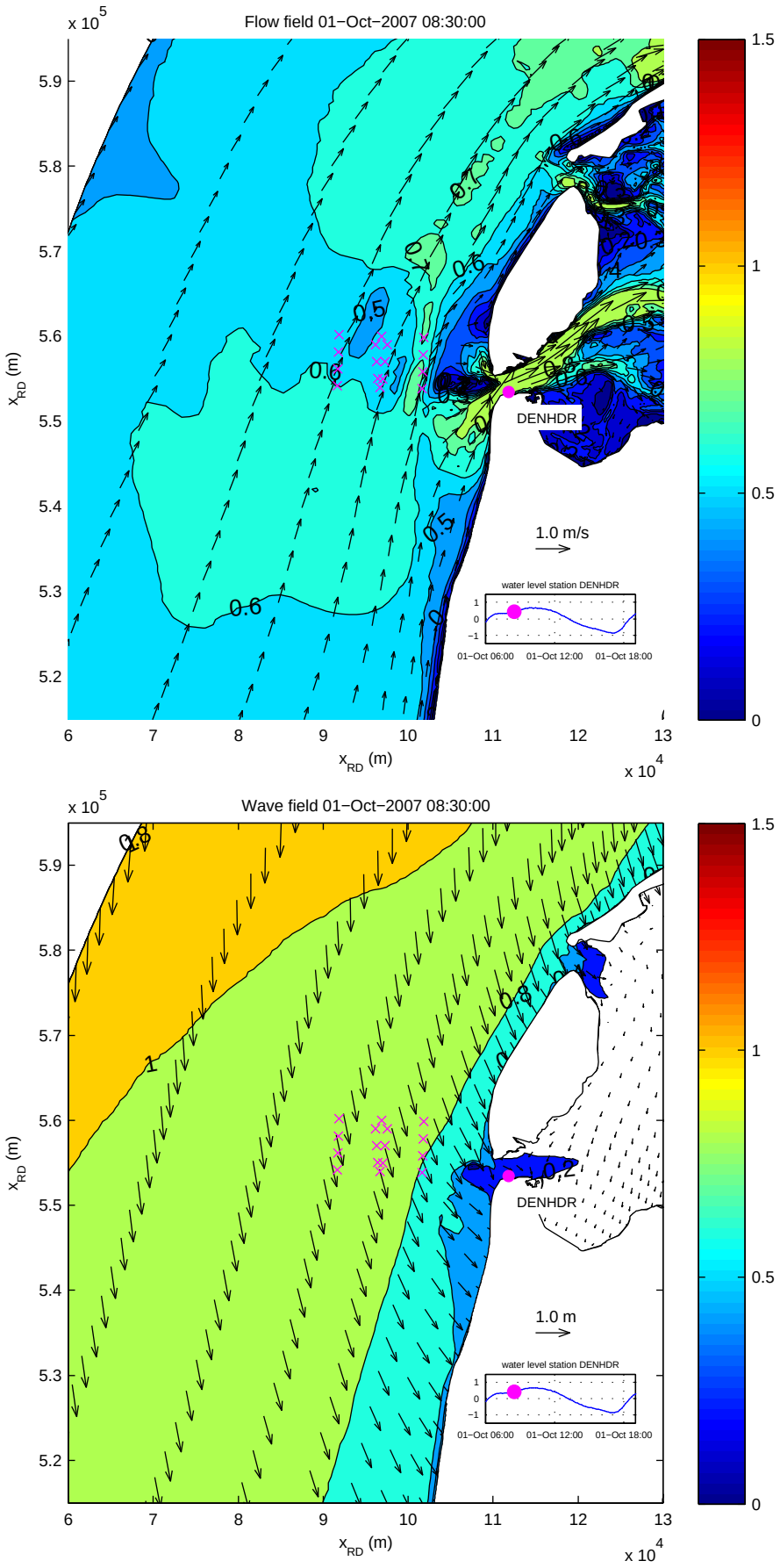

Simulated flow velocities in upper layer (m/s) and sigificant wave heights (m)
date and time: 01−Oct−2007 08:30:00
x−marks denote locations of T1 observations

Alkyon Hydraulic Consultancy & Research	A2273	Fig. 3.15

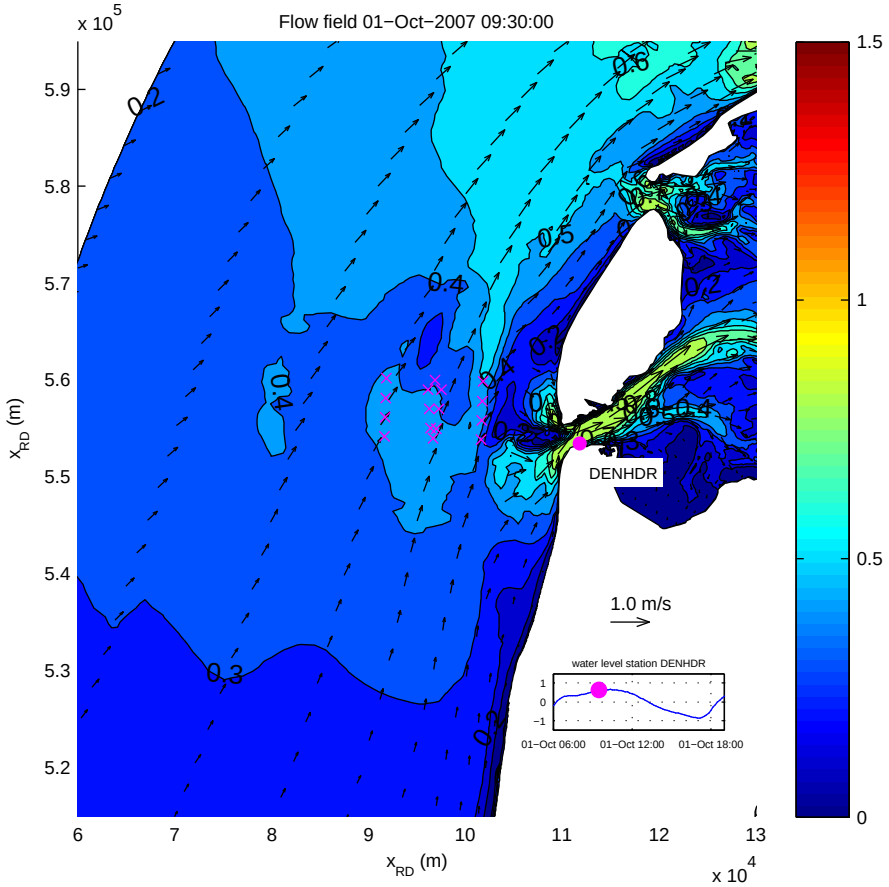

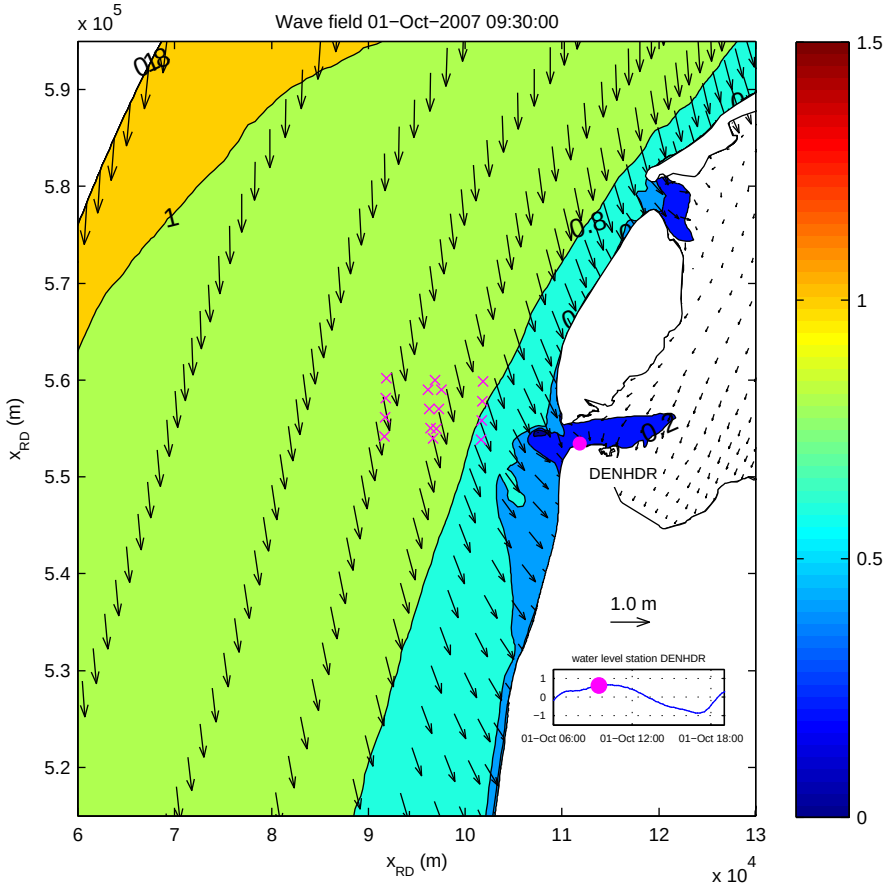

Simulated flow velocities in upper layer (m/s) and sigificant wave heights (m)
date and time: 01−Oct−2007 09:30:00
x−marks denote locations of T1 observations

Alkyon Hydraulic Consultancy & Research	A2273	Fig. 3.16

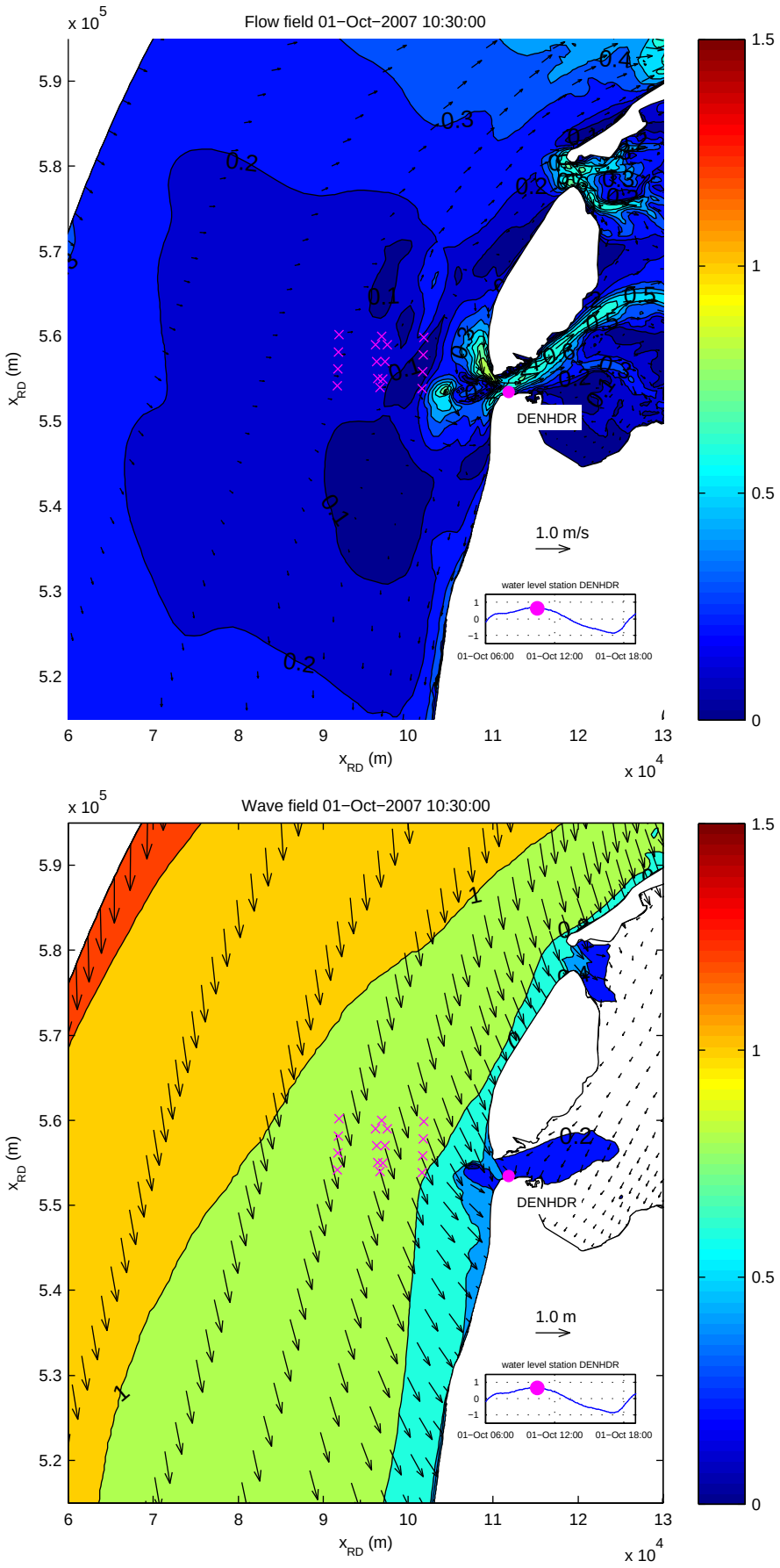

Simulated flow velocities in upper layer (m/s) and sigificant wave heights (m)
date and time: 01−Oct−2007 10:30:00
x−marks denote locations of T1 observations

Alkyon Hydraulic Consultancy & Research	A2273	Fig. 3.17

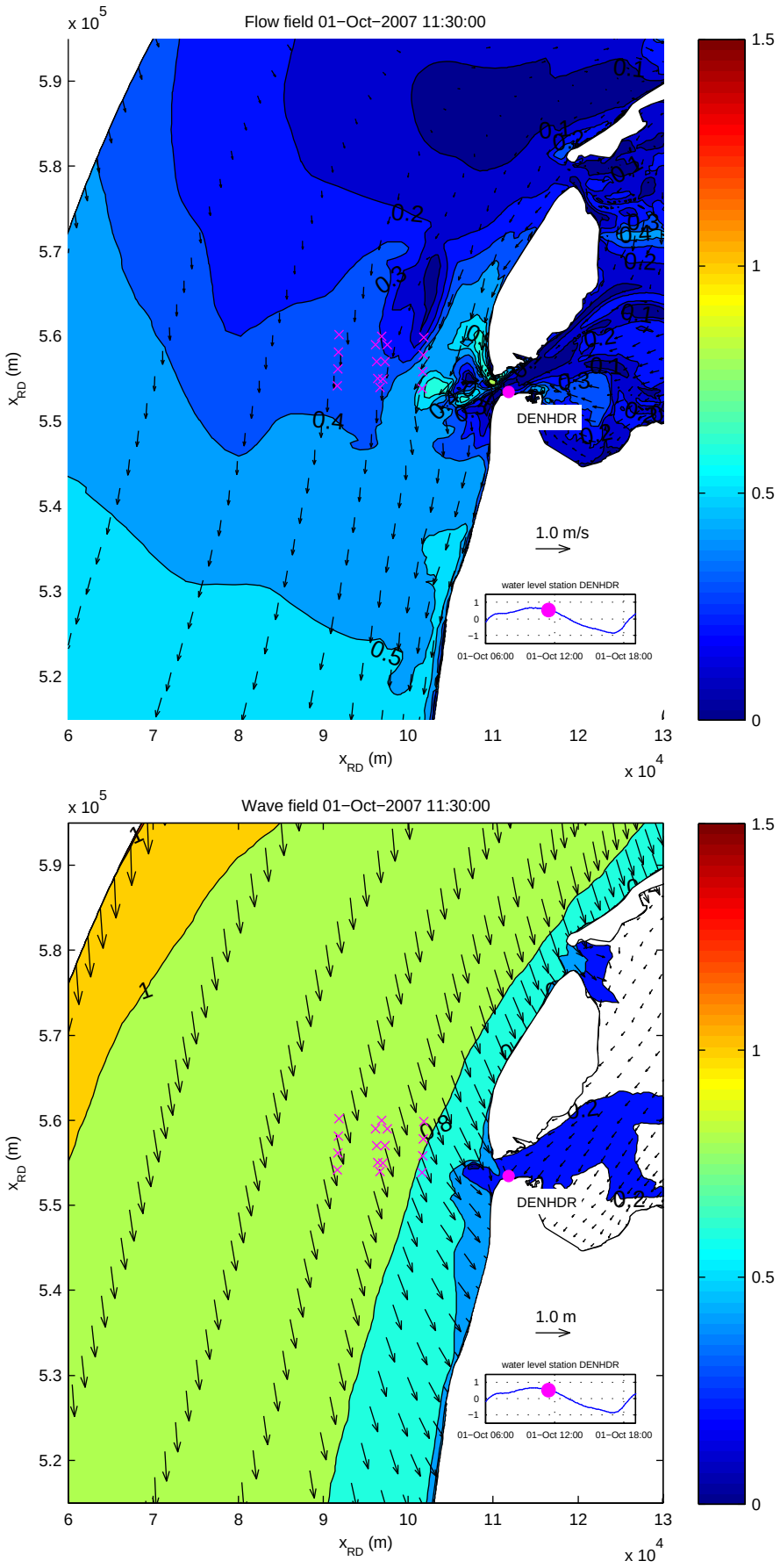

Simulated flow velocities in upper layer (m/s) and sigificant wave heights (m)
date and time: 01−Oct−2007 11:30:00
x−marks denote locations of T1 observations

Alkyon Hydraulic Consultancy & Research	A2273	Fig. 3.18

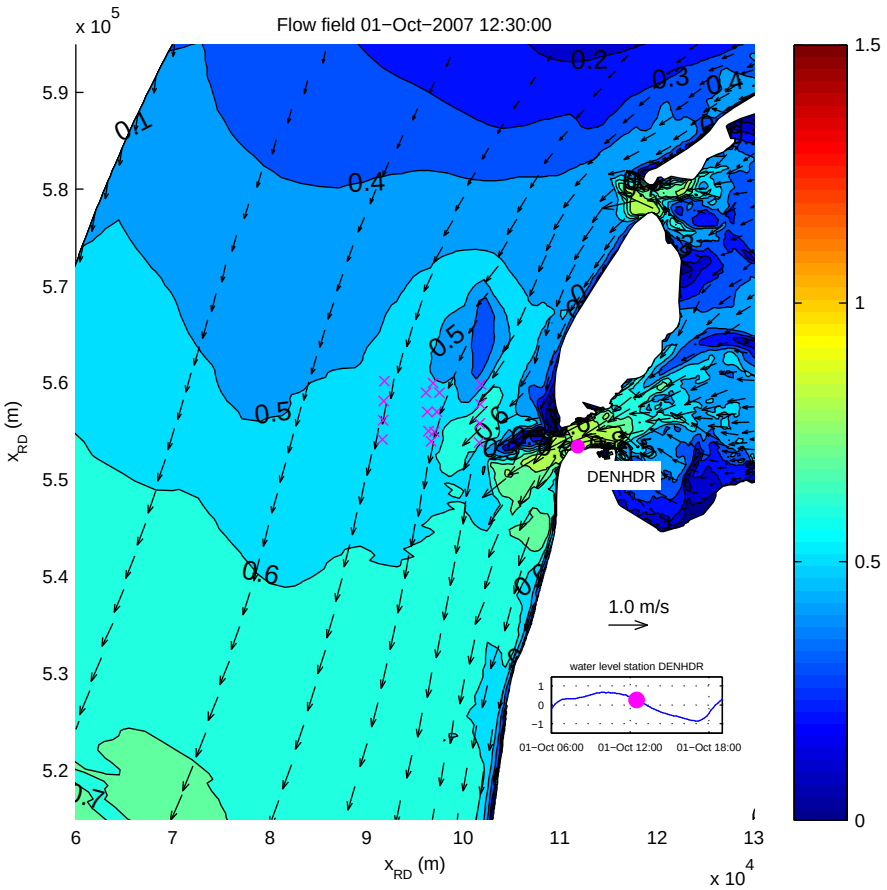

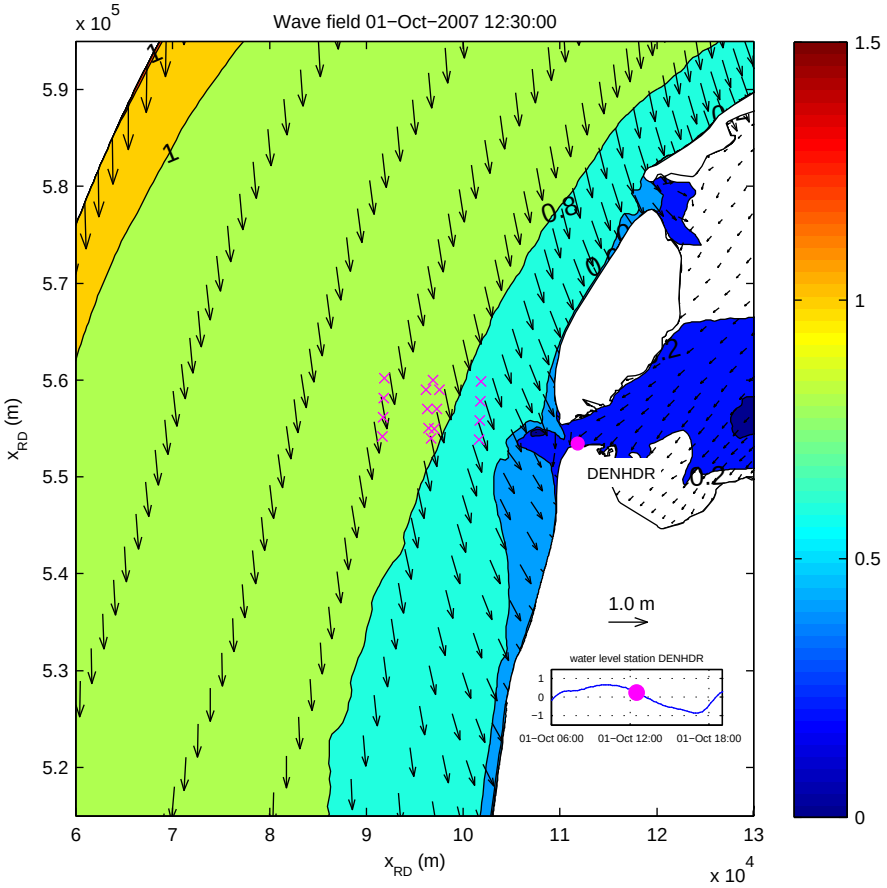

Simulated flow velocities in upper layer (m/s) and sigificant wave heights (m)
date and time: 01−Oct−2007 12:30:00
x−marks denote locations of T1 observations

Alkyon Hydraulic Consultancy & Research	A2273 Fig. 3.19

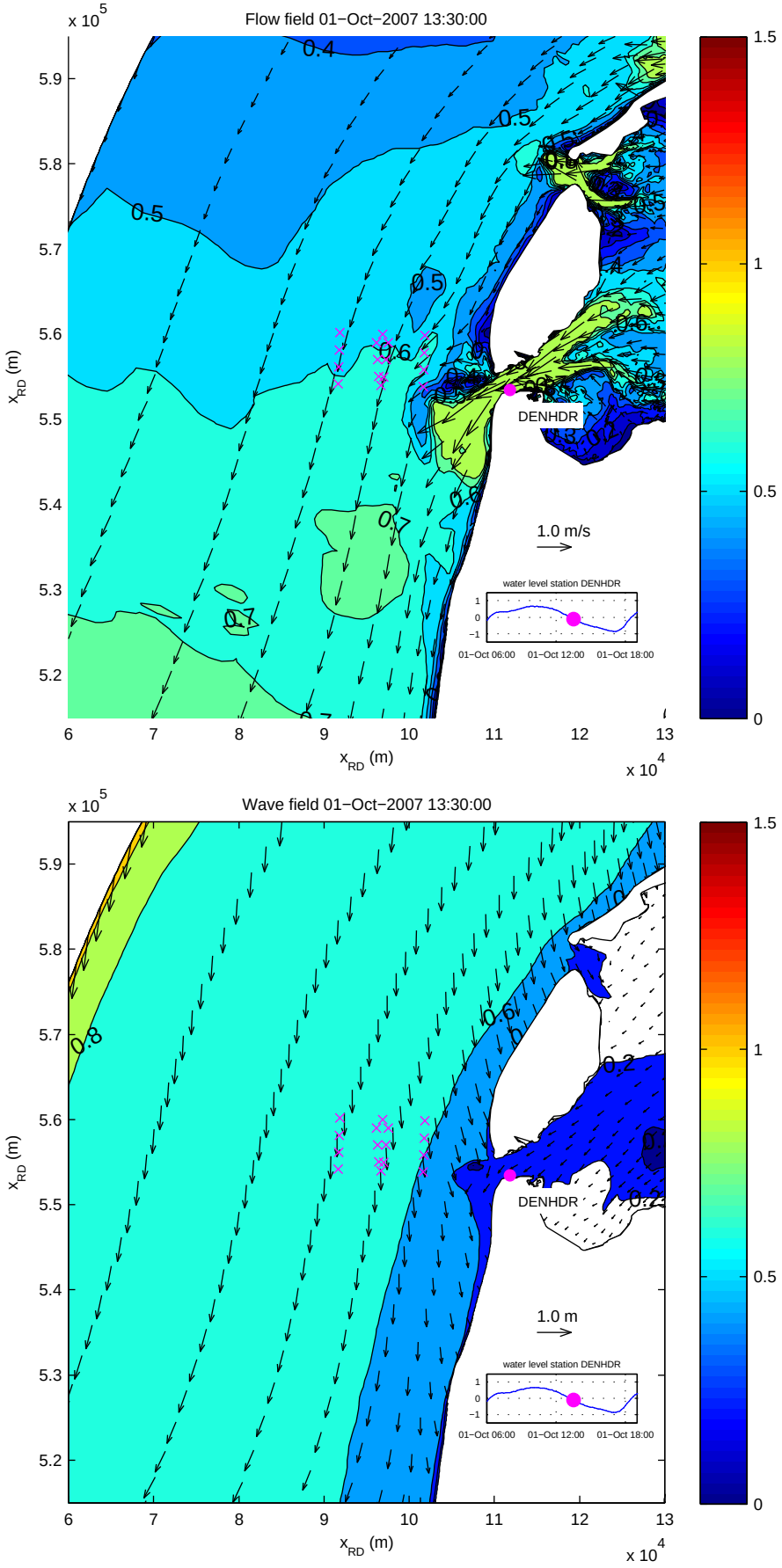

Simulated flow velocities in upper layer (m/s) and sigificant wave heights (m)
date and time: 01−Oct−2007 13:30:00
x−marks denote locations of T1 observations

Alkyon Hydraulic Consultancy & Research	A2273	Fig. 3.20

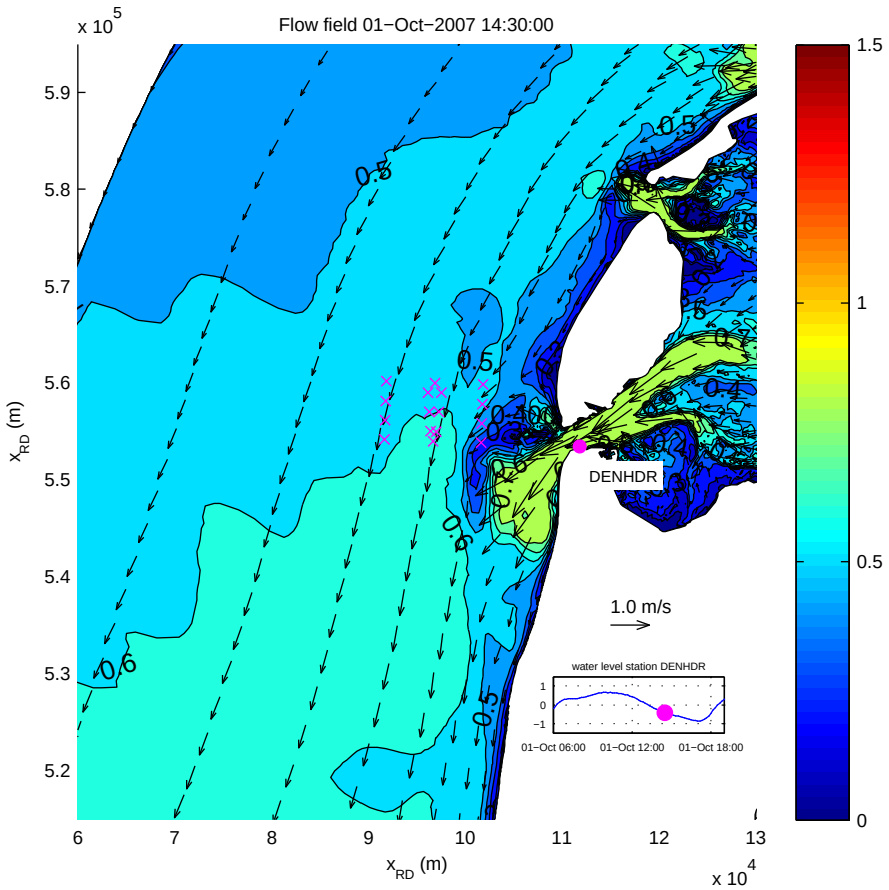

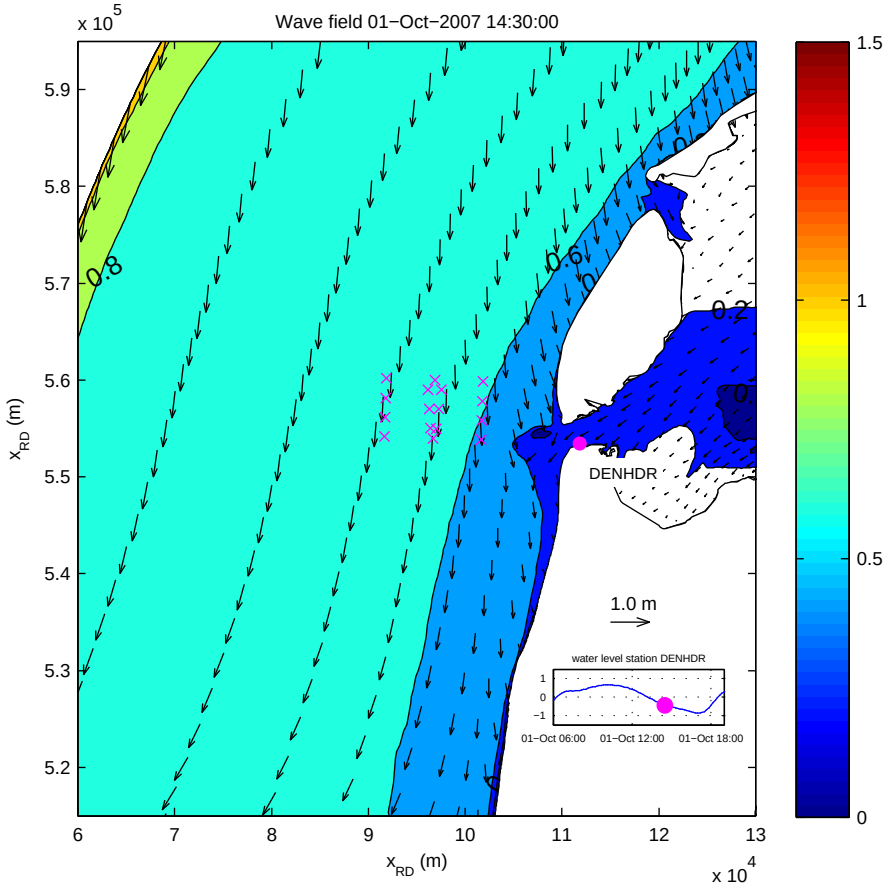

Simulated flow velocities in upper layer (m/s) and sigificant wave heights (m)
date and time: 01−Oct−2007 14:30:00
x−marks denote locations of T1 observations

Alkyon Hydraulic Consultancy & Research	A2273	Fig. 3.21

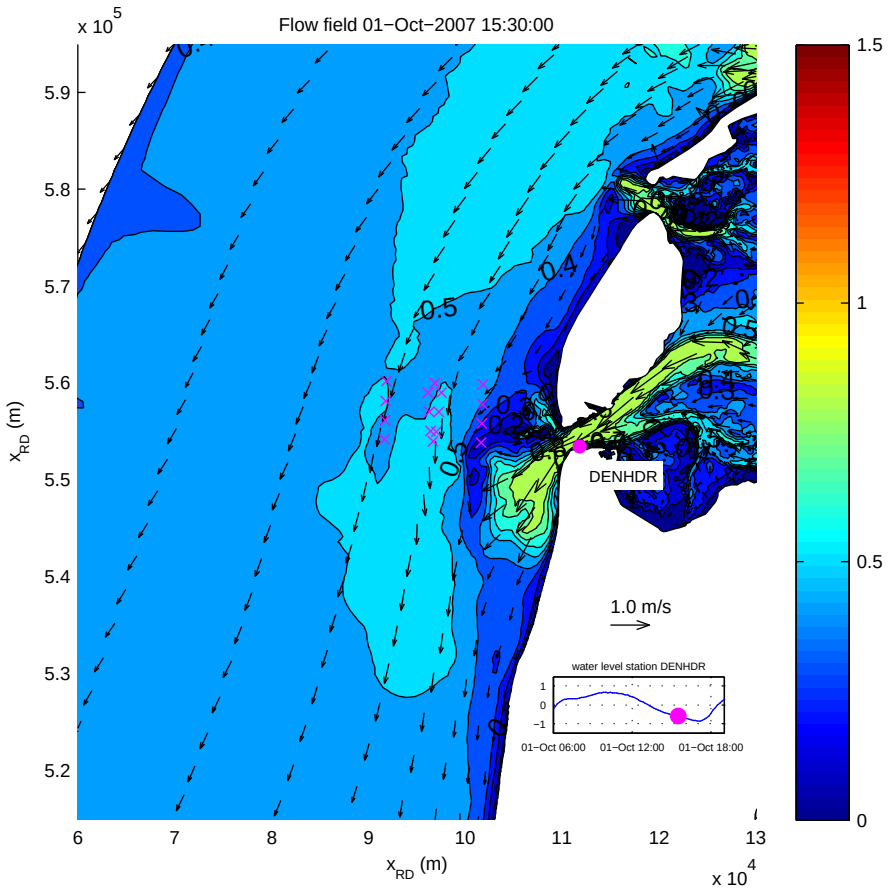

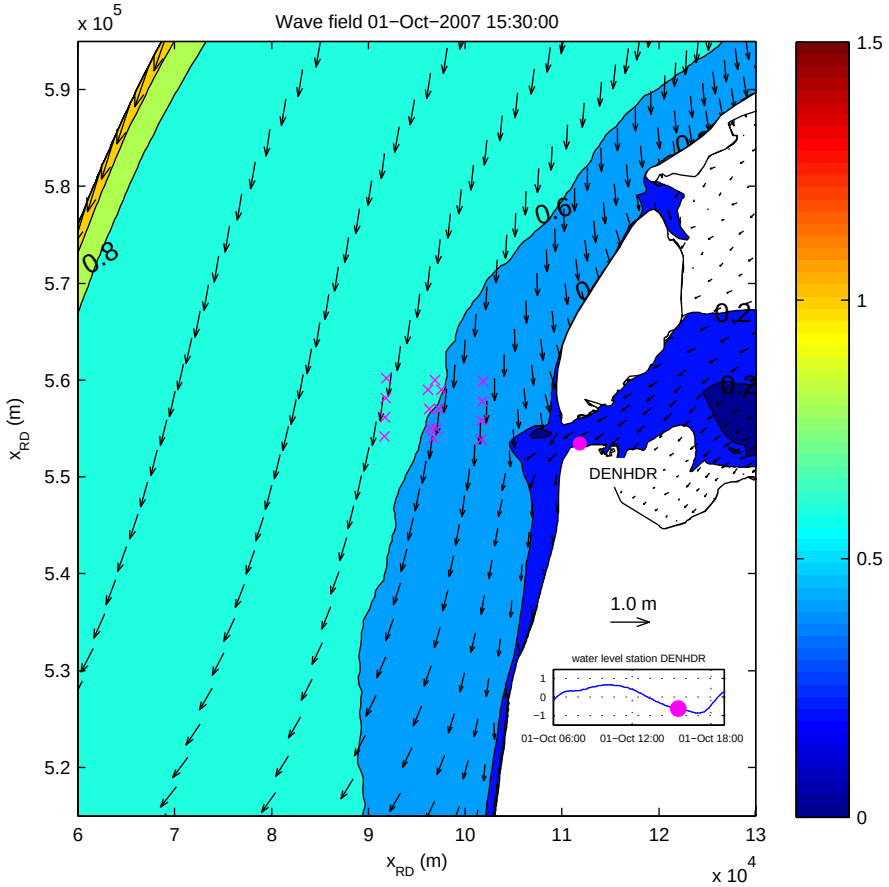

Simulated flow velocities in upper layer (m/s) and sigificant wave heights (m)
date and time: 01−Oct−2007 15:30:00
x−marks denote locations of T1 observations

Alkyon Hydraulic Consultancy & Research	A2273	Fig. 3.22

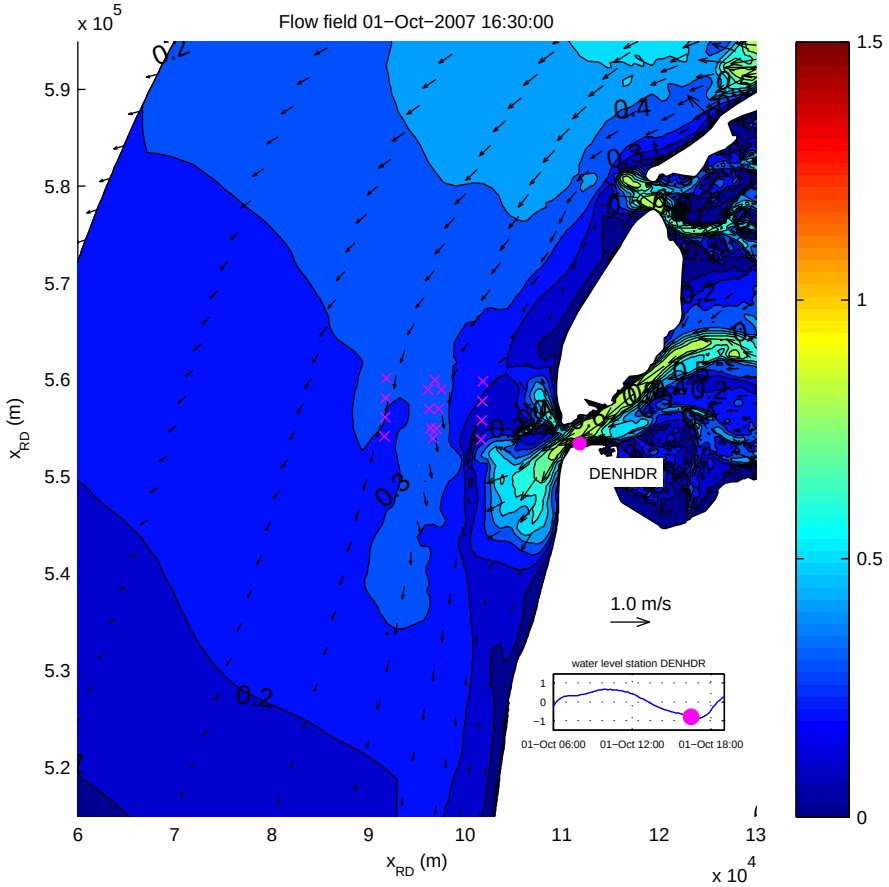

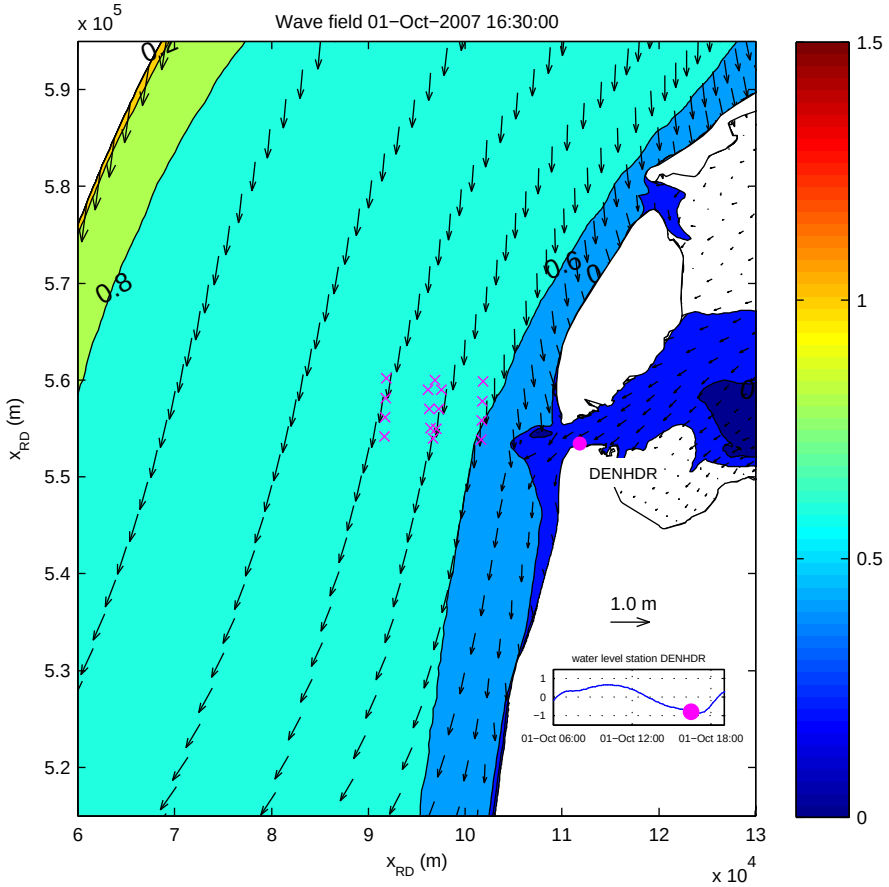

Simulated flow velocities in upper layer (m/s) and sigificant wave heights (m) date and time: 01−Oct−2007 16:30:00 x−marks denote locations of T1 observations		
Alkyon Hydraulic Consultancy & Research	A2273	Fig. 3.23

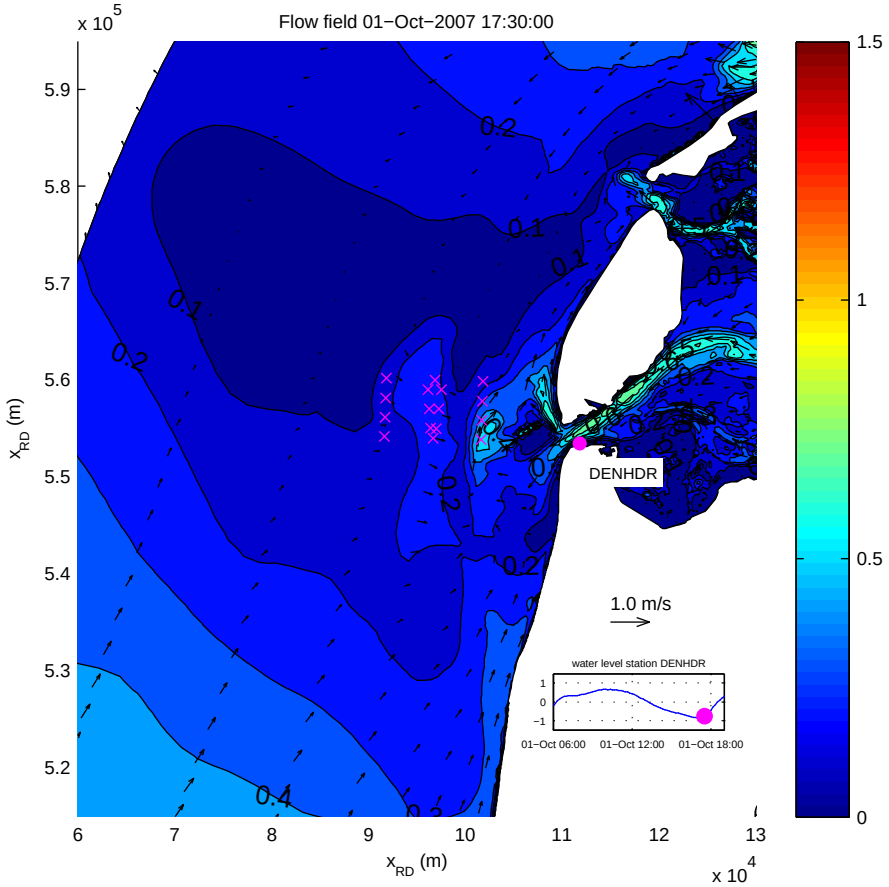

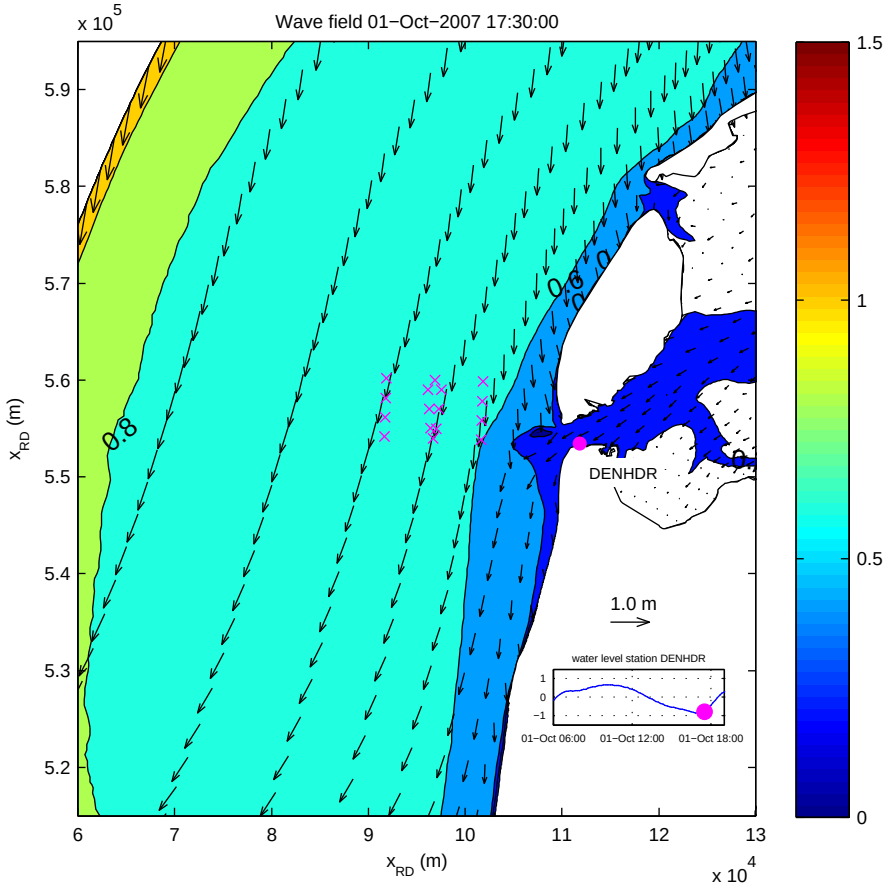

Simulated flow velocities in upper layer (m/s) and sigificant wave heights (m)
date and time: 01−Oct−2007 17:30:00
x−marks denote locations of T1 observations

Alkyon Hydraulic Consultancy & Research	A2273	Fig. 3.24

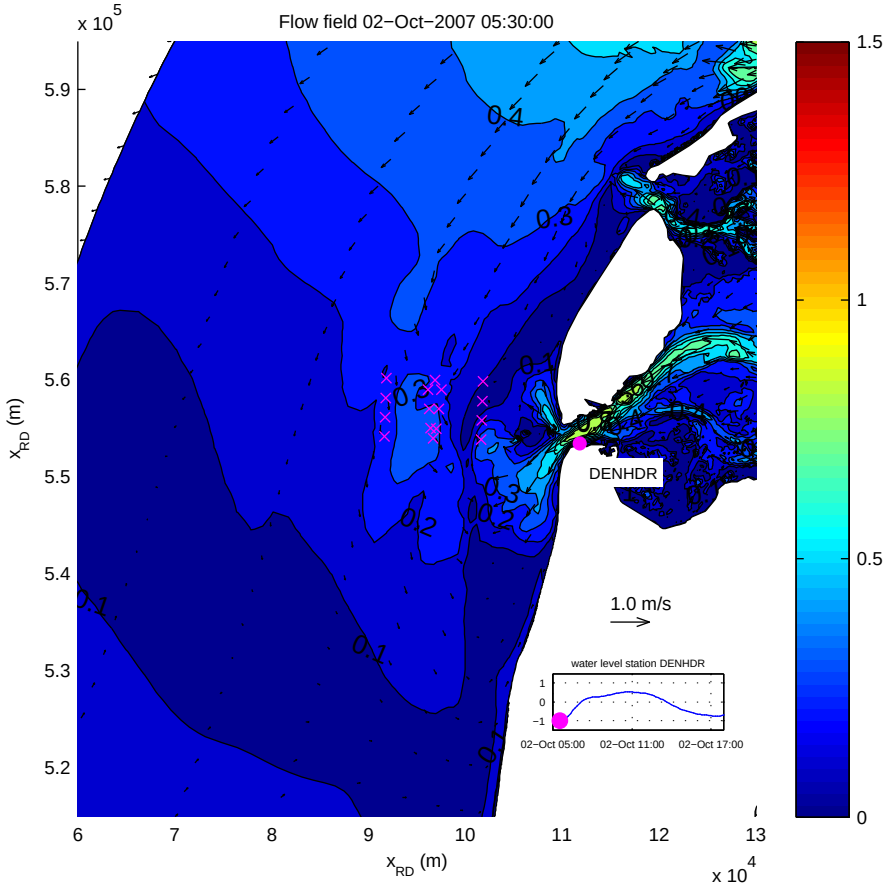

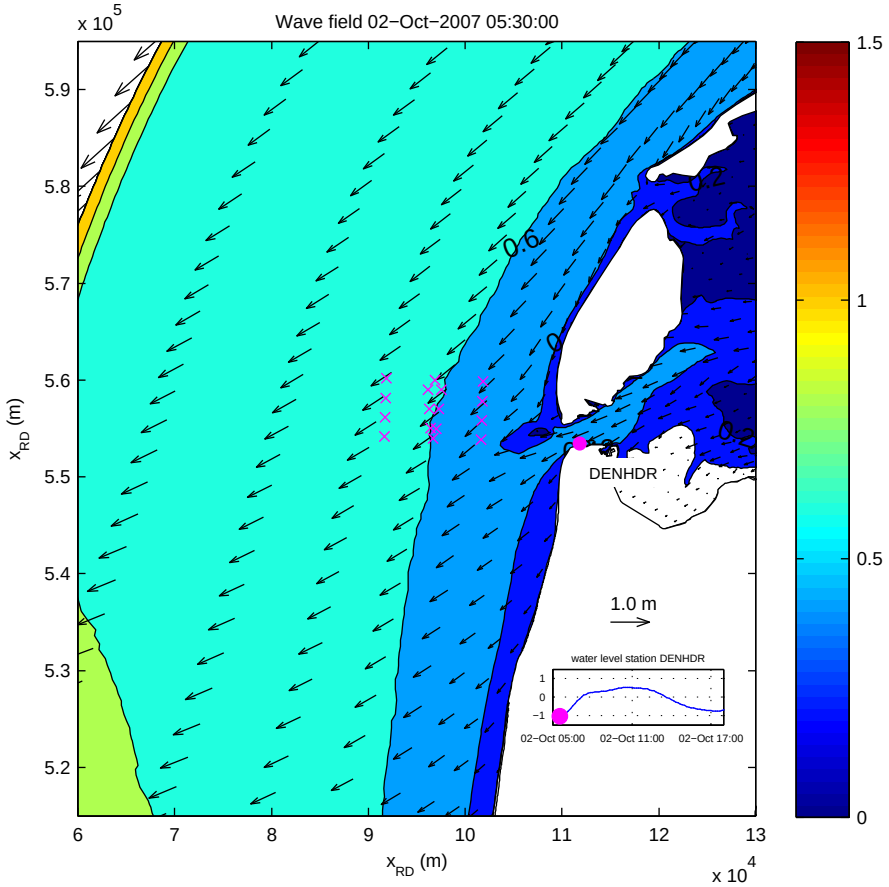

Simulated flow velocities in upper layer (m/s) and sigificant wave heights (m)
date and time: 02−Oct−2007 05:30:00
x−marks denote locations of T1 observations

Alkyon Hydraulic Consultancy & Research	A2273	Fig. 3.25

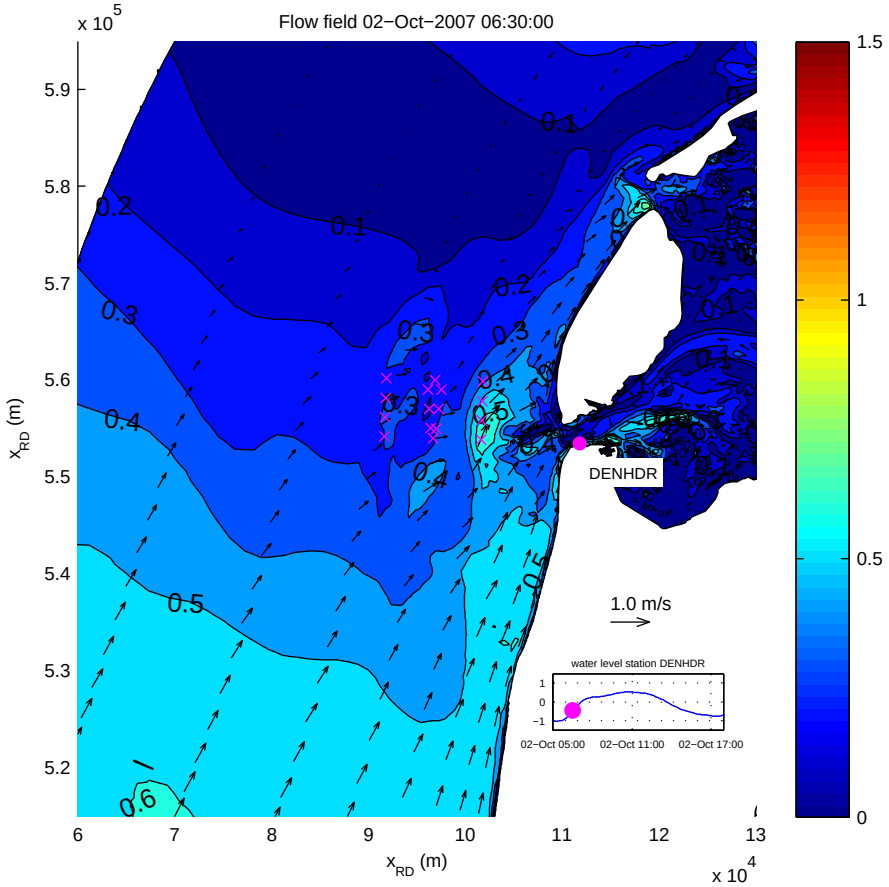

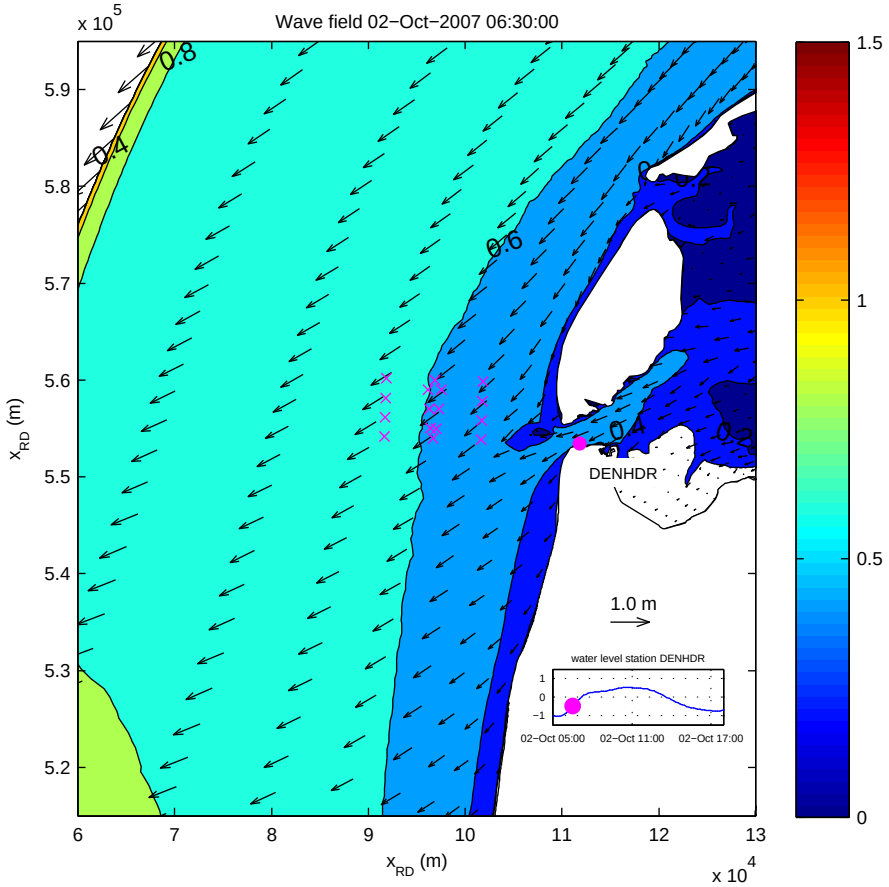

Simulated flow velocities in upper layer (m/s) and sigificant wave heights (m)
date and time: 02−Oct−2007 06:30:00
x−marks denote locations of T1 observations

Alkyon Hydraulic Consultancy & Research	A2273	Fig. 3.26

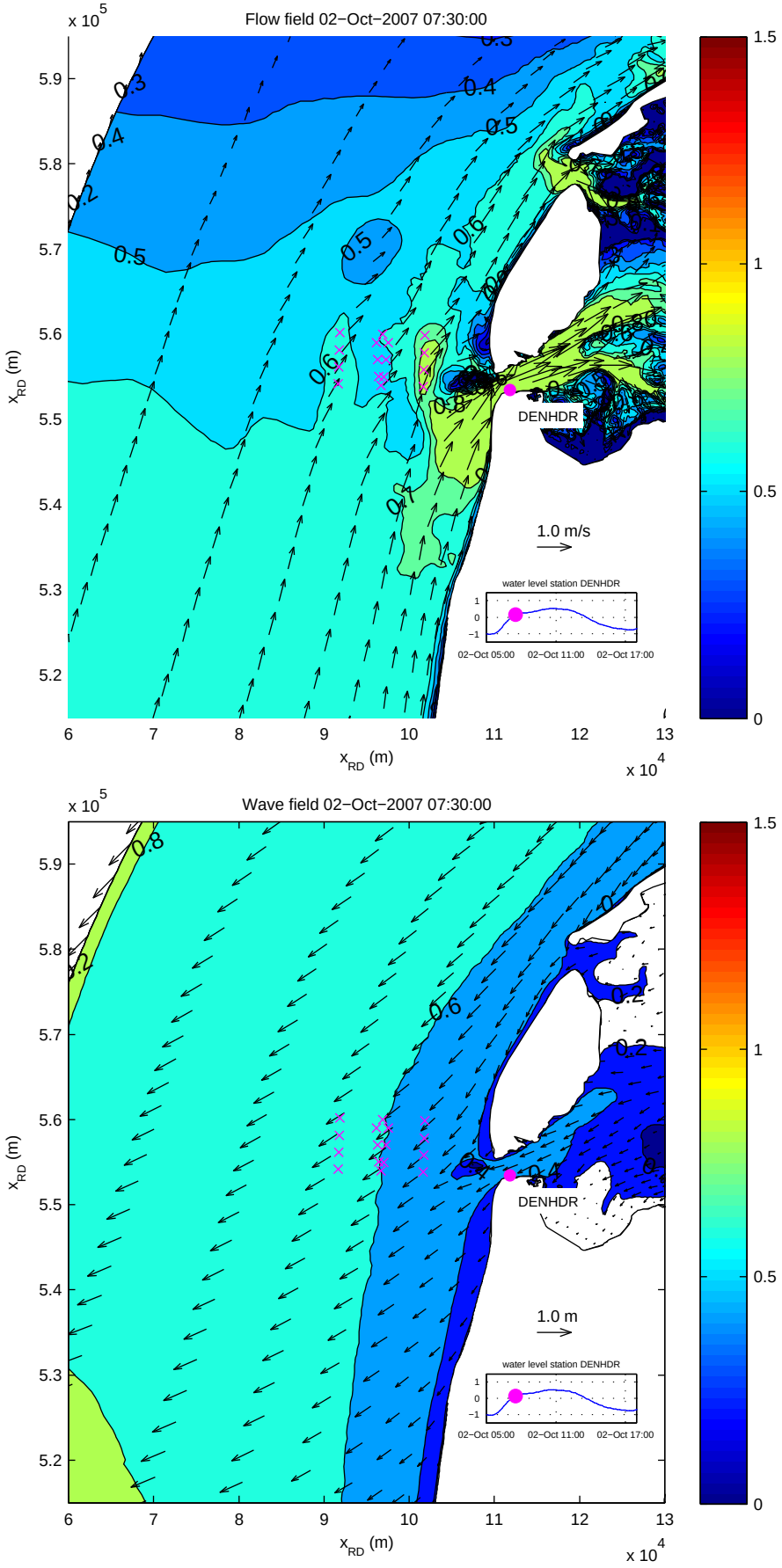

Simulated flow velocities in upper layer (m/s) and sigificant wave heights (m)
date and time: 02−Oct−2007 07:30:00
x−marks denote locations of T1 observations

Alkyon Hydraulic Consultancy & Research	A2273	Fig. 3.27

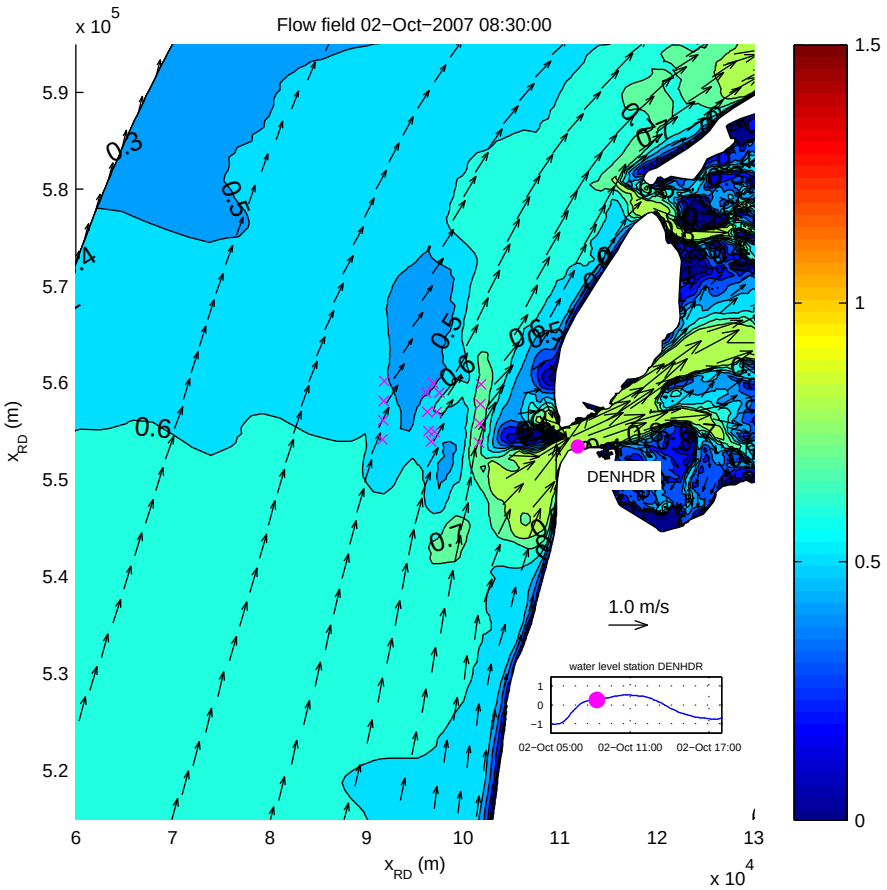

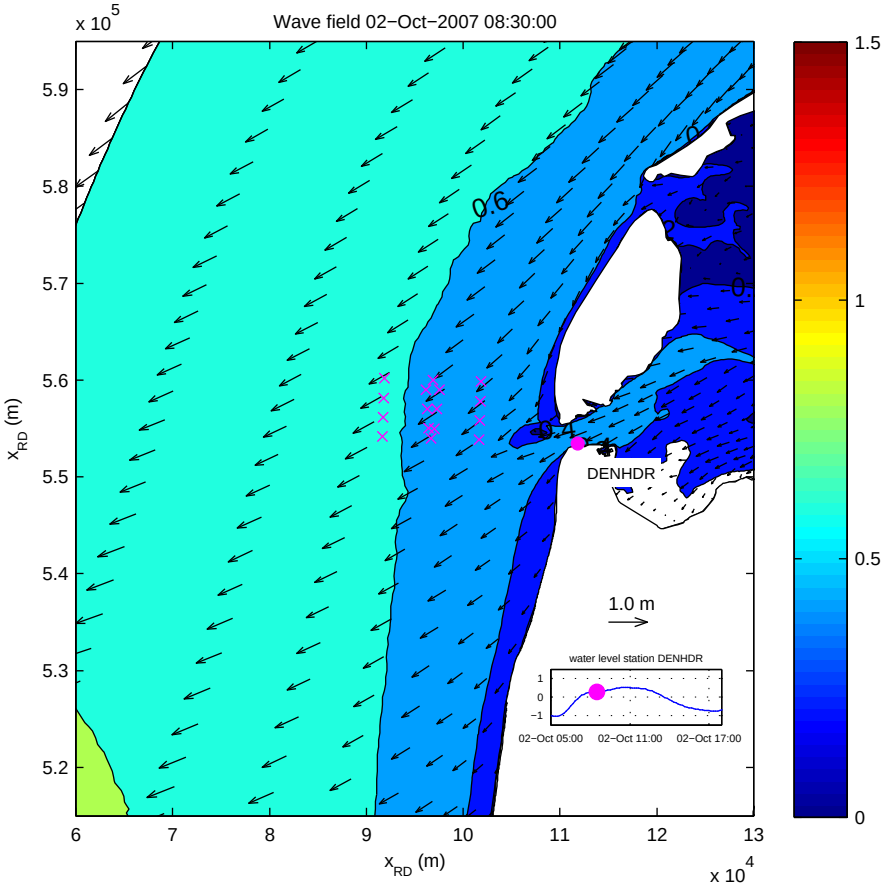

Simulated flow velocities in upper layer (m/s) and sigificant wave heights (m)
date and time: 02−Oct−2007 08:30:00
x−marks denote locations of T1 observations

Alkyon Hydraulic Consultancy & Research	A2273	Fig. 3.28

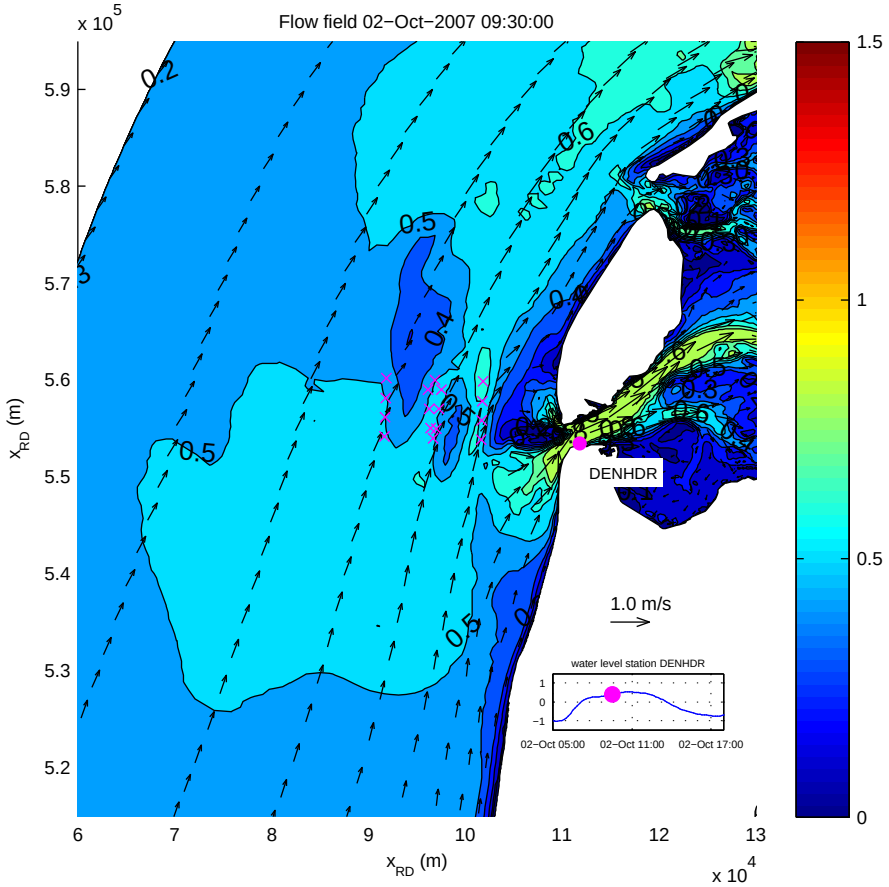

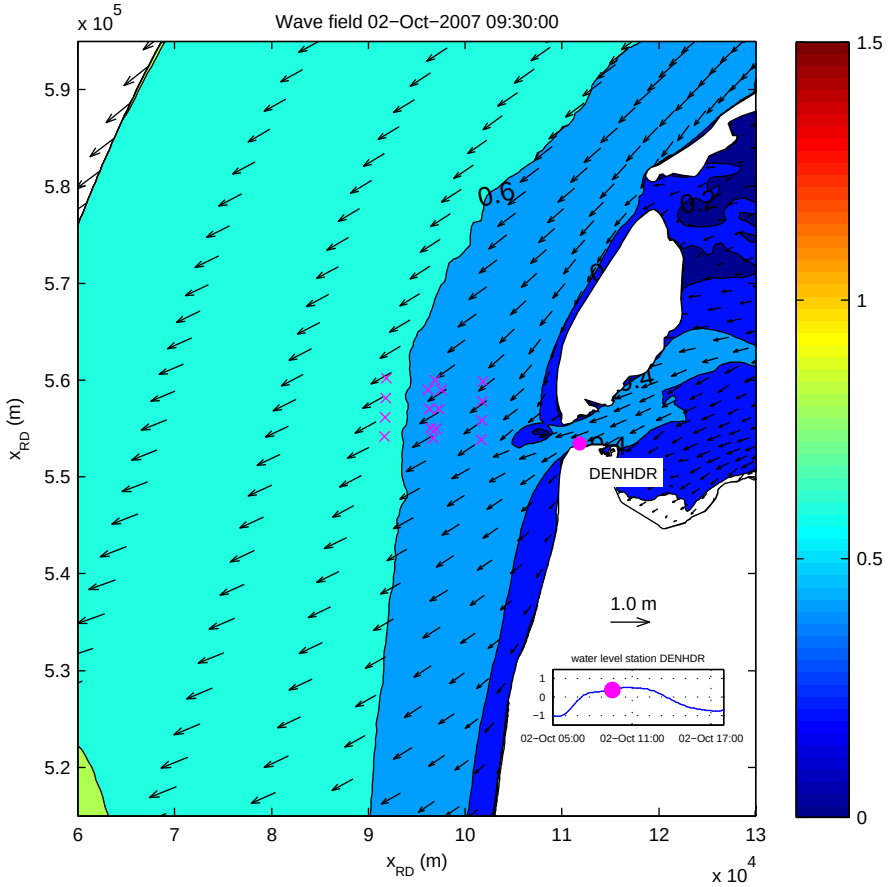

Simulated flow velocities in upper layer (m/s) and sigificant wave heights (m)
date and time: 02−Oct−2007 09:30:00
x−marks denote locations of T1 observations

Alkyon Hydraulic Consultancy & Research	A2273	Fig. 3.29

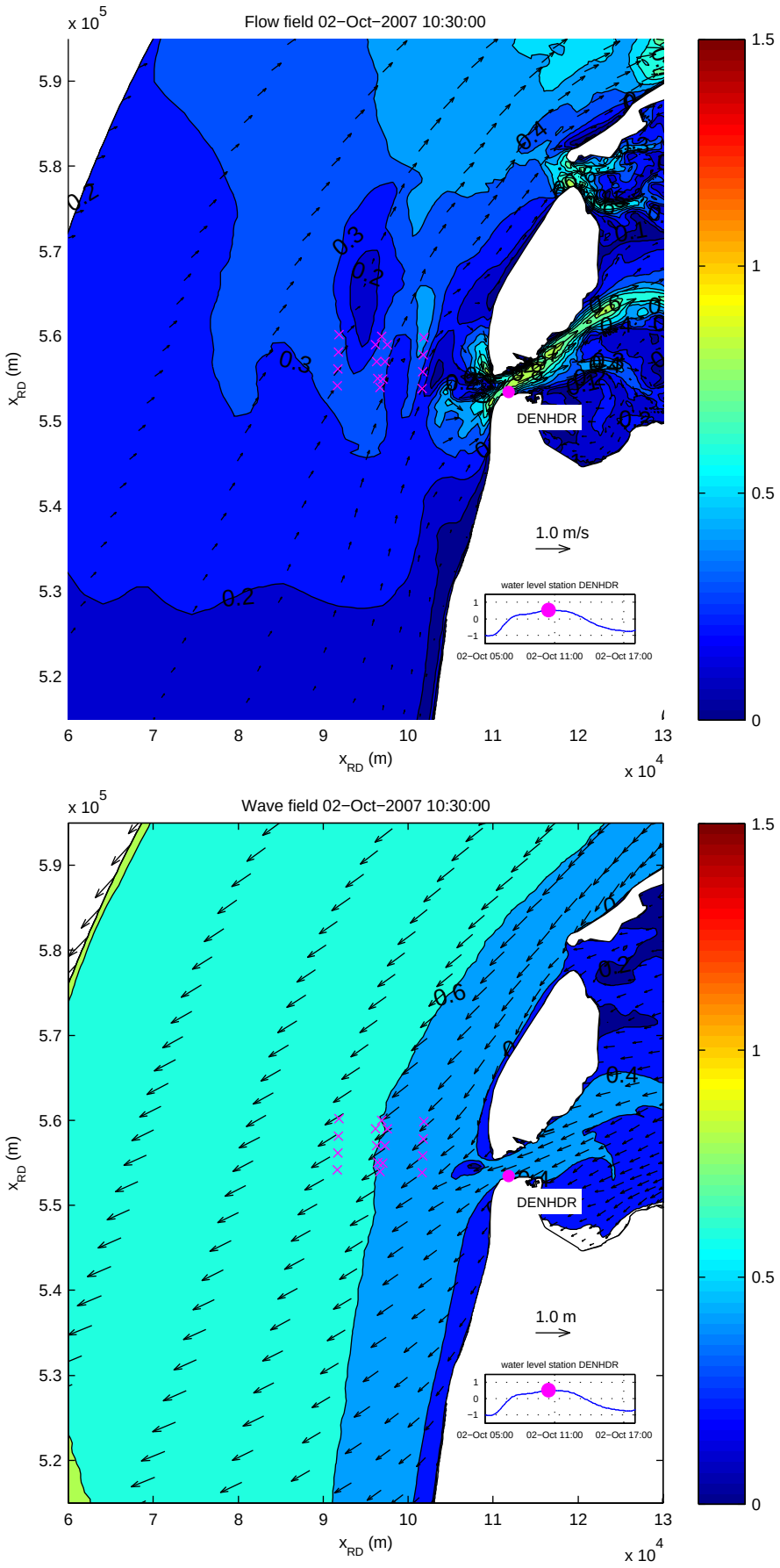

Simulated flow velocities in upper layer (m/s) and sigificant wave heights (m) date and time: 02−Oct−2007 10:30:00 x−marks denote locations of T1 observations		
Alkyon Hydraulic Consultancy & Research	A2273	Fig. 3.30

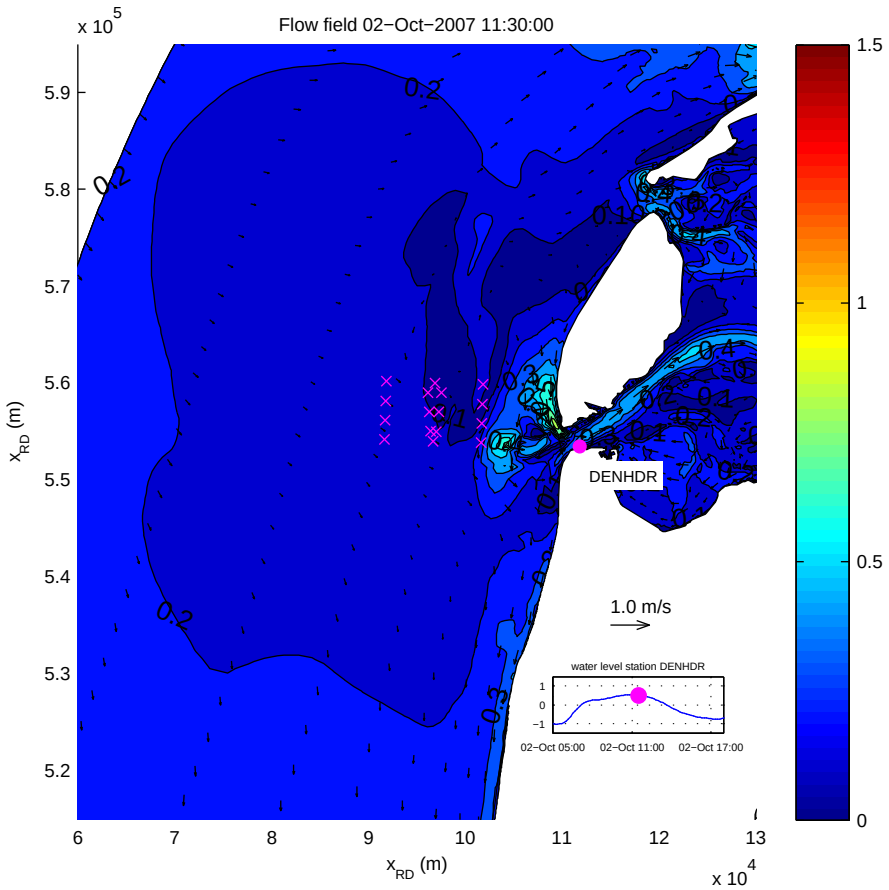

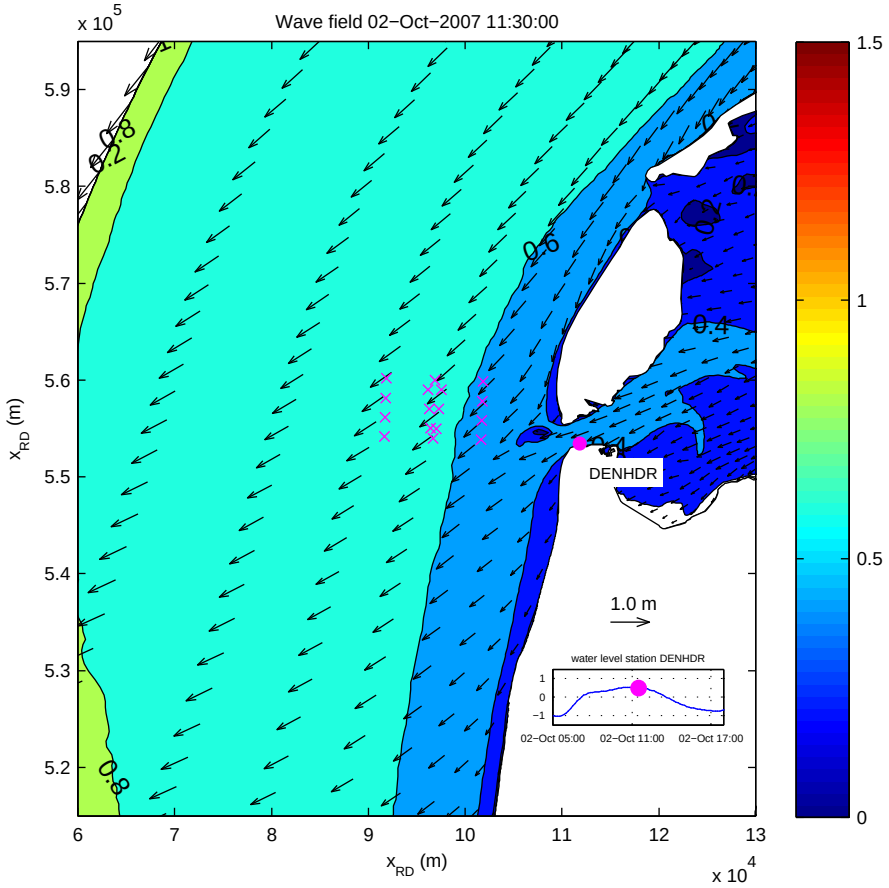

Simulated flow velocities in upper layer (m/s) and sigificant wave heights (m)
date and time: 02−Oct−2007 11:30:00
x−marks denote locations of T1 observations

Alkyon Hydraulic Consultancy & Research	A2273	Fig. 3.31

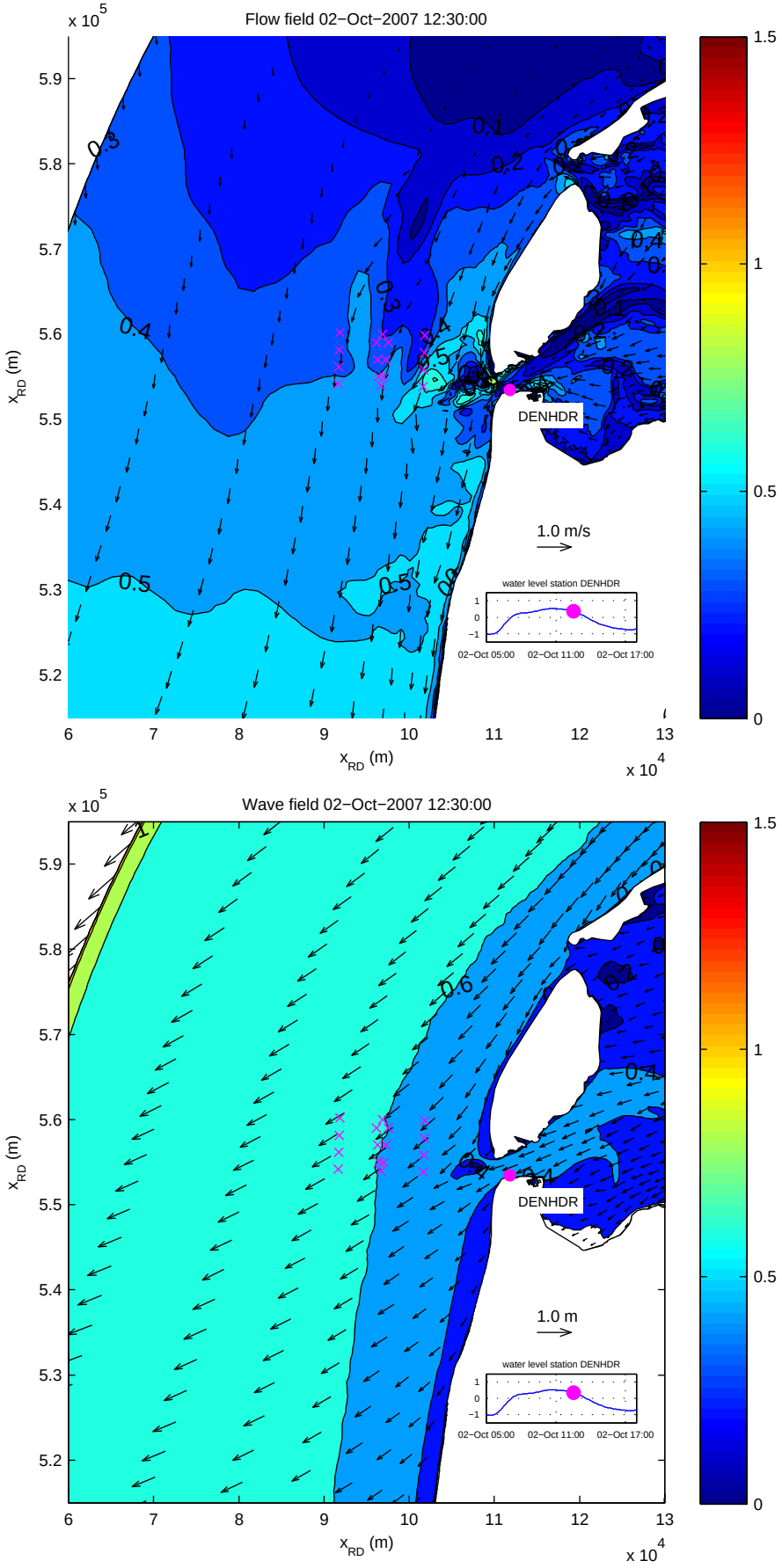

Simulated flow velocities in upper layer (m/s) and sigificant wave heights (m)
date and time: 02−Oct−2007 12:30:00
x−marks denote locations of T1 observations

Alkyon Hydraulic Consultancy & Research	A2273	Fig. 3.32

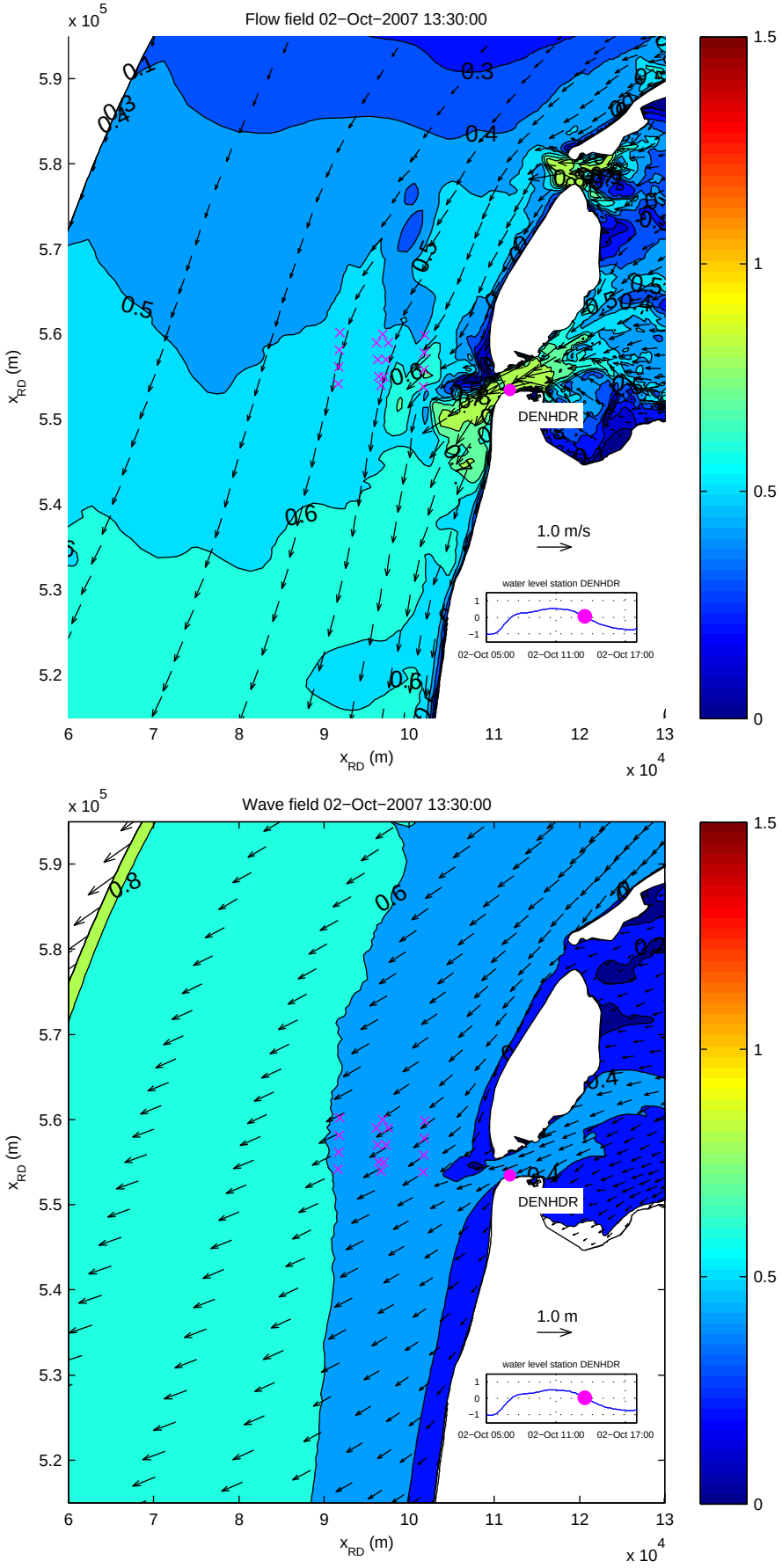

Simulated flow velocities in upper layer (m/s) and sigificant wave heights (m) date and time: 02−Oct−2007 13:30:00 x−marks denote locations of T1 observations		
Alkyon Hydraulic Consultancy & Research	A2273	Fig. 3.33

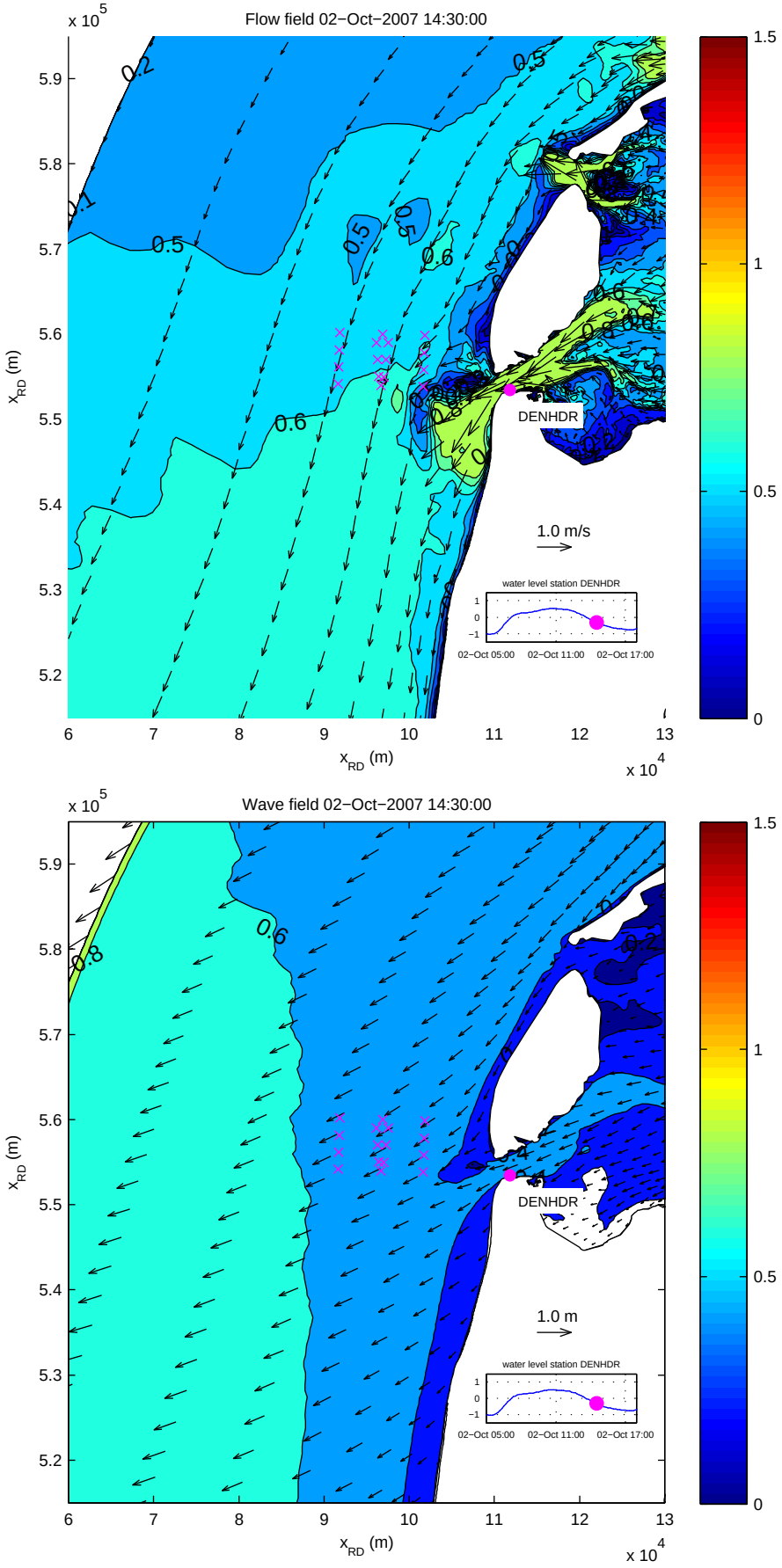

Simulated flow velocities in upper layer (m/s) and sigificant wave heights (m)
date and time: 02−Oct−2007 14:30:00
x−marks denote locations of T1 observations

Alkyon Hydraulic Consultancy & Research	A2273	Fig. 3.34

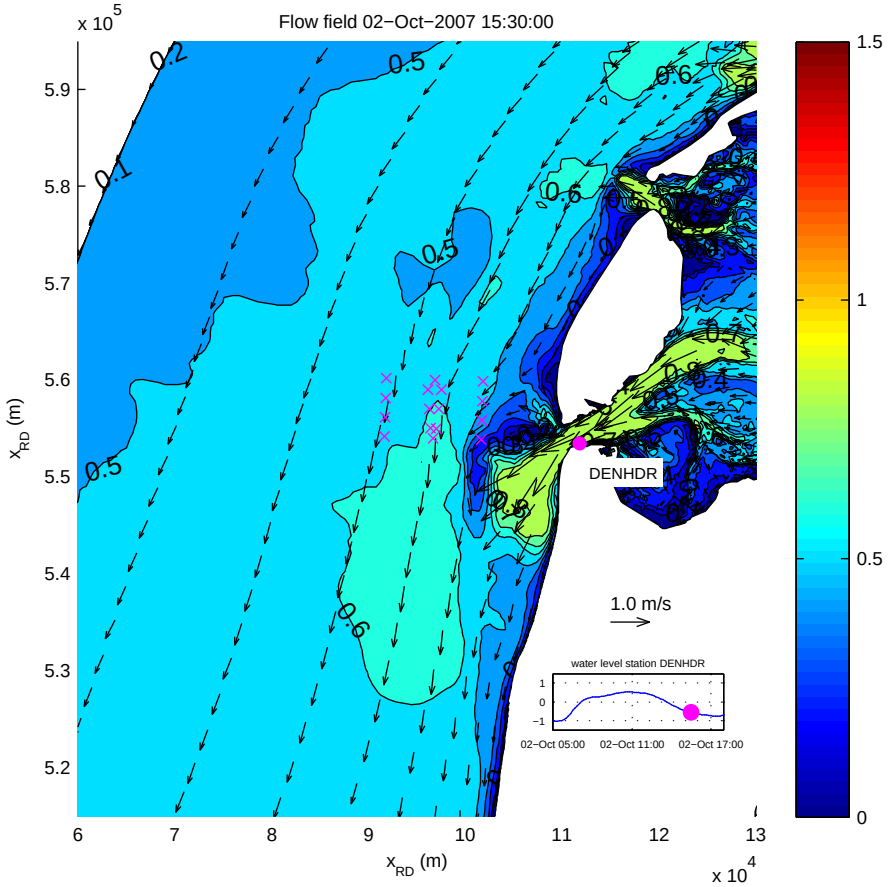

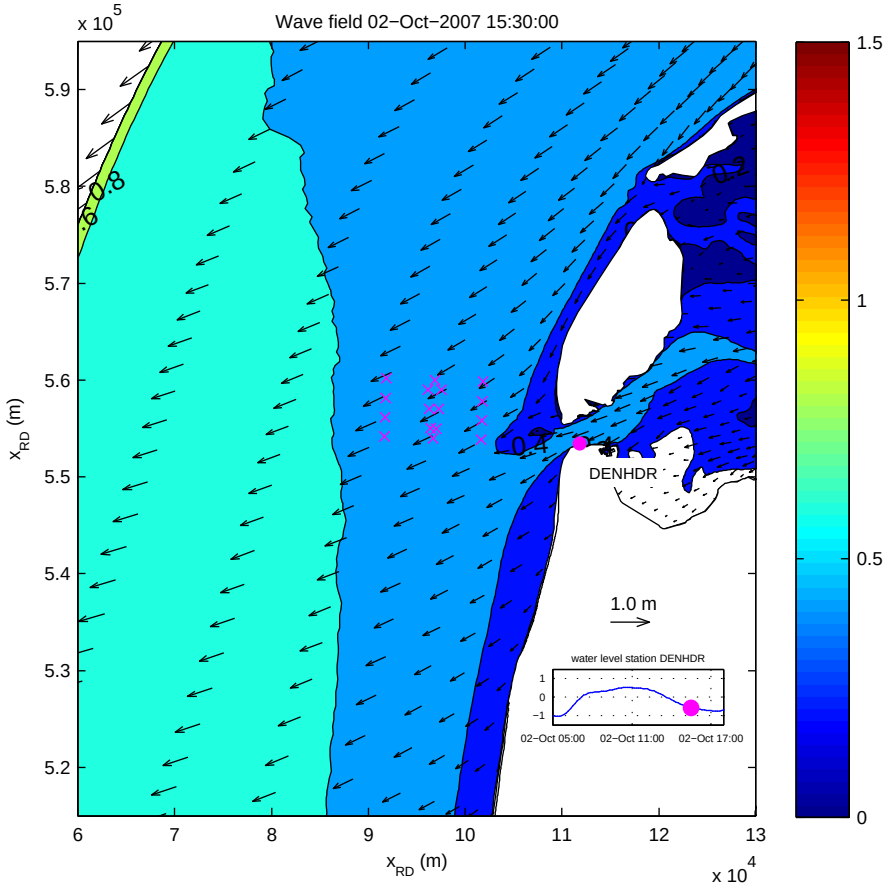

Simulated flow velocities in upper layer (m/s) and sigificant wave heights (m)
date and time: 02−Oct−2007 15:30:00
x−marks denote locations of T1 observations

Alkyon Hydraulic Consultancy & Research	A2273	Fig. 3.35

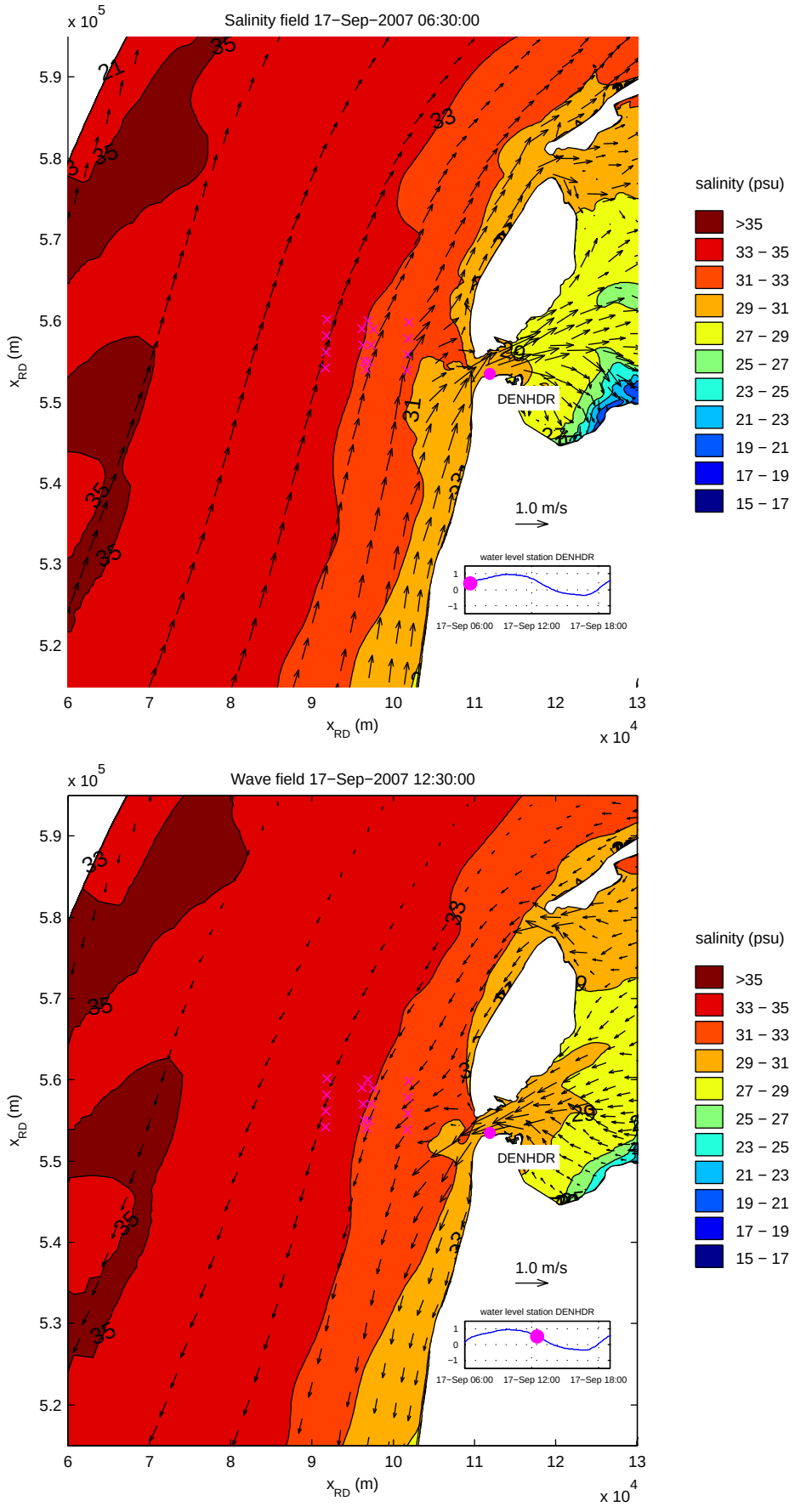

Simulated salinities (psu) in upper computational layer
date: 17−Sep−2007
x−marks denote locations of T1 observations

Alkyon Hydraulic Consultancy & Research | A2273 | Fig. 3.36

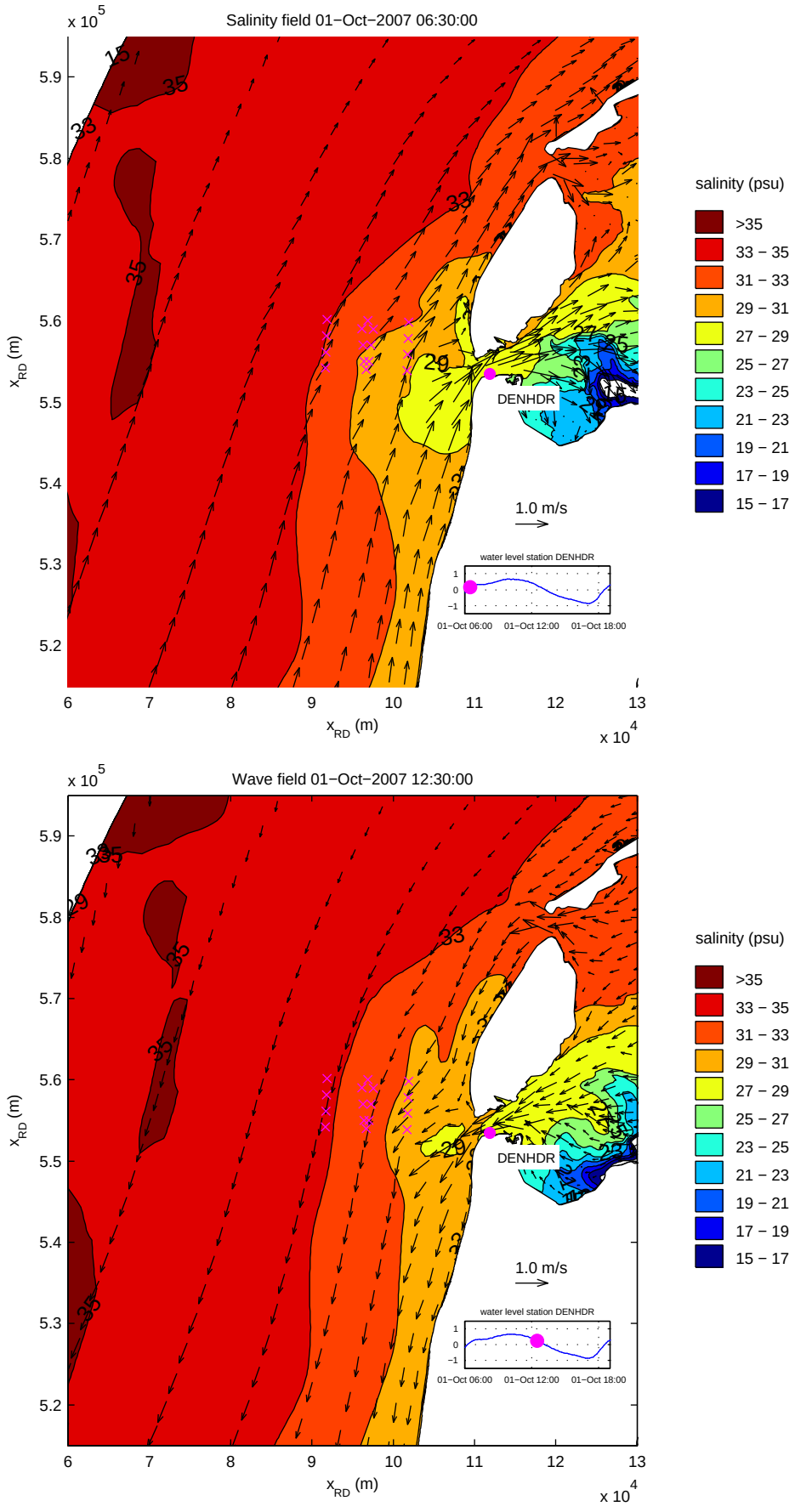

Simulated salinities (psu) in upper computational layer
date: 01−Oct−2007
x−marks denote locations of T1 observations

Alkyon Hydraulic Consultancy & Research	A2273	Fig. 3.37

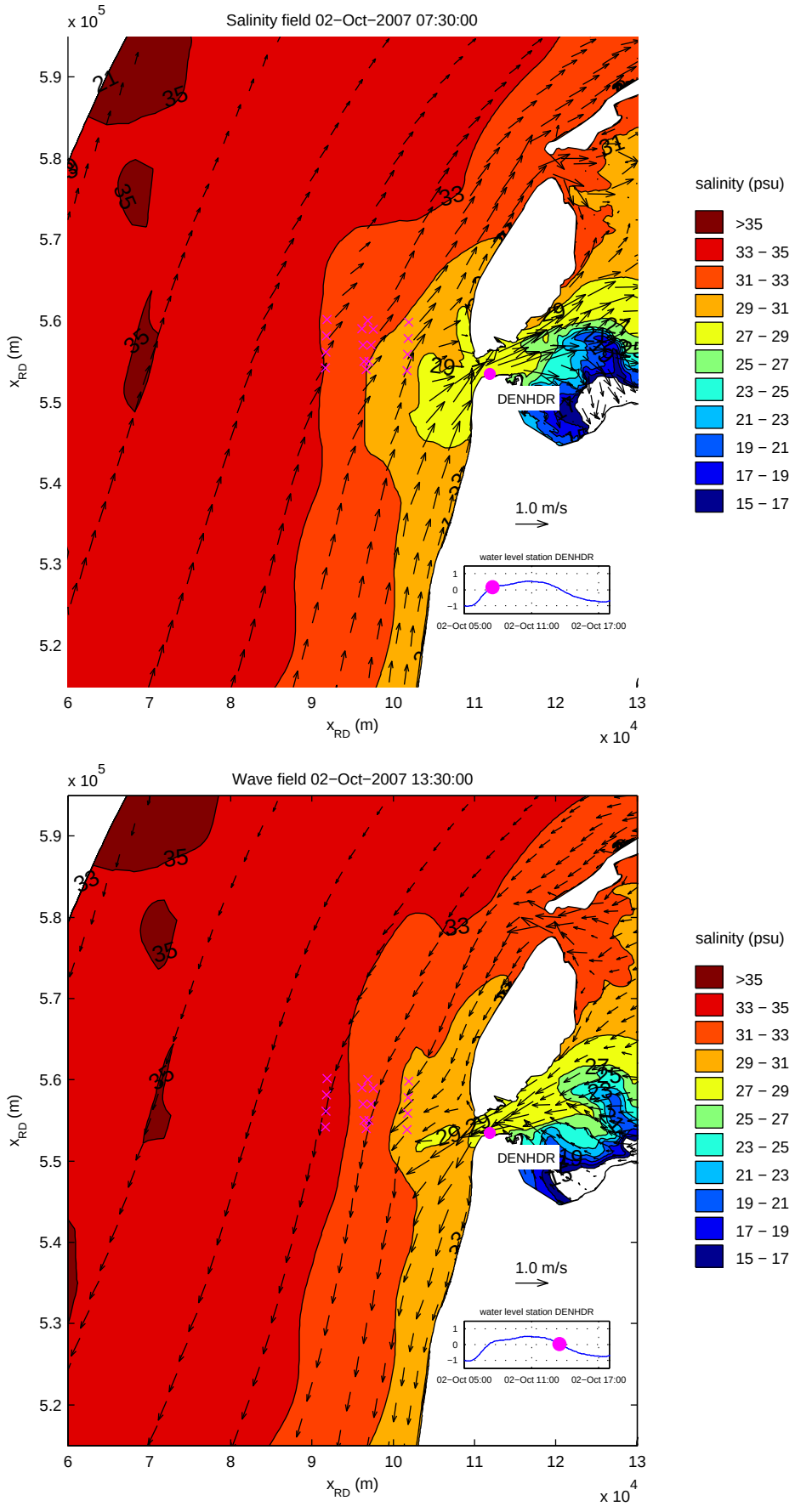

Simulated salinities (psu) in upper computational layer
date: 02−Oct−2007
x−marks denote locations of T1 observations

Alkyon Hydraulic Consultancy & Research	A2273	Fig. 3.38

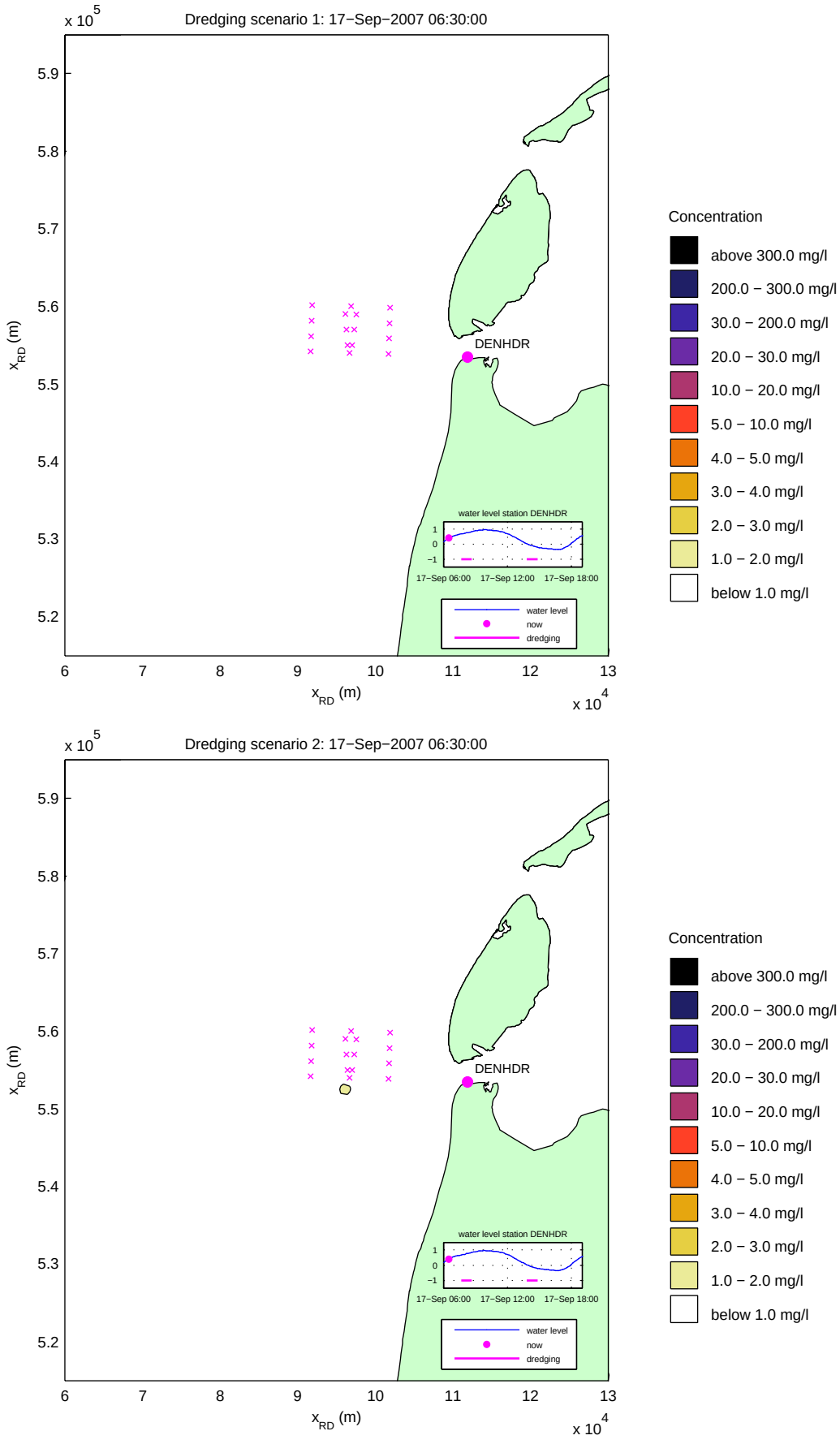

Simulated effect of overflow on silt concentrations (mg/l)
date and time: 17−Sep−2007 06:30:00
x−marks denote locations of T1 observations

Alkyon Hydraulic Consultancy & Research | A2273 | Fig. 3.39

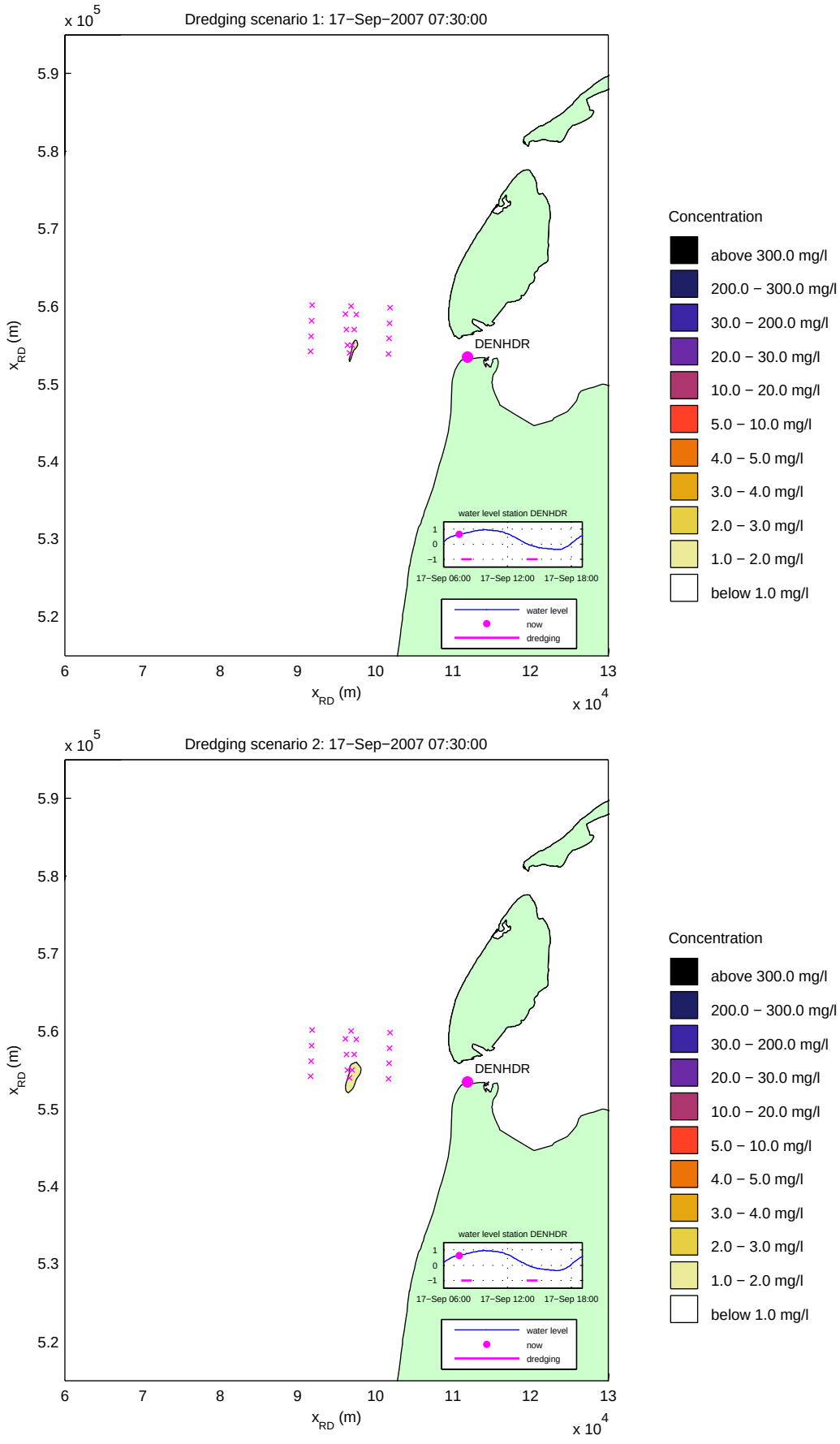

Simulated effect of overflow on silt concentrations (mg/l)
date and time: 17−Sep−2007 07:30:00
x−marks denote locations of T1 observations

Alkyon Hydraulic Consultancy & Research | A2273 | Fig. 3.40

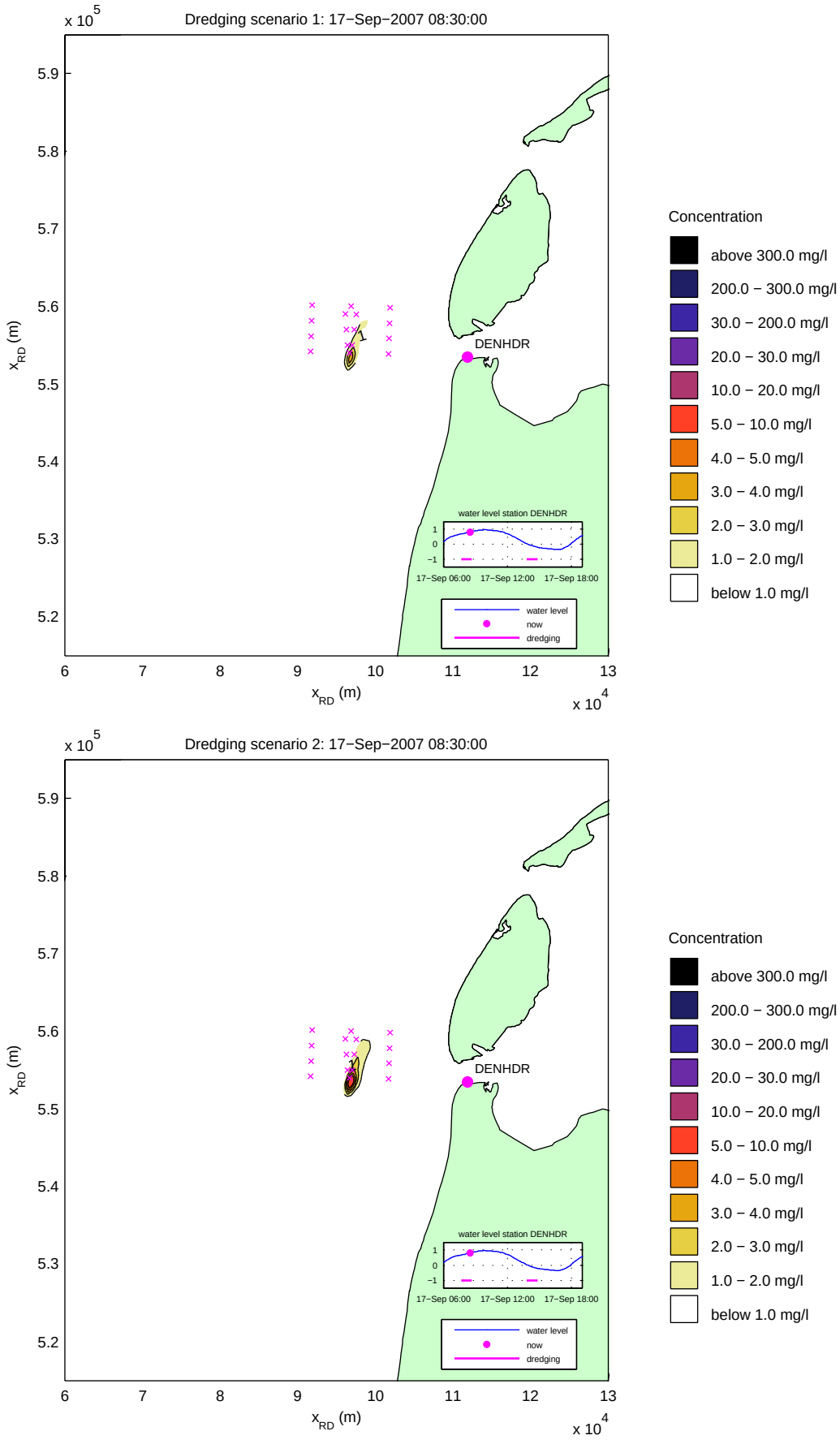

Simulated effect of overflow on silt concentrations (mg/l)
date and time: 17−Sep−2007 08:30:00
x−marks denote locations of T1 observations

Alkyon Hydraulic Consultancy & Research | A2273 | Fig. 3.41

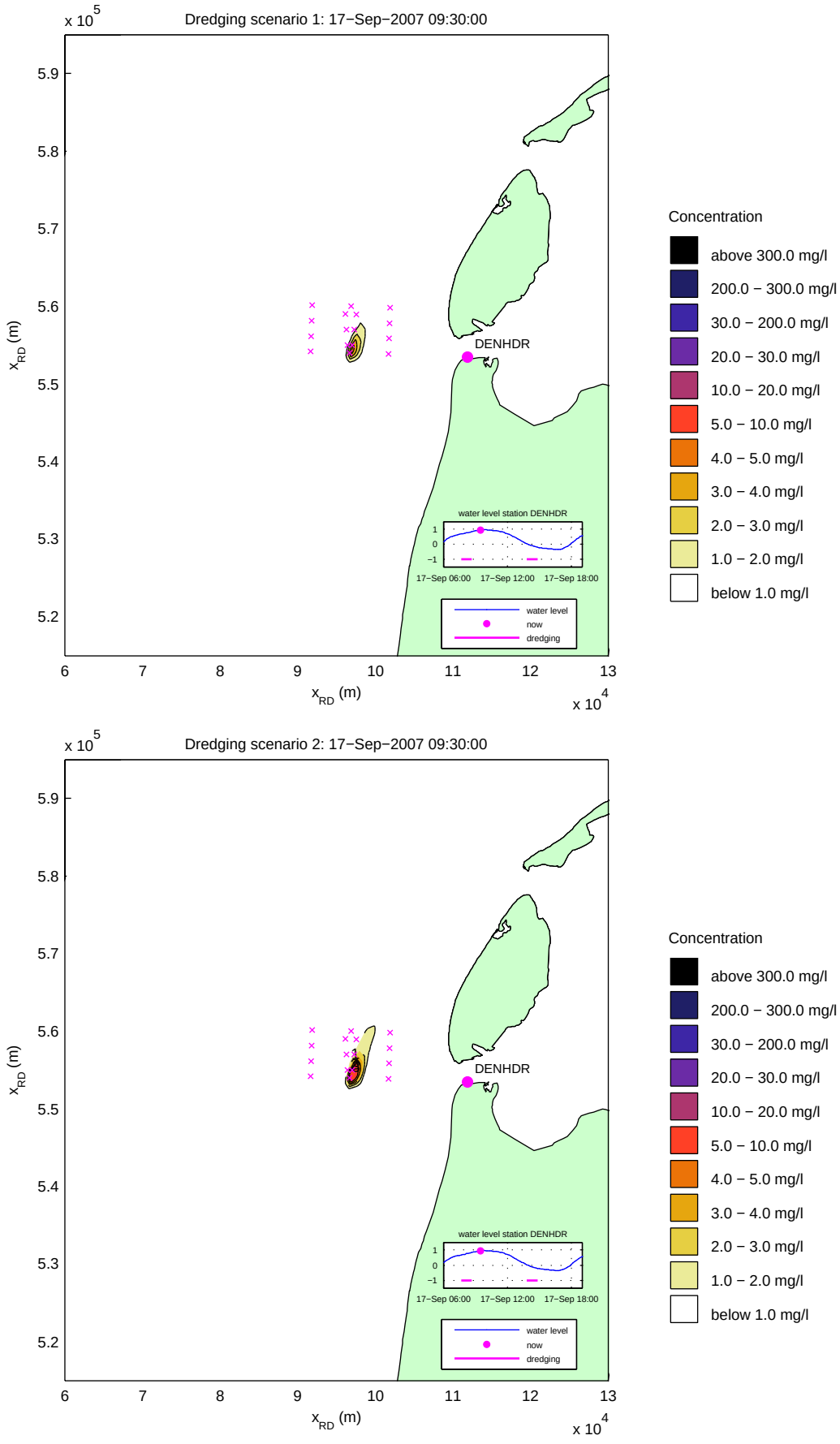

Simulated effect of overflow on silt concentrations (mg/l)
date and time: 17−Sep−2007 09:30:00
x−marks denote locations of T1 observations

Alkyon Hydraulic Consultancy & Research	A2273	Fig. 3.42

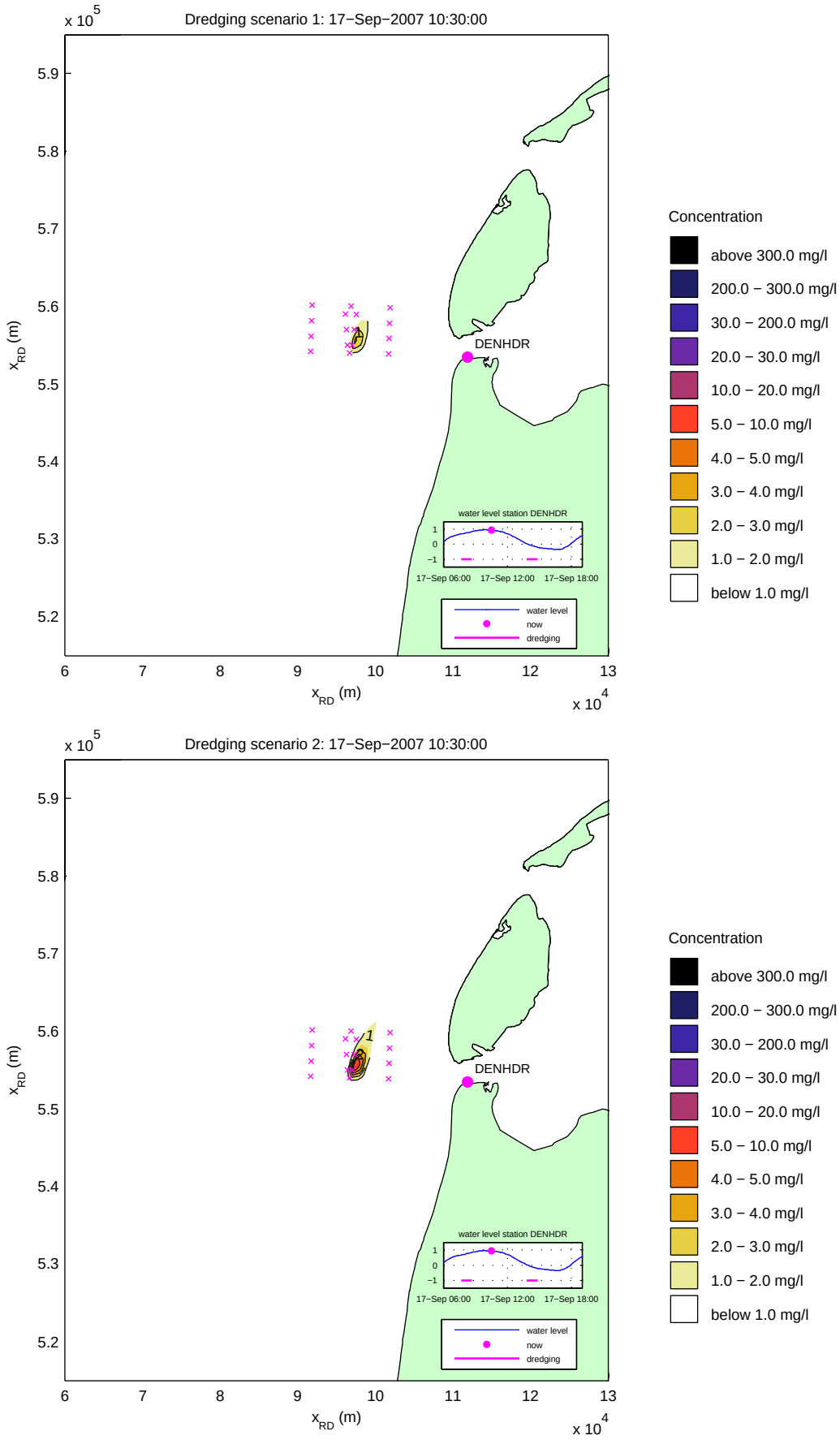

Simulated effect of overflow on silt concentrations (mg/l)
date and time: 17−Sep−2007 10:30:00
x−marks denote locations of T1 observations

Alkyon Hydraulic Consultancy & Research | A2273 | Fig. 3.43

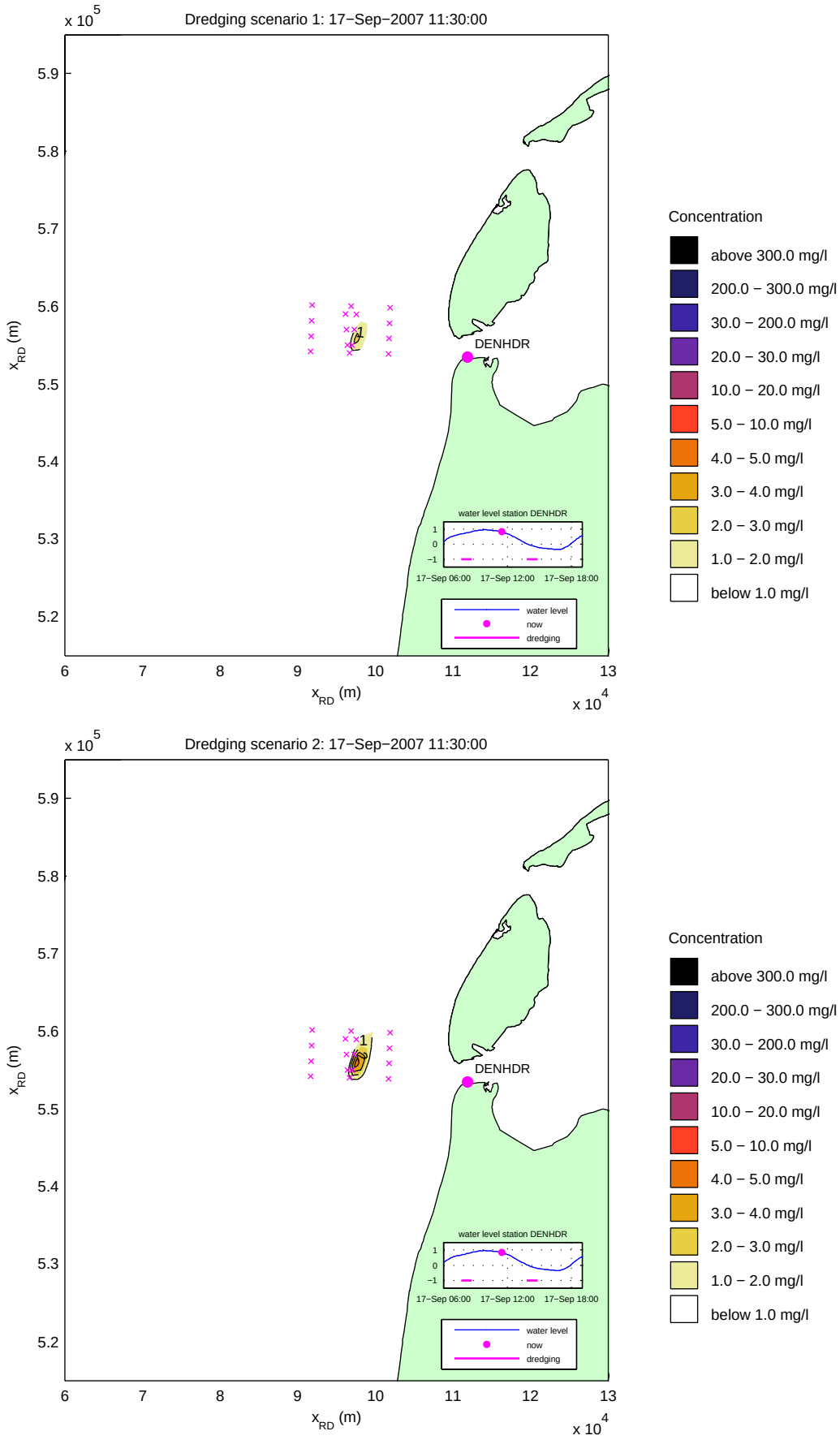

Simulated effect of overflow on silt concentrations (mg/l)
date and time: 17−Sep−2007 11:30:00
x−marks denote locations of T1 observations

Alkyon Hydraulic Consultancy & Research	A2273	Fig. 3.44

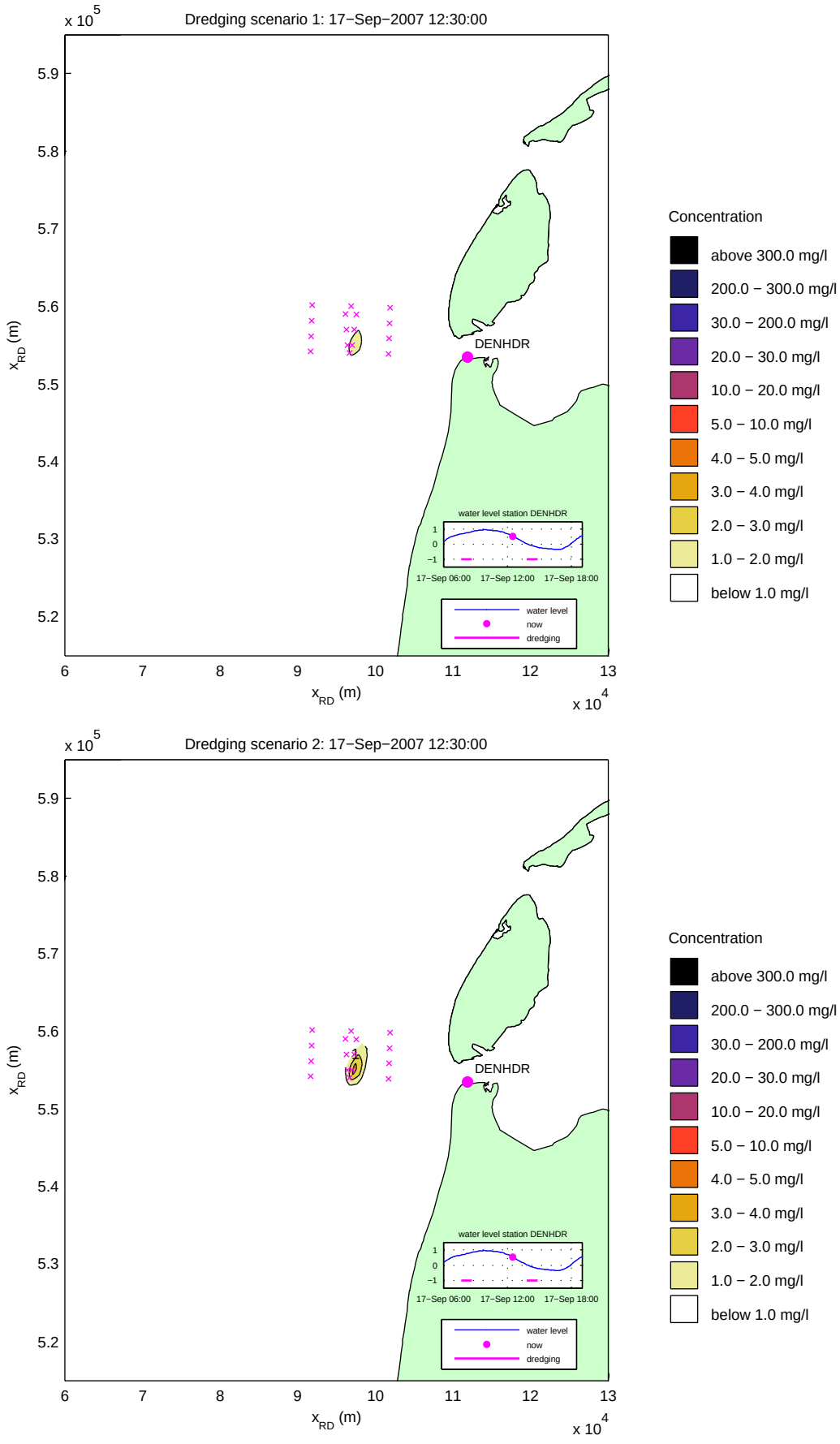

Simulated effect of overflow on silt concentrations (mg/l)
date and time: 17−Sep−2007 12:30:00
x−marks denote locations of T1 observations

Alkyon Hydraulic Consultancy & Research	A2273	Fig. 3.45

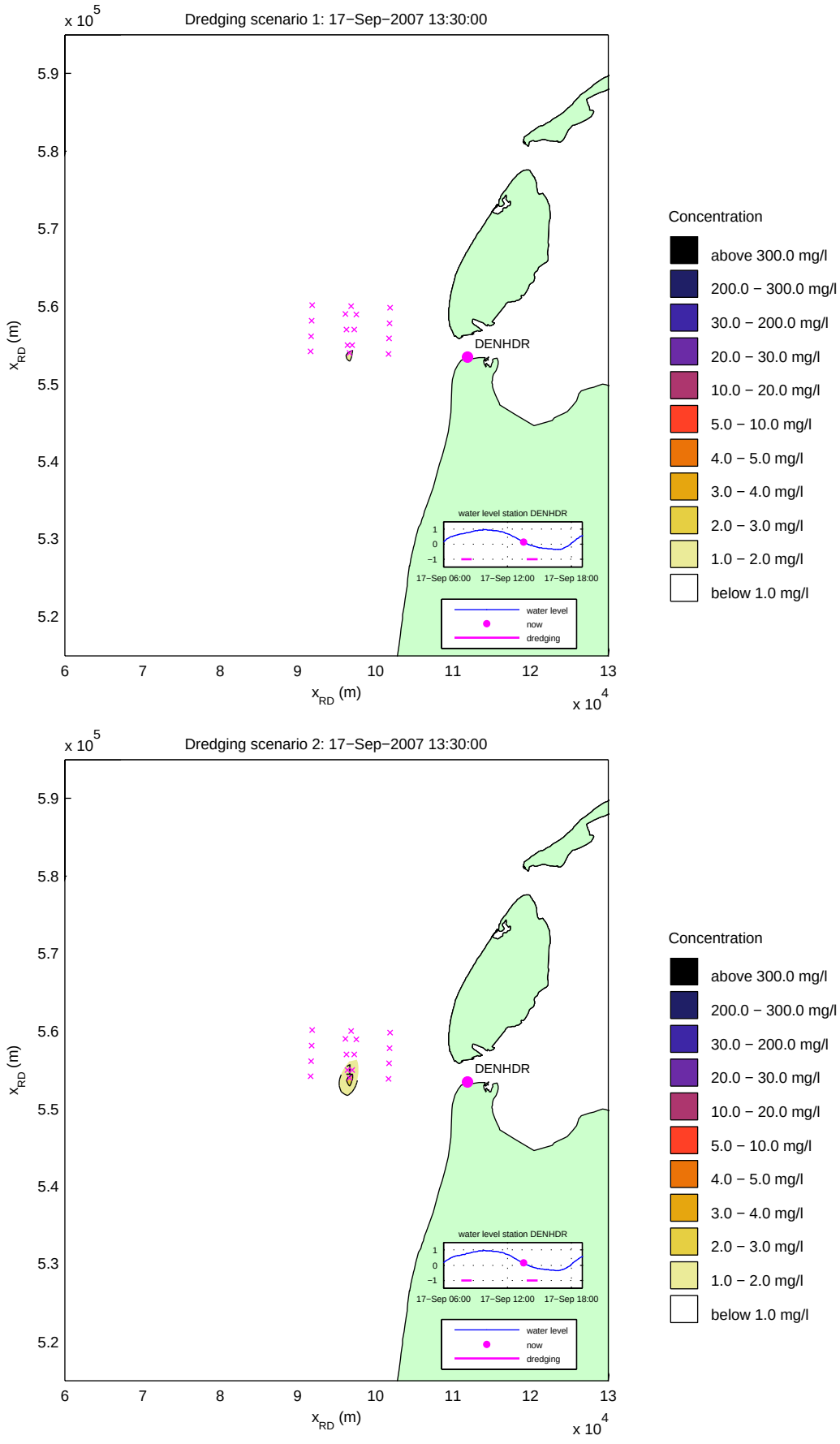

Simulated effect of overflow on silt concentrations (mg/l)
date and time: 17−Sep−2007 13:30:00
x−marks denote locations of T1 observations

Alkyon Hydraulic Consultancy & Research | A2273 | Fig. 3.46

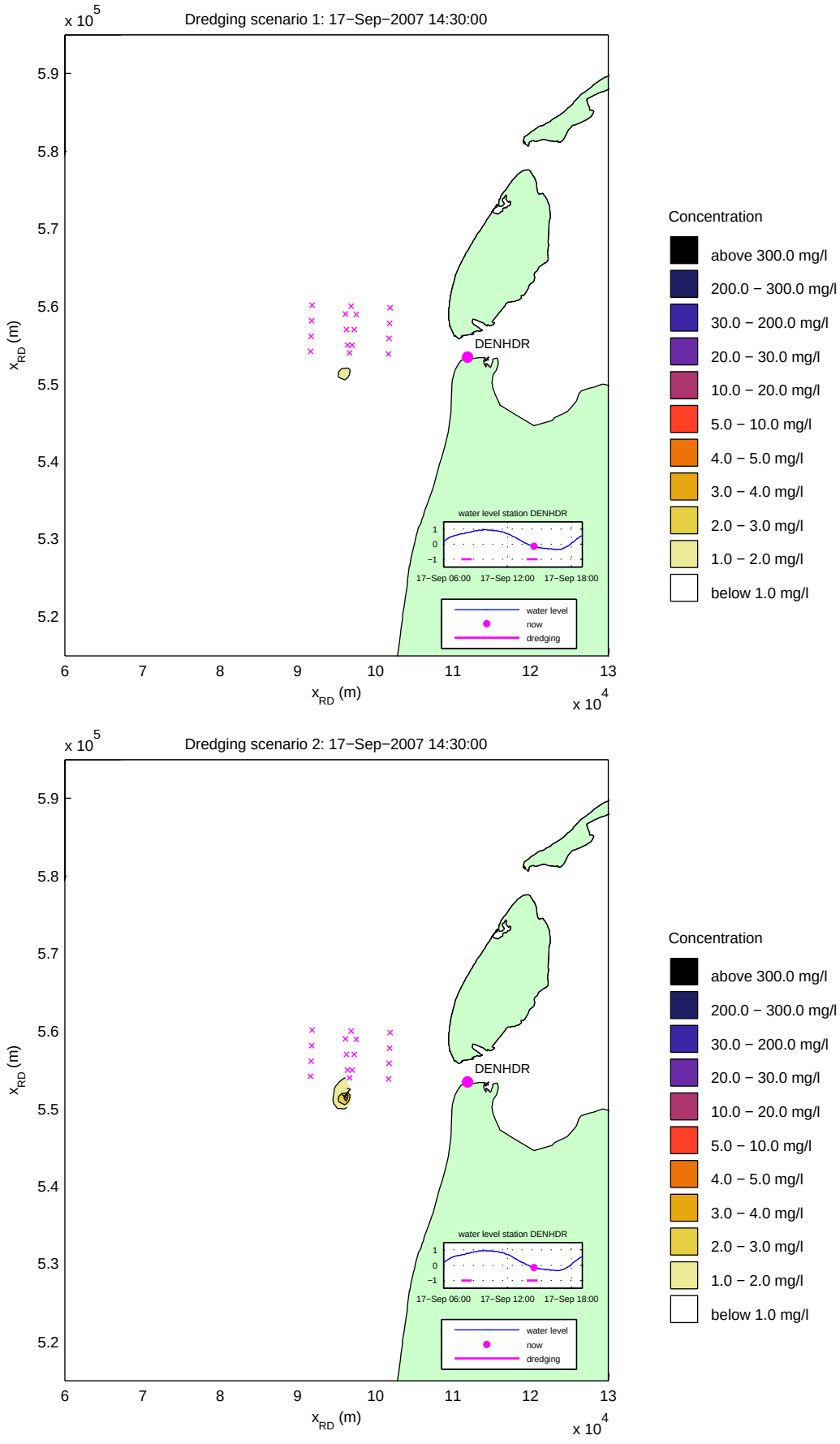

Simulated effect of overflow on silt concentrations (mg/l)
date and time: 17−Sep−2007 14:30:00
x−marks denote locations of T1 observations

Alkyon Hydraulic Consultancy & Research | A2273 | Fig. 3.47

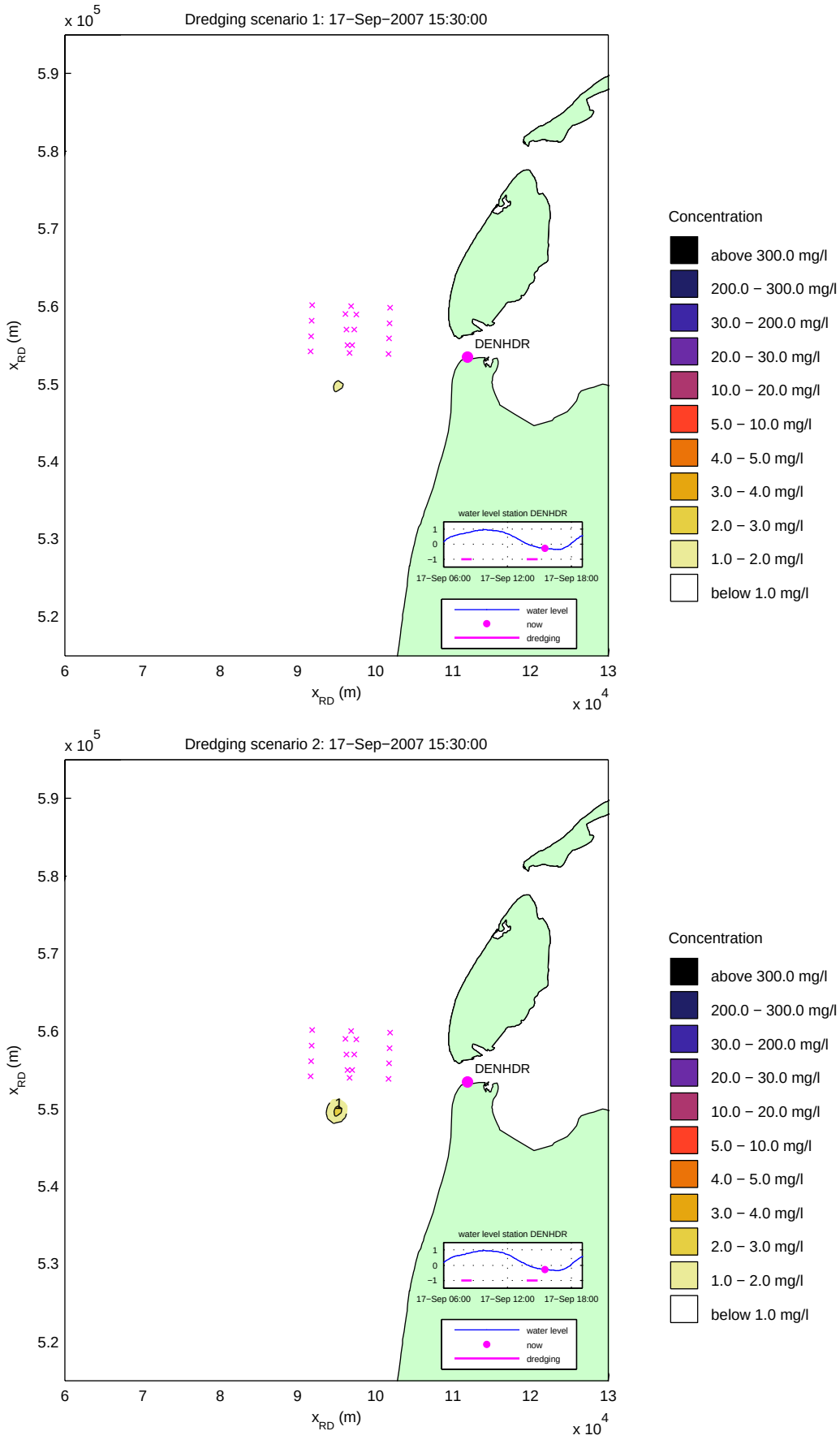

Simulated effect of overflow on silt concentrations (mg/l)
date and time: 17−Sep−2007 15:30:00
x−marks denote locations of T1 observations

Alkyon Hydraulic Consultancy & Research | A2273 | Fig. 3.48

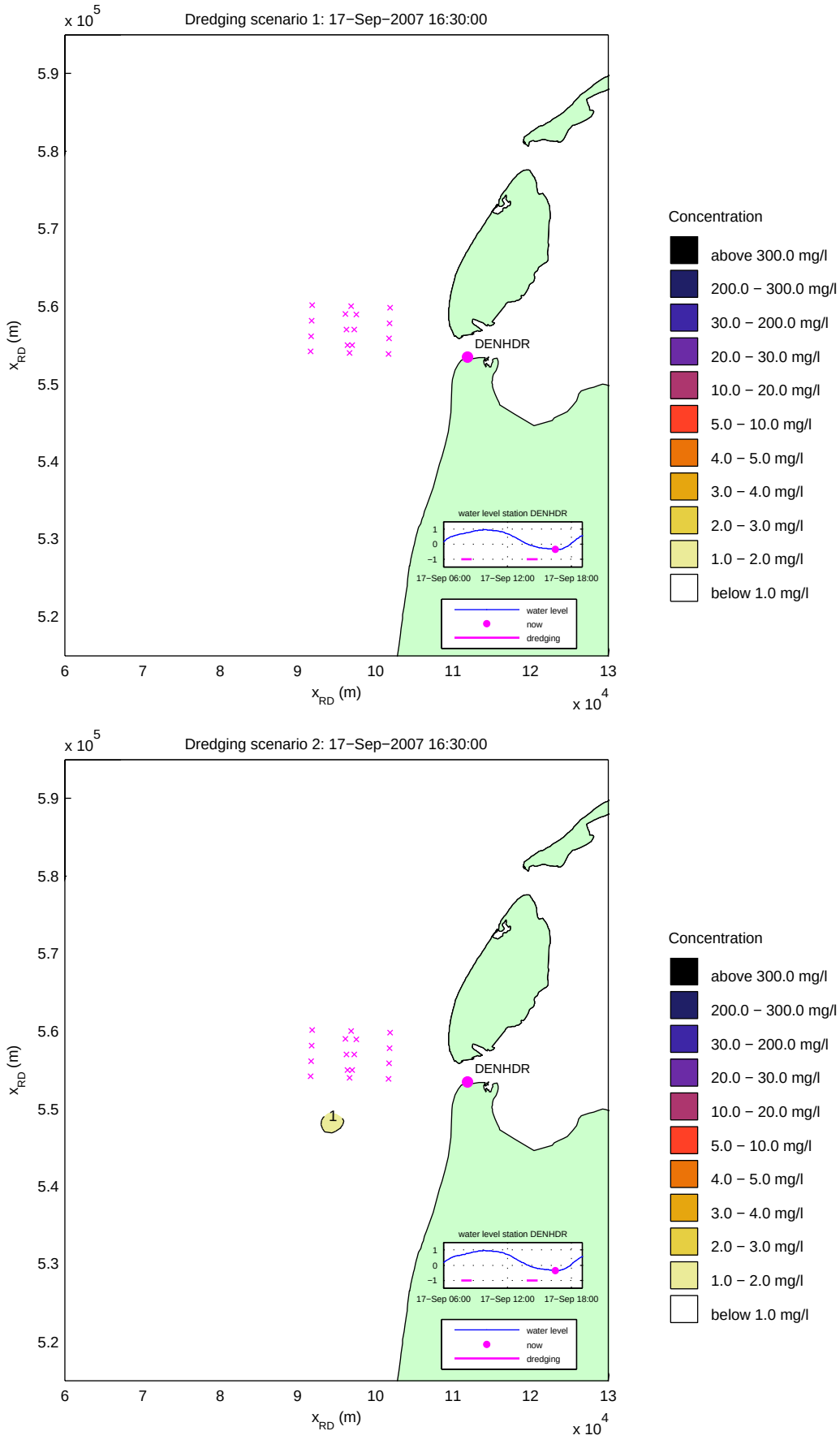

Simulated effect of overflow on silt concentrations (mg/l)
date and time: 17−Sep−2007 16:30:00
x−marks denote locations of T1 observations

Alkyon Hydraulic Consultancy & Research	A2273	Fig. 3.49

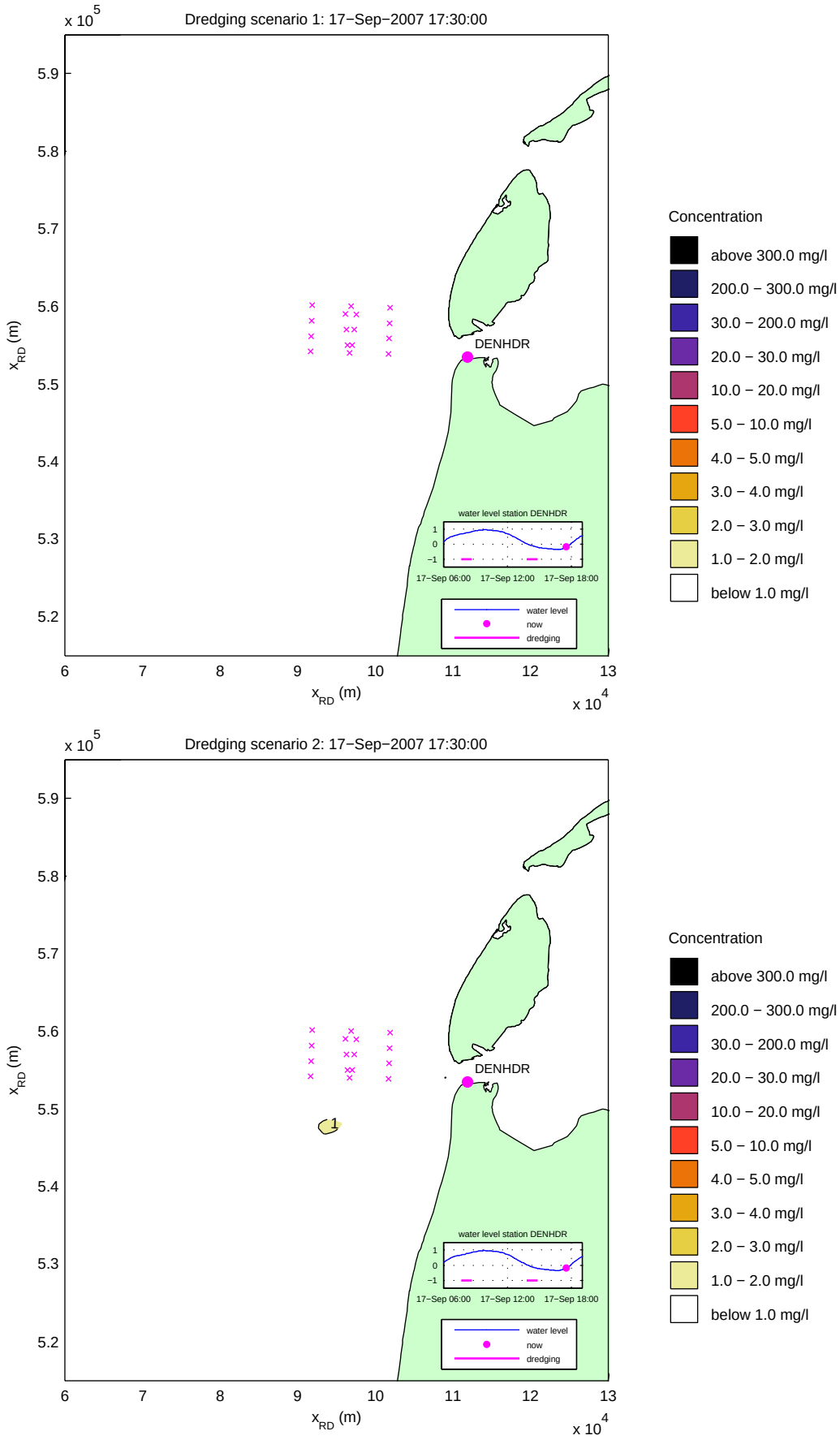

Simulated effect of overflow on silt concentrations (mg/l)
date and time: 17−Sep−2007 17:30:00
x−marks denote locations of T1 observations

Alkyon Hydraulic Consultancy & Research	A2273	Fig. 3.50

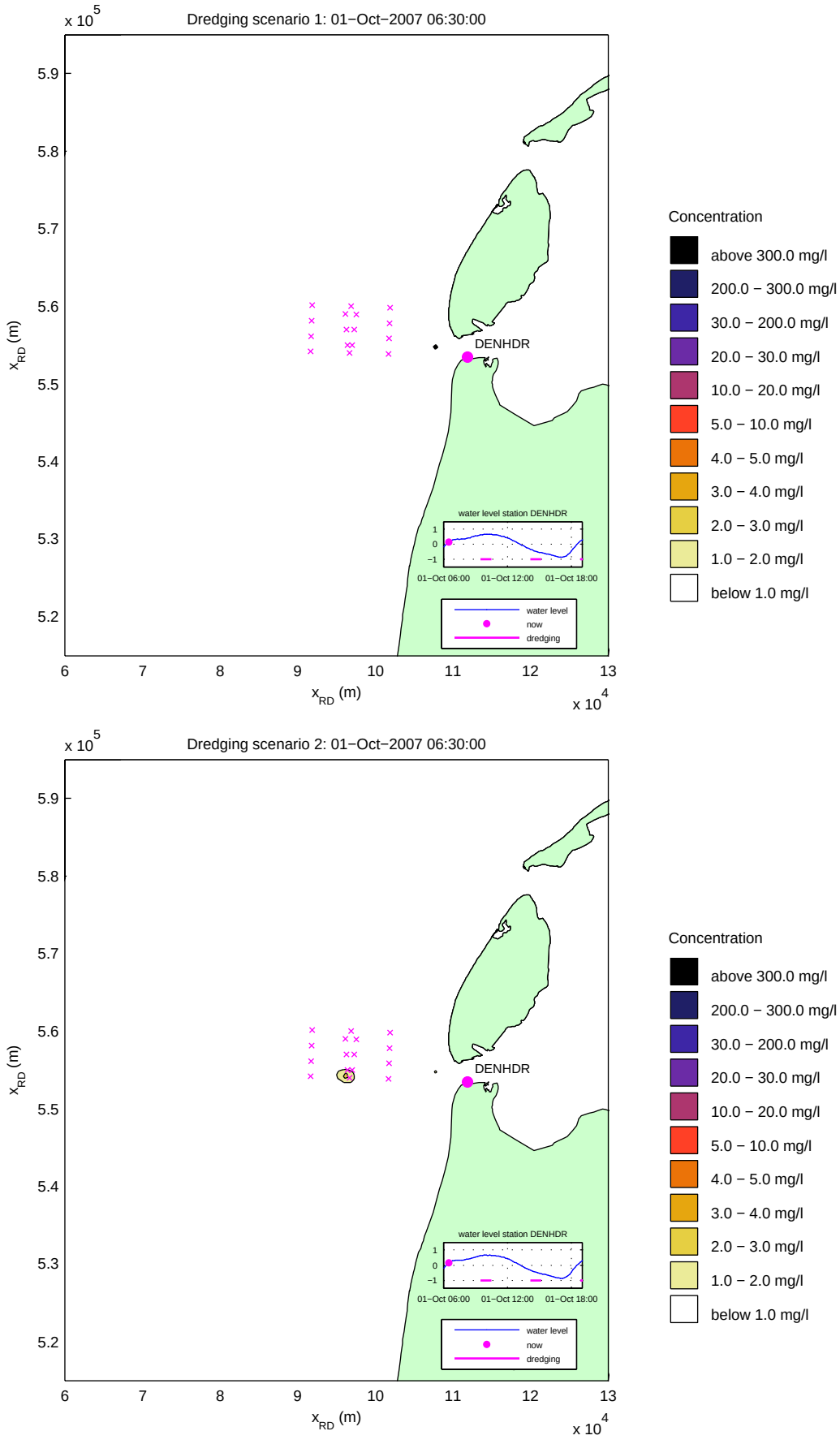

Simulated effect of overflow on silt concentrations (mg/l)
date and time: 01−Oct−2007 06:30:00
x−marks denote locations of T1 observations

Alkyon Hydraulic Consultancy & Research | A2273 | Fig. 3.51

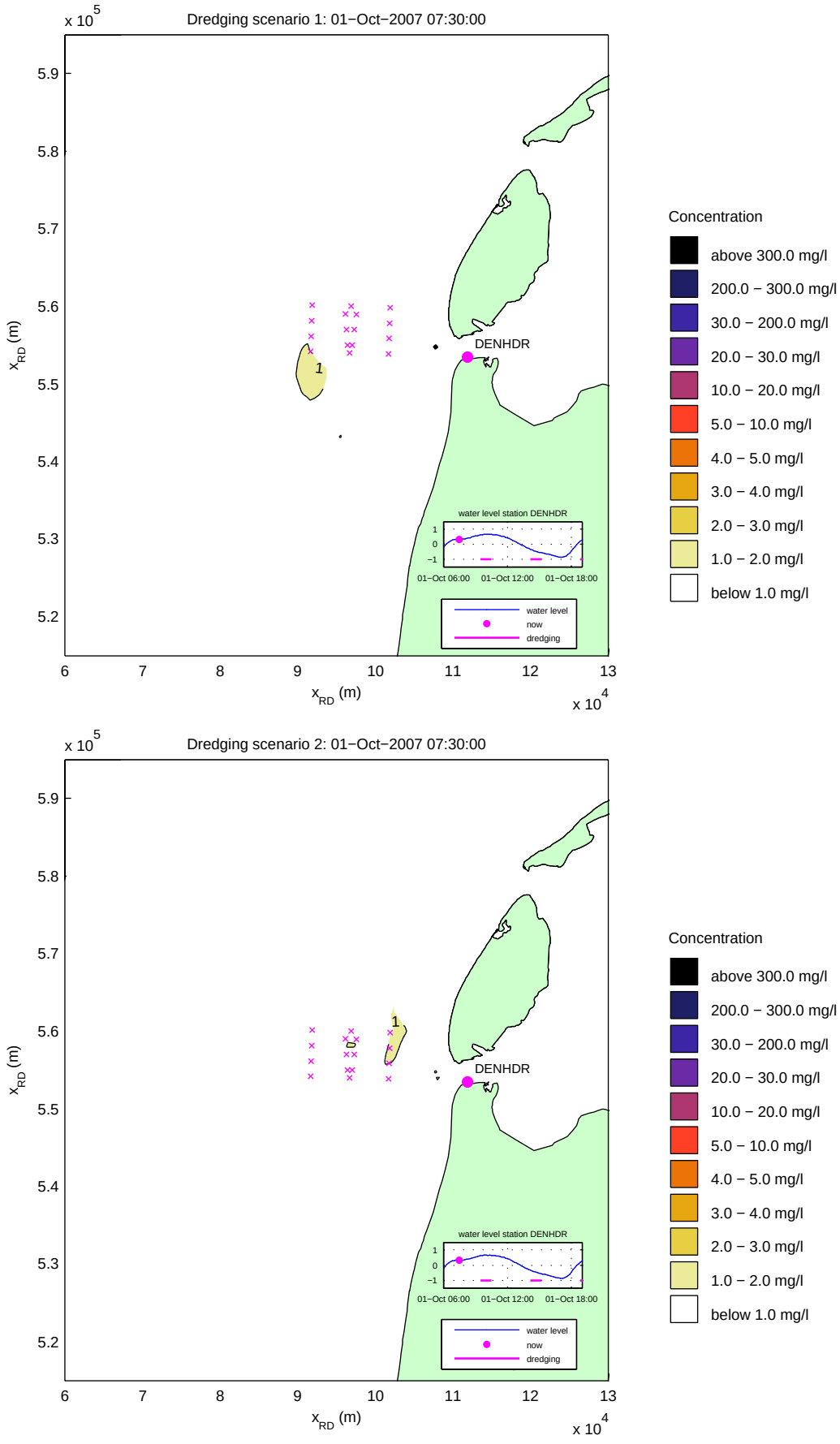

Simulated effect of overflow on silt concentrations (mg/l)
date and time: 01−Oct−2007 07:30:00
x−marks denote locations of T1 observations

Alkyon Hydraulic Consultancy & Research | A2273 | Fig. 3.52

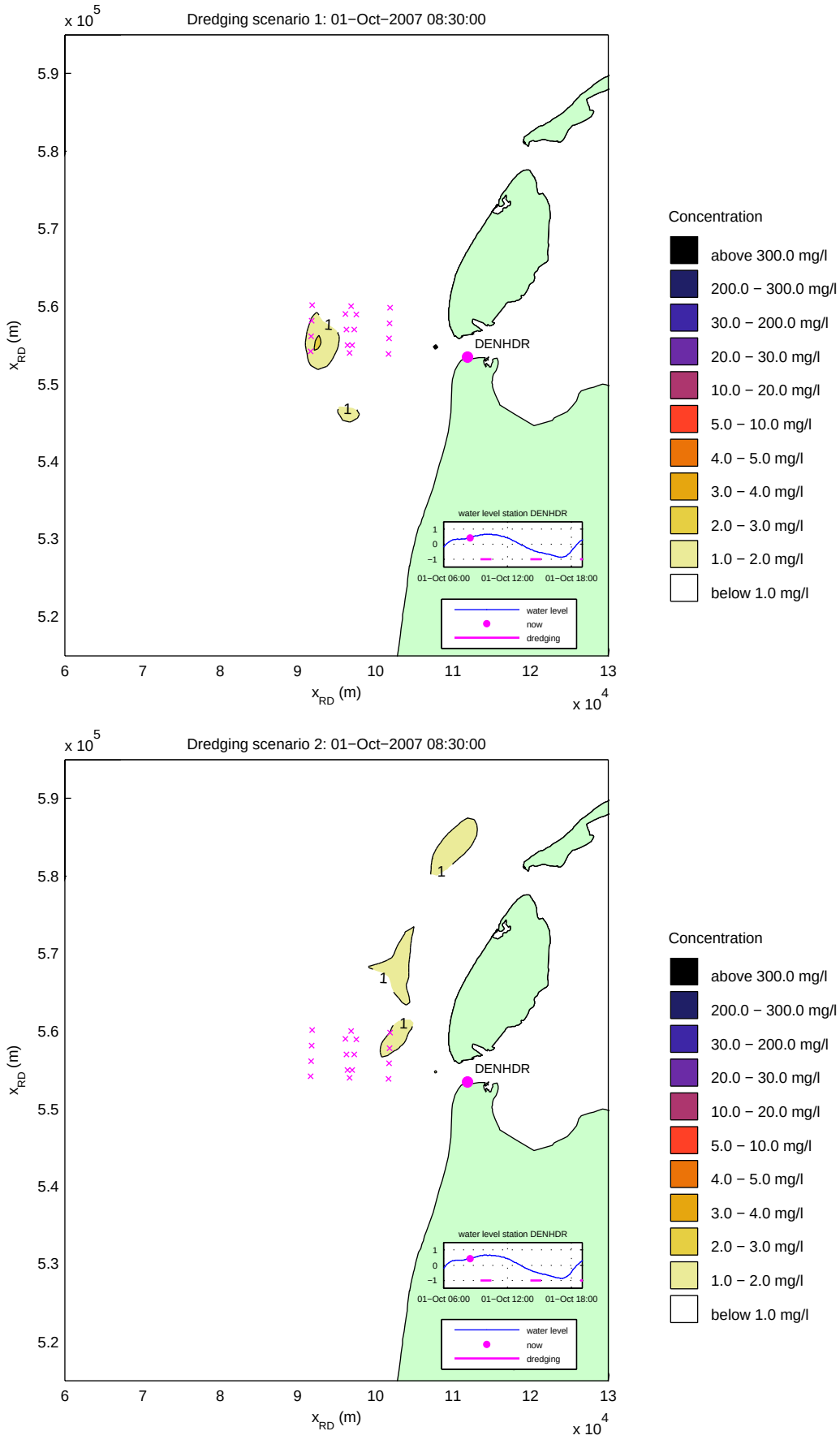

Simulated effect of overflow on silt concentrations (mg/l)
date and time: 01−Oct−2007 08:30:00
x−marks denote locations of T1 observations

Alkyon Hydraulic Consultancy & Research | A2273 | Fig. 3.53

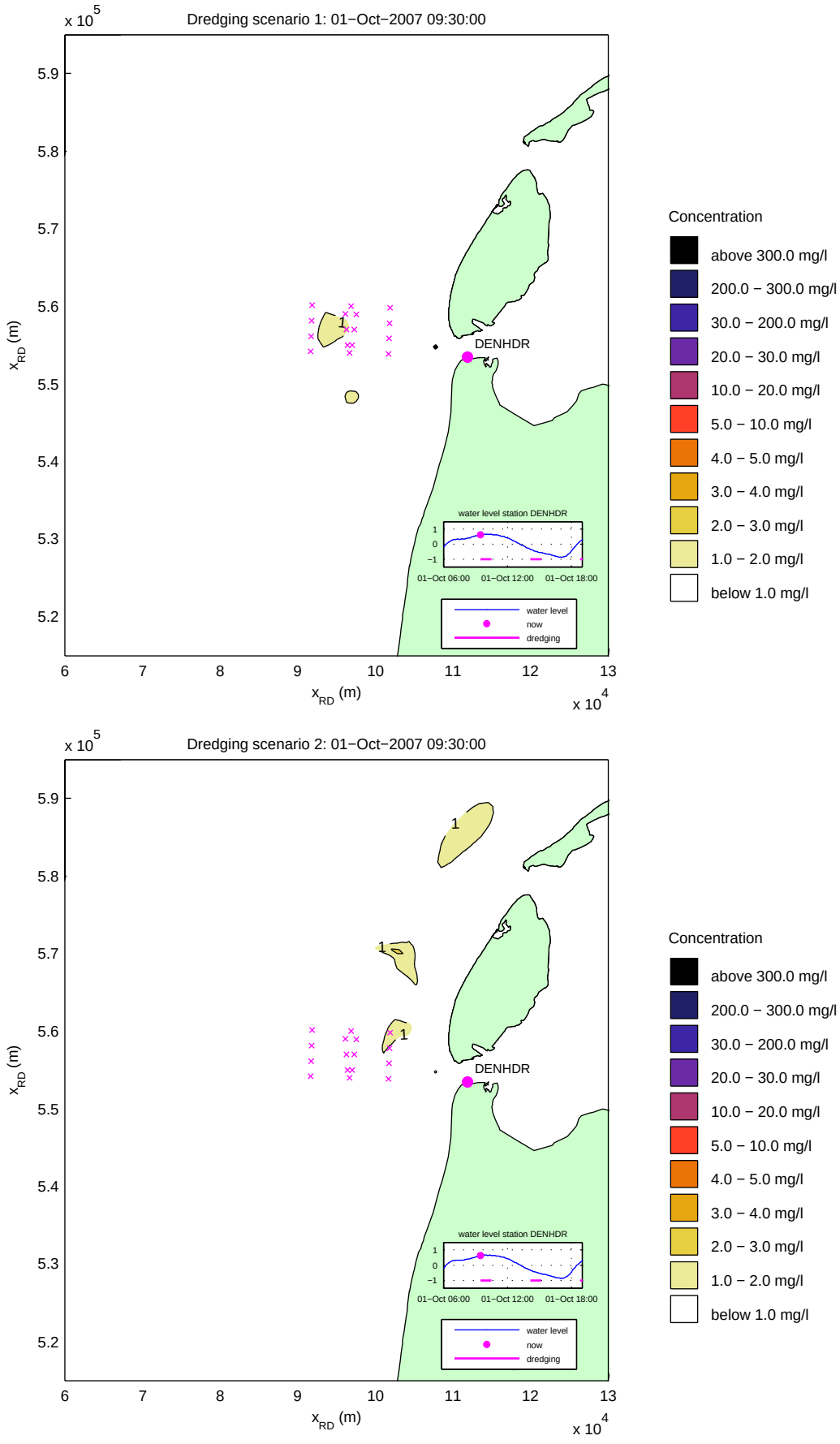

Simulated effect of overflow on silt concentrations (mg/l)
date and time: 01−Oct−2007 09:30:00
x−marks denote locations of T1 observations

Alkyon Hydraulic Consultancy & Research	A2273	Fig. 3.54

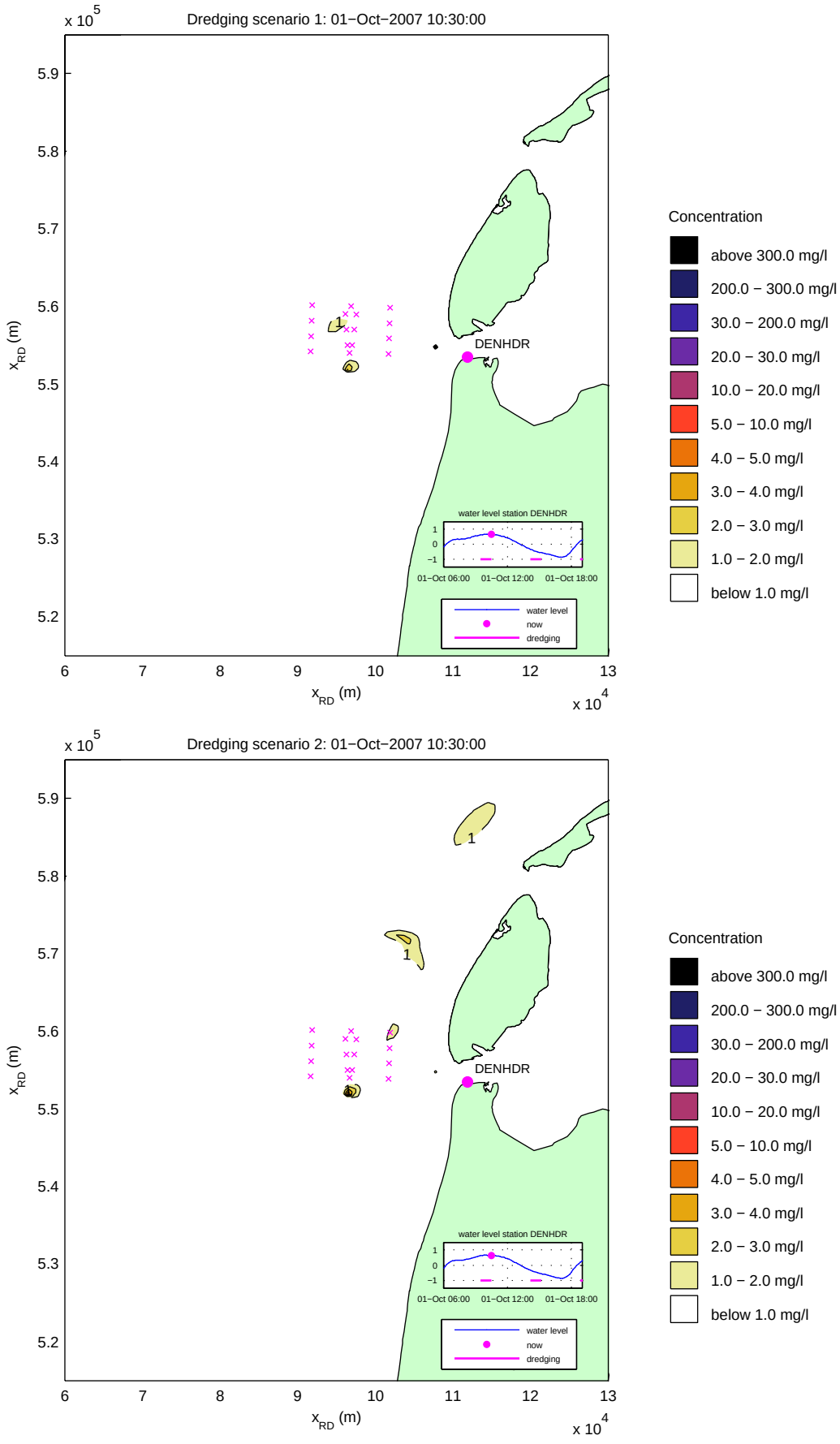

Simulated effect of overflow on silt concentrations (mg/l)
date and time: 01−Oct−2007 10:30:00
x−marks denote locations of T1 observations

Alkyon Hydraulic Consultancy & Research | A2273 | Fig. 3.55

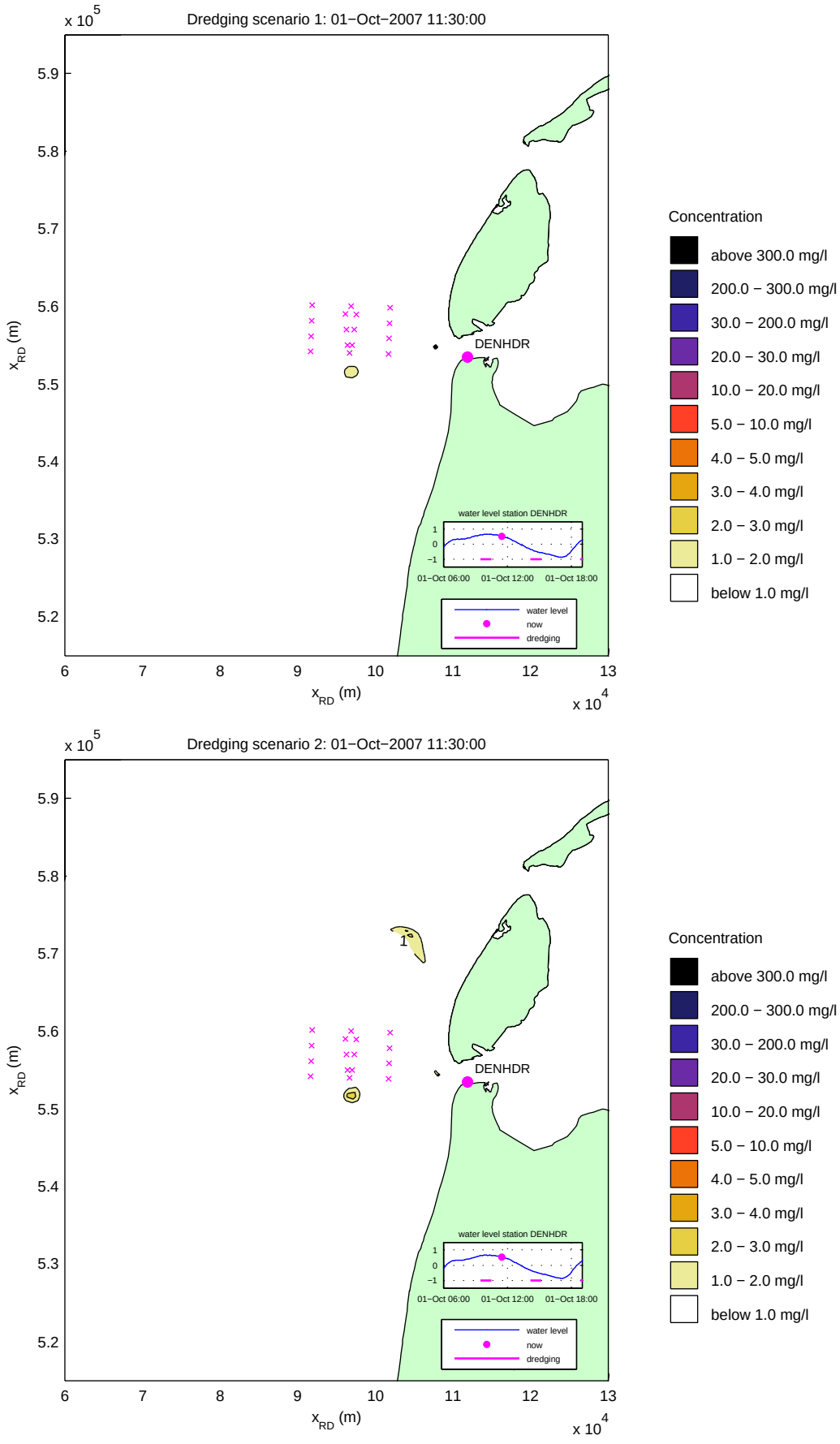

Simulated effect of overflow on silt concentrations (mg/l)
date and time: 01−Oct−2007 11:30:00
x−marks denote locations of T1 observations

Alkyon Hydraulic Consultancy & Research | A2273 | Fig. 3.56

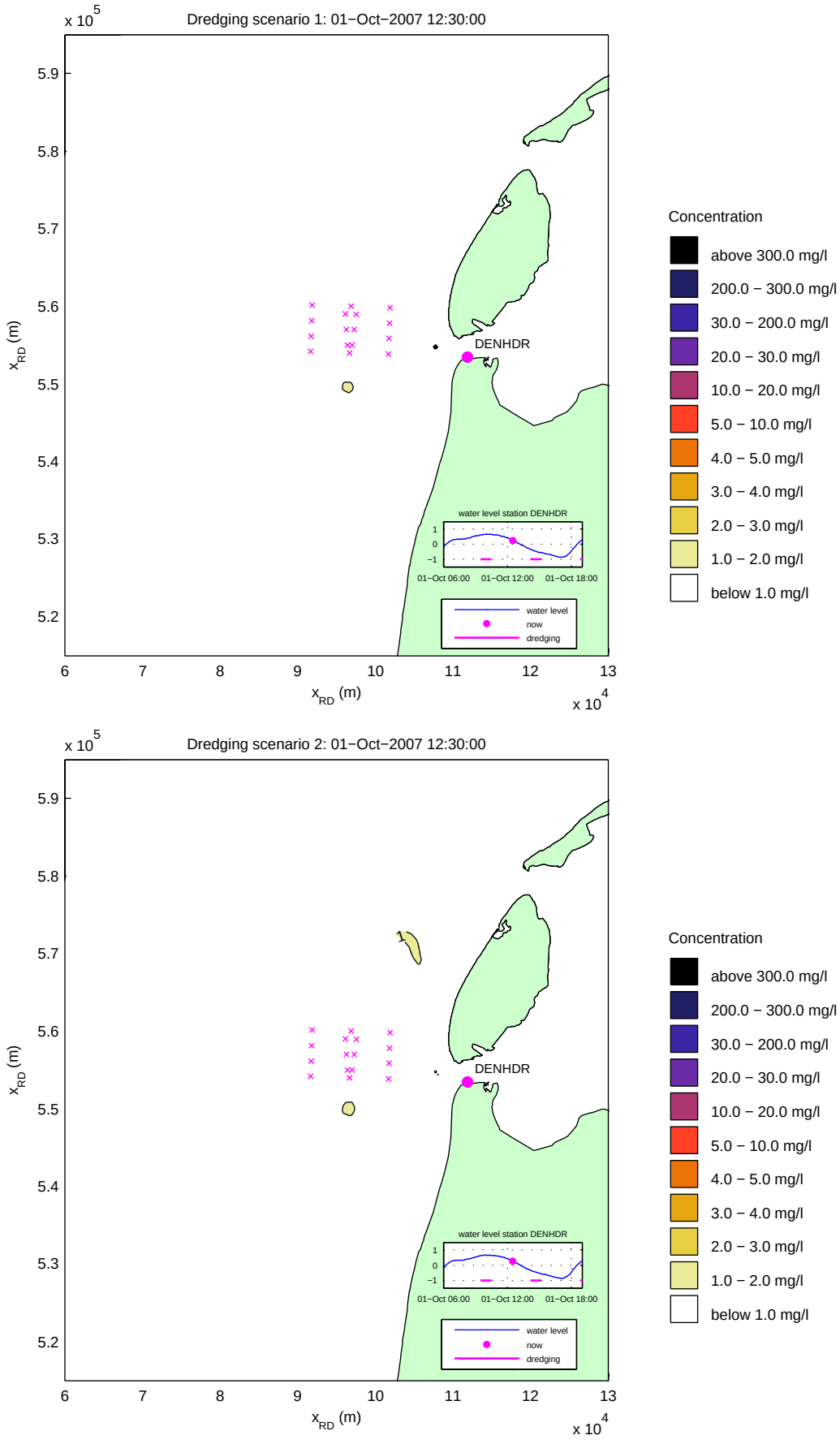

Simulated effect of overflow on silt concentrations (mg/l)
date and time: 01−Oct−2007 12:30:00
x−marks denote locations of T1 observations

Alkyon Hydraulic Consultancy & Research | A2273 | Fig. 3.57

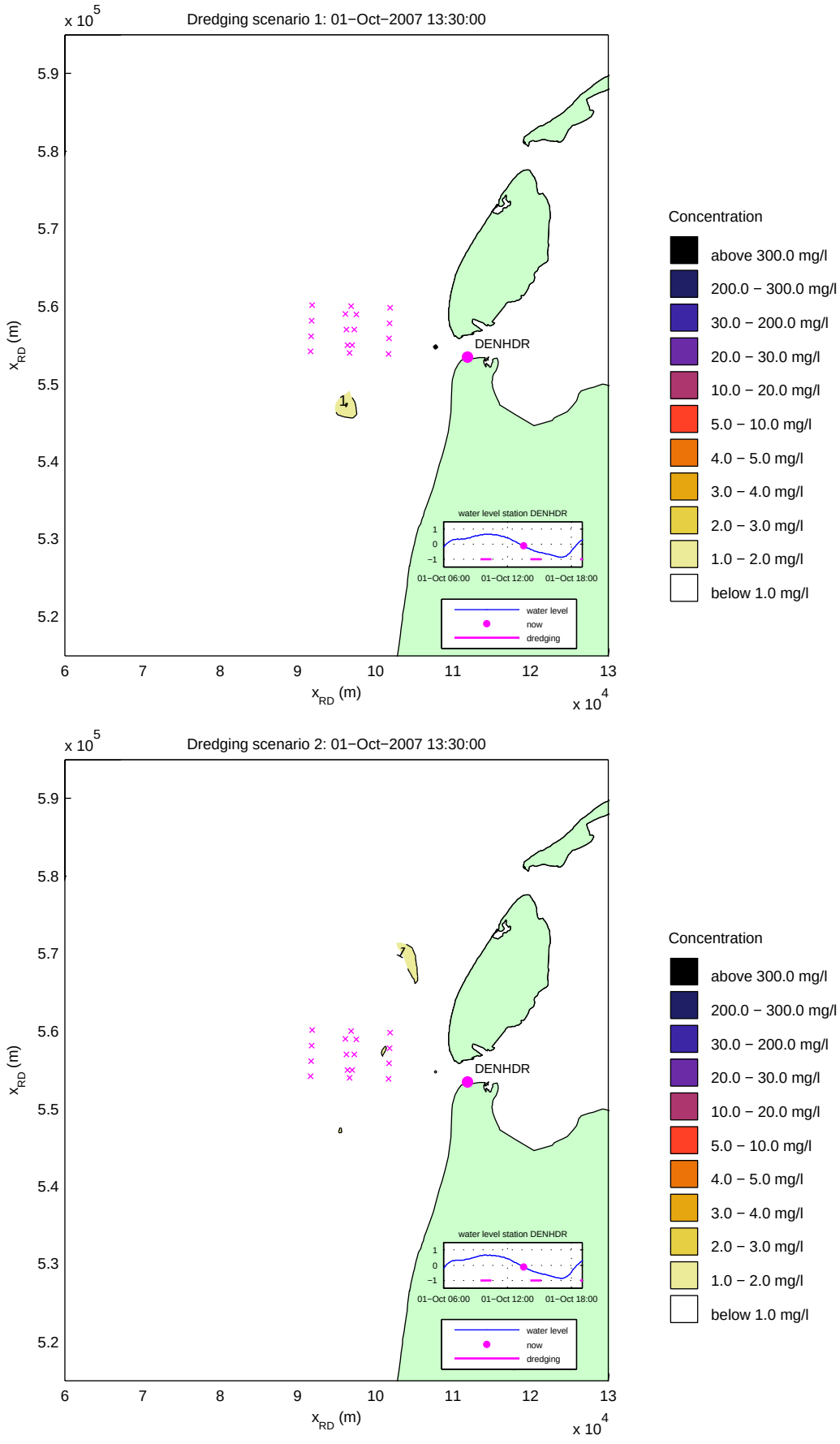

Simulated effect of overflow on silt concentrations (mg/l)
date and time: 01−Oct−2007 13:30:00
x−marks denote locations of T1 observations

Alkyon Hydraulic Consultancy & Research | A2273 | Fig. 3.58

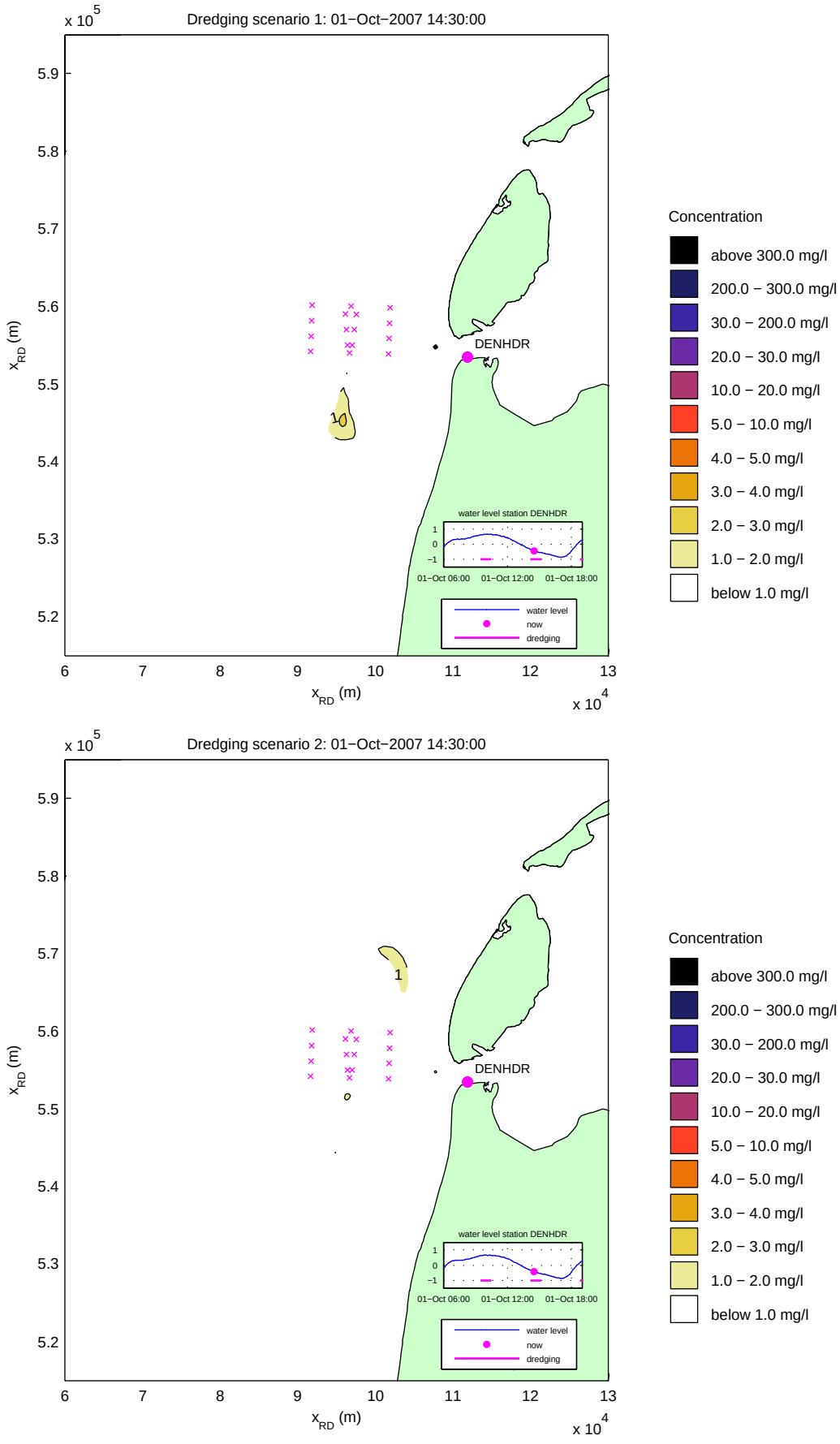

Simulated effect of overflow on silt concentrations (mg/l)
date and time: 01−Oct−2007 14:30:00
x−marks denote locations of T1 observations

Alkyon Hydraulic Consultancy & Research | A2273 | Fig. 3.59

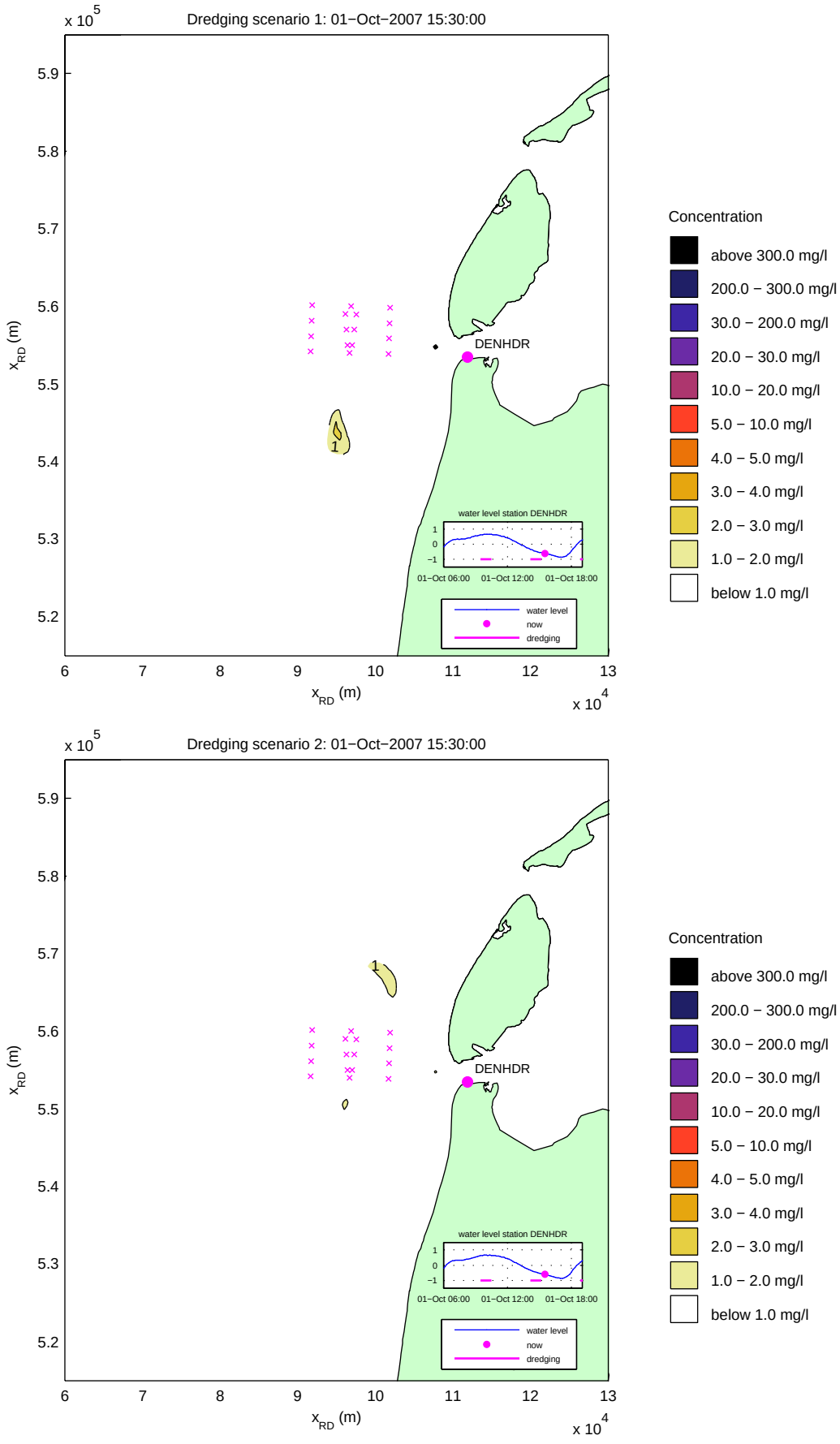

Simulated effect of overflow on silt concentrations (mg/l)
date and time: 01−Oct−2007 15:30:00
x−marks denote locations of T1 observations

Alkyon Hydraulic Consultancy & Research | A2273 | Fig. 3.60

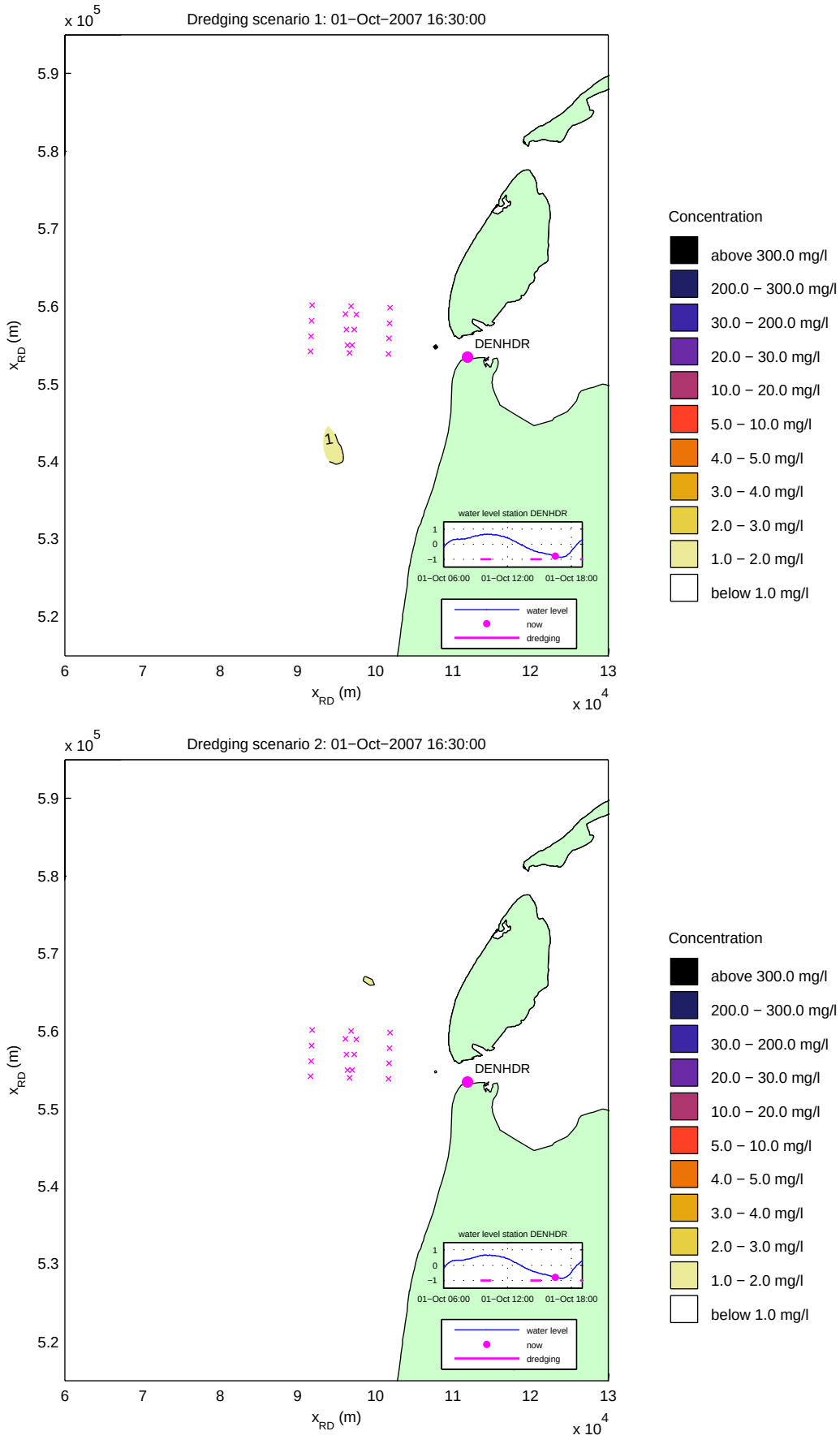

Simulated effect of overflow on silt concentrations (mg/l)
date and time: 01−Oct−2007 16:30:00
x−marks denote locations of T1 observations

Alkyon Hydraulic Consultancy & Research	A2273	Fig. 3.61

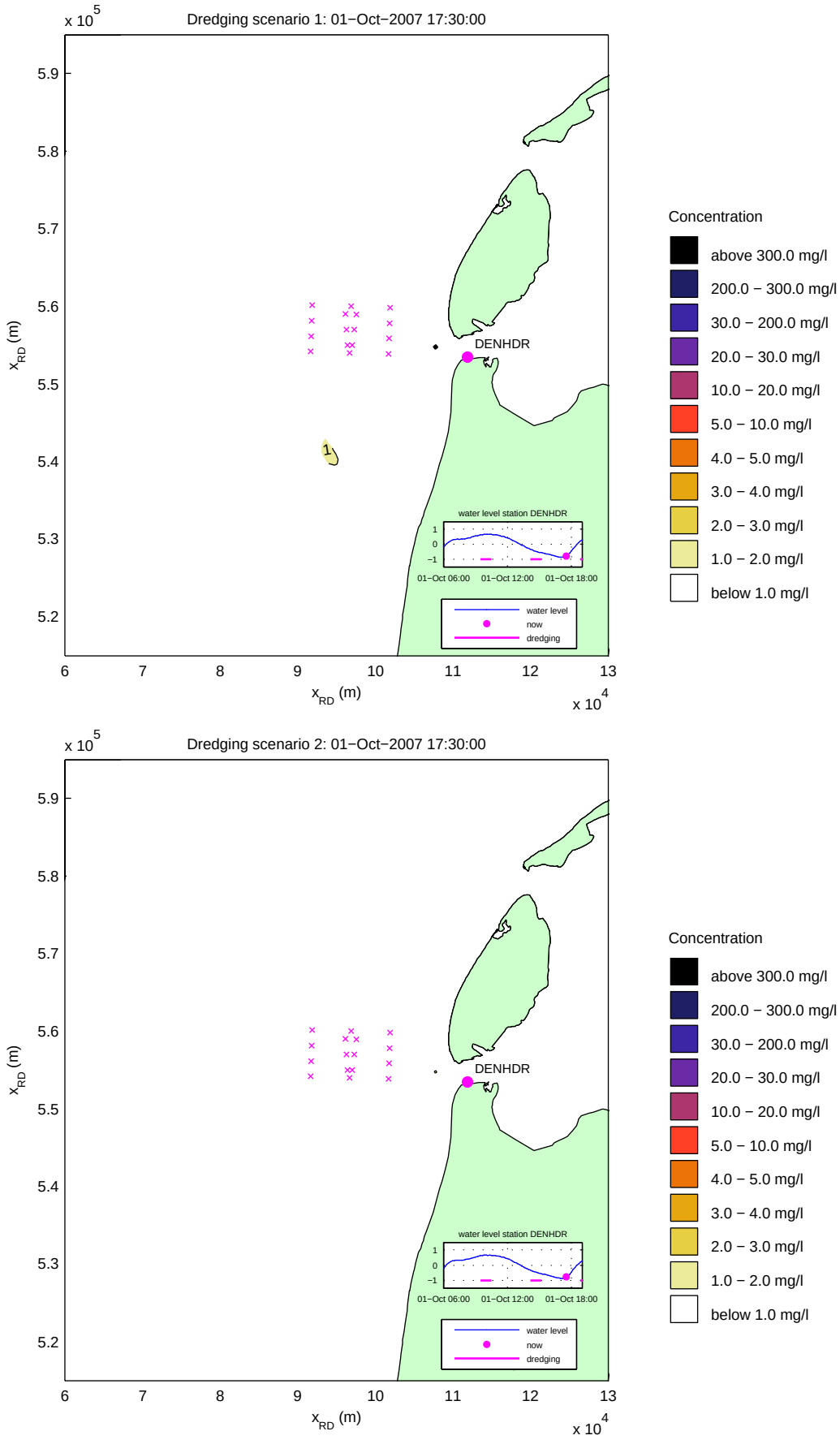

Simulated effect of overflow on silt concentrations (mg/l)
date and time: 01−Oct−2007 17:30:00
x−marks denote locations of T1 observations

Alkyon Hydraulic Consultancy & Research	A2273	Fig. 3.62

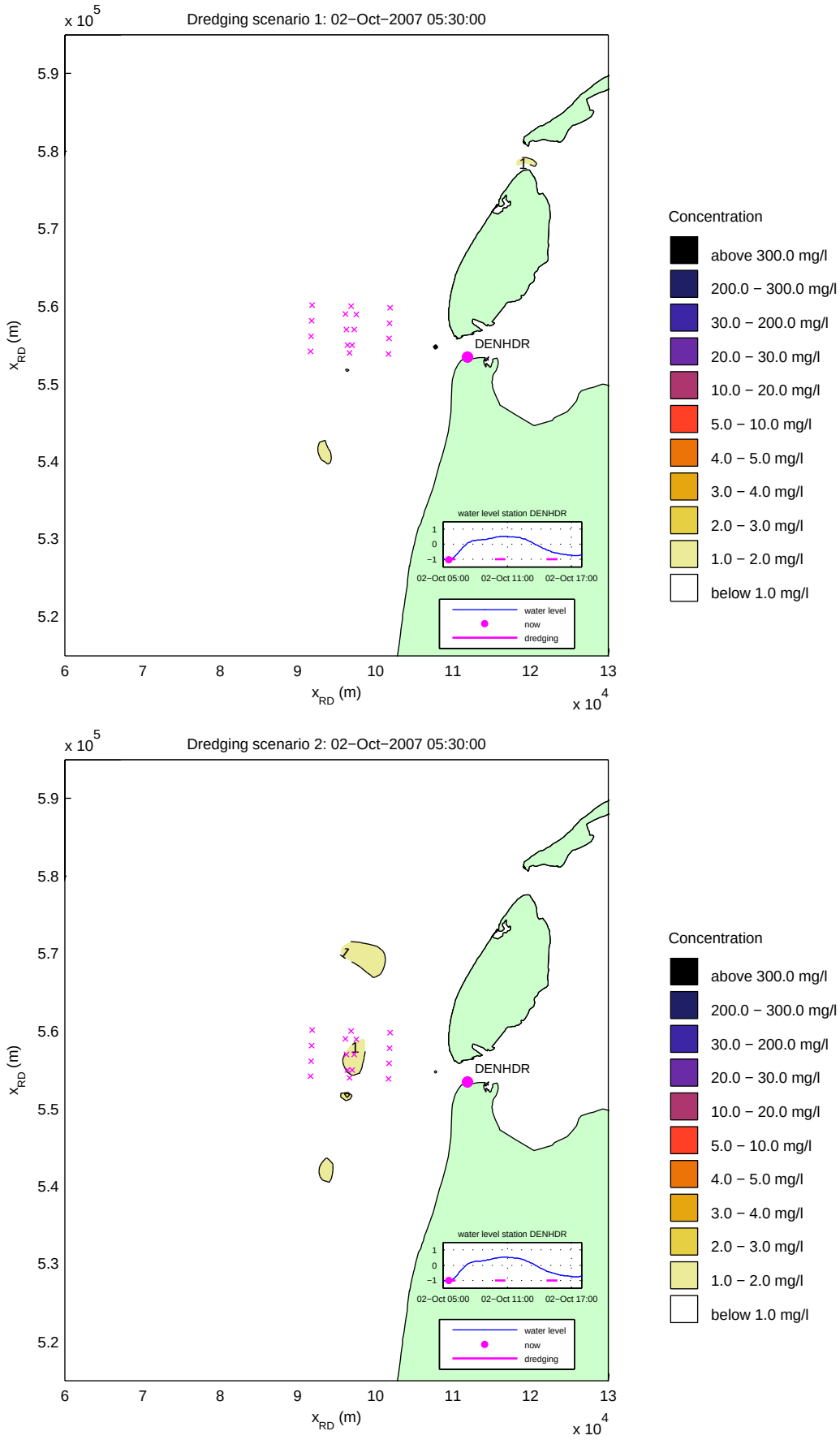

Simulated effect of overflow on silt concentrations (mg/l)
date and time: 02−Oct−2007 05:30:00
x−marks denote locations of T1 observations

Alkyon Hydraulic Consultancy & Research	A2273	Fig. 3.63

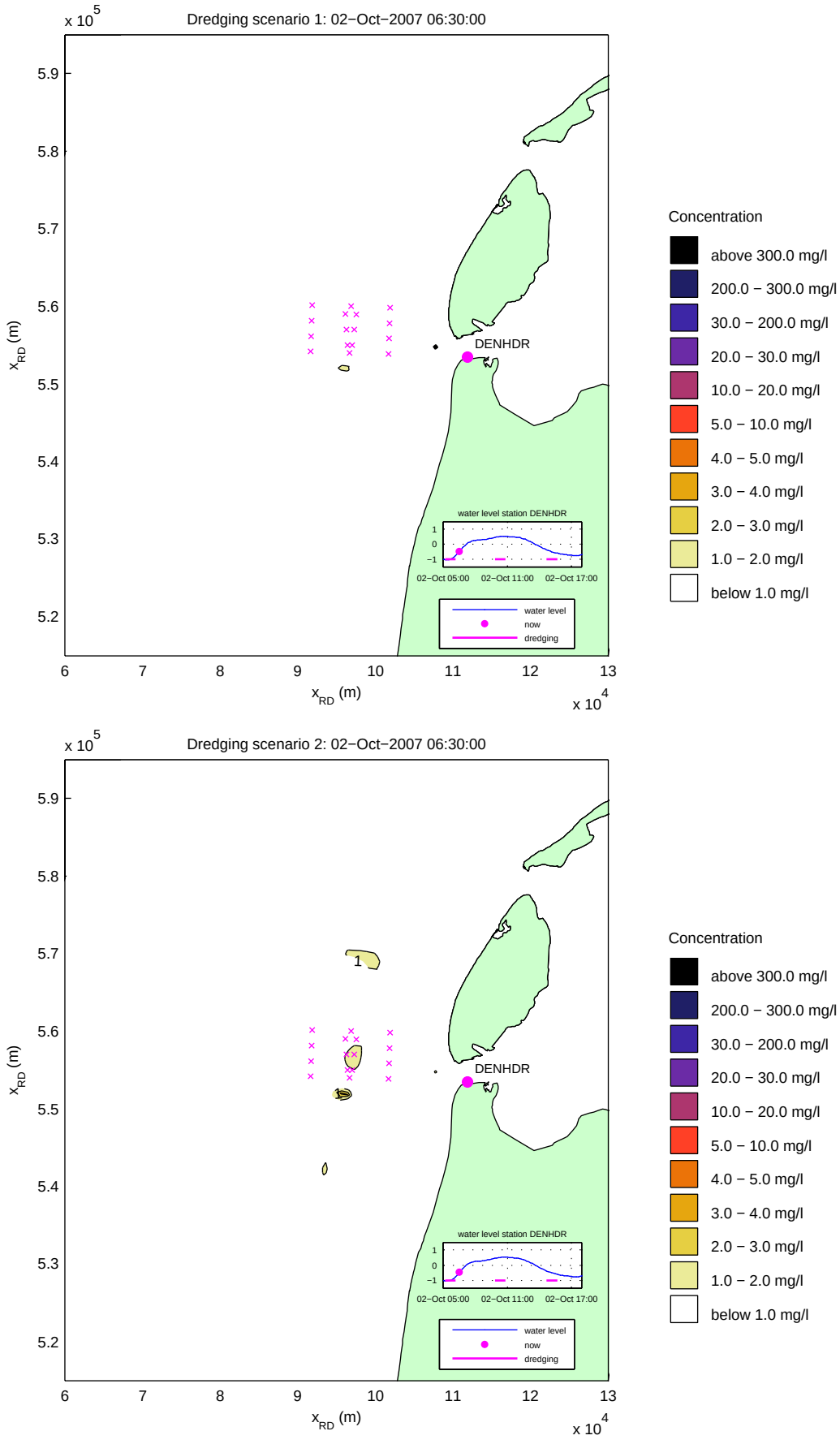

Simulated effect of overflow on silt concentrations (mg/l)
date and time: 02−Oct−2007 06:30:00
x−marks denote locations of T1 observations

Alkyon Hydraulic Consultancy & Research	A2273	Fig. 3.64

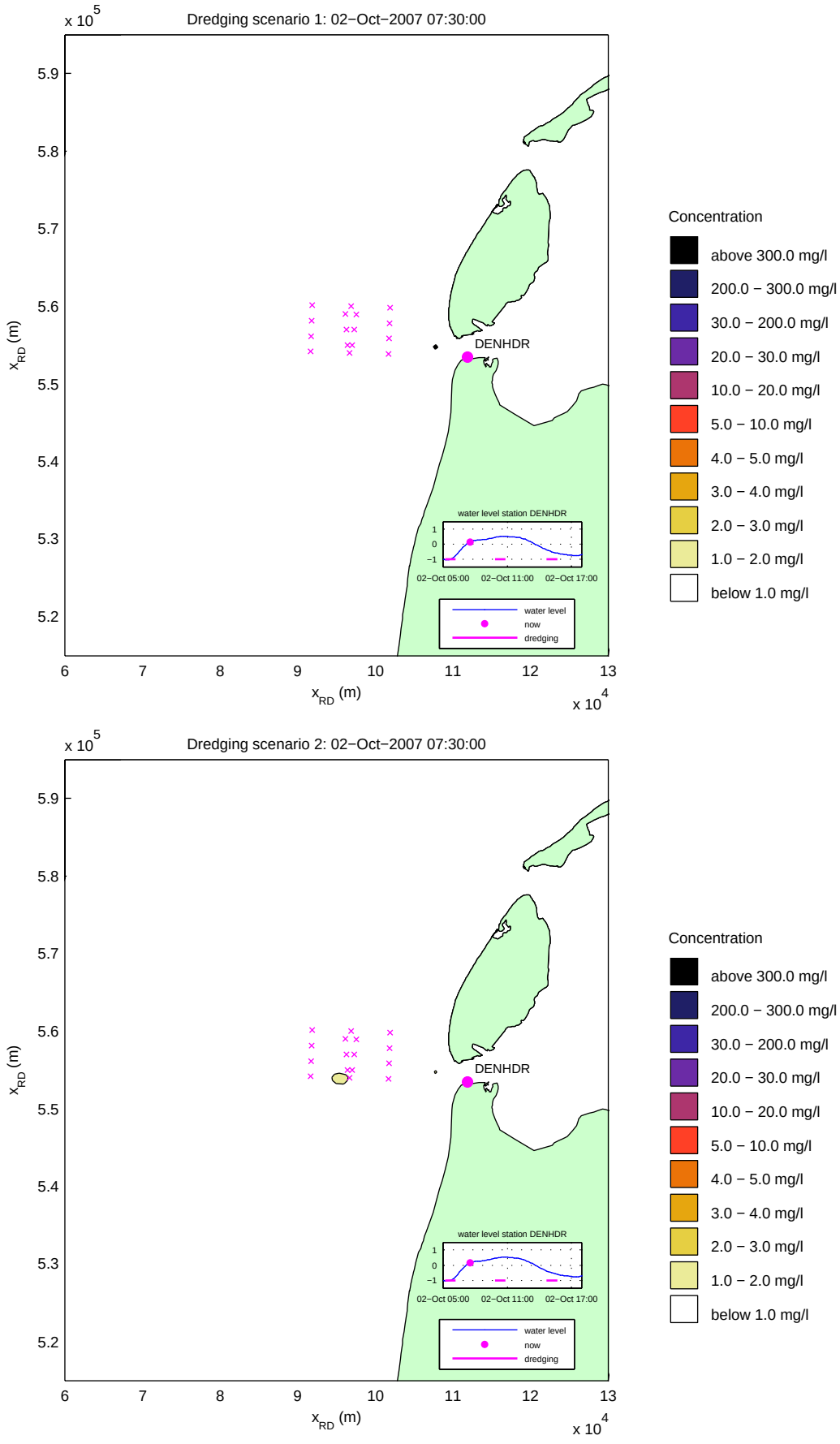

Simulated effect of overflow on silt concentrations (mg/l)
date and time: 02−Oct−2007 07:30:00
x−marks denote locations of T1 observations

Alkyon Hydraulic Consultancy & Research	A2273	Fig. 3.65

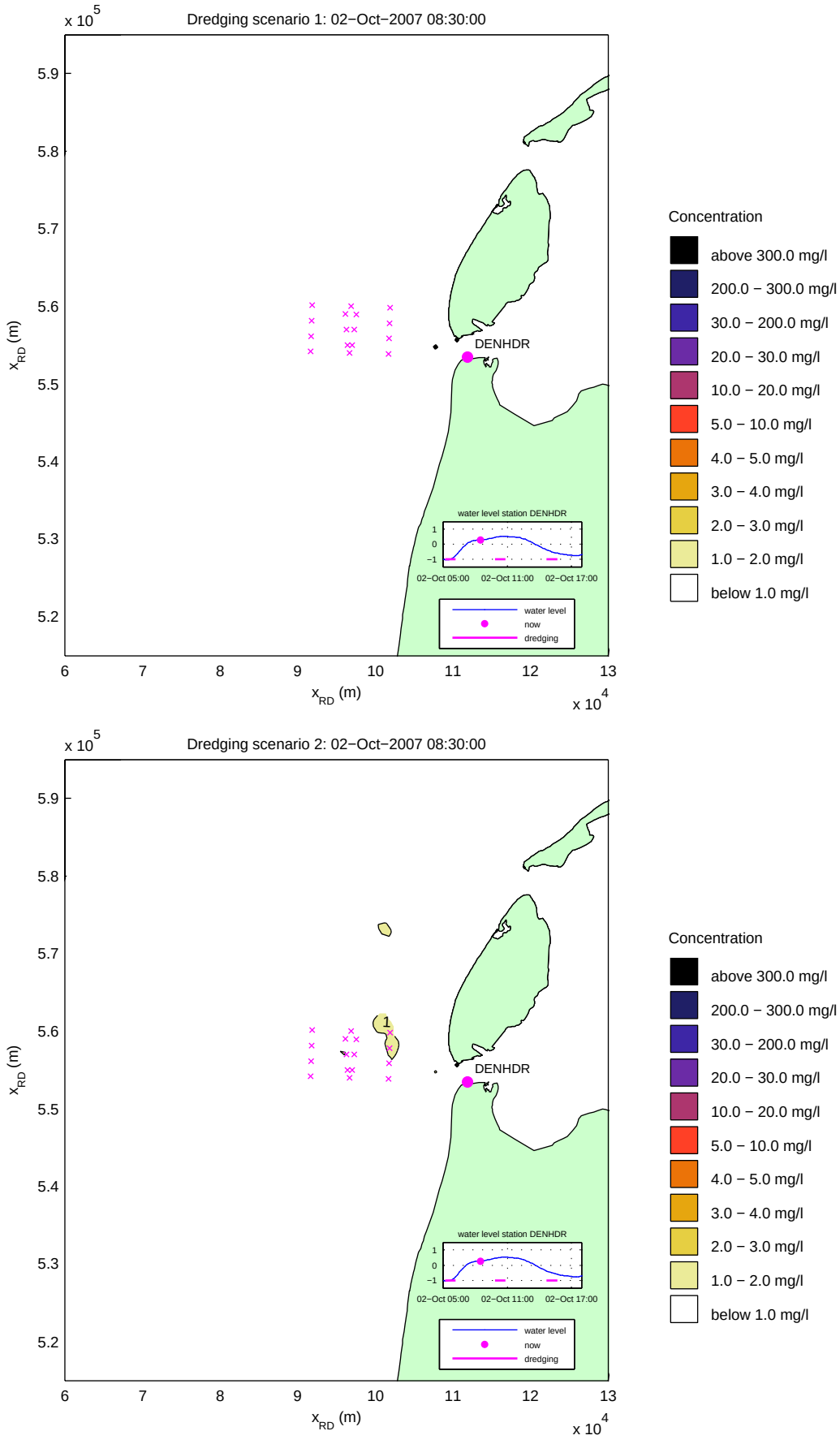

Simulated effect of overflow on silt concentrations (mg/l)
date and time: 02−Oct−2007 08:30:00
x−marks denote locations of T1 observations

Alkyon Hydraulic Consultancy & Research | A2273 | Fig. 3.66

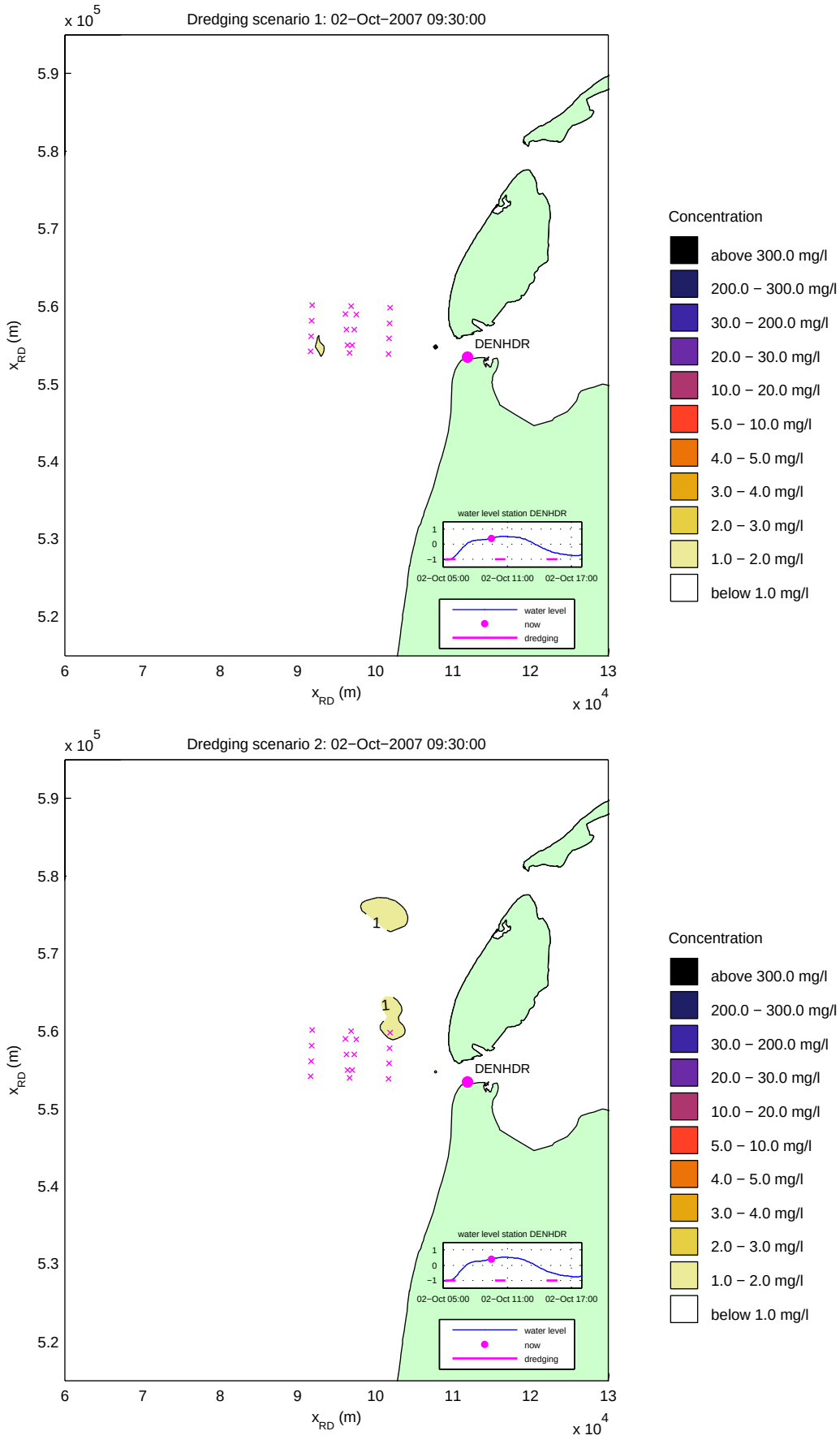

Simulated effect of overflow on silt concentrations (mg/l)
date and time: 02−Oct−2007 09:30:00
x−marks denote locations of T1 observations

Alkyon Hydraulic Consultancy & Research	A2273	Fig. 3.67

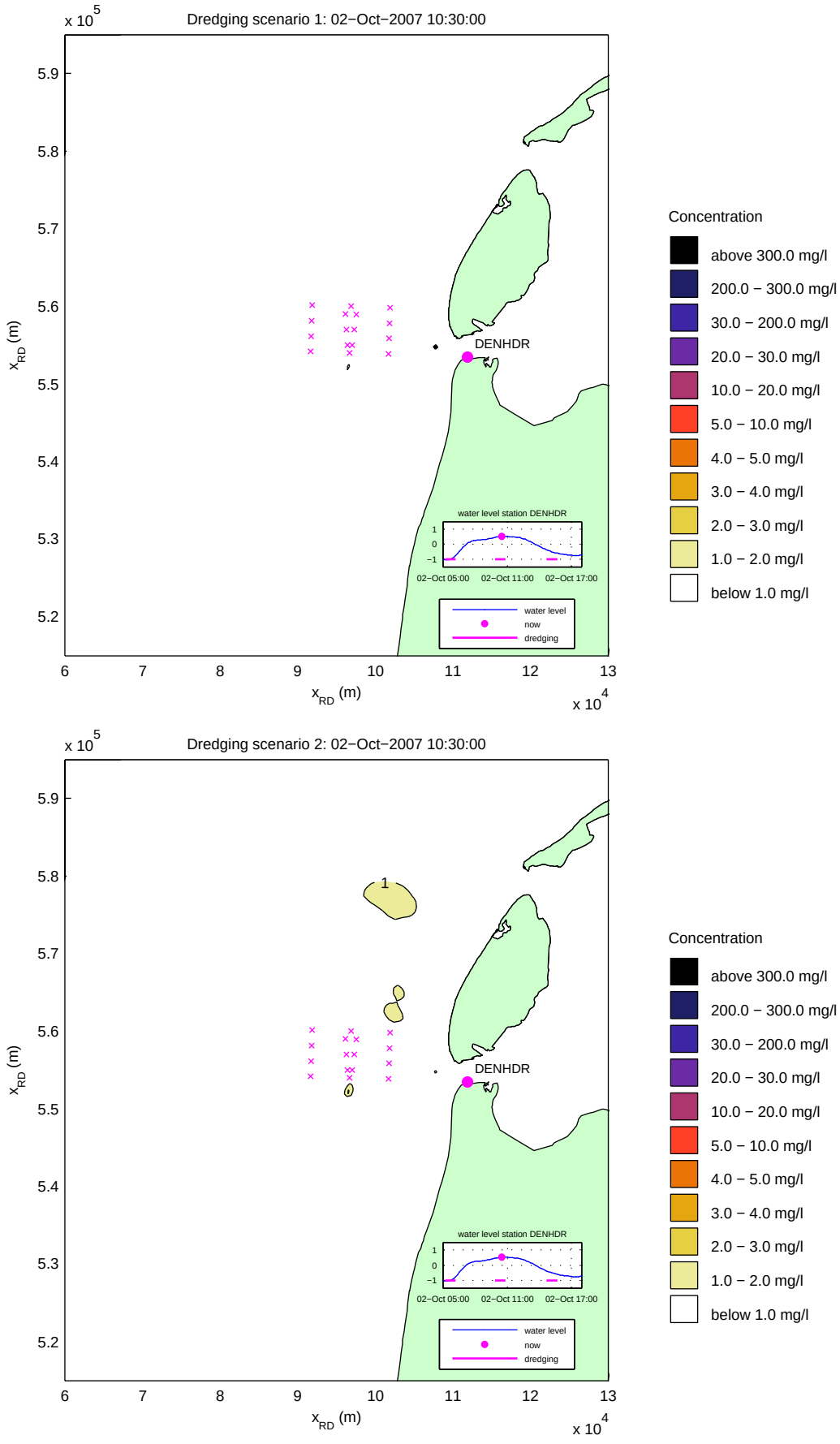

Simulated effect of overflow on silt concentrations (mg/l)
date and time: 02−Oct−2007 10:30:00
x−marks denote locations of T1 observations

Alkyon Hydraulic Consultancy & Research | A2273 | Fig. 3.68

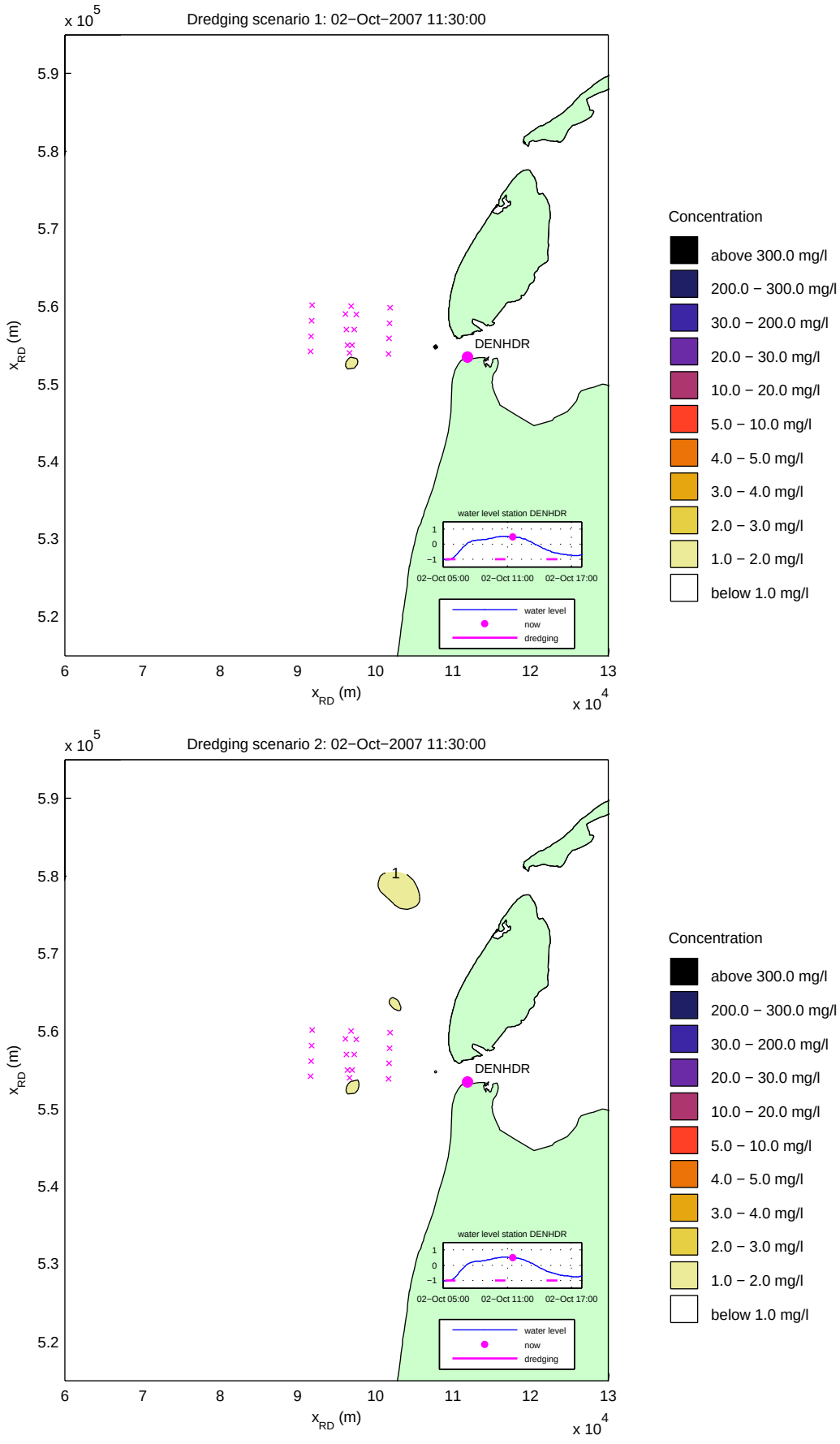

Simulated effect of overflow on silt concentrations (mg/l)
date and time: 02−Oct−2007 11:30:00
x−marks denote locations of T1 observations

Alkyon Hydraulic Consultancy & Research	A2273	Fig. 3.69

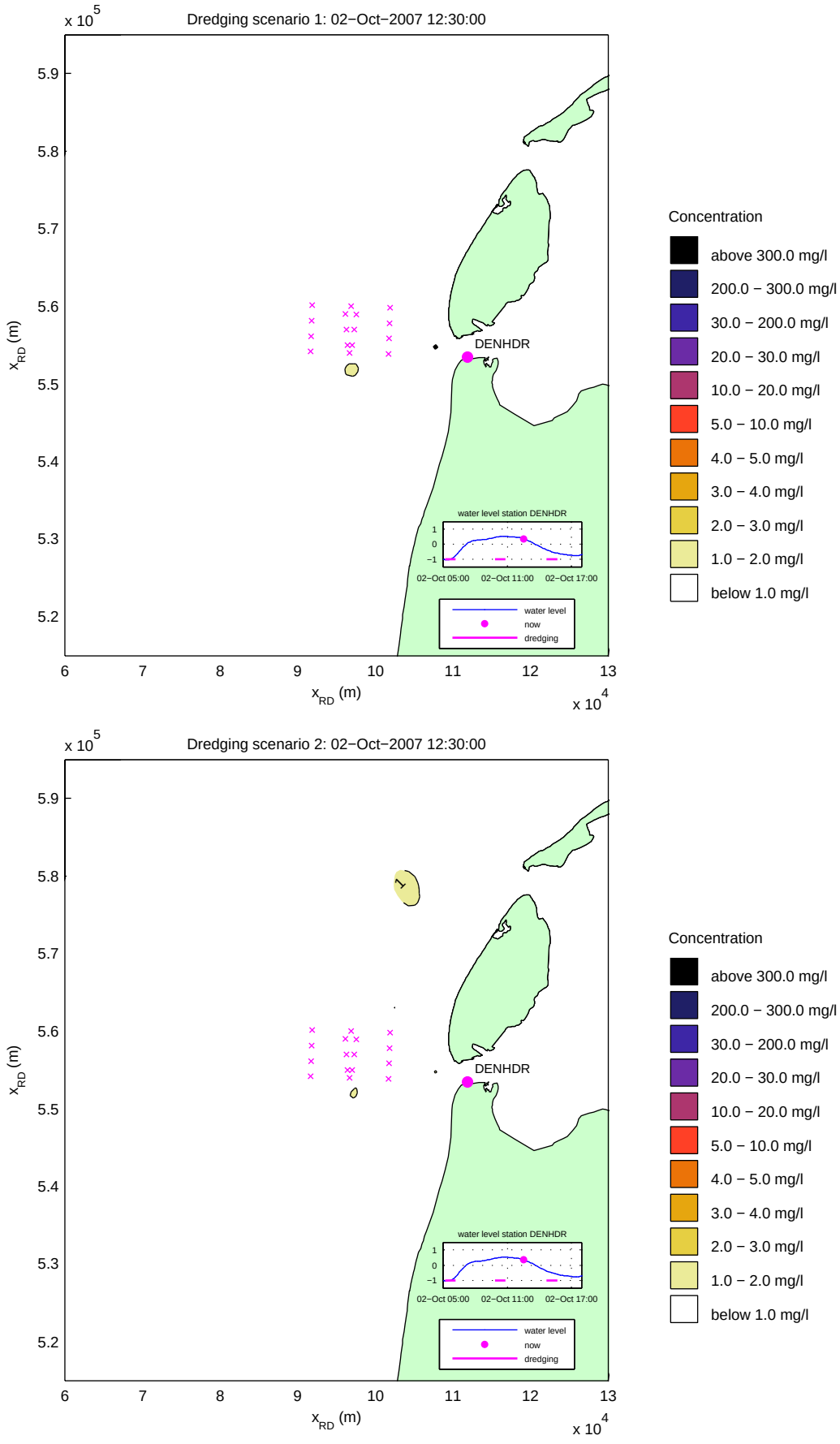

Simulated effect of overflow on silt concentrations (mg/l)
date and time: 02−Oct−2007 12:30:00
x−marks denote locations of T1 observations

Alkyon Hydraulic Consultancy & Research | A2273 | Fig. 3.70

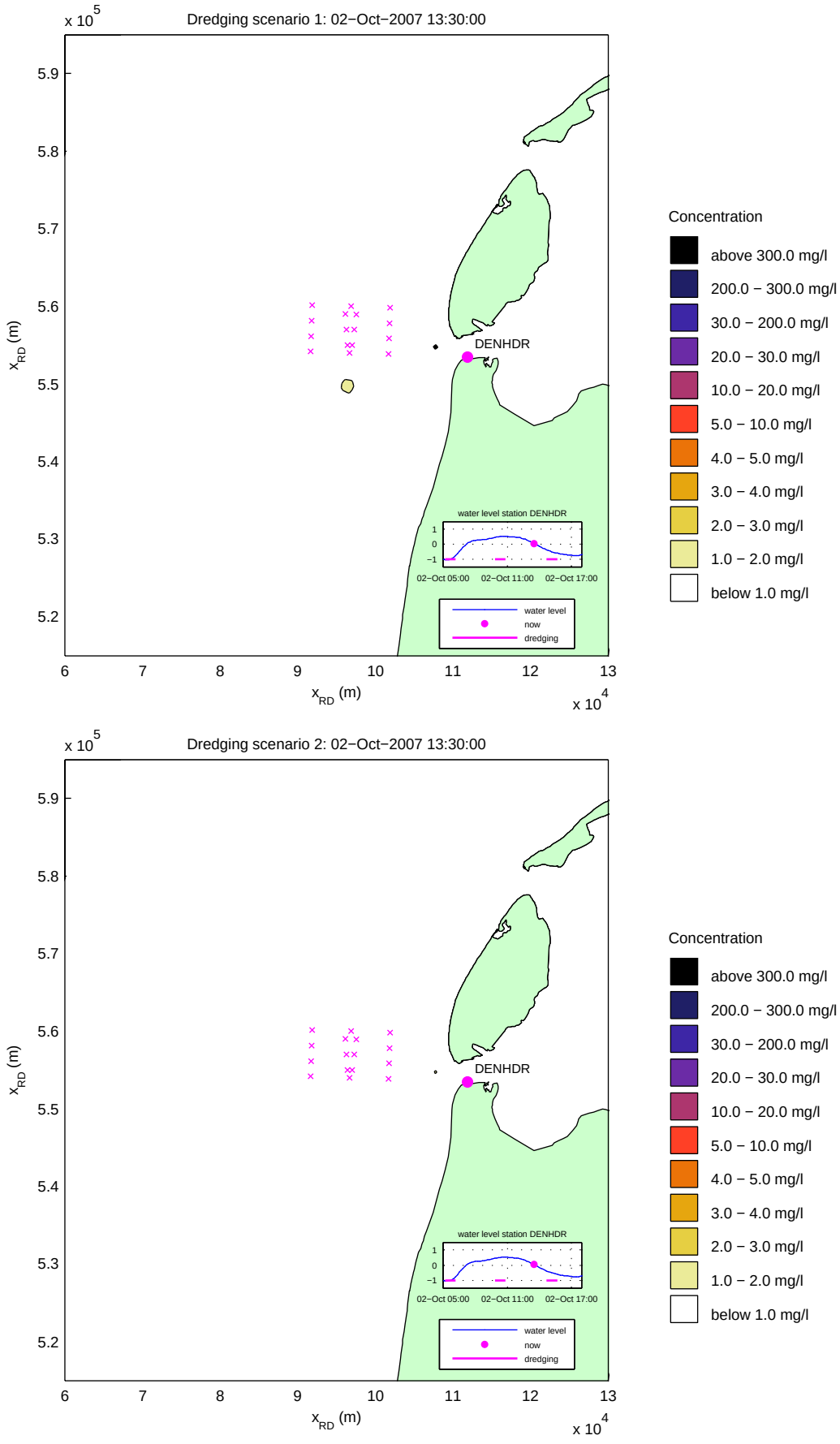

Simulated effect of overflow on silt concentrations (mg/l)
date and time: 02−Oct−2007 13:30:00
x−marks denote locations of T1 observations

Alkyon Hydraulic Consultancy & Research	A2273	Fig. 3.71

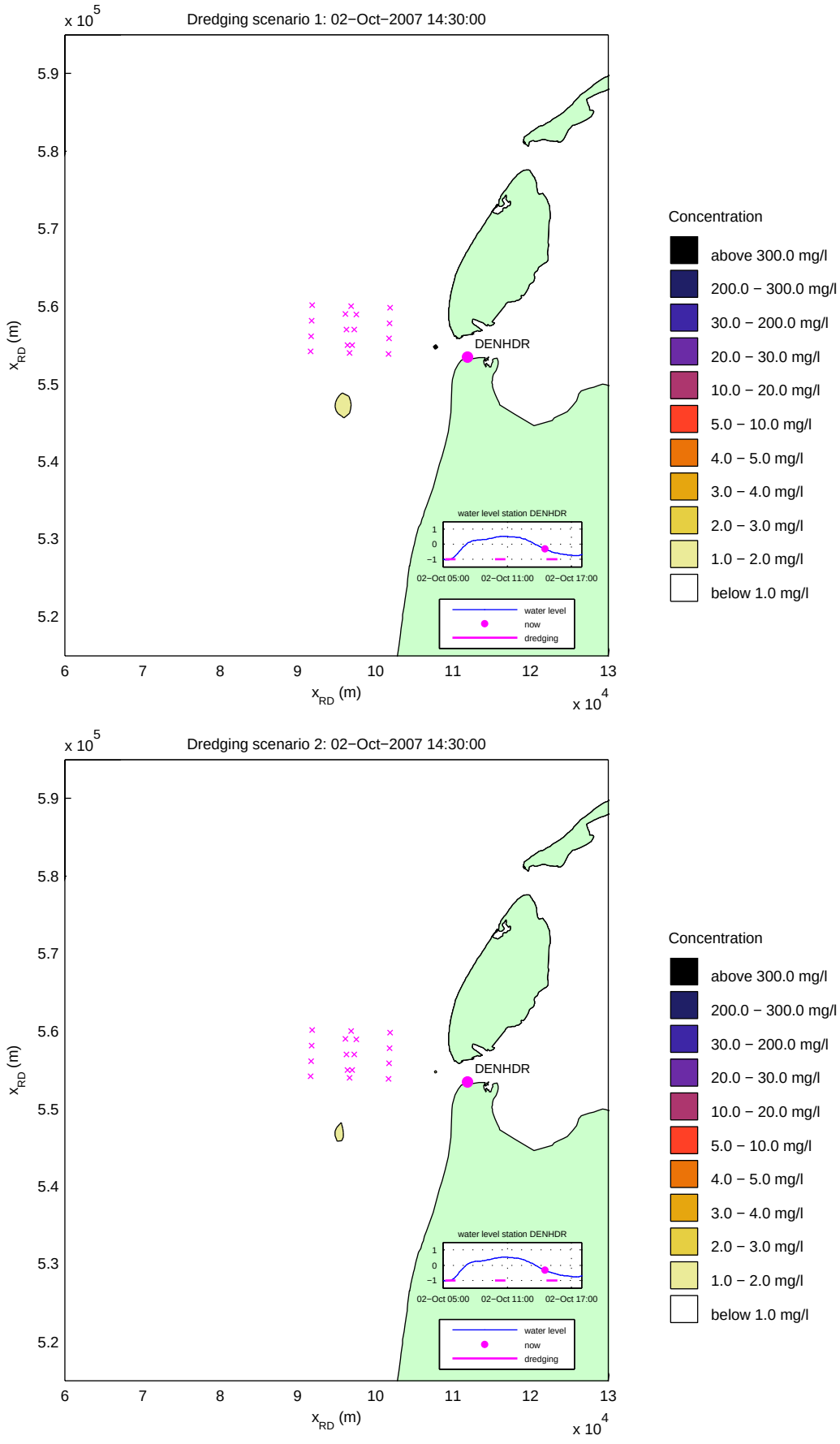

Simulated effect of overflow on silt concentrations (mg/l)
date and time: 02−Oct−2007 14:30:00
x−marks denote locations of T1 observations

Alkyon Hydraulic Consultancy & Research	A2273	Fig. 3.72

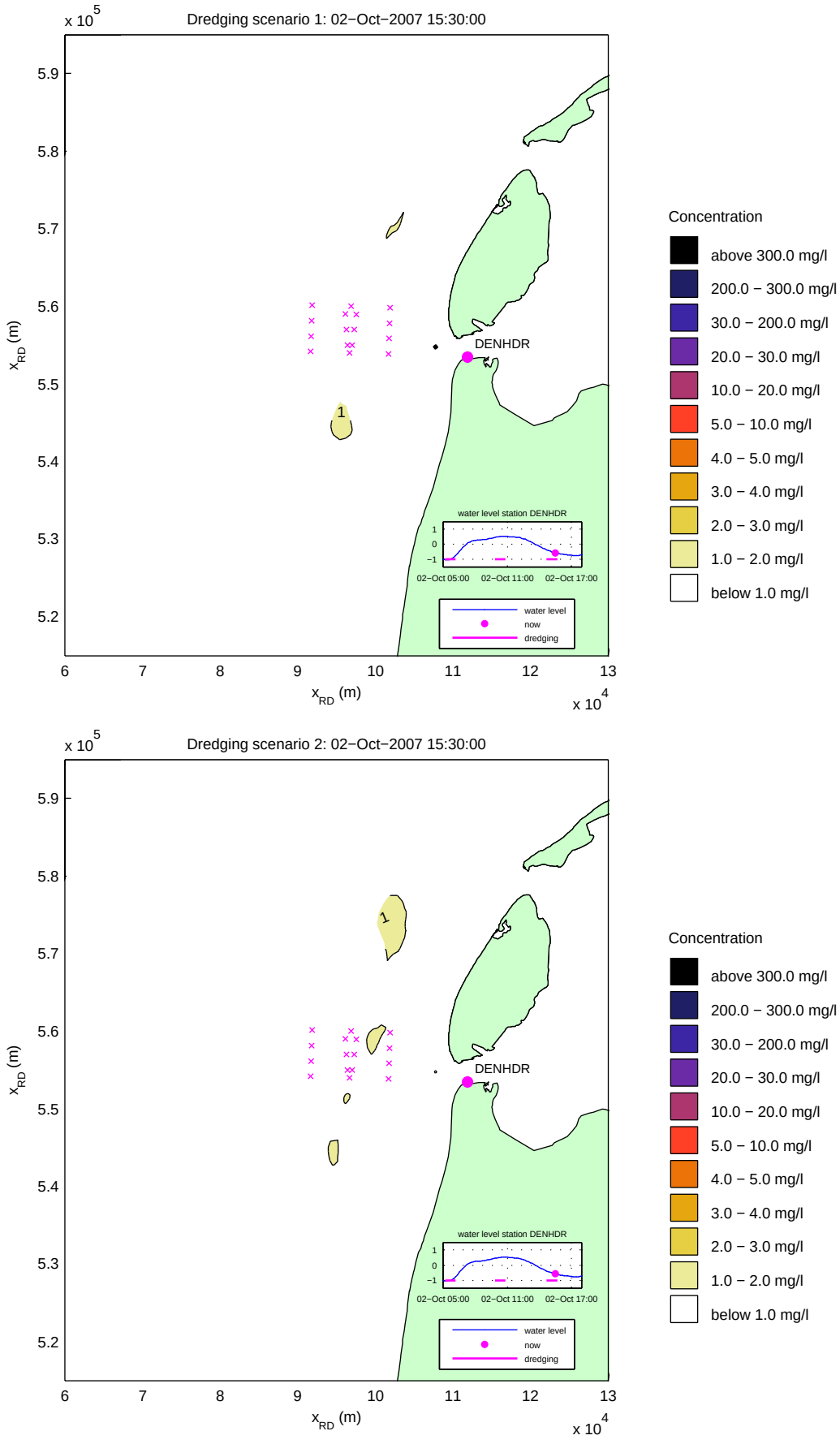

Simulated effect of overflow on silt concentrations (mg/l)
date and time: 02−Oct−2007 15:30:00
x−marks denote locations of T1 observations

Alkyon Hydraulic Consultancy & Research | A2273 | Fig. 3.73

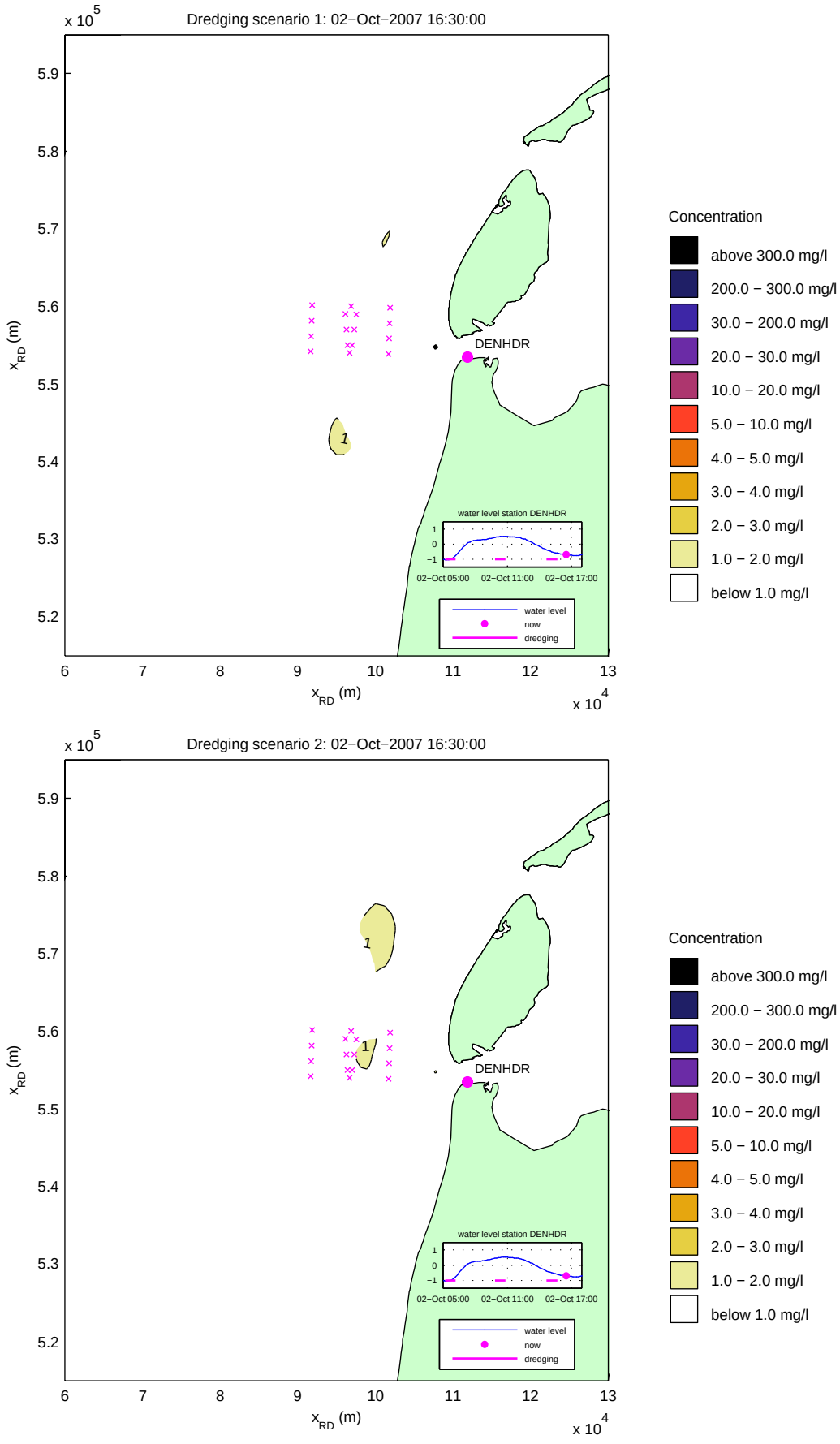

Simulated effect of overflow on silt concentrations (mg/l)
date and time: 02−Oct−2007 16:30:00
x−marks denote locations of T1 observations

Alkyon Hydraulic Consultancy & Research | A2273 | Fig. 3.74

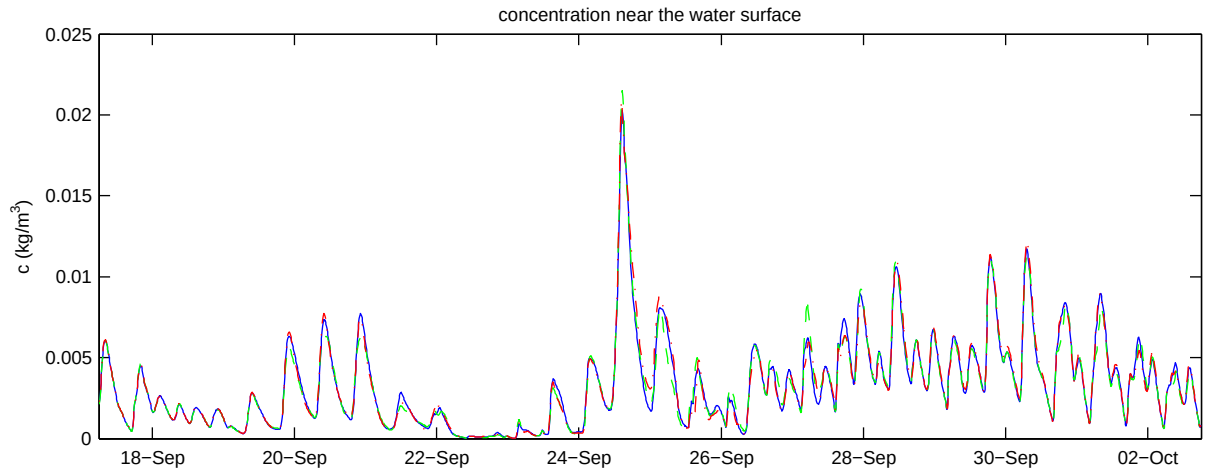

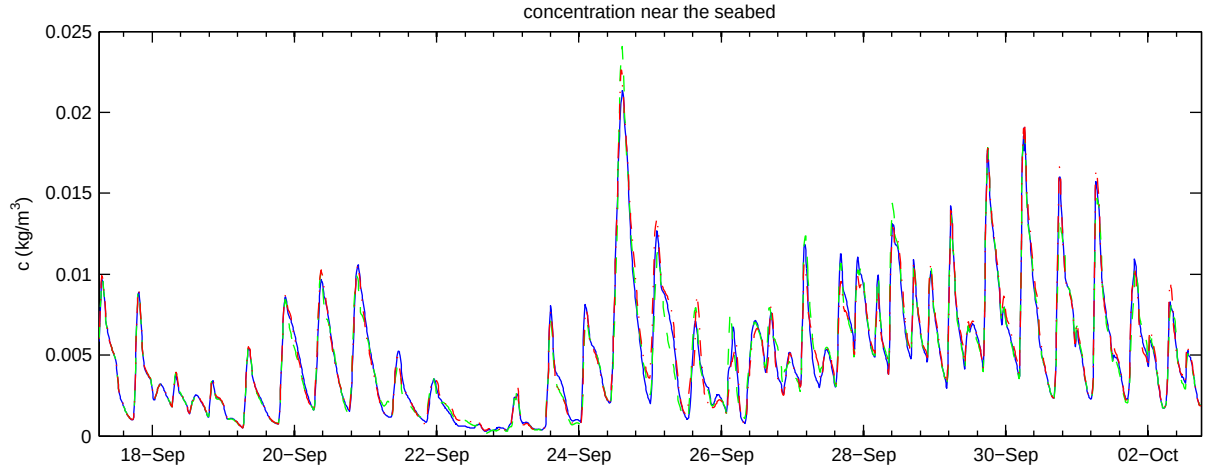

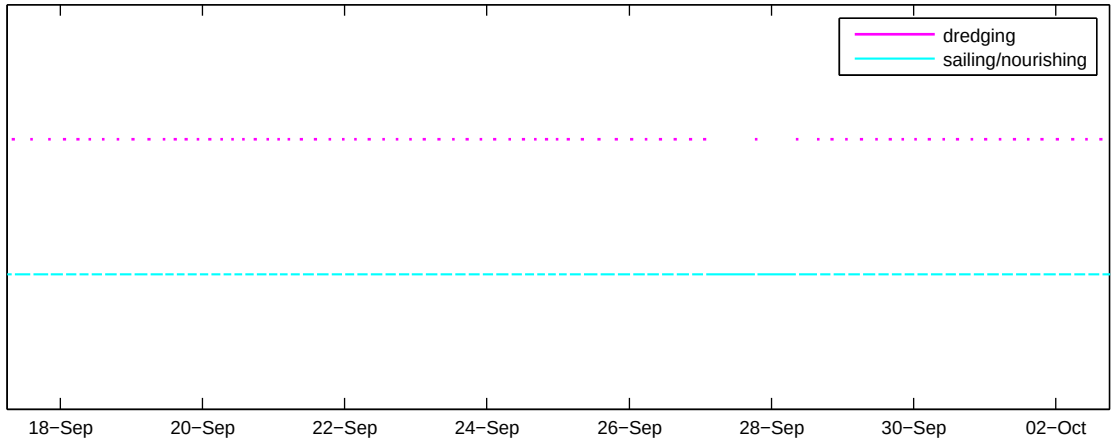

Simulated silt concentration time series with and without effect of overflow (mg/l) between 17−Sep−2007 06:00:00 and 02−Oct−2007 18:00:00		
Alkyon Hydraulic Consultancy & Research	A2273	Fig. 3.75

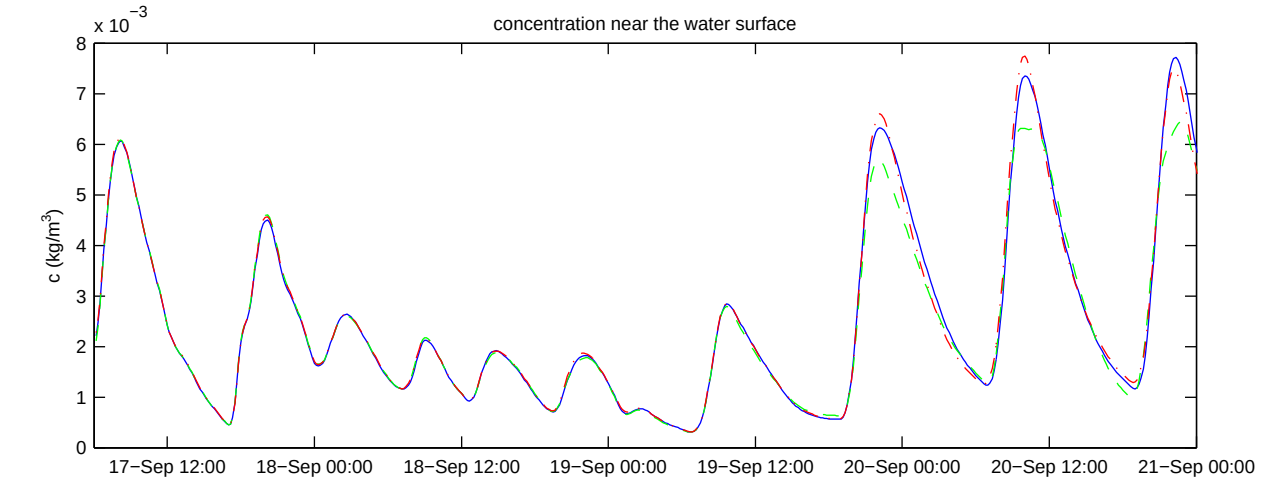

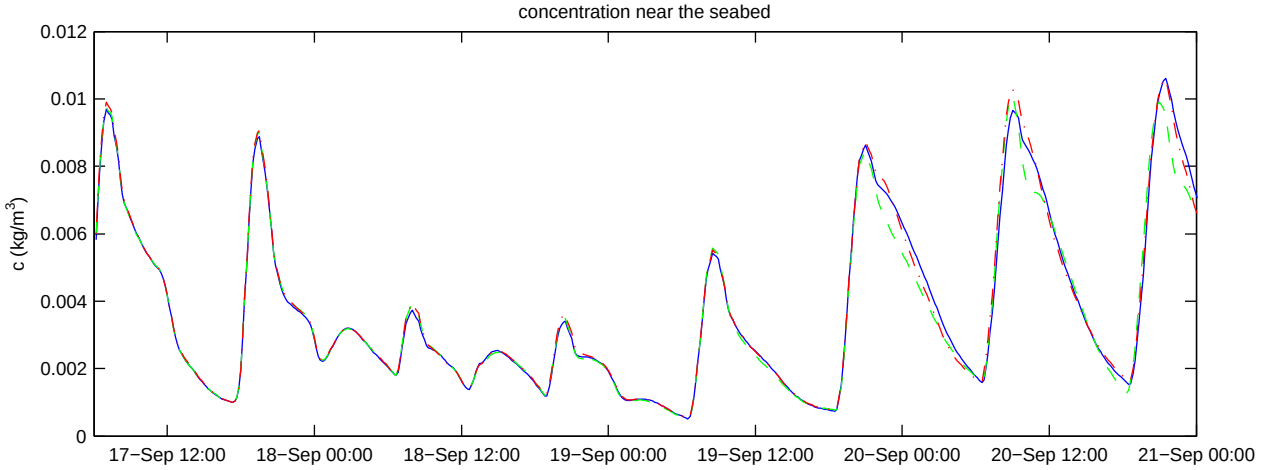

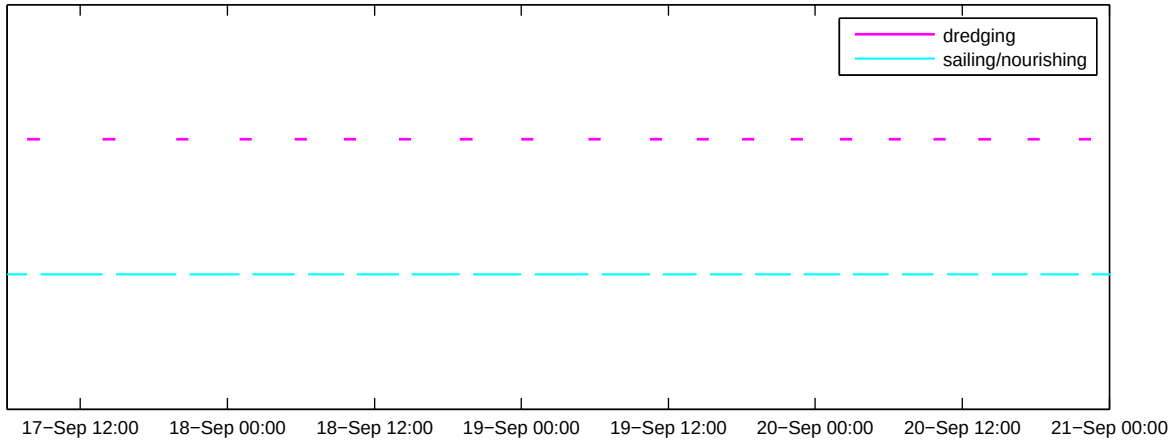

Simulated silt concentration time series with and without effect of overflow (mg/l) between 17−Sep−2007 06:00:00 and 22−Sep−2007 zoom in on previous figure		
Alkyon Hydraulic Consultancy & Research	A2273	Fig. 3.76

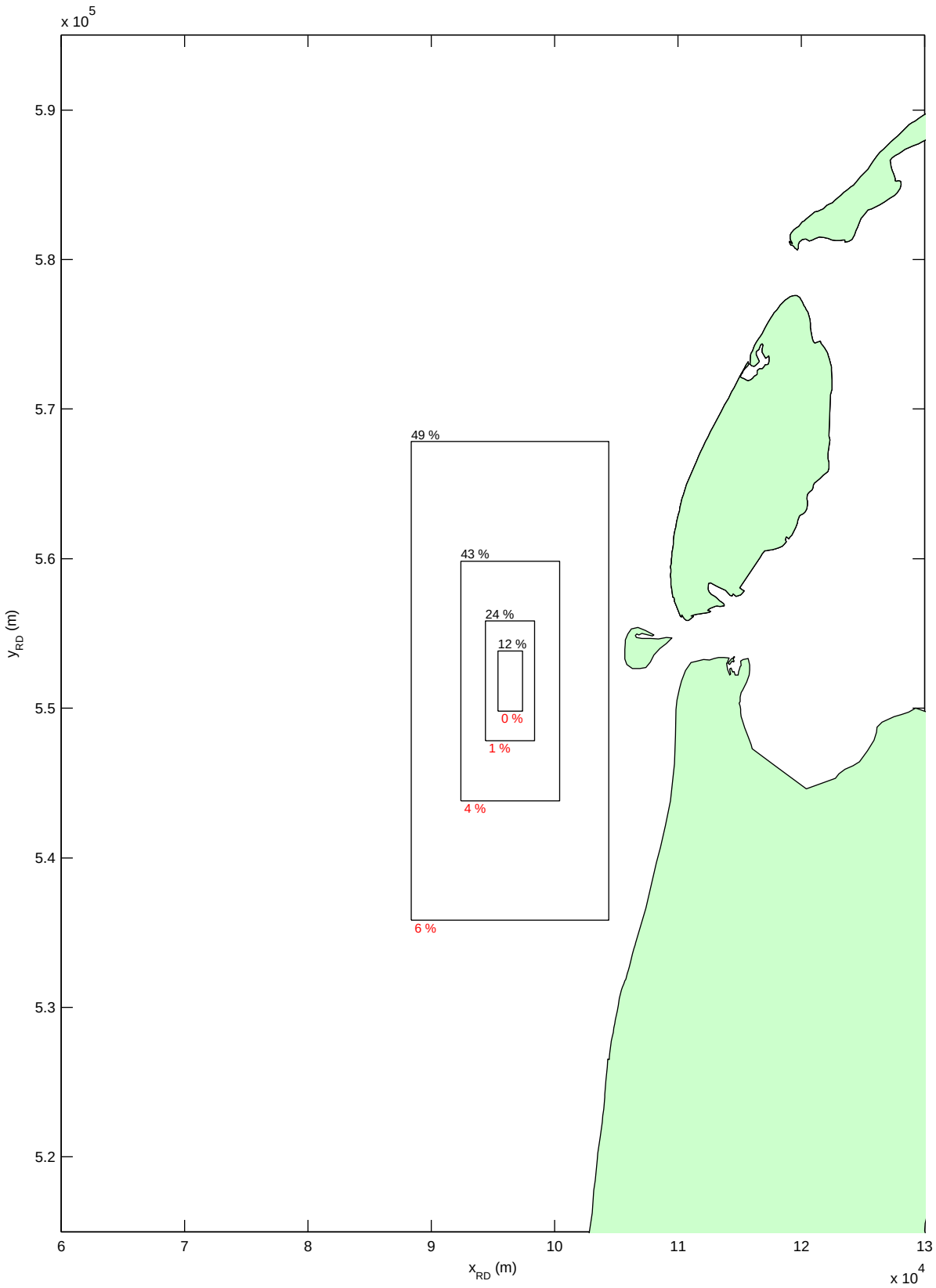

Areas and percentage of overflow sediment deposited (upper left corner) and percentage in suspension (lower left corner, red color) on 02−Oct−2007 23:30:00

Alkyon Hydraulic Consultancy & Research	A2273	Fig. 3.77

Appendix A

Description of the Van Rijn (2007) sediment transport model

Van Rijn (2007) sediment transport model

Van Rijn (2007) presents a unified view on sediment transport of fine silts to coarse sand and gravel by currents and waves. His model is now commonly referred to as the TRANSPOR2004 model (TR2004) which is an update of the TRANSPOR1993 model from Van Rijn (1993). TR2004 can handle bed load and suspended load transport. The model is fully predictive, meaning that only the basic hydrodynamic parameters and the basic sediment characteristics need to be known (Van Rijn, 2007 I).

To model suspended sediment transport, the most common approach is based on the advection-diffusion theory with downward transport due to gravity (settling) and the upward transport due to turbulent processes (mixing) (see eq.2.1). Van Rijn (1984; 1993; 2005; 2007) presented a prediction method for steady river flow. A bed roughness predictor is included and it is extended to the coastal flow regime by including wave-related mixing processes and by recalibrating the reference concentration using laboratory and field data of combined steady and oscillatory flow. Also the processes of flocculation and hindered settling for the fine silt and sand range are accounted for. This leads to a method which can be applied for a sediment size range from 8 to 2,000 µm and for the full hydrodynamic regime of quasi-steady river, tidal and coastal flow.

The sediment mixing coefficient for combined steady and oscillatory flow is modelled as:

$$\varepsilon_{s,cw} = \left[\left(\varepsilon_{s,c}\right)^2 + \left(\varepsilon_{s,w}\right)^2\right]^{0.5} \qquad \textit{eq. 4.1}$$

where the subscript *w* stands for the wave-related part and subscript c for the current-related part. The effect of sediment particles on the mixing of fluid momentum is taken into account which depends on the particle fall velocity and the bed-shear velocity. Also turbulence damping is taken into account as well as the effect of breaking waves.
The wave-related mixing coefficient in the upper half of the water column can be represented by:

$$\varepsilon_{s,w,\max} = 0.035\gamma_{br} h H_s / T_p \text{ , with } \varepsilon_{s,w,\max} \leq 0.05 \text{ m}^2/\text{s} \qquad \textit{eq. 4.2}$$

and the wave-related sediment mixing coefficient near the bed is described by:

$$\varepsilon_{s,w,bed} = 0.018\gamma_{br}\beta_w \delta_s U_{\delta,r} \qquad \textit{eq. 4.3}$$

T_p = peak wave period (s)
$U_{\delta,r}$ = representative near-bed peak orbital velocity based on significant wave height H_s (m/s)
β_w = coefficient = $1+2(w_s/u_{*,w})^2 \leq 1.5$
w_s = fall velocity of suspended sand (m/s)
$u_{*,w}$ = wave-related bed-shear velocity (m/s)
δ_s = thickness of mixing layer = $2\gamma_{br}\delta_w$ with limits $0.1 \leq \delta_s \leq 0.5$ m
δ_w = thickness of wave boundary layer = $0.36 A_\delta \left(A_\delta / k_{s,w,r}\right)^{-0.25}$ (m)
A_δ = peak orbital excursion based on significant wave height (m/s)

$k_{s,w,r}$ = wave-related bed roughness (m)
γ_{br} = empirical coefficient related to wave breaking = 1 + $(H_s/h - 0.4)^{0.5}$ (γ_{br} = 1 for $H_s/h \leq 0.4$)

The near-bed mixing parameter appears to increase slightly with increasing particle size in the range of 100-300 μm (Van Rijn, 1993). This is probably the result of centrifugal forces which are modelled by the β factor.

The near bed concentration, which is necessary to know for modelling sediment transport, can be modelled with the reference concentration close to the bed:

$$c_a = 0.015(1 - p_{clay}) f_{silt} \frac{d_{50}}{a} \frac{T^{1.5}}{D_*^{0.3}} \qquad \textit{eq. 4.4}$$

where:
p_{clay} = percentage of clay
f_{silt} = silt factor
a = reference level (m), where a is defined as the maximum value of half the wave- and half the current-related bed roughness with a minimum of 0.01 m. In the case of sheet flow conditions in the upper transport regime, the reference level is related to the sheet flow layer roughness (20 d_{50}) with a minimum value of 0.01 m.
T = dimensionless bed-shear stress
D_* = dimensionless particle parameter.

Settling velocity, flocculation and hindered settling

Important physical aspect included in this transport module is that the suspended sediment diameter increases with concentration due to flocculation effects. Van Rijn (2007a) presents a sediment fall velocity given by:

$$w_s = \phi_{floc} \phi_{hs} w_{s,0} \qquad \textit{eq. 4.5}$$

where ϕ_{floc} is the flocculation factor, ϕ_{hs} is the hindered settling factor, and $w_{s,0}$ is the sediment fall velocity of individual suspended particles in clear water (Van Rijn, 1993). The minimum fall velocity is set to 0.2 mm/s assuming a minimum floc size of about 16 μm .

The flocculation factor for particles finer than sand (d < 62 μm) and salinities larger than 5 ppt is represented by:

$$\phi_{floc} = \left[4 + \log\left(\frac{2c}{c_{gel}} \right) \right]^{\alpha} \qquad \textit{eq. 4.6}$$

with a minimum value of 1 and maximum of 10, and where $\alpha = d_{sand} / d_{50} - 1$ with $\alpha_{\min} = 0$ and $\alpha_{\max} = 3$, c is the mass concentration and c_{gel} is the gelling mass concentration (between 130 and 1722 kg/m^3). The α -factor caries linearly between 0 and 3 depending on the ratio of d_{sand} and d_{50}; $\alpha = 0$ for $d_{50} = 62$ μm (sand, $\phi_{floc} = 1$) and $\alpha = 3$

for $d_{50} \leq 16$ μm. The ϕ_{floc} factor gradually increases for particles decreasing from 62 μm to 16 μm. Flocculation is supposed to be fully active for a salinity value larger than about 5 ppt.

The transport module includes the commonly applied Richardson & Zaki (1954) expression for hindered settling, which is formulated in terms of the volume concentration as

$$\phi_{hs} = \left(1 - 0.65\frac{c_{vol}}{c_{vol,gel}}\right)^5 \qquad \textit{eq. 4.7}$$

where c_{vol} is the volume concentration and $c_{vol,gel}$ is the volume concentration for immobile sediment bed.

The effective sediment settling velocity including flocculation and hindered settling effects based on Equations (1)-(3) is shown in Figure 4.1 for three different particle sizes. The effective settling velocity of mud particles of 8 μm increases from 0.2 mm/s for c = 0.1 kg/m^3 to 2 mm/s for c = 2 kg/m^3. The flocculation process of mud particles of 16 μm proceeds somewhat slower. Hindered settling effects are dominant for c > 5 kg/m^3. The effective settling velocity of 32 μm particles increases from about 0.9 mm/s for c = 0.1 kg/m^3 to 2.2 mm/s for c = 30 kg/m^3.

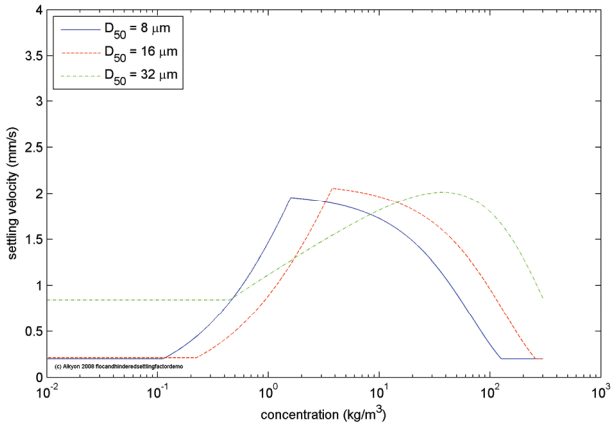

Figure 4.1 Effective settling velocity as a function of concentration for a bed of 8, 16 and 32 μm

Figure 4.2 shows examples of concentrations and settling velocities from test runs using a rectangular basin, illustrating the effect of a concentration dependent flocculation. The applied single suspended particle size is 26 μm. The depth-averaged velocity is 1 m/s. Figure 4.2 shows that under these conditions the settling velocity increases from about 0.5 mm/s in the upper part of the water column where the concentration are about 0.25 kg/m^3 to more than 1 mm/s near the bed where the concentrations are more than 1.5 kg/m^3.

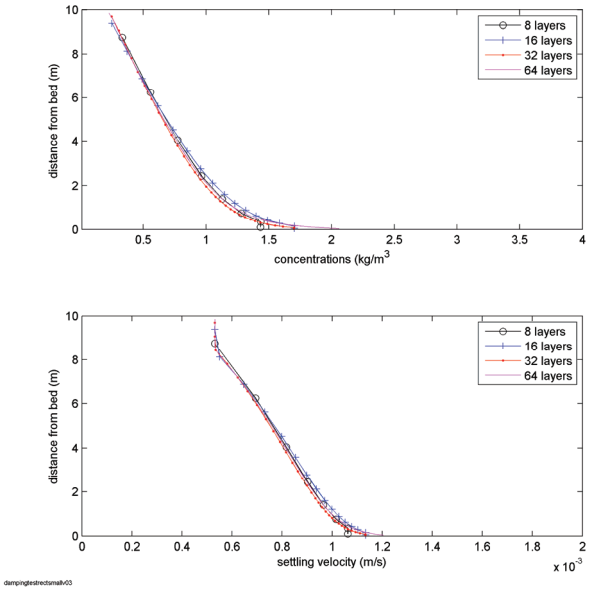

Figure 4.2 Examples of concentrations and settling velocities from DELFT3D test runs using different numbers of layers and based on a rectangular basin with a water depth of 10 m, a horizontally uniform sediment layer thickness, a depth-averaged velocity of 1 m/s and a single suspended sediment particle size of 26 μm .

Figure 4.2 also illustrates that the effect of changing the number of vertical layers on the concentrations is almost negligible under the applied conditions with uni-directional constant flow. Results from test runs using a harmonic boundary condition consisting of sinusoidal time series with a 1 m/s amplitude showed similar behaviour under maximum flow. However, the effect of the number of layers is more distinct during slack tide (small flow velocities). Figure 4.3 shows examples of vertical distributions of concentration and velocity during slack tide. Although the near bed concentrations are similar for the different simulations, higher up in the water column the concentration and the settling velocity decreases more rapidly when using more layers. The concentrations at mid depth are about 20% smaller when applying 64 layers instead of 8. This occurs only around slack tide. The results for higher current velocities are similar to those shown in Figure 4.2. Because of computational efficiency and the limited effect of the number of layers under these conditions we adopted 8 layers in our schematization. Realistically simulating the temporal behaviour of the vertical distribution of the high mud concentrations on the river Ems requires more layers but this is beyond the scope of the present study.

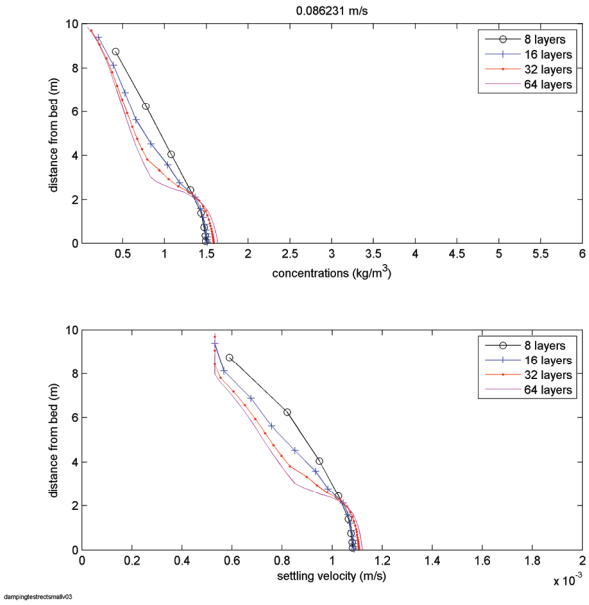

Figure 4.3 Examples of concentrations and settling velocities from DELFT3D test runs using a harmonic boundary condition with an amplitude of 1 m/s. The plot shows vertical distributions around slack tide (small flow velocity)